ADVANCED MODELLING OF OVOID BALLS

by

Christopher Holmes

A thesis submitted in partial
fulfilment of the requirements
for the degree of

Doctor of Philosophy

Loughborough University

Abstract

Sports played with an ovoid ball may be considered as minority sports in comparison to the numerous games played with spherical balls, however the ovoid ball market is considerable, with $84million spent on the purchasing of American footballs in the US alone (SGMA 2007b). In comparison to spherical balls, it is apparent that little research has been performed on ovoid types, which presented an opportunity for a detailed study into their dynamic properties in game related situations. With the development of this knowledge new ball design concepts have been investigated to improve consistency and performance, allowing manufacturers to create balls with improved physical characteristics.

Experimental procedures have been created which allow the dynamic behaviour of an ovoid ball to be characterised. It was found that the measured parameters varied depending upon the position of impact, orientation angle of the ball and the position of the valve at impact.

The inclusion of the valve within a rugby ball creates a non uniform mass distribution resulting in unstable rotation about the axis with the intermediate moment of inertia. This unstable rotation results in the ball performing a series of half twists, thus increasing the drag force during the flight and wobble. Prototype rugby balls have been manufactured with various mass distributions, allowing the effect on the unstable rotation to be analysed. Results showed that the inclusion of multiple valves, within the dynamically balanced bladder, resulted in stable rotation about all principle axes.

FE models have been created with isotropic and anisotropic material properties, with all models validated using experimental procedures. Results suggest that the anisotropic FE simulation accurately predicts the coefficient of restitution, contact time and deformation during experimental testing, and as a result it can be used to predict the dynamic behaviour of a rugby ball during various impact scenarios.

Using a thermo-bonded construction, it was shown that a novel rugby ball could be developed with a unique carcass configuration and outer panels with increased design flexibility. A number of carcass designs, based upon mathematical shapes, have been created which increase the consistency of the dynamic behaviour of the ball when impacted at different locations.

Acknowledgements

I would like to thank all those who not only made this research possible but enjoyable. Thanks go to my supervisors, Professor Roy Jones and Dr Andy Harland, for their enthusiasm, support and advice throughout the research. I am also grateful to Dr Tim Lucas and adidas for their continued support and enthusiasm towards the project during our numerous meetings, as well as providing assistance in the manufacture of the prototype rugby balls. My thanks also go to Professor Fred Yeadon and his infamous teddy bear, which began my interest in wobbly rotation many years ago.

I would like to thank the members of the Sports Technology Research Group who have not only provided friendship, but assistance and advice during testing, especially Steve Carr and Andrew Hallam for their technical support. I would particularly like to thank Jouni Ronkainen, for his continuing support and friendship throughout my time at Loughborough, and David Rogers, for his assistance during the Cardington hanger testing.

I would like to thank my parents for their support throughout my time in education, and finally Becky, who has helped me every step of the way whilst listening to me constantly talking about misbehaving balls with minimal complaint.

Publications Arising from this Work

Holmes, C., Jones, R. and Harland, A (2006). Ball launch characteristics of elite rugby union players. *Engineering of Sport.* 6 pp.211-216

Holmes, C., Jones, R. and Harland, A (2007). Design and development of a mechanical kicking simulator. *Journal of sports science and medicine.* 6. pp.211-216

Ronkanien, J., Holmes, C. and Harland, A (2008). A comparative study of ball launch measurement systems; soccer case study. *Engineering of Sport.* 7

Mitchell, C., Holmes, C. and Jones, R.(2008). Kicking in of rugby balls. *Engineering of Sport.* 7

"The dictionary is the only place that success comes before work. Hard work is the price we must pay for success. I think you can accomplish anything if you're willing to pay the price."

Vince Lombardi

Contents

Nomenclature

AF	American football
AFL	Australian rules football
CAD	Computer aided design
CFD	Computational fluid dynamics
CMM	Co-ordinate measuring machine
CoR	Coefficient of restitution
CHS	Prototype rugby ball
EPDM	Ethylene-propylene-diene-monomer
FA	Football association
FE	Finite element
FEA	Finite element analysis
FIFA	Fédération Internationale de Football Association
HSV	High speed video camera
IEC	International Electrotechnical commission
IRB	International rugby board
LED	Light emitting diode
MOI	Moment of inertia
NFL	National football league
PU	Polyurethane
RAF	Royal air force
RFU	Rugby football union
RGB	Rugby ball
SGMA	Sporting goods manufacturing association
SNR	Signal to noise ratio
TPU	Thermoplastic polyurethane

A	Cross sectional area
a	Radii of equilateral axis
b	Radii of polar axis
C_D	Drag coefficient
C_i	Material co-efficient proportional to shear modulus
d	Diameter of aperture

D_i	Material co-efficient proportional to bulk modulus
E	Elastic modulus
e	Coefficient of restitution
f	Focal length
F_A	Force due to air pressure
F_D	Drag force
fps	Frames per second
G	Shear modulus
g	Gravity
h	Height
h_1	Initial drop height
h_2	Rebound height
Ixx, Iyy, Izz	Moment of inertia about principle axes
I_1, I_2	Strain invariants
J	Total volume ratio
J^{el}	Elastic volume ratio
K	Bulk modulus
L_e	Length of element
l	Length
M	Mass of foot
m	Ball mass
N	Polynomial co-efficient
R	Horizontal range
S	Shape factor
r	Radius
T	Hang time
T_c	Contact time
t	Thickness of material
U	Strain energy potential
V_{Ball}	Ball velocity
V_{Foot}	Foot velocity
v_1	Inbound ball velocity
v_2	Outbound ball velocity
w	Width

x	x-axis
y	y-axis
z	z-axis
β	Stiffness proportionate Rayleigh damping
γ	Shear strain
ε	Strain
ε_x	Axial strain
ε_y	Transverse strain
$\lambda_1, \lambda_2, \lambda_3$	Principal stretches
ν	Poisson's ratio
ϱ	Fluid density
σ	Stress
τ	Shear stress
ω	Angular velocity

Chapter 1

Introduction

1 Introduction

There are over 50 games played with balls which are generally spherical, but a small number are played with ovoid balls. Ovoid balls are generally used in team games and they may be considered minority sports in comparison to soccer, for example. However they represent a significant business sector with the NFL Superbowl and rugby World Cup attracting global viewing audiences. In comparison to spherical balls, it is apparent that little research has been performed on ovoid types, which presented the opportunity for a detailed study into their dynamic properties in game related situations. With the development of this knowledge new ball design concepts were investigated to improve consistency and performance, allowing manufacturers to create a ball with improved physical characteristics.

There are three main sports played using an ovoid ball, rugby, American/Canadian football and Australians rules football. The main area of interest for this research was rugby and American football, therefore a brief history of the two sports follows.

1.1 History of Ovoid Ball Sports

Rugby Football is said to have originated from Rugby School, whose initial rules only allowed the handling of the ball if it was caught once airborne. In the 1820's a boy named William Webb Ellis was said to have run with the ball, towards the opponent's goal line, with this practice becoming the norm by the 1840's. Players leaving Rugby School would take the game with them, and as a result clubs began to form not only in England but in the colonies. The different clubs were all playing the game with varying rules, so in 1870 Edwin Ash, secretary of the Richmond Club put a letter in the newspapers which said "Those who play the rugby-type game should meet to form a code of practice as various clubs play to rules which differ from others, which makes the game difficult to play". On 26th January 1871 a meeting was held in London attended by over thirty people from twenty two clubs and schools, and as a result of this meeting the Rugby Football Union (RFU) was founded (RFU 2005).

American and Canadian football are said to have been directly descended from both Association Football and Rugby Football in the early 1820's. A game known as 'ballown' was also played around that time by students from Princeton University. Players were allowed to use both their feet and their fists to advance the ball, with the main aim to advance the ball past the opposing players. Harvard University also played a similar game between freshman and sophomore classes on the first Monday of a new school year, with the rough nature of the game leading to the event being dubbed 'bloody Monday'.

On November 6th 1869 the first game was played between Rutgers and Princeton Universities, with the game using modified London Football Association rules (NFL 2005). On November 23rd 1876, representatives from Harvard, Columbia, Princeton and Yale met at Massasoit House to create the standard American Football rules. This event later became known as the Massasoit Convention, and the rules adopted were very similar to those of Rugby Football. Between 1880 and 1883 Yale coach Walter Camp introduced a number of changes to the rules of American Football, with Walter Camp continuing to edit the rulebook until his death in 1925.

The number of registered rugby union players in 2005 was 3.41million, with over 1.19million of those playing in England (IRB 2005). In the same year 19.9million Americans played American football, with 14.1 million of those playing the non contact variation of the game, flag football (SGMA 2007a)

1.2 Manufacture of Ovoid Balls

The construction of an ovoid ball consists of a number of layered panels constructed around a rubber bladder. The variation between different manufacturers and different ball types comes in terms of the governing body rules, manufacturing methods and the materials used. The ball specifications are given by the appropriate sport governing body, but generally consist of four panels, stitched together along the principle axis. A brief overview of the manufacturing methods for a rugby ball and American football follow.

1.2.1 Manufacture of a Rugby Ball

Today the initial manufacturing process involves the construction of the woven fabric, which is used within the outer panel of the majority of ovoid balls. Two layers of fabric are fed through a series of rollers and bonded together using liquid resin, allowing the

sheets of woven fabric to be aligned at different material orientation angles, enabling the optimisation of the dynamic properties of the ball.

The rubber compound used to create the outer panel material is then fed through a series of rollers to remove air and compress the material to the correct thickness. Woven fabric sheets are then fed between rollers with the rubber compound, to create the complete outer panel material. The panels are placed into a press, allowing the rubber to be vulcanised under the combination of heat and pressure, whilst adding the ball's surface texture. The sections of panel material are then screen printed and stamped to the correct panel dimensions, with a hole inserted into one of the panels, which is later used during the bladder insertion.

In order to conform to the regulations detailed by the governing body (IRB), a set of four panels and the latex bladder are weighed, and a contact adhesive is used to attach the bladder to the outer panel. The manual stitching procedure is completed using waxed thread, with the ball initially sewn together inside out, and only a small gap left along one end of a seam. This area is then used to turn the ball the right side out, and the stitching process is completed. The completed rugby ball will then be inflated to the correct match pressure and undergo a series of checks, both visually (defects in seams and panels) and physically (weight, length and circumference measured).

1.2.2 Manufacture of an American Football

The woven fabric used within the construction of an American football is created in an identical way to that of a rugby ball, with the only difference occurring in the method of attachment to the outer panel. A tanned cowhide is stamped into equally shaped panels, with the panels trimmed to a uniform thickness and weight in order to meet official specifications. The trimming process occurs because no two cowhides used during the manufacture are identical. The leather panels will then be stamped with manufacturer and association logos, and the edges of the outer leather sewn to the woven fabric. Holes are punched into the combined panel to allow the insertion of the laces at a later stage, and a second woven fabric piece is sewn in to reinforce the lacing area. The four panels will then be sewn together inside out on a heavy duty lockstitch sewing machine, leaving the area of the laces unstitched, as this is used in the bladder insertion process.

The leather is softened using steam and the balls are then turned the right side out, which is necessary for the insertion of the bladder. The bladder is inserted through the opening in the lace region and the ball is pre-laced with a heavy linen thread. The balls undergo a pre-moulding process during which they are inflated to a pressure of 80psi, in order to identify any possible problems with the bladder or seams. The balls are then partially deflated ready for the lacing procedure.

The lacing procedure is a difficult skill to accomplish and is only performed by a small team of specialist workers within a factory, with each ball double laced with a gridcord material. The balls are re-inflated to the standard 13psi pressure to allow a series of final checks to be performed, both visual (seams, end seams, deflects within leather), and physical (length, width, circumference and weight). Figure 1.1 depicts key stages during the manufacture of American footballs.

Stitching of panels

Insertion of bladder

Insertion of laces

Figure 1.1 Manufacture of American footballs (Wilson 2005)

1.3 Research Objective and Thesis Outline

There is little published knowledge regarding the dynamic behaviour of ovoid balls, with no measure of performance defined within the specification of the relative governing bodies. The construction of ovoid balls has changed very little since the foundation of the games, although the ovoid ball market is considerable, with $84million spent on the purchasing of American footballs during 2006 in the US alone (SGMA 2007b). The research aims to investigate the dynamic properties of ovoid balls, focusing on the rugby and American football, through the use of advanced experimental measurement procedures and finite element models. Benchmarking of various ovoid balls will develop an understanding of the dynamic performance of ovoid balls, which will allow the manufacture of prototype ovoid balls, with improved physical characteristics.

Currently there is little knowledge regarding the dynamic properties of ovoid balls, with the governing bodies of the various sports detailing the ball specification as a number of static dimensions. These static dimensions give no indication of how the ball will behave during game related situations. Discussions with elite players (Holmes 2006) have shown that players have developed an understanding of the variation between ovoid balls produced by different manufacturers and are having to adjust their tactics to suit the brand of ball being used. The non spherical nature of an ovoid ball also results in a variation of the dynamic properties depending upon impact location. It is important to gain an understanding of the dynamic properties with respect to impact location and the variation between different ovoid ball brands and types. Chapter 3 details the development of a rebound test which allows the dynamic properties of ovoid balls to be assessed during normal impacts, and describes the difficulties of ensuring the rebound direction was normal to the impact surface after contact.

The bounce of an ovoid ball is of particular interest as, during a rugby game, players will use the bounce of the ball to their advantage and this has become a major tool in an attacking player's skill base. The non spherical nature of the ovoid ball will result in different bounce characteristics dependent upon the impact location, original ball angle and out-of-balance forces. Chapter 4 describes the development of a ball bounce characterisation test, which allows the bounce of an ovoid ball to be re-created under controlled laboratory conditions. The bounce characterisation test will examine the effect of valve placement and initial ball orientation during the bounce of an ovoid ball.

In order to develop an understanding of the behaviour of ovoid balls during game related situations it is important to establish the launch parameters that elite players can achieve during the various kicks that are utilised during a game. Chapter 5 describes the first study to detail the ball launch characteristics of elite rugby union players. The data from this study was used within Chapter 6, which describes the development of a high speed ball launch mechanism and method for calculating possible errors associated with the use of high speed cameras, which were used throughout the research.

In order to develop an understanding of the mechanical behaviour of an ovoid ball during a dynamic impact, an isotropic finite element model was developed. Chapter 7 details the procedure for the characterisation of the shape and the material properties of

an ovoid ball. The model was pressurised and subjected to numerous impact scenarios which were validated using data from the experimental testing procedures developed during previous chapters. Phenomenon visible during the end impact of the isotropic model highlighted the need for developing an anisotropic finite element model in Chapter 8.

It has been demonstrated during elite player testing that large levels of spin can be imparted onto a rugby ball during a kick. It is important to characterise the effect of rotation on the flight of an ovoid ball. Chapter 9 investigates the effect of rotating the ball about the different principal axes, and how the mass distribution within an ovoid ball can have a detrimental effect during its flight.

The creation of these dynamic tests will allow the benchmarking of various ovoid balls to develop an understanding of their dynamic performance. The aim of the research is then to develop an ovoid ball with improved physical characteristics, which will occur in two distinct phases. Firstly the development of a technology that can be implemented into a current stitched ovoid ball, and secondly a novel ovoid ball constructed utilising the thermo-bonding method, currently used during the manufacture of elite soccer balls. Chapter 10 details the design and evaluation of a dynamically balanced bladder technology which can be implemented into a stitched rugby ball. Chapter 11 describes the ball flight characterisation of the prototype stitched rugby balls within a large indoor facility, which negates the effect of external conditions such as the wind. Chapter 12 details the design of a novel rugby ball, constructed using the thermo bonded method.

Chapter 2

Literature Review

2 Introduction

The purpose of this chapter is to review science and practice regarding ovoid ball behaviour, however research reveals that literature concerning this type of ball is limited. Most sports balls are spherical and as might be expected there has been considerable research into their dynamics dating back to Cariolis (1835). The major part of the literature review therefore concerns performance and design of spherical balls but given their construction and similarity of impact conditions, valid comparisons can be made to ovoid balls. In general the test methods employed are also applicable to the ovoid ball situation. The section will review the coefficient of restitution, contact time, contact area and deformation during experimental impacts, and also provide a review of current ball modelling techniques. The material characterisation is an important aspect of modelling and methods used to assess woven fabrics which are used in the construction of ovoid balls are reviewed. An overview of the aerodynamics of ovoid balls provides an insight into the behaviour of the ball during game related situations.

2.1 Ball Impact Mechanics

There are few publications regarding the impact mechanics of ovoid balls during dynamic situations. The mechanics of spherical sports balls during normal impacts will be reviewed in order to gain some insight into the behaviour of ovoid balls. Normal impacts involve balls impacting a rigid surface, deforming about three axes, then rebounding in the same direction as the initial motion. During an oblique impact the frictional force opposing the direction of the horizontal motion will reduce the ball's velocity during the contact phase and the forces acting during contact will impart spin onto the ball after impact.

An evaluation of normal impacts has been investigated, as this type of situation provides an effective means of validating both computational and numerical models. Typical parameters used for validation are coefficient of restitution (CoR), contact time, contact area and deformation.

2.1.1 Coefficient of Restitution

During a simple impact, energy will be lost causing the ball to rebound at a lower velocity, and in the case of a dropped ball from 2m it will rebound to a reduced height. The amount of energy lost is described as a ratio between the inbound velocity and the outbound velocity, commonly known as the coefficient of restitution (CoR).

$$e = \frac{v_2}{v_1}$$

e - coefficient of restitution

v_1 - initial velocity (m s^{-1})

v_2 - rebound velocity (m s^{-1})

Equation 2.1 Coefficient of restitution

The elasticity of an impact will determine the value of the CoR, and was described by Hay (1993) as the ability of a body to return to its original shape once it has been deformed. A perfectly elastic impact will result in zero energy loss CoR=1, whilst a perfectly plastic impact results in a zero rebound height, CoR= 0, with the CoR of sports balls generally somewhere in between.

To analyse the CoR of different sports balls, Hay (1993) conducted a simple experiment involving releasing balls from a height of 1.83m onto a hardwood surface and measuring the rebound height. Results varied from 0.89 to 0.31 for a 'superball' and cricket ball respectively, with the variation in results attributed to the material and construction of the balls.

Previous investigations have shown that the impact surface, inflation pressure, inbound velocity and temperature all affect the CoR of sports balls. Hay (1993) examined the effect of the impact surface when measuring the rebound height of a volleyball when released from 1.83m. Results noted that the CoR would vary from 0.42 to 0.76 during impact with a gymnastics mat and artificial grass respectively, with the lower CoR attributed to the higher damping associated with the foam material of the mat. The important case of a consistent impact surface is evident if a fair comparison is to be made between results.

The effect of internal pressure on CoR was first examined by Holmes and Bell (1985). A simple experimental procedure was used to measure the rebound height of a number of

soccer balls of varying construction, which were released from a height of 3m and impacted a natural turf and concrete surface, at pressures ranging between 0.6 and 1.1 bar. Results showed a reduction in CoR of 5.1%, when comparing a soccer ball at 0.6 and 1.1 bar. The effect of pressure in an inflatable sphere was re-examined by Bridge (1998a), who dropped an inflatable 'play ball' from a height of 1m. It was noted that the CoR increased as a function of pressure with the curve corresponding to an exponent of n=-0.62, with the reduction attributed to the energy losses occurring during impact. The CoR is dependent upon the ratio between the energy stored by the compression of the air during impact and the amount of energy transferred into surface waves, as they propagate away from the impact area. Increasing the pressure results in a lower level of distortion, which reduces the compression within the ball during impact, and the energy lost in the form of surface waves. Bridge (1998b) also presented a refined model which accounted for the adiabatic expansion of air inside the ball during contact. The propagation of the surface waves, which travel up and down the ball, affect its behaviour with the wave speed determined by the material density and the surface tension created by the internal pressure. The dampening of these surface waves results in a significant energy loss.

Daish (1972) stated that the greater the velocity prior to impact, the greater the compression and therefore the greater the energy loss. Bridge (1998a) examined this theory whilst impacting balls with an inbound velocity ranging from 1-7m/s. It was noted that the efficiency of the rebound (CoR) decreased linearly with an increase in impact velocity. Bernstein (1977) stated that the CoR was a function of the approach speed, when measuring the first 20 bounces of a solid plastic bead released from the height of 1m. Falcon et al (1998) examined the behaviour of a solid tungsten carbide bead bouncing onto a rigid surface containing a force sensor, from a release height of 2mm. The bead was allowed to continue impacting the sensor for a number of bounces and the CoR was calculated using the flight time between two successive bounces. It was stated that the CoR would remain constant during the first 80 impacts, with a value of 0.97, before decreasing for the final impacts. The authors stated that the CoR was not only a function of the material properties, but also a characterisation of the way in which the energy dissipation occurs. It was noted that the energy loss would occur in three forms, 1) the creation of surface and volumetric waves and vibrational modes stored in the bead and plate after collision, 2) plastic deformation of the bead and plate and 3) the

energy dissipation due to the viscoelastic properties of the bead and plate. It was stated that the viscoelastic properties of the material provided the greatest mechanism of energy loss.

Drane and Sherwood (2004) examined the changes in CoR of baseballs with respect to the temperature of the ball. The baseballs were impacted with an ash wall, at velocities of 60 and 100mph, with the temperatures ranging from 25 to 120 °F. Results showed a 2% increase in CoR between 40 to 120°F impacts, whilst exposing the baseball to subfreezing temperatures (25°F) resulted in a 3% reduction in CoR.

In summary, hollow sports ball CoR;

- Reduces with inbound velocity
- Increases with increase in temperature and internal pressure
- Varies with impact surface

2.1.1.1 CoR Measurement

The most common method of measuring the CoR of a sports ball is a rebound test, in which a ball is released from a height of approximately 2m. It has been stated that CoR is dependent upon the inbound velocity, but only a few governing bodies specify CoR values at playing speeds, e.g. golf. The capture of the rebound height using video camera is the most common method of determining the CoR of a sports ball, with the placement of a vertical scale within the field of view allowing direct measurement of the rebound height. Brody (1990) stated that parallax errors associated with the use of image capture devices may result in a ±1cm error when measuring the rebound height.

Bernstein (1977) described a measurement procedure for the CoR of a collision between a solid plastic bead and a rigid surface. The sound of impact was detected using a microphone, amplified, and used to produce transverse deflections on a pen recorder. Analysis of this data allowed the time interval between successive impacts to be calculated, during which the ball will spend an equal amount of time rising and falling. This method assumed that CoR was independent of velocity, which has since been proved incorrect.

Stensgaard and Laesgaard (2001) developed Bernstein's approach by creating an automated method of CoR capture, using a PC sound card and microphone arrangement. The authors captured the time interval between the bounces of a steel ball released from a height of 3-5cm, with the high sampling frequency also allowing contact time to be calculated. During impacts with a stainless steel plate it was found that a small indentation would be created on the surface, allowing an estimation of contact stress to be calculated. The authors noted that the plastic deformation in the stainless steel plate was a considerable energy loss mechanism.

High speed video imagery (HSV) is also commonly used to determine a value of CoR during impact with high inbound velocities. Dynamic test methods developed by Price (2005) involved launching soccer balls horizontally into a plate at velocities approaching 80mph, rendering the use of a sound measurement system inappropriate due to the single nature of the impact. A standard 25Hz video capture system would not be an acceptable tool for analysis, due to the high ball velocity and lower capture rate. High speed video allows the CoR to be calculated accurately, with effective camera placement reducing any parallax errors. An appropriate frame rate needs to be selected depending on ball velocity.

2.1.2 Contact Time

The majority of ball games involve striking the ball with an implement, whether a foot in soccer or a club as in golf. Daish (1972) stated that it is a characteristic of such impacts that they are all over in a very short space of time, usually a small fraction of a second, and will decrease with an increase in velocity until the duration reaches a steady state value. The author stated the difference in contact times between golf (0.5 ms) and tennis (5ms) was due to the 'give of the strings in the racket'. Gugan (2000) studied the effect of impacting a wooden mallet with a Jaques croquet ball at velocities ranging from 2.19 to 5.50 m/s. The author stated that contact time decreased from 0.97 to 0.79ms with an increase in velocity, with the contact times similar to those stated by Daish for golf.

Bridge (1998a) examined the effect of increasing inbound velocity and inflation pressure on the contact time during impact. The impact velocity ranged from 1-6 m/s during experimentation, and it was noted that contact time decreased with an increase in initial velocity. The contact time was measured by covering the ball in a metal foil, which

created a circuit between the ball and the contact plate for the duration of the impact. The curves fitted to the data have power law exponents in the range -0.13 to -0.20. Contact time decreased with an increase in inflation pressure (10 to 90 kPa), with contact time reducing according to the power law with exponents ranging from -0.25 to -0.34. The reduction in contact time was attributed to the lower levels of deformation caused by the increase in inflation pressure.

Armstrong et al (1988) examined the effect of varying the inflation pressure on the measured contact time of a soccer ball. Trials were carried out at 6, 9 and 12 psi, with the soccer balls released from a height of 6m onto a force plate allowing the contact time to be analysed. It was noted that the contact duration decreased from 12.402 to 11.676 ms, for 6 and 12 psi respectively.

Levendusky et al (1988) inflated twenty soccer balls to a pressure of 9psi. The balls were divided evenly due to their construction, into moulded and stitched balls, and released from a height of 18.09m onto a rigid flat surface, which contained an AMTI biomechanics force plate. The peak force, impulse, contact duration and rise time were analysed. The study concluded that the contact time for the stitched soccer balls was 5% greater than that of the moulded ball.

Falcon et al (1998) stated that according to Hertz theory, the duration of a collision (T_c) between a bead and a surface can be calculated using Equation 2.2.

$$T_c \alpha v^{-1/5}$$

T_c - contact time (sec)

v - initial velocity (ms)

Equation 2.2 Hertz theory

Equation 2.2 states that the lower the velocity before impact, the greater the duration of the impact. The author impacted a solid tungsten carbide bead onto a rigid surface containing a force sensor, and stated that the contact time increased with a reduction in velocity. Hertz (1881) developed a theory for the impact of a solid sphere against a flat plate which assumed non sphere deformation, however the majority of sports balls will experience considerable deformation during impact. Jones (2002) used a pressure bar gauge to measure the impact of a golf ball at a range of game related velocities, 1.4 to 67

m/s. The paper noted that the Hertz theory of impact was capable of accurately modelling the details of the impact over a full range of impact velocities.

Johnson et al (1972) describe how a trip wire was attached to a soccer ball, covered with copper foil, and projected vertically onto a metal rigid plate. The circuit completed during the time of contact allowing the contact time to be analysed, with contact times ranging between 8.3 to 7.5 ms for 2.6 to 7.52 m/s respectively.

Cross (1999) examined the contact time of a variety of sports balls, as well as a steel and plasticene ball. The study showed that contact times ranged from 5.75 to 0.94ms for the tennis and golf ball respectively. The steel ball had the lowest contact duration at 0.13 ms.

In summary hollow sports ball contact time;

- Reduces with inbound velocity and internal pressure
- Varies with ball construction and stiffness

2.1.2.1 Contact Time Measurement

Three main techniques have been utilised for the measurement of contact time during an impact, the force plate, high speed imaging and electrical circuits. The majority of the literature described above, has utilised the force plate during the analysis of the contact duration, and shown it to be a valid measurement tool. Roberts et al (2001) stated that the force plate method is restrictive as it is only an accurate measure of impact duration between a ball and a rigid surface. Impacts involving a moving implement or non flat surfaces are not suitable for this type of measurement procedure.

High speed imaging is a common method used to determine the contact duration of an impact. However the accuracy is limited to the frame rate of the camera, and problems may arise if there is a need to capture dynamic impacts during play. Roberts et al (2001) noted that the camera placement is critical in order to reduce errors, so this method is generally used during an impact where the contact location can be predicted, with either the ball or surface stationary prior to impact.

Electrical circuits have been used to analyse contact times in golf (Cochran and Stobbs 1968, Hocknell et al 1998 and Roberts et al 2001), play balls (Bridge 1998) and football (Johnson et al 1972). This method involves creating an electrical circuit between the contact surface and the ball. Hocknell used a tin 100 μm copper strip to cover the equator of the ball and the circuit was completed through a trailing wire and a metal club head. As previously stated Johnson et al covered the entire surface of a soccer ball in copper foil, and carried out rebound tests at various heights.

2.1.3 Contact Area

Dowell et al (1991) studied the effect of releasing sports balls onto a force plate from various heights, with impact velocities ranging from 4.9 to 8.4 m/s. The sports balls were divided into two classifications, compressible (racquetball, soccer ball, basketball and handball) and compact (golf ball and baseball). A steel ball was also analysed during the study to provide a means of comparison. Carbon paper was placed over a clean sheet of typing paper onto an impact force plate, and during the contact phase of an impact the carbon paper would produce an imprint on the typing paper. This image was analysed and used to calculate the diameter of the contact area to the nearest millimetre. An increase in velocity correlated to an increase in contact area for all ball types. The basketball and steel ball measured a contact area of 171.6 cm^2 and 0.343 cm^2, respectively.

Bridge (1998a) used a similar method to determine the contact area of an impact with a play ball, whilst adjusting the inflation pressure and initial velocity. A thin sheet of sandpaper replaced the carbon paper used by Dowell et al. (1991). The author states that an increase in inbound velocity results to an increase in contact area, whilst an increase in inflation pressure caused a reduction.

Gugan (2000) analysed the contact area during impacts between a Jacques croquet ball and a wooden mallet. The contact area was measured using the carbon paper method, with the author noting that the impressions were usually close to circular. The author stated that the experimental results showed good agreement with Hertz theory of elastic impact.

Johnson et al (1972) covered the impact plate with a fine chalk powder in order to establish the contact area of soccer ball impacts at varying inbound velocities. The author states a linear increase in contact area with impact speed. The theoretical model within the paper overestimated the contact area, in comparison to experimental results, as the experimental model did not taken into account the bending of the sidewalls throughout compression.

2.1.4 Deformation

Daish (1972) stated that deformation of a golf ball during an impact was the main energy loss mechanism. Manufacturers can increase the CoR of a sports ball by reducing the deformation experienced under a load, which in golf would be described as a high compression ball. However a decrease in the deformation of an impact may affect the sensation that player receives from the contact. Daish stated that the sensation from hitting a high compression ball may be less pleasant than a softer one, but will result in it travelling further.

Dowell et al (1991) measured the contact area of a number of sports balls and it was found that the contact area increased with velocity. The contact area is directly related to the deformation experienced within the ball, and as expected the greater the compressibility the more deformation the ball experienced.

Hubbard and Stronge (2001) studied the deformation of a hollow spherical ball upon impact with a hard flat surface. The thin walled shell in question was a table tennis ball. The paper utilises a theory developed by Updike and Kalnins (1970) to analyse the deformations in an elastic spherical shell, compressed against a flat surface. The theory states that the deformation occurs in three phases. 1) An initial stage of small deflection in which the shell flattens against the surface, 2) Once the deflection exceeds a critical value, buckling or snap through takes place resulting in the formation of a small inverted spherical cap, 3) During larger deflections, circumferential buckling of the inverted cap occurs, producing a set of three or four lobes. During the second phase, the velocity of the inverted cap is directly opposed to the velocity of the shell. This results in the parts of the ball having opposite accelerations, which will directly affect the CoR.

Tatara (1993) used high speed imaging techniques to examine the behaviour of a soft sphere during an impact. It was noted that the deformation during impact was found to be local and limited to the contact area. The authors also noted that the ball was seen to be very slow in the upward velocity or even to stand still instantaneously. This phenomenon was attributed to the oscillations in the ball, produced as the impact area began to contract and expand after contact.

Hocknell et al (1996) studied the effect of elastic deformations during a golf ball impact. Laser Doppler vibrometry was used to calculate the deformation of the ball to a resolution better than 0.1mm, in the direction of impact and perpendicular to it. Hocknell later used this measurement method as a way of validating an FE model of a golf ball impact. The method had the advantages of high accuracy and was non-contacting.

2.1.5 FE Modelling of Ball Impacts

Finite element modelling will be used throughout the research as an effective tool for predicting the behaviour of an ovoid ball during impact conditions. The following section will review the FE modelling used to recreate ball impact scenarios.

Hocknell et al (1998a, 1998b) examined the mechanical behaviour of a golf club head impacting a ball. A three dimensional co-ordinate measuring machine was used to capture the surface of an existing golf club, allowing its shape to be recreated in surface modelling software. This shape was discretised into a mesh of 2D quadrilateral shell elements, with wedge elements arranged in an isosahedron structure, used to represent the ball. The model was validated using laser vibrometry to measure the club head mode shapes under excitation, and the deformation of the ball measured during an impact demonstrated good agreement between experimental and simulation results. The model was used to assess stress, strain, velocity and the modal analysis.

Asai et al (2002) examined the impact between the foot and a soccer ball during a curve kick, with the leg and ball meshed using hexahedron and shell elements respectively. The human foot and leg is a very complex structure, which was simplified and defined using homogenous material properties. Details of the material properties of the ball were not discussed in the paper. The model was validated using a high speed video camera

operating at 4,500fps, with comparisons made between the experimental and simulation velocities of the toe. The deformation of the ball during contact was analysed, and good agreement was found between the experimental and simulation results for toe velocity and ball deformation. Other parameters such as contact time and the ball velocity were not validated, yet the model was used to examine impact phenomenon that occurs during an instep kick. The effect of impact point on the ball was examined, and the authors stated that as the offset distance from the centre of the ball increases, the spin rate and velocity increase and reduce respectively. Once the offset distance exceeds the radius of the ball, the spin rate begins to decrease, as does the contact area and time.

Cordingley (2002) developed an FE tennis ball model using a material definition of the synthetic rubber core, simulated outer cloth material and with the viscoelastic behaviour of the ball defined using an external damping coefficient. The author stated that the geometry and element choice can have a significant effect on the impact characteristics of the model and these effects were minimised by the creation of a high density isosahedral mesh. The author showed that it was possible to tune the model parameters in order to fit the coefficient of restitution and stiffness. The models were validated using high speed video capture of both normal and oblique impacts, and a good agreement was found between experimental and simulation data.

Price (2005) examined the dynamic behaviour of a soccer ball using a series of FE models constructed from shell elements. A thirty two panel manually stitched soccer ball was modelled, which included a region to represent the stitching. The author stated that the stitching region was stiffer than the panel region by a factor of five, resulting in a skeletal-like structure within the ball. It was found that the woven fabric used during the construction of a soccer ball was anisotropic and this affected the deformation characteristics of the ball. The effect of anisotropy was also examined with the construction of a carcass model to represent the internal structure of a thermo bonded soccer ball. The author noted that during high speed impacts distortion would occur at maximum deformation due to the shear strains within the carcass material. The carcass model was subsequently used as a design tool for the optimisation of the material anisotropy, in order to provide a ball with improved consistency of impact characteristics. High speed video and force plate results were used to validate the soccer ball models and their components.

2.2 Material Characterisation

As discussed in Chapter 1, rubber like materials and woven fabrics are used in the construction of the bladder and outer panels of an ovoid ball. The following section gives an overview of the mechanical properties of these materials in order to accurately recreate the material response within an FE model. Particular attention is given to the anisotropy exhibited in the woven fabric found in the outer panels.

2.2.1 Isotropic Materials

Daniel and Ishai (2006) define an isotropic material as one with the same properties in all directions or that its properties are independent of the orientation of the reference axis. An isotropic material under axial loading will undergo deformation in the load direction. An applied tensile load will result in the extension of the length of a material and the stress and strain of a material can be derived by calculating the cross sectional area and original length of the specimen. The stress and strain of a material are related by the elastic modulus defined in Equation 2.3.

$$E = \frac{\sigma}{\varepsilon}$$

E - elastic modulus
σ - stress
ε - strain

Equation 2.3 Elastic modulus

During the uniaxial loading of a specimen, a transverse deformation will also occur, and the ratio of axial strain to transverse strain is defined as the Poisson ratio, which can be calculated using Equation 2.4.

$$\nu = -\frac{\varepsilon_y}{\varepsilon_x}$$

ν - Poisson ratio
ε_x - axial strain
ε_y - transverse strain

Equation 2.4 Poisson's ratio

Price (2005) noted that the axial strain would be proportional to the transverse strain if 1) the applied force is constant throughout loading, 2) the material is homogenous (it has the same composition and elastic properties at every point), and 3) the material is isotropic (the elastic properties are the same in all direction perpendicular to the longitudinal axis)

During pure shear loading a material will undergo shear deformation when loading is applied to the externals faces of the specimen's geometry. The shear modulus can be calculated using Equation 2.5

$$\tau = G\gamma$$

τ - Shear stress
G - shear modulus
γ - shear strain

Equation 2.5 Shear modulus

During compression a material will resist the change in volume, and this resistance is described as the bulk modulus. The bulk modulus is related to the elastic modulus and Poisson's ratio, defined by Equation 2.6

$$K = \frac{E}{3(1-2\nu)}$$

K - bulk modulus
E - elastic modulus
ν - Poisson's ratio

Equation 2.6 Bulk modulus

For an isotropic homogenous material, the relationship between the elastic modulus, shear modulus and Poisson's ratio can be defined by Equation 2.7

$$G = \frac{E}{2(1+\nu)}$$

Equation 2.7 Relationship between elastic modulus, shear modulus and Poisson's ratio

2.2.2 Rubber Material

Natural rubber, or polyisoprene, is found in the sap of the Hevea Brasiliensis tree, mainly cultivated in Malaysia. Ciesielski (1999) stated that the material, when modified by vulcanisation, has the remarkable ability to substantially return to its original shape after being stretched considerably. It can be argued that the most significant step in sports ball development was the discovery of vulcanisation by Dunlop in 1839. A piece of natural rubber has a mass of long polymer chains which are entangled, often described as spaghetti. During the loading of the material the chains disentangle, and there is a degree of slippage as the material begins to straighten out. Ciesielski noted that during the vulcanisation the overall elasticity of the material increases, by locking the chains to each other, reducing the amount of slippage that the chains can undergo.

Figure 2.1 depicts the stress strain response of a rubber during uniaxial loading. It can be seen that the loading of the material is non linear, creating an S shaped curve that can be categorised into three sections. The initial strain occurs at a rapid rate, which can be attributed to the random orientation of the polymer chains, whilst the second portion of the graph depicts a more linear response, with a reduction in the elastic modulus. During this phase of the loading, the polymer chains undergo a rotation about one of the carbon atoms. The final response of the material is much stiffer resulting in an increase in the gradient of the curve, which is attributed to the straightening of the coiled structure of the molecular chain. This type of deformation requires a greater amount of energy resulting in an increase in the force required to extend the material.

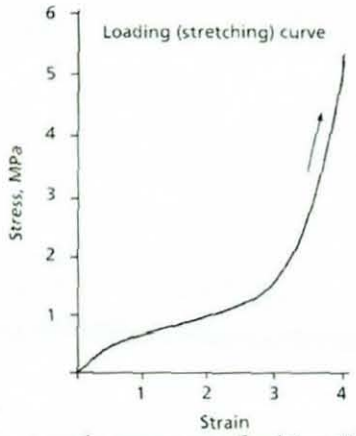

Figure 2.1 Stress strain response of rubber (Ciesielski 1999)

2.2.3 Woven Fabrics

A material is anisotropic when its properties vary depending upon the direction in which they are loaded. Woven fabrics used within the construction of sports balls are anisotropic and Price (2005) showed that this effect can cause non uniform deformation during impact scenarios. A woven fabric is constructed from interlacing two sets of yarns at right angles to each other, known as the warp and the weft, depicted in the plain weave in Figure 2.2. The material bias exists at 45° to the orientation of the warp and the weft. The orientation of the yarns will determine the properties of the fabric, and can be bi-axial or tri-axial in type. A bi-axial arrangement consists of yarns orthogonally orientated, whilst a tri-axial configuration consists of three yarns orientated at -60, 90 and 60°, which results in a reduction of the anisotropy within the fabric.

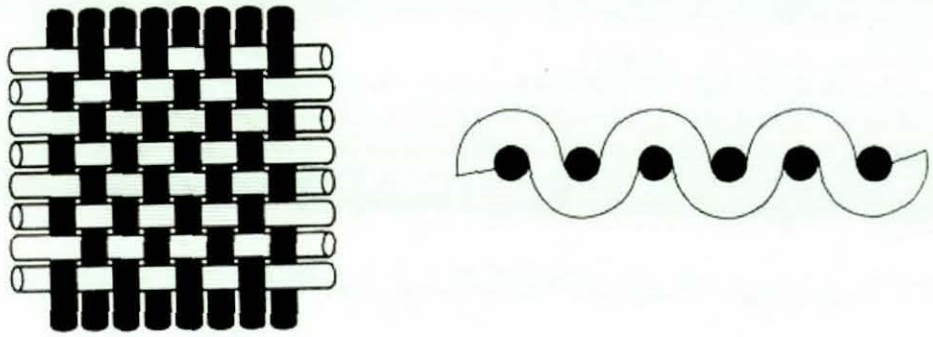

Figure 2.2 Warp and weft of a plain weave (Price et al 2005)

Woven fabrics can be categorised by the repeated pattern of the interlaced yarns, with plain, twill and satin weaves. The plain weave, depicted in Figure 2.2, is the simplest and most common type of weave and is found in a wide range of fabrics, with the warp yarn passing alternately over and under one of the weft yarns (Price et al 2005). The plain weave has the highest frequency of yarn interlacing which results in a weave with high strength. Figure 2.3 depicts the twill and satin weaves. The twill weave has a reduction in the interlacing and produces diagonal lines on the cloth which can either be left or right handed. The direction of the weave on the back of the cloth is opposite to the twill line on the front face. Twill weaves have fewer interlacings which results in more yarns per inch than a plain weave, creating a stronger, more compact, heavier and durable weave. The satin weave only contains one interlacing for each warp yarn and each weft yarn, and is designated by the number of harnesses that they require in weaving. Price et al (2005) stated that for a five harness satin weave, there are only five interlacings in the repeat of the weave, with a harness value above eight proving uneconomical. The structural integrity of the satin weave is reduced in comparison to the plain weave, due to the low levels of interlacing, but it provides a smooth texture to the upper surface.

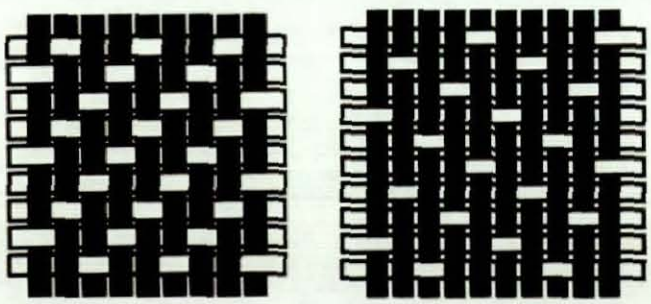

Figure 2.3 A 45°right hand twill weave and a five harness satin weave (Price et al 2005)

Hearle (1969) examined the straining of a woven fabric along the yarn direction and noted that the straining occurred in three distinct phases (Figure 2.4). 1) Straining occurs with a high elastic modulus attributed to the friction between the interacting yarns within each of the crossovers, 2) the decrimping stage, during which the undulations within the yarns are removed, resulting in the flattening of the yarns and a reduction in the elastic modulus, and 3) the extension of the individual yarns, which results in the increase of the elastic modulus.

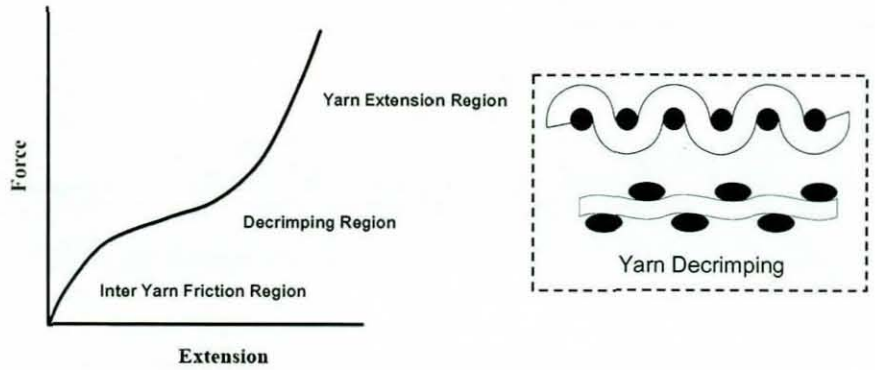

Figure 2.4 Stress strain response and the decrimping of the yarns (adapted from Hearle 1969)

Hearle (1969) stated that during loading of a woven fabric along the bias, a trellising effect occurs with the extension due to the rotation of the yarns at the cross over points, rather than extension of the yarns. This effect results in a low elastic modulus and is depicted in Figure 2.5. As the straining continues, the only mechanism preventing the straining is the friction between the yarns at the cross over points. Sidhu et al (2001) noted that during the continuation of loading, a locking angle will be reached and the rotation of the yarn stops. This results in the extension of the yarns rather than the rotation of the crossover points, resulting in an increase in the elastic modulus.

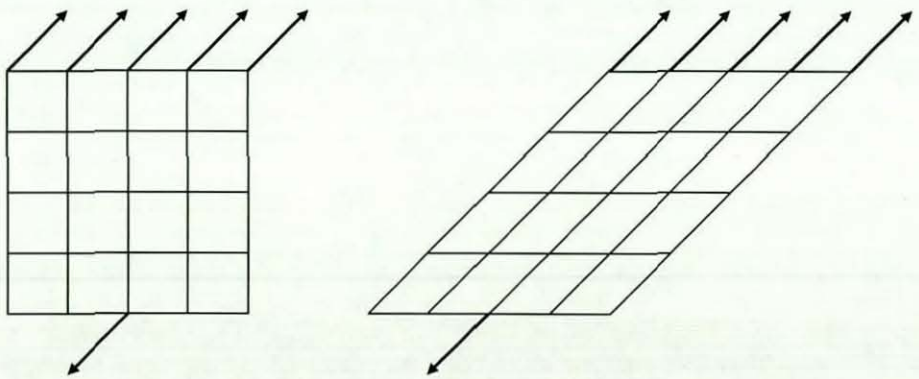

Figure 2.5 Trellising effect during straining along the bias

Sun et al (2004) carried out theoretical and experimental testing examining the effect of the varying the spacing between the warp and the weft. The author stated that the spacing ratio and the yarn diameter have more of an effect on the Poisson's ratio than the elastic modulus of the yarn. Kong et al (2004) examined the effect of varying the stitch density, stitch tension and stitch placement under bias extension, and stated that the extension occurred by rotation, sliding and compaction of the yarns. The author stated that the bias resistance increased with the density and in line tension of the yarns, because of increased frictional resistance. The insertion of stitches through intersecting yarns, as opposed to the normal undulating weave, resulted in an increased resistance to the sliding process, which in turn increased the bias resistance. The author noted that the insertion of the stitches resulted in premature crimping and wrinkling of the yarns.

2.3 Ball Aerodynamics

The aerodynamics of ovoid balls can be reviewed in three separate sections, experimental wind tunnel testing, flight of the pass and flight of the kick. The dynamics of passing will concentrate on the effect of rifle spin, which is a significant factor in an American football punt and rugby spiral kick. The affects of tumble spin occurring in place and drop kicking will also be reviewed. In order to gain an understanding of the basics of aerodynamics, a short review of spherical sport ball aerodynamics follows.

2.3.1 Spherical Balls

A sports ball travelling through air will have thin layer of fluid adjacent to the surface, described as the boundary layer, which is crucial to its motion. The layer may either be laminar or turbulent, depending on the airflow conditions, with the laminar airflow described as uniform, allowing easy separation from the ball's surface at the centre line. Neilson (2003) stated that if the boundary layer grows sufficiently or if the airflow turbulence intensity is increased then local instabilities develop and the laminar structure in the boundary layer becomes turbulent. A turbulent boundary layer will remain attached to a larger proportion of the surface, which causes a smaller wake (Figure 2.6).

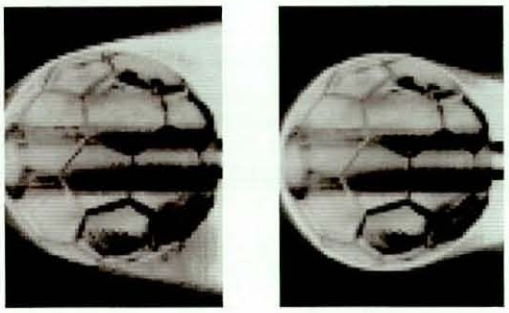

Figure 2.6 a) Laminar flow b) Turbulent flow (Carre 2005)

The wake is the major component of the drag force, Equation 2.8, which is the resistive force acting against the forward motion of the ball.

$$F_D = \frac{1}{2} C_D \rho A V^2$$

F_D - drag force

C_D - drag coefficient

ρ - density of air

V - velocity

A - cross-sectional area

Equation 2.8 Drag force

The Reynolds number is a dimensionless constant that is used to define the nature of the airflow around a given shape. The point at which the airflow changes from laminar to turbulent is described as the critical Reynolds number, and is highly dependent upon the surface roughness of the ball (Figure 2.7). Early golfers noticed that scuffed balls would travel further than a new smooth ball, and this discovery resulted in the modern dimpled balls seen today. The dimples create turbulence which reduces drag in a similar way to roughening the surface, and Aoki et al (2002) noted that as the boundary layer on the surface is disturbed, it transfers to turbulent flow, the separation point moves to the downstream side and the wake area lessens. The authors noted that the number and the depth of the dimples affect the drag force.

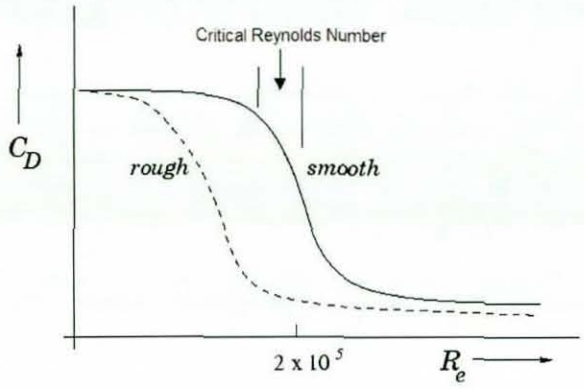

Figure 2.7 Effect of surface roughness

The use of spin is considered a significant factor affecting the flight of a sports ball. A ball rotating clockwise, whilst moving from right to left, creates a pressure differential between the top and the bottom of the sphere. The pressure differential, created according to Bernoulli's principle is due to the air at the top of the ball travelling faster in comparison to the bottom. Bernoulli's principle states that regions of higher velocity in a fluid correspond to regions of lower pressure in the fluid and that the pressure differential will produce a force perpendicular to the velocity vector of the sphere. An increase in velocity at the top of the ball, in comparison to the bottom will create an upwards force, known as the Magnus force which is depicted in Figure 2.8. The magnitude of the Magnus force is dependant upon the spin rate and the ratio of air speed to periphery speed. Neilson (2003) noted that a slow moving ball with a large amount of spin will generate a larger Magnus force than a fast moving ball with an equal amount of spin.

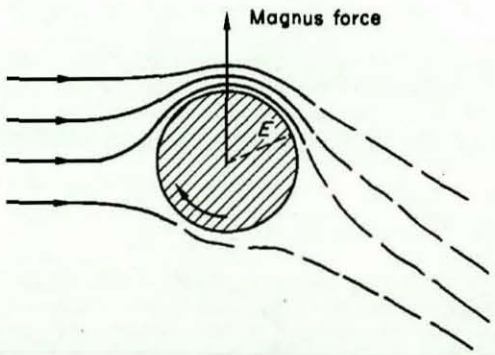

Figure 2.8 Magnus force experienced by a rotating ball (Daish 1972)

2.3.2 Ovoid Balls

2.3.2.1 Wind Tunnel Testing

An ovoid ball can be described as a prolate spheroid, which has three principle axes, depicted in Figure 2.9. Throughout the research the principle axes, yy and zz, will be defined as the equilateral axes whilst xx will be defined as the polar axis.

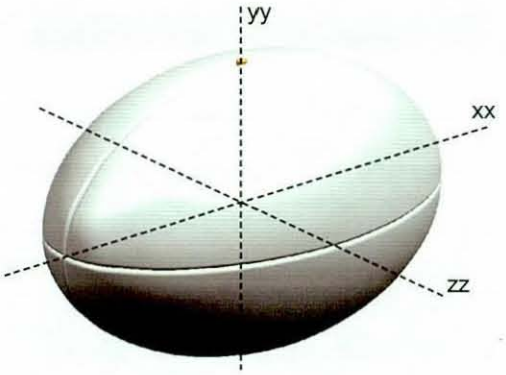

Figure 2.9 Principle axes of an ovoid ball

Wind tunnel testing to determine aerodynamic coefficients is normal practice in high technology industries where high speed objects are translated in a fluid. There has been significant wind tunnel testing of sports balls over many years in order to improve their performance. This has improved knowledge of ball characteristics but the testing is generally done with the ball stationary. In general, flying sports balls are spinning and it is difficult to provide experimental set-ups to spin the ball without affecting the airflow. There is therefore limited experimental data associated with spinning balls.

Rae and Streit (2002) measured the drag coefficient of a Wilson NFL football, which was filled with expanding foam and mounted onto a shaft with a motor and strain gauges. The football was placed in a wind tunnel and experienced wind speeds of 26.82 m/s, whilst rotating about the polar axis at 600rpm, with the polar axis facing the upstream airflow. The authors noted that the spin has a negligible effect on the normal and axial forces, but has a large effect on the side force. The authors recommend that a value of 0.14 is used for the drag coefficient of an American football when travelling nose first, and to use a cosine variation to achieve a value for the various ball orientations between 0 and 90°.

Luthander and Rydberg (1939) stated that the drag co-efficient is reduced when a sphere is spinning on an axis parallel to the flow past the sphere. Watts and Moore (2003)

examined this theory whilst rotating an American football positioned with its equilateral axis aligned with the direction of wind. The authors noted that the drag force was consistently lower when the ball was spinning at 600rpm, and that the decrease in drag force was wind velocity dependent, and ranged from 73.1% to 7.9% for 2.8m/s and 22.7m/s respectively. The drag force has two components, viscous drag, caused by viscous force on the surface of the object, and form drag, a low pressure wake at the rear of the object. It was noted that the viscous drag was the larger of the two components at low velocities, but this ratio was reversed with an increase in wind speed. The drag coefficients stated by Watts and Moore ranged from 0.05 to 0.06, which was one third that reported by Rae and Streit (2002). Differences between the values obtained experimentally were attributed to the variations in the footballs studied and possible experimental errors stated by Rae and Streit.

Alam et al (2005) studied the lift and drag forces of a rugby and Australian Rules football (AFL) measured experimentally, with wind speeds ranging from 60 to 140kph with no spin applied to the balls. The author states that the drag coefficient for the rugby ball was higher than that of the AFL ball when the polar axis was facing the upstream flow, 0.18 and 0.1 respectively. The authors noted that the drag coefficient increased dramatically when the ball was rotated, stating that the flow structures with an equilateral axis facing the upstream flow was complex and had similar trends, for both ball types. Alam stated that the flow separations were complex and time varying, with the separation starting at a position ¾ of the length of the ball along its polar axis, when positioned with the polar axis facing the upstream flow.

A comparison of the drag coefficients at varying yaw angles, noted a lack of symmetry during the measurement of both the rugby and AFL balls (Figure 2.10). The lack of symmetry was attributed to the non symmetrical nature of the balls due to manufacturing errors, creating a lack of symmetry with respect to the air flow and force balance. Wantanabe (1982) examined the effect of hysteresis when experimentally measuring the drag coefficient of a 20 cm aluminium sphere in the critical Reynolds number range. The author rotated the sphere at 5° intervals and noted that the drag coefficient did not create a symmetrical output. The author stated that the previous history of the upstream flow would affect the current results, creating a hysteresis loop, which may be attributed to the non symmetrical nature of the results presented by Alam et al (2006). In order to

overcome the effect of hysteresis, measurements should be taken from -90 to 90°, and 90 to -90°, and a comparison made.

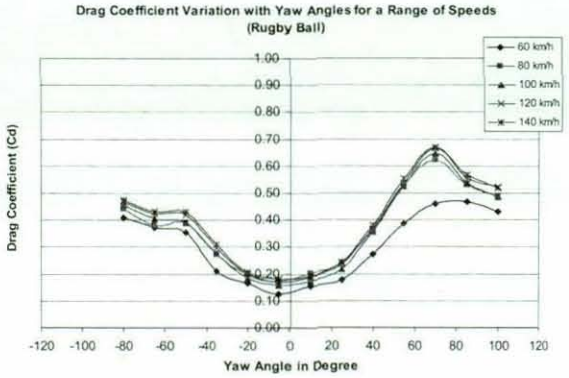

Figure 2.10 Drag coefficients – experimental measurement (Alam et al 2006)

As a continuation of this work, Alam et al (2006) presented a comparison of simulation and experimental data for the drag coefficient of the rugby ball. A simplified smooth oval shape was meshed and the computational fluid dynamics (CFD) software Fluent 6.1 was used to simulate the field flow at velocities ranging from 60 to 120kph, with the yaw angle varying from -90 to 90°. The author noted that no Reynolds number variation was found in the CFD analysis and that drag coefficients produced a symmetrical response about a 0° yaw angle, unlike the experimental data. The drag coefficient with the polar axis facing the upstream flow was predicted at 0.15 which compares to the 0.18 measured during experimental testing. Figure 2.11 depicts the drag coefficient predicted during CFD simulations, and allows comparison to the experimental results in Figure 2.10.

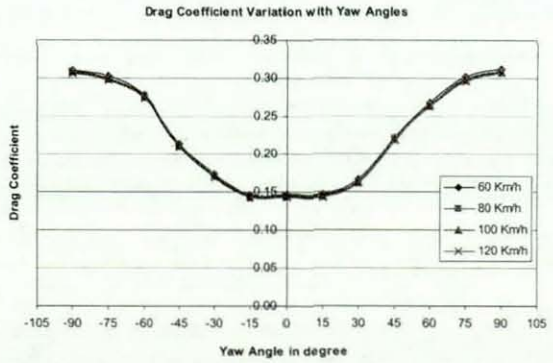

Figure 2.11 Drag coefficients – CFD (Alam et al 2006)

The results indicate the difficulty in experimental validation of simulation results but also the difficulties experienced in achieving realistic experimental set-ups.

2.3.2.2 Passing Dynamics

In rugby and Australian Rules football the length of pass is generally short so it can be argued that aerodynamic effect will be minimal. However in American football long pass distances are comparable to kicks. Little analysis has been undertaken on rugby passes but there is knowledge for American footballs. The orientation of an American football during a punt or quarterback pass will depend on the conservation of angular momentum and Brancazio (1985b) stated that the spin axis of an American football will maintain a constant orientation providing angular momentum is conserved. This type of behaviour is rarely exhibited during game situations and in general the orientation of the football will track the trajectory of its flight (Figure 2.12b)

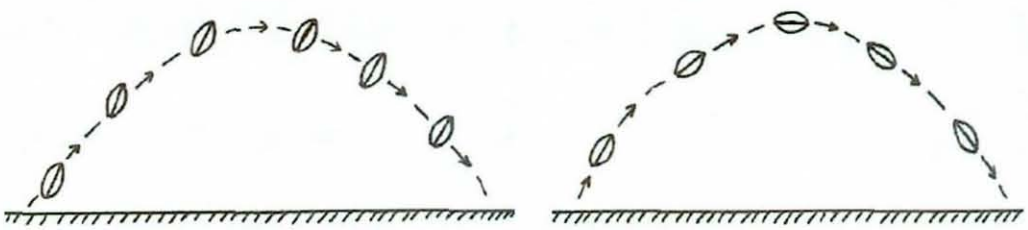

Figure 2.12 Orientation of spin axis a) angular momentum is conserved b) not conserved

During flight a force F_A is created by the air pressure acting on the leading face of the football, which can be resolved into a single drag force acting through a point known as the centre of pressure (Figure 2.13). The torque (N) about the centre of the ball can be calculated using $N = F_A D \sin \theta$.

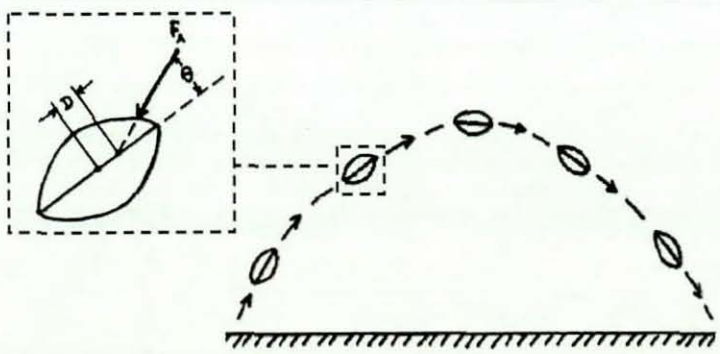

Figure 2.13 Torque produced by the drag force (Brancazio 1985b)

When initially launched a football's spin axis will be initially aligned with its trajectory, creating no torque, however the trajectory of a football is curved and so an angle will begin to develop between the axis of spin and the trajectory, creating a torque described

above. In response the football will align to reduce this angle to return the torque to zero, resulting in the nose angle of the ball constantly changing throughout the flight. This situation only occurs when a football is launched with its axis aligned with its trajectory and with sufficient spin.

Brancazio (1987) examined the theory of a 'wobbly' forward pass, and stated that if a football was passed with no precession then the ball will only rotate about one axis, and the author noted that this is the hallmark of a good quarterback. During precession an object will have an angular velocity about the axis of spin (polar axis), but will also have an angular velocity about another axis. This effect causes the object to precess about this axis at a fixed angle, which results in the tip of the football tracing out a cone shape, rather than a single point (Figure 2.14b). The author states that a precession would arise if a small amount of rotational motion was applied about a second axis, causing a wobble to be imparted onto the ball. It was noted that in order to throw a non wobbling forward pass, the quarterback must keep their wrist locked as the ball leaves their fingers, as any slight rotation about the wrist will apply an angular velocity about an equilateral axis. The author describes a 'wobble to spin ratio' which is the rate of the precession to the rate of the spin about the polar axis, and states that this is a fixed quantity as it depends upon the principle moments of inertia. Rae (2003) examined a number of images of forward passes thrown during NFL games, and stated a wobble to spin ratio of 0.56, which was similar to the 0.6 stated by Brancazio. Brancazio (1987) also stated a theoretical estimation for the drag force value of 0.1 which was considerably higher than the value measured by Watts and Moore (2003) and Rae and Streit (2002). The author also noted that drag force was ten times greater for a football travelling broadside compared with one travelling at the same velocity nose first.

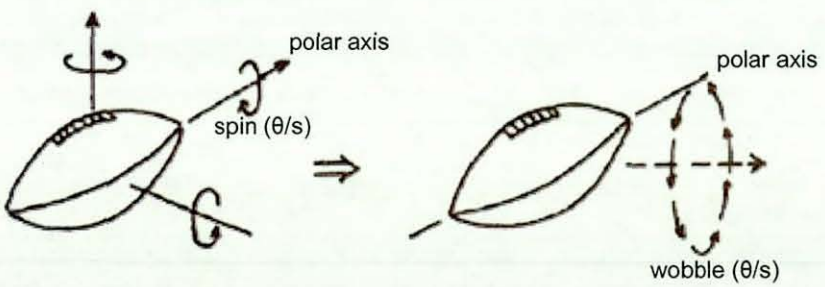

Figure 2.14 a) Principle axes of rotation b) wobble created during flight (Brancazio 1987)

Rae (2003) examined the effect of lateral curvature during a forward pass, and stated that the reorientation of a ball during flight (Figure 2.12b), generated a gyroscopic torque to

the left or right of the trajectory. The author noted that the ball responds by turning its nose to one side of the flight path or slightly above it. The interaction between the additional gyroscopic torque and the aerodynamic torque creates a small curvature in the flight path, consequently a right handed player would produce lateral curve to their right side. This phenomenon is known in ballistics literature as drift.

Nowak (2003) created an onboard flight data recorder to allow the capture of the flight dynamics of an American football. The system consisted of a number of accelerometers designed to measure acceleration in two orthogonal directions every 5ms. The flight of any sports ball can be divided into two phases, 1) The launch phase during which the athlete imparts translational and angular accelerations, and 2) The free flight phase where the accelerations are dictated by aerodynamic and gravitational forces. Nowark stated that during a forward pass the transition from launch phase to free flight takes 0.4 seconds and the total flight is only 3 seconds in duration. During the flight the ball rotated at an angular velocity of 600rpm, with a reduction of spin, attributed to the anti-spin torque and changing orientation of the ball, with a spin to wobble ratio of 1.8. The main restriction of the author's work was that a normal American football was not used during the testing due to the complexity of placing electronics inside an inflatable sports ball. Instead a 'Nerf' ball was used which is a type of foam recreational ball that has a similar shape to an American football, although smaller in size.

2.3.2.3 Kicking Dynamics

The literature reviewed within the following section relates to the kicking dynamics of American and Australian Rules football. There is currently little literature regarding the kicking dynamics of rugby balls.

Brancazio (1987) stated that during a kick-off, tumble axis spin will be imparted onto the ball, and unless affected by strong torque forces its flight will be very stable, with its axis of spin maintaining a constant direction in space without precessional motion.

Brancazio (1985a) noted the dilemma of a kicker during a punt and kick off within the game of American football. The kicker's purpose within this game situation is to send the ball as far down the field as possible, whilst keeping the ball in flight for as long as possible, helping the team to gain maximum yardage. The dilemma of the kicker is to

make a trade off between distance and "hang time" by varying the angle of the ball's launch. Brancazio developed Equations 2.9 and 2.10 to calculate the distance and "hang time" of a punted American football using launch velocity and angle. Theoretical values obtained neglect the effect of ball orientation, spin and air viscous forces. 26 NFL games were analysed involving 206 kick offs (21 kickers) and 238 punts (24 kickers). Distance was measured from the kicker's foot to the point where the ball was caught or hit the ground (±1yard), and hang time was measured with a digital stopwatch (± 0.1 sec). Average hang time and yardage for kick off and punt were 4.0sec 63yrd and 4.2sec 50yrd respectively.

$$R = \frac{v_o^{\,2}}{g}\sin 2\theta_o$$

R - horizontal range

T - hang time

v_o - launch velocity

θ_o - launch angle

Equation 2.9 - Horizontal distance of a punt

$$T = \frac{2v_o \sin\theta_o}{g}$$

Equation 2.10 - Hang time of a punt

Brancazio (1985b) discussed the effect of the unusual aerodynamic shape of an American football, and its significant role in determining the technique and strategies involved in kicking. The cross sectional area of a football varies from $0.076m^2$ ($0.25\ ft^2$) to $0.125m^2$ ($0.41ft^2$), which equates to drag coefficients of 0.1 (nose first) and 0.6 (broadside). Brancazio noted that a professional player can achieve velocities of 70mph and 80 mph for a punt and kick off respectively, and that the elevation angle should be 45° and 60° for a kick off and punt respectively in order to maximise distance and hang time for each kick.

Hartschuh (2002) examined the kicking leg and ball launch characteristics of thirteen American football punts captured using a 30Hz video camera. The kicking motion was divided into two sections, 1) the backswing during which the knee, shin, ankle and toe velocity were similar, and 2) approaching impact where the knee begins to slow, shin velocity was constant, ankle and toe accelerate to maximum velocity at impact. The author stated a typical toe velocity of 19.5m/s, whilst the ball was dropped at 4m/s

before impact. Ball velocity was measured at 24.5±0.6m/s at an angle of 49.4±1.5°. When compared to theoretical values, air resistance reduced the distance of punts by 24-33% and had a negligible effect on hang time.

Macmillian (1975) examined the main aspects that determine the flight of a kicked Australian Rules football. A 400Hz high speed video camera was used to capture the kicking action of a drop punt, a drop kick and a stab kick, and the author states that the drop punt had the highest foot velocity (23.74 m/s) but achieved the lowest ball velocity (24.99 m/s). The author noted that the transfer of momentum between the foot and the ball was an area of further study. Macmillian stated that the launch angle was a simple function of the path of the foot during contact, whilst the angular velocity at the knee was the major determinant of the foot velocity, which in turn determined the ball velocity.

Cunningham and Dowell (1976) examined the effect of air resistance whilst performing three variations of an American football punt. The three trajectories analysed were punt I - a football landing on its forward tip, punt II - a football landing parallel to the ground and punt III - a football landing on its backwards tip. The launch conditions of the three types of punt were analysed using high speed imaging, and the authors made a comparison between the experimental and theoretical distances achieved for each punt. A constant k was determined by dividing the experimental and theoretical distances, and it was noted that k was 0.44, 0.46 and 0.48 for punts III, II and I respectively.

2.4 Conclusions

The literature review detailed the ball impact mechanics of spherical balls during a normal impact, as there is little knowledge regarding the dynamic behaviour of ovoid balls. The coefficient of restitution provides a measure of the loss of kinetic energy during contact, and it is affected by the inbound velocity, internal pressure, ball construction and dimensions. It was noted that the viscoelastic material properties, formation of surface waves and plastic deformation also affect the coefficient of restitution.

The contact time, contact area and deformation are found to vary with inbound velocity, inflation pressure, ball construction and stiffness. It was noted that the contact time

shows good agreement with Hertz theory of interacting bodies, which is generally used to describe contact between solid balls with minimal deformation during contact.

It has been demonstrated that the creation of FE models can provide accurate simulated results. Force plates, vibrometry and high speed video capture have all been demonstrated as useful tools in the validation of FE models. It has been shown by Cordingley (2002) that it is possible to tune the model parameters in order to fit the coefficient of restitution and stiffness Price (2005) demonstrated the effect on non-uniform deformation during a high speed impact of a soccer ball, caused by the material anisotropy.

Woven fabrics used extensively within the construction of hollow sports balls have significant anisotropy. A review of literature has found that the deformation mechanism will vary depending upon the orientation, with a trellising effect occurring along the bias.

An overview of the aerodynamics provided an insight into a complex subject. Wind tunnel results show that the drag force varies depending upon the position of the ball, with the maximum and minimum values occurring when the equilateral and polar axes face the upstream flow respectively. The drag coefficients stated by various authors ranged from 0.05 to 0.1, with the polar axis of an American football facing the upstream flow. The significant variation in results was attributed to differences in experimental set up and balls measured. During the flight of an American football with rifle spin, it was noted that a force was created by the air pressure acting on the leading face of the football, creating a torque. The football will vary its position throughout flight in order to minimise this torque value, resulting in the realignment of the ball as it tracks the trajectory of flight. Brancazio (1987) stated that if an American football was passed with spin about only one axis of rotation then it will spin perfectly during flight. However if a small amount of rotational motion is given to a second axis then precession will occur, causing the ball to wobble. Literature suggests a wobble to spin ratio of 0.56 to 0.6.

The non uniform shape of an ovoid ball will affect its dynamic behaviour in comparison to the spherical sports balls examined by the previous research. This phenomenon needs to be quantified and will be a key area of interest during this research, with the development of testing procedures to recreate dynamic impacts. The merits of using FE

modelling as a predictive tool have been described within this literature review, and will be used throughout this research to gain an understanding of the behaviour of ovoid balls during game related situations, and to speculate on future designs.

Chapter 3

Development of Rebound Test

3 Introduction

There are over fifty games played with balls which are generally spherical but a small number are played with ovoid balls, which presents particular problems with specification and assessment. This chapter details the need for dynamic assessment of ovoid ball performance, and describes the design and development of the rebound test. Testing has been carried out on a number of different types of ovoid balls and the results are detailed below.

3.1 Specification of Ovoid Balls

The specifications for ovoid sports balls are established by the relevant sport's governing bodies, and consider a number of basic criteria such as the number of panels, dimensions, weight and pressure at the start of play, detailed in Appendix A. The parameters defined are all static dimensions, but factors determining how the ball will perform under play conditions are not measured. The simplest test to measure dynamic performance, used by the majority of governing bodies for spherical balls, is a drop test which effectively measures the coefficient of restitution (CoR). Normally this is a slow speed test with the ball being dropped from around 2 metres. The shape of an ovoid ball means that this type of measurement procedure is difficult to achieve because a dropped ovoid ball will generally not bounce normal to the impact surface. The specified ball dimensions indicate major and minor values with no indication of shape. Ovoid balls can therefore behave differently in game related situations. In addition only a small number of panels are allowed which means that considerable differences can occur depending on impact position, particularly from the ends. The investigation reported here relates to the development of a drop test procedure which provides an accurate and repeatable method for measurement of CoR for ovoid balls at major and minor dimensions.

3.2 Development of Ovoid Ball Rebound Testing Device

One of the most significant sports ball properties is the reaction to impact, which is generally specified as coefficient of restitution. During an impact, energy will be lost causing the ball to rebound at a lower velocity and in the case of a simple normal impact

with a rigid surface, a ball dropped from 2 m will rebound to a reduced height. The coefficient of restitution is described as the ratio between the inbound velocity and the outbound velocity and is an indication of the energy retained during the impact. Since position is generally easier to measure than velocity the ratio of the initial height to the rebound height represents the square of the CoR (Equation 3.1)..

$$e = \frac{v_2}{v_1}$$

$$e = \sqrt{\frac{h_2}{h_1}}$$

e - Coefficient of restitution
v_1 - Initial velocity
v_2 - Rebound velocity
h_1 - Initial drop height
h_2 - Rebound height

Equation 3.1. Coefficient of Restitution

The elasticity of an impact will largely determine the value of the CoR with elasticity being defined as the ability of a body to return to its original shape once it has been deformed (Hay 1993). A perfectly elastic impact will result in zero energy loss CoR=1, and a perfectly plastic impact results in a zero rebound height, CoR= 0. The most common method of effectively measuring CoR for sport balls is a rebound test where a ball is dropped from a known height.

3.2.1 FIFA Specification

In 1996 the governing body for soccer FIFA (Federation International Football Association) introduced the Denominations Program to standardise the quality of soccer balls. The FIFA specification for soccer balls involves seven laboratory based tests to assess specific ball parameters. 'FIFA approved' or 'FIFA inspected' balls carry an approved logo and FIFA state that such a designation on a football indicates that it has been tested officially and found to be in compliance with specific technical requirements, different for each category and additional to the minimum specifications stipulated in Law 2 (FIFA 2006).

The rebound, water absorption and shape and size retention testing procedures are dynamic tests. The rebound test involves dropping a ball from a height of 2m onto a steel plate, and measuring the height to which it rebounds. The recording of the rebound height, using a video camera, is the most common method of determining the CoR of a

sports ball. A vertical scale is generally placed in the camera's field of view, and used to measure the highest point of rebound. CoR can be determined from the ratio between the two heights. Since the FIFA test parameters are respected internationally they could form the basis for development of a series of laboratory based tests for ovoid balls.

3.2.2 Development of Holding Mechanism

Large hollow balls allowed to fall freely under their own weight tend to deviate during the drop due to out of balance, air currents etc, causing the ball to rebound at an angle to the impact surface. Elementary tests by the author allowing free drop of an ovoid ball showed considerable ball deviation during the drop and orientation of the ball axis during impact. The resulting rebound was seldom vertical and generally the ball motion contains spin, making the evaluation of CoR extremely difficult. The FIFA rebound test overcame this effect by supporting the soccer ball upon a metal ring at a height of 2m. The ring then falls under gravity carrying the ball which impacts with a steel cylinder, and the rebound height is analysed using images from a 25Hz video camera. Because the ball motion is controlled during the drop the rebound is generally vertical. It was decided to adopt the FIFA method and modify the supporting ring to allow ovoid balls of various specifications to be held both horizontally and vertically. This allows the ball to impact at its end, and at any position around its centre, but in order to accurately assess the CoR it is necessary to ensure that the ball bounces vertically after impact.

Initial testing showed that the aerodynamic properties of an ovoid ball, whilst impacting around its centre, resulted in the ball initially leaving the holding ring as it fell under gravity. This resulted in a lack of control of the impact position, and spin was imparted onto the ball due to the off centre impact. The tumble axis spin resulted in the ball impacting the side of the drop test machine. Modifications were made to the holding mechanism to ensure the ball remained in contact with the holding ring and sprung steel supports were attached to the mechanism providing a minimal supporting force (measured at 5.6N) to either end of the ball during a centre impact (Figure 3.1). Upon impact with the steel cylinder, the holding mechanism continues to fall, and the constraining force of the holding mechanism is removed. As a result the ball was free to rebound upwards along its inbound path, allowing a valid measurement of vertical rebound velocity. During preliminary testing the angle at which the ball rebounds relative to the impact surface, was measured for a number of ovoid balls in order to determine

the validity of the CoR measurement. The maximum deviation angle occurred during end impacts and the absolute mean value was measured as 2.8° (n=15), in comparison to 1.2° (n=15) measured during soccer ball impacts.

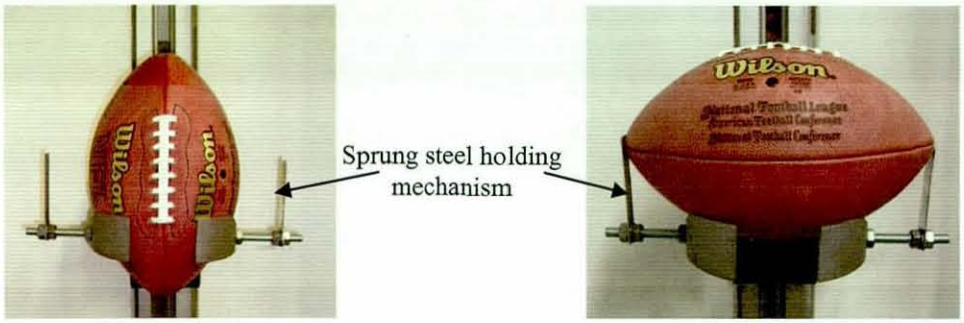

Figure 3.1 Holding mechanism a) vertical impact b) centre impact

3.3 Methodology

The dynamic properties of eight different balls, representing all ovoid ball types (rugby union, rugby league, American football and Australian rules) were evaluated using the rebound test, detailed in Table 3.1. The aim of the study was to determine the differences that exist between different ball types and the effect of different impact positions on CoR and contact time. Manufacturers of sports balls aim to produce balls which perform consistently in play and interviews with elite players (Holmes 2006, Neilson 2003), indicate that ball bounce variability is a more significant factor with ovoid balls than soccer balls. During game related impacts players are unlikely to have the ability or time to adjust their point of contact, and therefore require a uniform value for CoR independent of the position of impact to avoid inconsistent performance. The study measures ball impacts at a number of different positions to allow the effect of various features such as the seams, valve and laces to be analysed.

Table 3.1 Ovoid ball details

Ball No	Sport	Type	No of Panels
1	Rugby Union	International Match Ball	4
2	Rugby Union	International Match Ball	4
3	Rugby Union	International Match Ball	4
4	Rugby League	Match Ball	8
5	American Football	Professional Game Ball	4
6	American Football	College Game Ball	4
7	American Football	High School Game Ball	5
8	Australian Rules	Match Ball	4

The inflation pressure of the balls was standardised for the different ball types, rugby – 9psi, American football – 13psi and Australian Rules – 11psi (as recommended by manufacturers). For each ball type, three balls were evaluated, allowing manufacturing variability to be accounted for. The rugby balls and Australian Rules football were impacted in four locations, end, seam, centre of panel and valve (Figure 3.2). The American footballs were impacted at an extra fifth location, the lace (N.B. Japanese rugby balls may also have a lace, but this is unusual and so this ball was not evaluated). Each test position was impacted five times to allow a mean value to be established.

A Photron Fastcam APX high speed video camera (HSV) was used to capture the movement of the ball before and after impact. The HSV was positioned perpendicular to the travel of the ball at a distance 2m from the camera, and operated at a frame rate of 2000Hz (Figure 3.3).

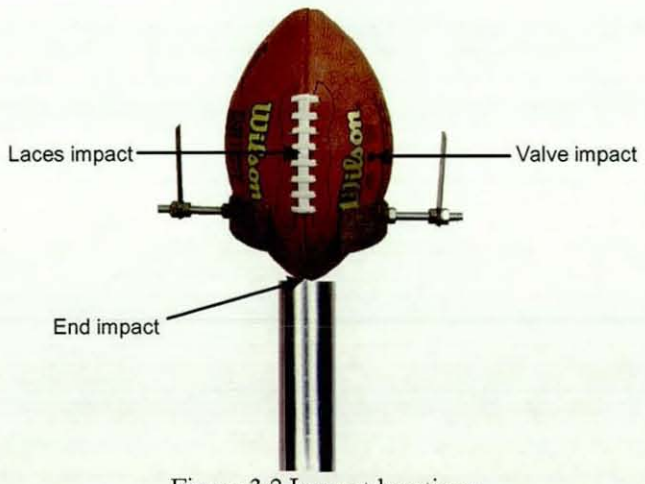

Figure 3.2 Impact locations

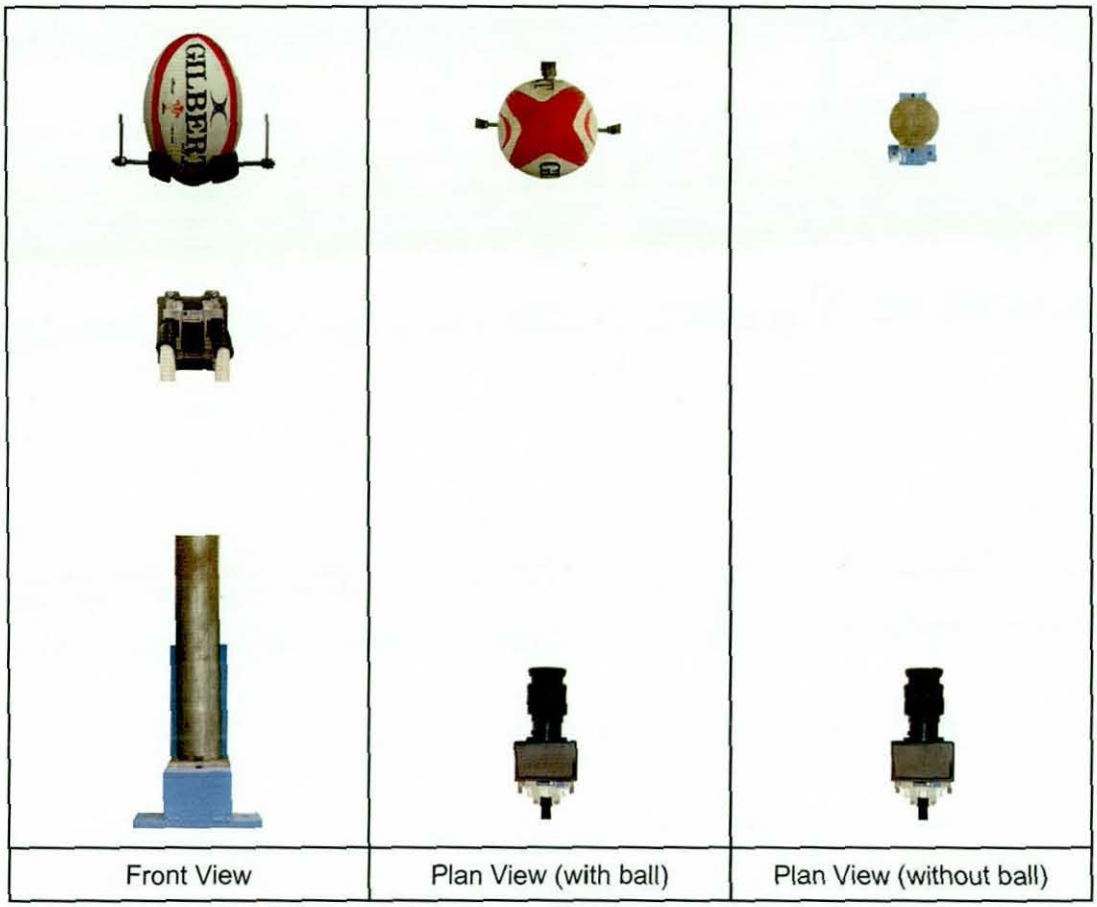

Figure 3.3 Rebound test setup

3.4 Analysis

The high-speed camera recording was digitised using Image Pro Plus software, and the ball velocity and contact time calculated (Figure 3.4). The software allows the displacement of the centre of the ball to be calculated over a given time interval and the position of the centre of the ball was measured at 120 and 20 frames before contact, and then at 20 and 120 frames after the final moment of contact. This allows the inbound and outbound velocities to be calculated. The contact time was measured as the length of time that the ball is in contact with the rigid surface, (by scrutinising the recorded frames).

Figure 3.4 CoR measurement procedure

In order to minimise measurement error attributed to the ball movement not being perpendicular to the camera's field of view, the position of the camera was carefully aligned using a digital inclinometer. The repeatability of the analysis was determined by analysing the same impact a number of times. The uncertainty of the CoR analysis was calculated to be ±0.008 (95% confidence) and of the contact time to be ±0.52ms (95% confidence).

3.5 Results

The mean (+1SD) CoR and contact time results are shown in graphical form in Figures 3.5 and 3.6. Lace impact results are only shown for the American footballs (AF 1, AF 2 and AF 3).

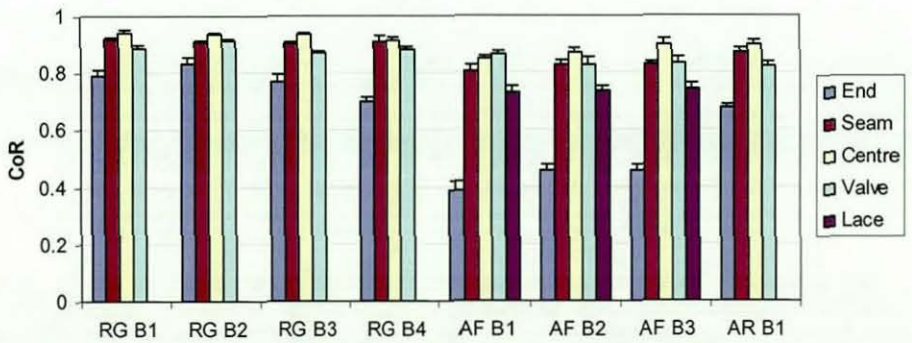

Figure 3.5 CoR measured during rebound test

It can be seen that ovoid balls produce a similar trend irrespective of brand or type with impacts on the end of the ball resulting in a significant drop in CoR. This reduction was greatest for the American footballs and is exemplified for impacts involving AF 1, resulting in a maximum CoR drop of 42% in comparison to a centre panel impact. The rugby balls produced higher CoR values across all impact positions in comparison to the American footballs and the highest CoR was measured during a centre of panel impact, and ranged from 0.91 to 0.96. Seam, valve and lace impacts result in a reduction in CoR, in comparison to a centre impact.

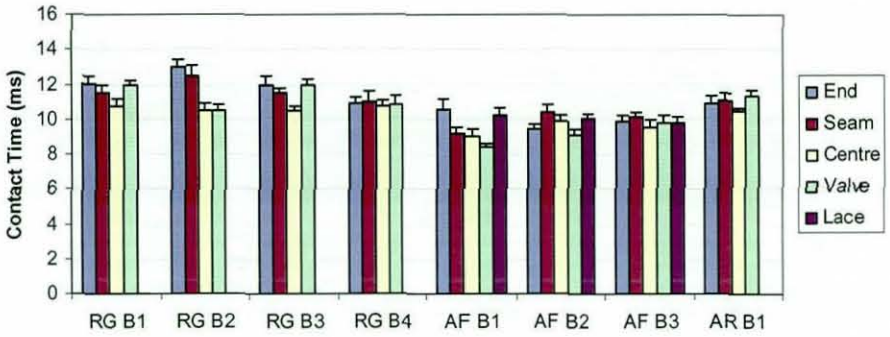

Figure 3.6 Contact time measured during rebound test

Unlike the measurements of CoR, ovoid balls produced different trends for contact time irrespective of brand or type. The three four-panel rugby balls, RGB 1, RGB 2 and RGB 3, have the highest contact time during an end impact and the lowest contact time during a centre panel impact. These results relate to the lowest and highest CoR respectively. Seam and valve impacts also produce an increase in contact time for this type of ovoid ball. The RGB 4 rugby ball produces a consistent value for contact time across all impact positions. This trend is also seen for impacts involving the American football, AF 3 with the fifth panel.

3.6 Discussions

A reduction in CoR was demonstrated during an end impact for all ovoid balls, irrespective of ball type. The maximum CoR was measured during a centre of the panel impact, whilst a reduction was also noted during valve, seam and laces impacts. Price (2005) stated that the seam region in a soccer ball has a significantly higher stiffness in comparison to the centre of the panel. The variation in material properties and construction may explain the differences between the CoR values measured at the different impact regions.

It is apparent from the test that the CoR of the ball was highest during centre of the panel impacts. However it is interesting to note that the current trend in rugby open play kicking is to impact towards the rear of the ball which should result in a reduction in distance. This may be because of players' comfort or control. However American football punting tends to impact on the side of the panels as impact with the end causes significant pain.

The contact time varied greatly from ball to ball, but the general trend showed the lowest contact time occurred from a centre of the panel impact, directly relating to the highest measured value of CoR. Impacts involving stiffer regions of the ball resulted in an increased contact time. RGB 4, with eight panels, exhibited an increased uniformity when comparing contact time across all impact positions. A reduction in the distance between the centre of the panel and the nearest seam resulted in an increased level of stiffness at the centre of the panel. The reduction in the width of the panels, due to the increased number, may result in contact between the rigid surface and the seams during a centre of the panel impact. The summation of these two factors resulted in a reduction in difference between seam and centre of the panel impact, with respect to contact time. This effect can also be seen during impacts involving the American Football, AF 3 ball, with the fifth panel.

3.7 Determination of Stiffness

In order to allow the comparison between the stiffness of an ovoid and spherical ball, a uniaxial material test machine was used to compress the balls between two rigid plates under quasi-static loading conditions. The balls were compressed by 30mm with a strain rate of 500mm/min, with the ovoid ball being compressed both at the end and centre of the panel in order to account for the non spherical shape (Figure 3.7).

Figure 3.7 Quasi-static compression

The balls were each inflated to the recommended match pressure of 9psi and 14.5psi (1bar) for rugby and soccer balls respectively, allowing the effect of pressure to also be examined. Figure 3.8 depicts the force compression curves of a rugby and soccer ball when compressed by 30mm.

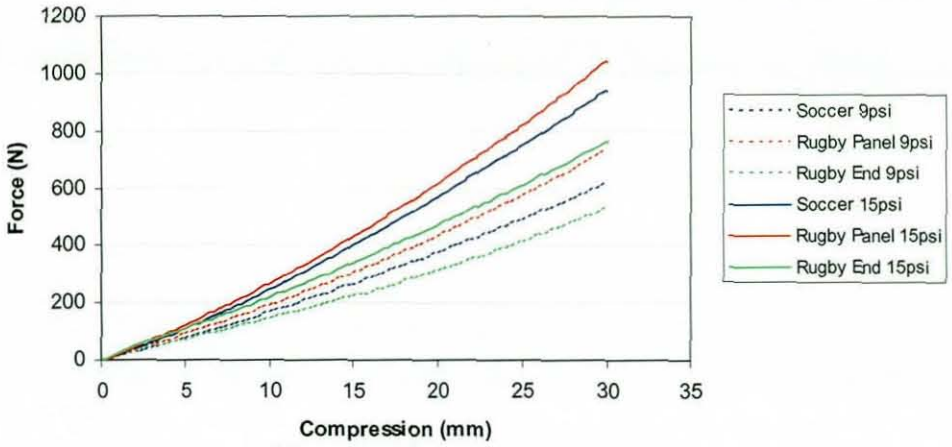

Figure 3.8 Force compression curve

Results show that the balls produced stiffer responses when inflated to a higher pressure, which was expected, with the force taken to compress the rugby ball at the centre of the panel increasing by 313N to 1046N. The results indicated that the end of the rugby ball required the minimum force to compress the ball 30mm, however contact time results from the rebound test suggested the end was a stiffer part of the ball. During compression it was noted that both areas of the ball, in contact with the rigid plates, would compress a similar amount. The amount of volumetric compression was dependent upon the ball type and compression location, and would affect the amount of force required to produce the deformation. CAD models of the rugby and soccer ball were used to calculate the surface area of the plate in contact with each of the balls during compression (Figure 3.9). The surface areas were 0.021, 0.026 and 0.17m^2 for the soccer ball, centre of the panel and end of the rugby ball respectively.

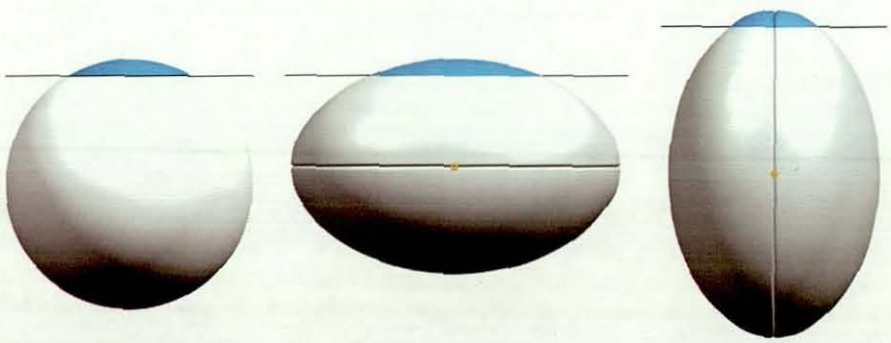
Figure 3.9 Calculated surface area during maximum compression

The non-spherical shape of a rugby ball may also affect the comparison of different compression sites, which is an effect shown during the compression of incompressible materials such as rubber. The uniaxial compression of incompressible rubber blocks bonded to rigid end plates, has shown that the relationship between stress and strain in the test piece is dependent upon the so called 'shape factor' (Horton et al 2002). The 'shape factor' defines the ratio of the loaded cross-sectional area to the total force-free area (Figure 3.10), and is exploited during the design of rubber springs and mountings.

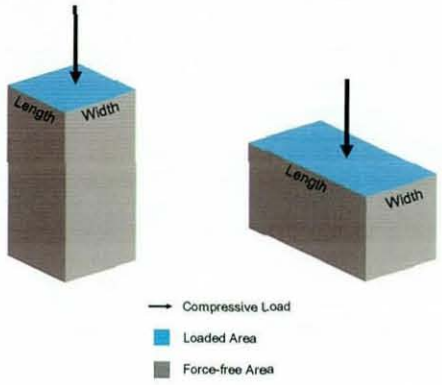

Figure 3.10 Shape factor

A rugby ball represents a shape similar to that of a rectangular block, which has a shape factor (S) defined in Equation 3.2 (Gent 2001).

$$S = \frac{lw}{2h(l+w)}$$

l – length
w – width
h – height

Equation 3.2. Shape factor for a rectangular prism

A rectangular rubber block will be stiffer when positioned with a larger loaded area due to the lower 'shape factor' value. This effect should be considered when comparing results from compression testing of non symmetrical shapes such as a rugby ball. Although a rugby ball is not an incompressible material, the increase in stiffness during a centre panel compression may not be due to stiffer nature of the material, but the effect of the shape being compressed.

3.8 Conclusions

This study provides the first comprehensive means of assessing the coefficient of restitution and contact time of an ovoid ball during a normal impact. The dynamic properties of eight different balls, representing all ovoid ball types (rugby union, rugby league American football and Australian rules) were evaluated using the developed rebound test. It was shown that when examining the CoR of ovoid balls that they produce a similar trend irrespective of brand or type, with end impacts resulting in a significant drop in CoR in comparison to centre of the panel impacts. The highest CoR was measured during a centre of the panel impact, and ranged from 0.85 to 0.96. Seam, valve and lace impacts result in a reduction in CoR, in comparison to a centre panel impact and can be attributed to the variation in material properties and construction between the end, seam, valve and laces in comparison to the centre of the panel.

Unlike the CoR results, ovoid balls produced very different contact time trends. The measured value of contact time was directly related to the stiffness of the impact region. Seam, valve and lace impacts resulted in an increase in contact time in comparison with the centre of the panel impact. Increasing the number of panels used to manufacture an ovoid ball caused a decrease in stiffness variation between the centre of the panel and the seam, due to the reduction in seam width. The reduction in stiffness variation directly results to an increased level of consistency for contact time between impact positions.

Material testing results by Price (2005) showed that the stitching region within a soccer ball has a significantly higher stiffness in comparison to the centre of the panel. The end of the rugby ball consists of four panels converging to a single point, increasing the stiffness in this area. During the quasi-static compression of a rugby and soccer ball it was found that the force taken to compress 30mm was greatest at the centre of the panel and lowest during an end compression. The discrepancy between this result and the material testing values could be due to non-uniform volumes being compressed at the different positions, and also the effect of the 'shape factor'.

Chapter 4

Ovoid Ball Bounce Characterisation

4 Introduction

The ovoid shape of a rugby ball means that when it interacts with the pitch there is considerable uncertainty with the direction of bounce. Factors which affect the 'bounce' are the balls' shape, orientation of the ball at impact, out of balance, ball velocity, coefficient of restitution and interface friction. The uncertainty surrounding the bounce of a rugby ball is accepted by players and plays a significant part in the ethos of the game. However elite players have a perception of whether bounce variation is acceptable or unacceptable. The following chapter details the design of a measurement system which allows the bounce of an ovoid ball to be accurately measured under controlled conditions. Results are presented for impacts involving two different rugby ball types with varying valve mass, and the effect of the impact location, original ball angle and out-of-balance were examined. The effect of uneven mass distribution, resulting in out-of-balance forces, was measured and its effect on the bounce characteristics investigated.

4.1 Ovoid Ball Bounce

The bounce of an ovoid ball is not as predictable as that of a spherical ball and therefore its characteristics post impact are difficult to measure. A survey of relevant literature has not revealed any analysis of the bounce of ovoid balls. Testing procedures have been developed to allow the effect of the surface friction of spherical balls to be analysed. Cotton (2008) developed an oblique impact procedure in which a soccer ball was fired using a ball launcher at a velocity of 25m/s onto a steel plate. The angle of the impact plate and the effect of wet and dry conditions were examined. Results showed that at 25m/s an increase in impact plate angle resulted in an increase in rebound angle (90° rebound angle during normal impact). The effect of the ball's spin rate was also examined and as might be expected it was found that the highest spin rate was recorded during impacts with the lowest rebound angle. Daish (1972) conducted an overview of the impact mechanics involved during oblique impacts, and observed a reduction in outbound angle due to the loss of energy during the collision and the relationship between spin pre and post impact. Daish stated that during a simple oblique impact

without spin, a spherical ball will rebound with an outbound angle identical to the inbound angle.

An ovoid ball will make contact with the ground during a number of different game related situations. The bounce characteristics of the ball after the impact have different levels of importance depending upon the ovoid ball game being played. During a game of American football there are few situations in which the ball will purposely make contact with the ground as the ball will become 'unplayable', by either team, if a player drops a pass before they have control of the ball. One instance in which the ball bounce is favourable is the drop kick, where the ball makes contact with the ground before being struck, which can be used in a game of American football to score an extra point after a touchdown. This practice is rarely attempted due to the difficult nature of the skill, in comparison to the safer option of the field goal. In January 2006 New England Patriots quarterback Doug Flutie kicked a drop kick in a game against the Miami Dolphins, 65 years since the last successful attempt. During a game of rugby union, the bounce of the ball is very important, as it is often used to the advantage of the team during various kick types, i.e. grubber kick (ball bounces a number of times along the ground), drop goal/restart (ball makes contact with the ground before kicked) and chip (ball is kicked over the defensive line and generally allowed to bounce before being collected by the attacking team). It is for this reason that the bounce characteristics of two rugby balls have been assessed using a new test procedure.

4.2 Testing Procedure

Due to the non spherical nature of the ovoid ball, the impact position of the ball cannot be controlled if the ball is allowed to fall freely under gravity. In order to assess ovoid ball bounce the rebound test procedure developed in Chapter 3, has been used to characterise the bounce of an ovoid ball. The supporting ring has been designed to allow the ball to impact the rigid steel cylinder anvil at a known angle, after being dropped from a height of 2m. The position of the rigid impact cylinder was adjusted to allow contact with the bottom of the rugby ball irrespective of initial ball angle. Each ball was impacted 5 times, with the valve facing upwards, downwards, right and an impact in the centre of the panel (valve right and upwards), depicted in Figure 4.1. The variation in impact position allowed the effect of the mass and placement of the valve on the bounce characteristics to be determined. Two rugby ball types were analysed with varying valve

mass, and three balls per type were impacted with an initial ball angle of 15, 30, 45, 60 and 75°. Laser levels were used to aid the placement of the ball so that the angle of the ball could remain constant throughout the testing, irrespective of impact position. The impact velocity of the ball varied depending upon the balls position, and ranged from 5.3 to 5.5m/s. The accuracy of the ball placement was measured by analysing a series of still images, and was calculated to ± 1.79°.

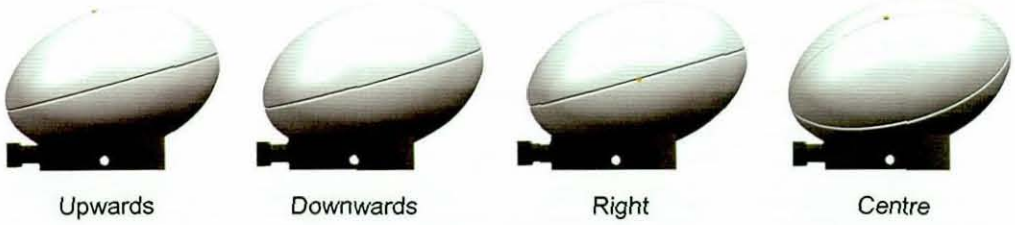

Figure 4.1 Ball valve position during a 15° impact orientation

Two Photron APX HSV cameras operating at 2000 frames per second, with a shutter speed of 1/4000s, operating at a maximum resolution of 1024 x 1024 pixels, were used to capture the motion of the ball before and after impact with the rigid cylinder. The capture sequence of both cameras was started using a single manual trigger to allow synchronisation of the captured images. Figure 4.2 shows a simplified diagram of the testing setup.

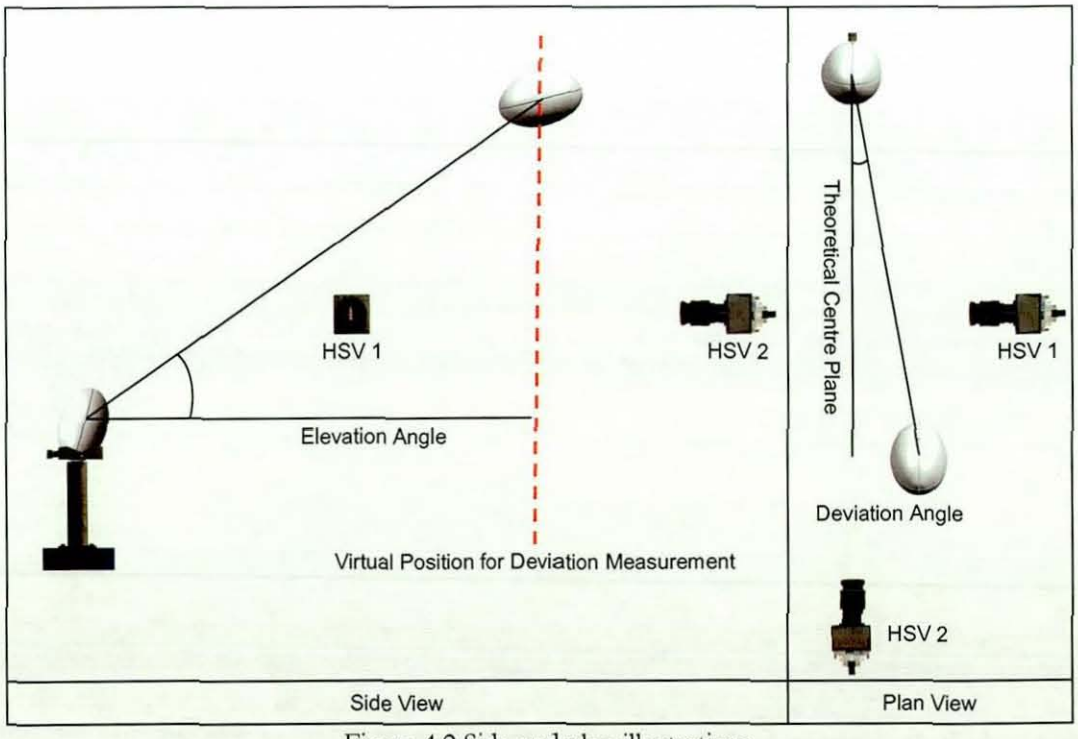

Figure 4.2 Side and plan illustrations

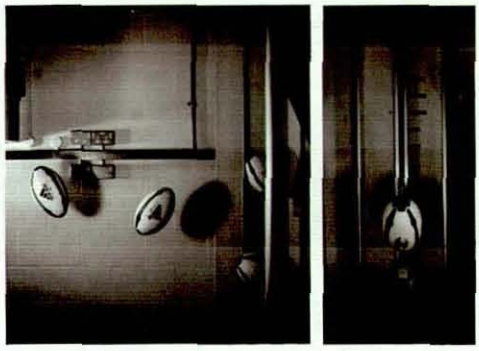

Figure 4.3 Composite image depicting ball flight from HSV 1 and HSV 2 respectively

4.3 Analysis

Images captured using HSV 1 were digitised using Image Pro Plus allowing the x and y pixel co-ordinate position to be obtained at two positions, a known time interval apart. The co-ordinate values were then used to calculate the 2D ball velocity and elevation angle in the plane perpendicular to the camera. The angle of the ball at the two positions was measured and used to calculate the change in angle during a known time interval, allowing the spin rate to be determined. HSV 2 was accurately positioned using laser levels to ensure that the centre x pixel aligned with the centre of the rigid cylinder and the line of motion of the falling supporting ring. The digitisation of the images captured using HSV 2 allowed the lateral deviation of the ball to be determined at the point of contact with the rigid cylinder, and at a known time interval after impact. The synchronisation of the two HSV cameras, allowed the rugby ball's 3D position in space to be calculated, which in turn allowed the deviation angle of the ball to be determined (Figure 4.4).

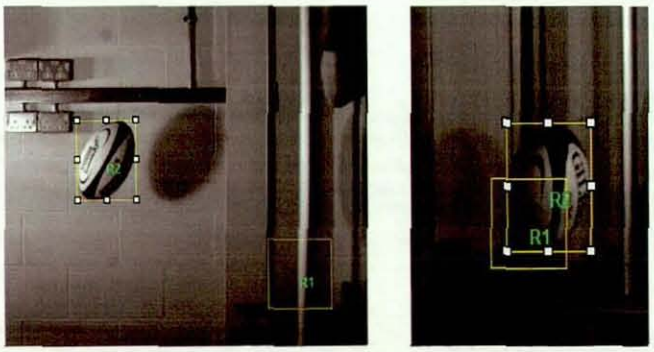

Figure 4.4 Determination of rugby balls 3D position

The repeatability of the analysis was determined by analysing the same impact a number of times. The uncertainty of CoR was calculated to be ±0.02, the elevation angle ±0.13° the deviation angle ±0.17°and the spin rate ±2.7rpm all measured to levels of 95% confidence.

4.4 Results

4.4.1 Ball Launch Characteristics

Figures 4.5 – 4.7 depict the ratio of inbound to outbound ball velocity (CoR), elevation angle and spin rate for the rugby balls set at 45°, illustrating the effect of valve placement during the impact. Similar trends are exhibited in the results for all ball orientation angles measured.

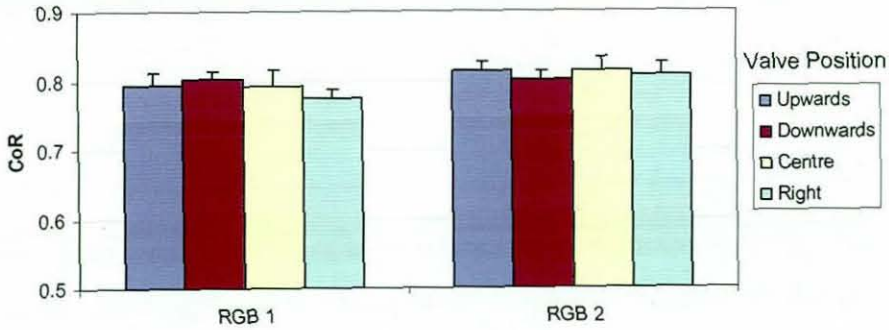

Figure 4.5 CoR: 45° ball angle

The CoR remained fairly consistent apart from a reduction measured for the RGB 1 ball during the valve right impact. The ball velocity was measured in a plane normal to the HSV camera and a reduction in ball velocity could be due to an increase in the ball velocity out of the plane of the camera, which was not measured.

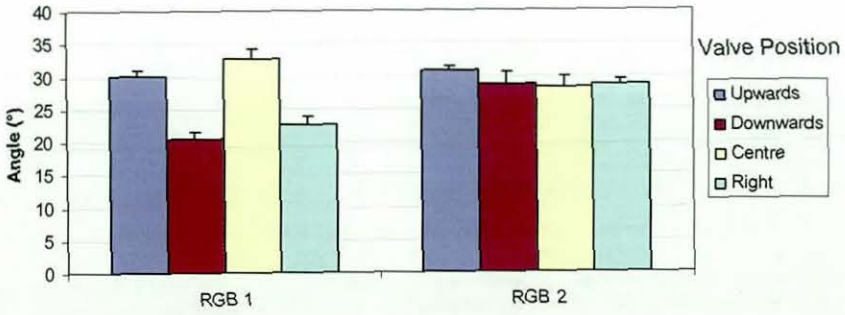

Figure 4.6 Elevation angle: 45° ball angle

It was noted that the elevation angle remained reasonably consistent during all impact orientations for the RGB 2 ball, with the maximum variation of 2.6° between mean values, however the position of the valve during the impact caused a variation in the elevation angle for the RGB 1 ball. The minimum elevation angle was measured when the valve was facing downwards, whilst the maximum was measured during a centre of the panel impact, an increase of 59.2%, (12.1°).

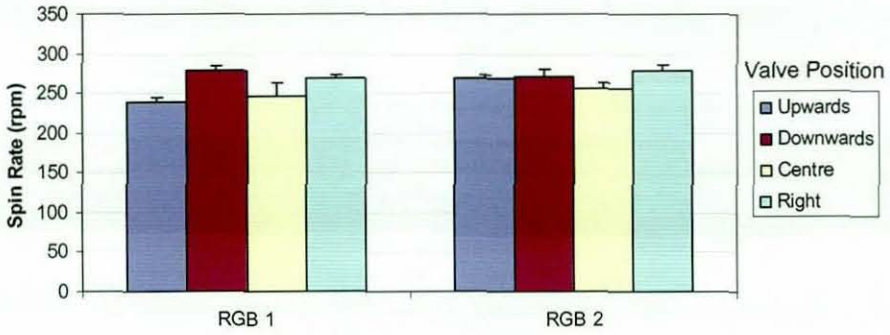

Figure 4.7 Spin rate: 45° ball angle

The position of the valve during impact affected the measured spin rate of the RGB 1 and RGB 2, with an increase in spin rate during a valve down impact. Higher spin rate values correspond to the impact locations with a lower measured elevation angle.

Figures 4.8 – 4.10 depict the mean value for CoR, elevation angle and spin rate calculated using the data from all ball orientation angles. 0 and 90° values are taken from the *rebound test, Chapter 3.*

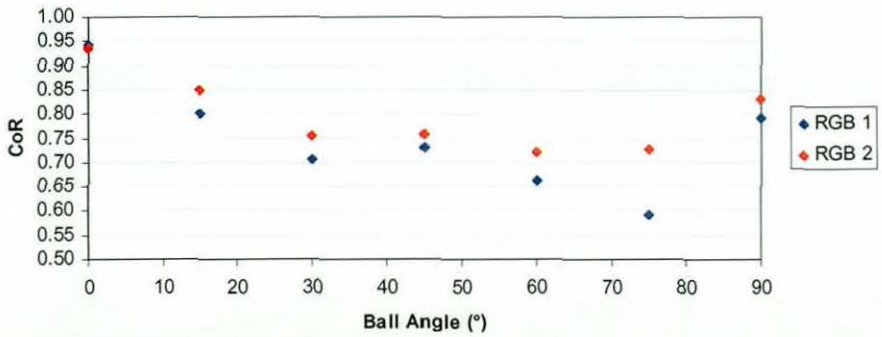

Figure 4.8 CoR

The ratio between inbound and outbound ball velocity for the RGB 2 ball was consistently higher across all ball orientation angles. This result corresponds to the CoR values measured during the rebound test in Chapter 3. Both rugby balls exhibit a similar trend with the ratio decreasing as the angle of orientation increases. This was expected as the impact location moves from the centre of the panel, 0°, towards the end of the rugby ball. The CoR was lower from 15 to 75° than the measured value of CoR at 90° (end impact) for both balls. The pre impact energy will be converted into ball velocity and spin post impact during impacts and the reduction in ball velocity could be due to the energy used to create the spin which can be neglected for a 90° impact.

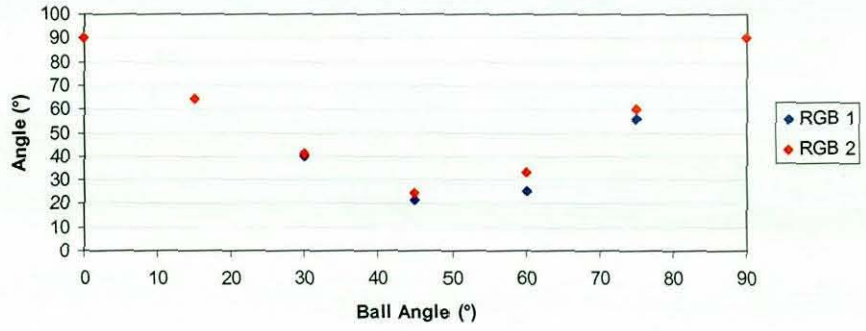

Figure 4.9 Elevation angle

The elevation angle for both balls shows a similar U shaped trend. The maximum elevation angle is measured at both 0 and 90° ball orientation angles, whilst the minimum recorded value is measured at 45° (21.3°).

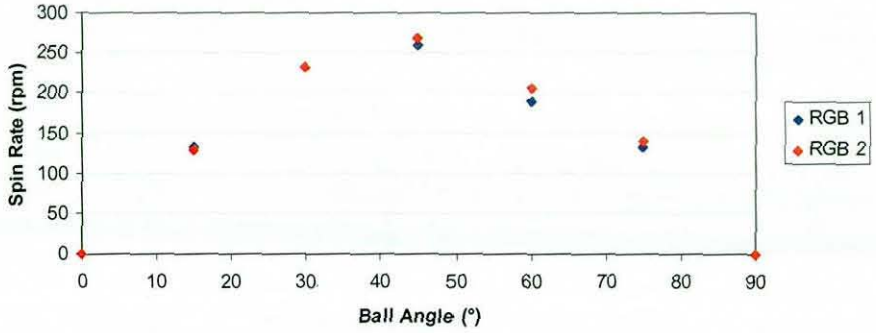

Figure 4.10 Spin rate

The results for spin rate show an inverted U trend for both rugby balls. The minimum spin rate was recorded at both 0 and 90° (rebound test), whilst the maximum value of 268rpm was measured for the RGB 2 ball during a 45° ball orientation impact. Results show that a low elevation angle corresponds with a high spin rate (45°), whilst a high elevation angle corresponds to a low spin rate as demonstrated during a normal impact.

4.4.2 Deviation Angle

Figure 4.11 depicts the x and y co-ordinates measured using HSV2 at a known distance 1m from the impact position. The figure details the results for impacts with a 45° ball orientation, although similar trends were demonstrated across all angles. The theoretical centre plane of the ball's flight (Figure 4.2), after impact was determined and the rugby ball's deviation from this line in pixels was calculated. A calibration image allowed each

of the x and y pixel co-ordinates measured to be converted into a vertical position, relative to the camera image, and the distance away from the theoretical centre line of the ball's flight to be measured.

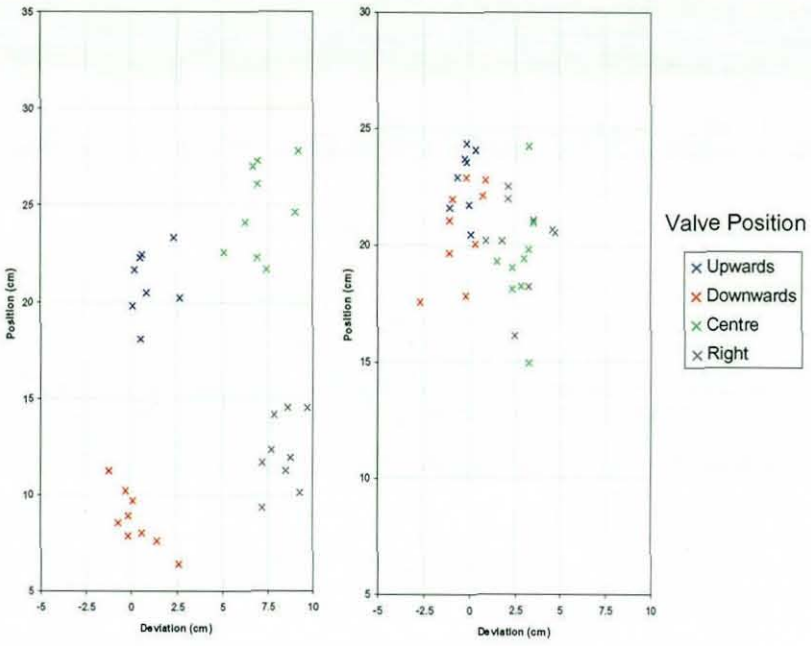

Figure 4.11 a) Deviation (RGB 1) b) Deviation (RGB 2)

The impacts with RGB 1 rugby ball showed an increase in the spread of the ball position data, at the known distance, both horizontally and vertically, in comparison to the RGB 2 ball. Figure 4.11 a) demonstrates the effect of impacting a rugby ball with a greater valve mass, with each valve position forming a cluster of points. Impacts with the valve upwards and downwards produced little lateral deviation for both rugby balls, although the ball with the larger valve mass demonstrated a variation in vertical position between the clusters of points. This was validated by the reduction in elevation angle recorded by the HSV 1 camera. Impacting the ball in the centre of the panel resulted in lateral deviation towards the right, whilst its vertical position was located in between the upwards and downwards positions, as the valve was centrally positioned. Impacts with the RGB 2 ball resulted in a reduction in the spread of ball positions, and although each valve position produced a cluster of data points, the difference between each cluster was less than that of RGB 1. Impacts with an off-centre valve position resulted in an increase in deviation from the theoretical centre plane, although this value was greatly reduced in comparison to RGB 1 ball.

Figures 4.12 - 4.16 depict the deviation angle calculated using the synchronisation of the two HSV cameras.

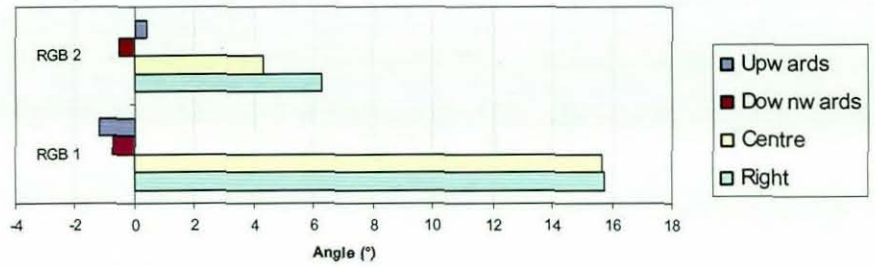

Figure 4.12 Deviation angle: 15° ball orientation

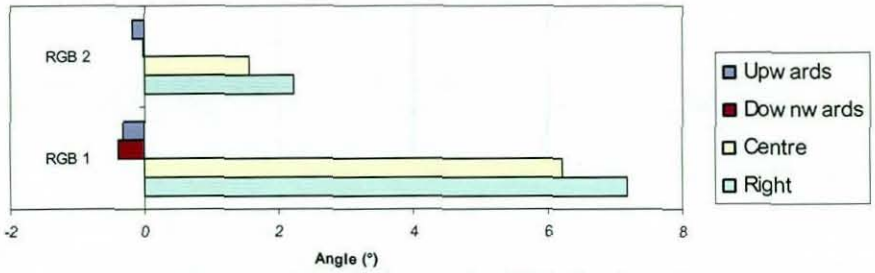

Figure 4.13 Deviation angle: 30° ball orientation

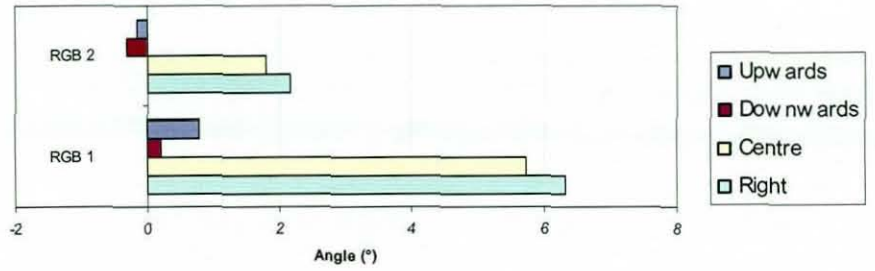

Figure 4.14 Deviation angle: 45° ball orientation

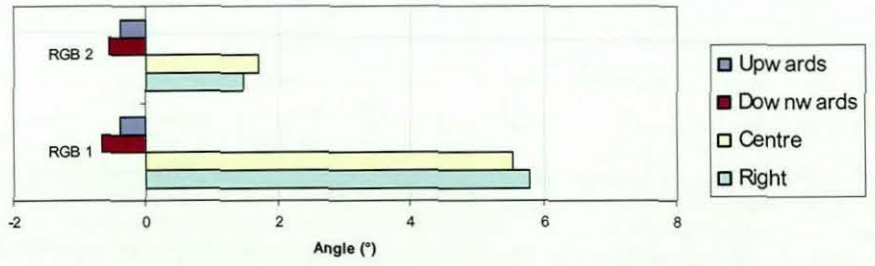

Figure 4.15 Deviation angle: 60° ball orientation

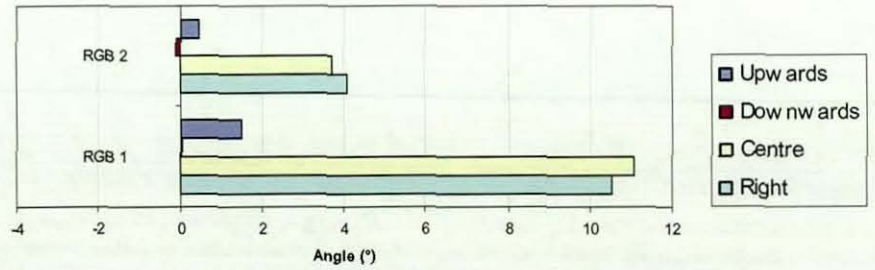

Figure 4.16 Deviation angle: 75° ball orientation

All rugby balls show the same trend in results, irrespective of initial ball orientation angle, with the maximum deviation angle recorded at 15 and 75° ball orientation. The minimum deviation angle was measured during impacts with the valve in the upwards or downwards position, whilst the maximum deviation angle was measured when the valve was placed off centre.

4.5 Trajectory Simulation

During the bounce characterisation procedure, restriction of space within the laboratory environment did not allow the ball's position to be recorded at the point of impact with the second bounce. The trajectory of a particle in motion whilst under the influence of a uniform gravitational field is assumed to follow a parabolic path, neglecting air resistance and forces due to spin. The parabolic trajectories of projectiles were first discovered by Galileo and later proven by Sir Isaac Newton. Equations of motion can be used to determine the x and y position of a particle at incremental stages throughout the trajectory. The trajectory of the projectile can be broken down into a series of smaller arcs over which the velocity can be treated as constant. Daish (1972), states that the assumption of constant velocity during parabolic flight will not introduce any great measurement error. The number of divisions of the trajectory will not only affect the accuracy of the resultant parabola but the number of calculations needed.

Matrix Laboratory (MATLAB) software was created by the chairman of the computer science department, Cleve Moler, at the University of New Mexico. In 1984 Cleve Moler and Jack Little founded the company MathWorks to allow the commercialisation of the MATLAB product. MATLAB allows numerical calculation to be carried out in an efficient manner using matrix manipulation, and a code was constructed to allow the calculation of the trajectory of the ball using the experimental data from the ovoid ball bounce test. The x and y components of the ball velocity were derived from the mean values for the elevation angle and ball velocity. The position of the projectile was calculated at known time intervals (1ms), whilst a gravitational acceleration of -9.81m/s was applied vertically. The results assume that the object was travelling within a vacuum, therefore air resistance and the effect of the ball's spin were not taken into account. The simulation was allowed to calculate the trajectory of the ball until a negative horizontal position was reached, hence contact with ground level. The movement in the z direction was simulated by applying the deviation angle, measured experimentally, to the calculated

horizontal and vertical trajectory. Figures 4.17 and 4.18 depict the trajectory of balls RGB 1 and RGB 2

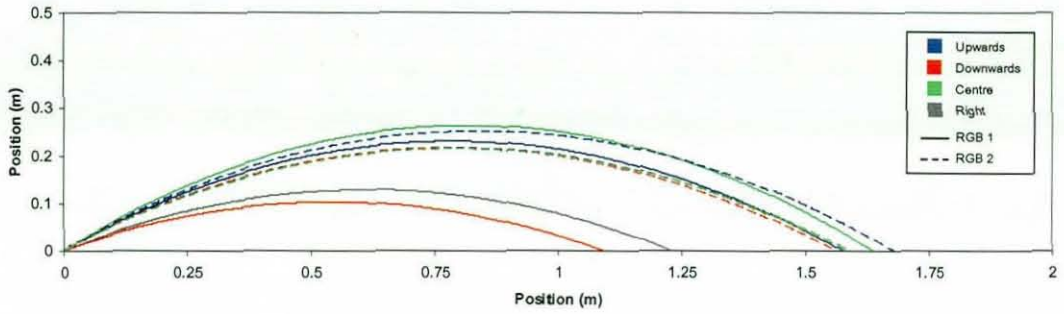

Figure 4.17 Ball Trajectory at 45° ball orientation (side view)

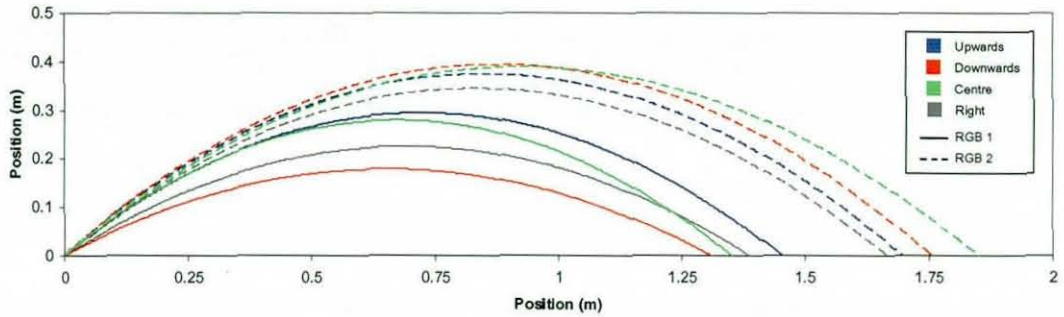

Figure 4.18 Ball Trajectory at 60° ball orientation (side view)

Results from the trajectory simulations demonstrate that the RGB 2 ball produced more consistent trajectories irrespective of valve position on impact. The difference in elevation angle caused by rotating the valve position during impacts with the RGB 1 ball, results in variation between trajectories, and this effect is exemplified at a 45° ball orientation angle. The increase in elevation angle at 60° results in a steeper trajectory for all of the impact positions and ball types, causing an increase in the horizontal and vertical distance travelled. During experimental testing the RGB 2 ball demonstrated a greater elevation angle and ball velocity and this resulted in a greater vertical and horizontal distance travelled throughout the trajectory. During impacts with a 60° ball orientation angle, a maximum hang time of 0.568s was calculated during a centre of the panel impact with the RGB 2 ball, whilst the minimum hang time was 0.384s for the RGB 1 ball during a valve down impact.

The experimental values of standard deviation for the elevation angle, ball velocity and deviation angle were used to determine the range of impact positions expected whilst impacting the ball in the different valve positions. Figures 4.19 and 4.20 depict the mean impact position and 1SD for ball orientation angles of 45 and 60° respectively, which were deemed to be representative of the balls' bounce characteristics.

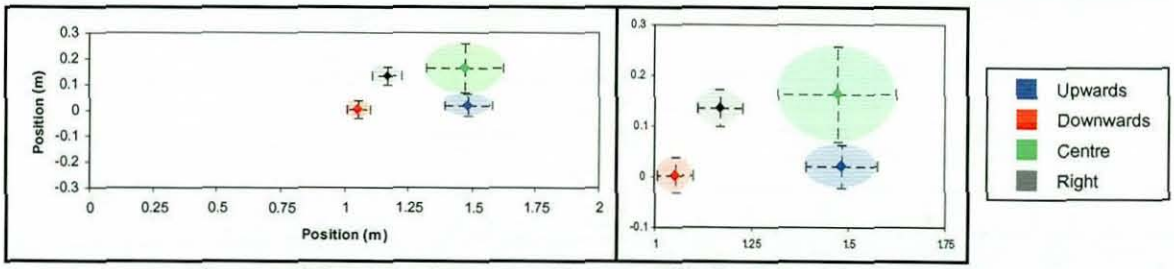

Figure 4.19a) RGB 1 impact position at 45° ball orientation (plan view)

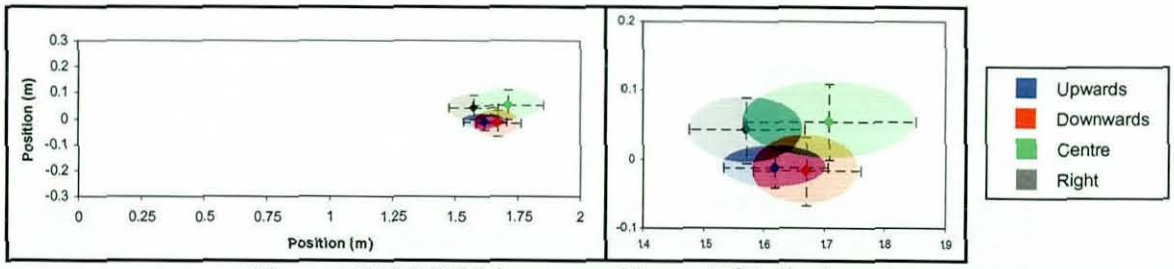

Figure 4.19b) RGB 2 impact position at 45° ball orientation

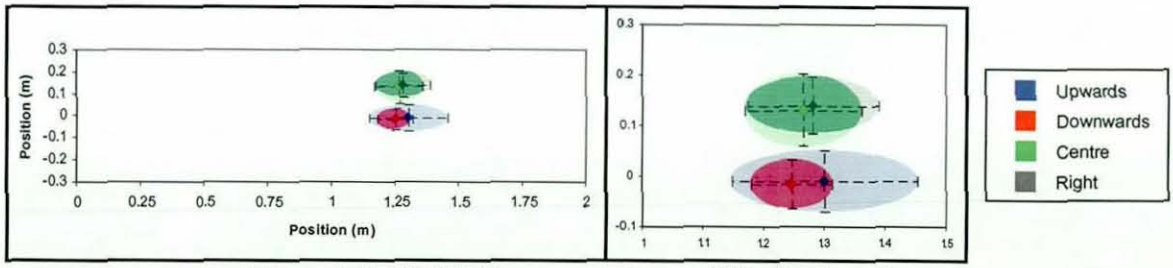

Figure 4.20a) RGB 1 impact position at 60° ball orientation

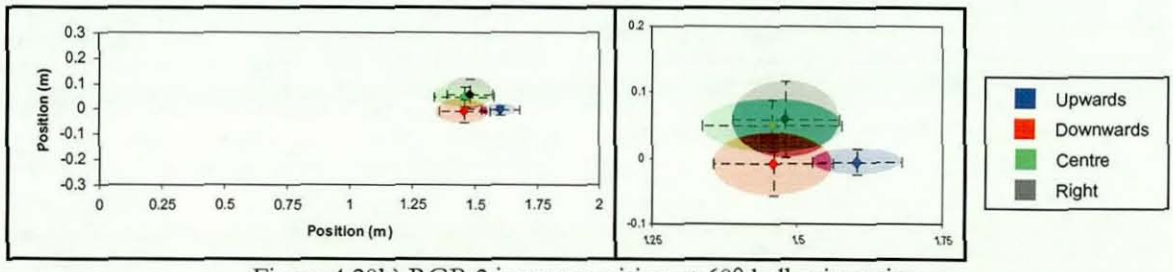

Figure 4.20b) RGB 2 impact position at 60° ball orientation

Impacting the RGB 1 ball in different valve positions caused an increased variation in the horizontal and lateral position of the second bounce. This effect was visible at all ball orientation angles. Impacting the RGB 1 ball with the valve to the right caused a maximum lateral deviation of 0.14m in comparison to the valve upwards or downwards. This value was a 94% (0.07m) increase compared with the RGB 2 ball for the 45° ball orientation angle and impact position. Impacting the RGB 1 ball in the valve upwards position resulted in an increase in horizontal distance of 43% (0.43m), in comparison to a valve downwards position for the same type of ball. A similar comparison for the RGB 2 ball only showed a 10% (0.14m) increase.

4.6 Out-of-Balance Forces

4.6.1 Introduction

The development of the bounce characterisation test has shown the effect of the mass distribution within an ovoid ball, and how it influences game related impacts. The inclusion of the valve within the bladder, and also the laces for an American football and Australian rules ball, affects the mass distribution, causing an unbalance. The mass of the valve can range from 10-25g, whilst the laces weigh around 7g. Top quality ovoid balls are hand stitched and manufacturing variability will result in an inconsistent ball shape, resulting in additional mass variability. Out-of-balance forces may also have a significant effect on ball flight dynamics, e.g. wobble and precession. A method has been developed to assess the out-of-balance forces of an ovoid ball whilst the ball is rotated about both the polar and equilateral axes. The two rugby balls examined during the bounce characterisation and two American footballs were measured in order to assess typical values for both ovoid ball types.

4.6.2 Theory of Unbalance

The rotation of engineering components about a fixed axis in order to assess undesirable unbalance is common practice. This practice is used to determine the unbalance caused due to the tangential displacement of the centre of mass from the centroid of the object. The displacement of the centre of mass from the centroid causes a centripetal force during rotation, which can generally be minimised by adding or subtracting mass from the perimeter of the part. Neilson (2003) described the procedure used to measure the out-of-balance of soccer balls, using a vertical balancing machine. This procedure allowed the point of unbalance to be determined. Then the spherical ball was rotated so that the

axis of ball rotation lies within a plane normal to the line passing through the centre of mass and the centroid. The inclusion of a valve within a rugby ball will cause the centre of mass to displace from the centroid (Figure 4.21), causing an unbalance. The orientation of the ball will affect the displacement of the centre of mass, causing varying levels of unbalance, dependant upon the axis of rotation.

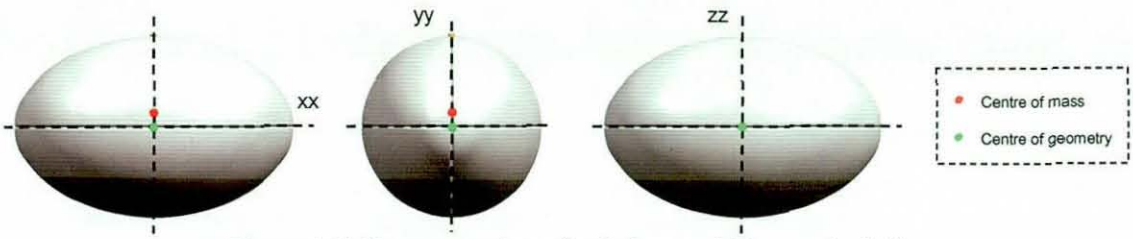

Figure 4.21 Representation of unbalance within a rugby ball

4.7 Equipment

A vertical balance machine was used to determine the out-of-balance forces that exists within a number of different ovoid balls. Two ball fixtures were created to allow the unbalance to be measured about the polar and equilateral axes.

4.7.1 Vertical Balancing Machine

Figure 4.22 depicts the vertical balancing machine manufactured by Universal Balancing Ltd for adidas. The appropriate ball fixture was mounted onto the spindle in order to prevent lateral movement. The drive unit within the machine rotates the component to the correct rotational velocity, defined by the user, and maintains this velocity throughout the test period. The vibration generated by the unbalance of the rotated component was measured around the rotating spindle, using a bi-morph element. This low power electromechanical transducer is capable of converting mechanical or acoustic energy to electrical energy, producing a voltage signal in the form of a sinusoidal wave. The peak amplitude of the sinusoidal wave is proportional to the acceleration of the vibration, which is then converted to an amplitude proportional voltage, and amplified for analysis, using an integrated circuit.

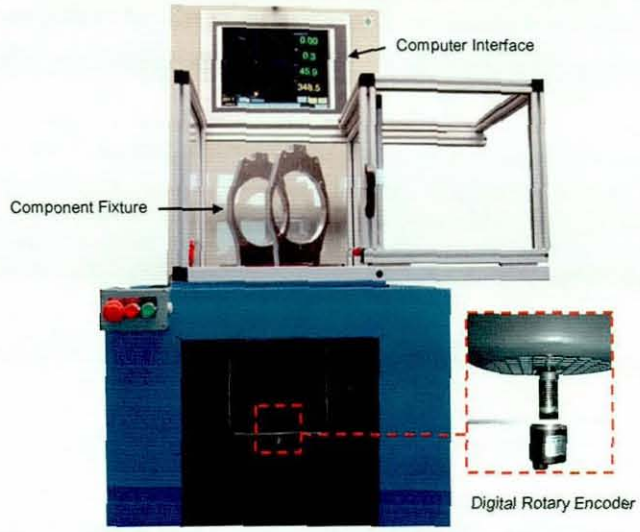

Figure 4.22 Representation of vertical balancing machine

A digital rotary optical encoder is mounted onto the machine's main spindle generating a square wave for each revolution of the mounted fixture. The analysis of the position of the peak vibrational response from the rotating spindle is compared with the data from the rotary encoder, allowing the orientation angle of the unbalance to be measured. This information is displayed to give the user to define the position of the unbalance in real time (Figure 4.23).

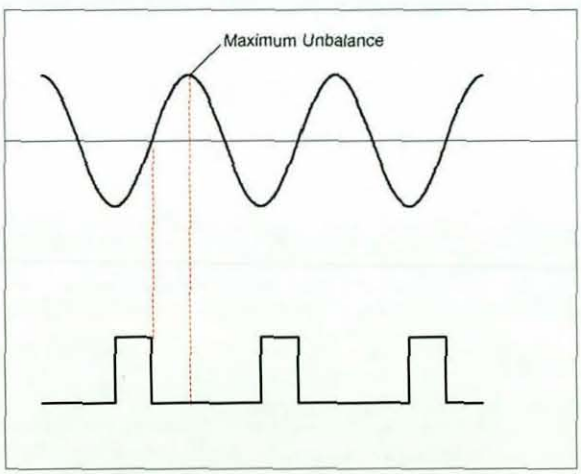

Figure 4.23a) Sinusoidal wave (vibration) and square wave (rotation)

Figure 4.23b) Computer interface

4.7.2 Fixture

Two fixtures were developed to allow the out-of-balance of ovoid balls to be measured about the main axes of spin, with a simple design allowing easy attachment to the rotating spindle. Figure 4.24 depicts the fixture used to measure the out-of-balance about the polar axis. In order to take an accurate measurement, the fixture needed to be rigid, so an appropriate size was determined to allow the measurement of a ball. Inserts were constructed to allow the measurement of smaller ovoid balls, such as American footballs and Australian Rules footballs. The fixture contained a tapered centre to allow the correct alignment of the slightly deflated ball, in order to ensure that the ball's centre of geometry was in the centre of the fixture. The ball was then inflated to within the constraints of the fixture, with the restraining ring slightly tapered to prevent movement of the ball, within the fixture, during rotation.

Figure 4.24 Fixture used to measure unbalance about the polar axis

Figure 4.25 depicts the fixture used to measure the unbalance when rotating an ovoid ball about the equilateral axes. The fixture consists of two plates with a tapered hole measuring 165mm in diameter, to restrain the ball during rotation. The base of the fixture allows easy attachment to the rotating spindle, whilst the distance between the plates can be adjusted to accommodate balls of varying sizes. The distance between the spindle centre and each plate was kept consistent in order to create a symmetrical fixture. Inserts can be placed within the plates, to allow the measurement of smaller balls such as American footballs and Australian Rules footballs. Marks were placed on the ball, the correct distance to the inside edge of the plate, to allow accurate placement of the ball within the fixture. A slightly deflated ball was placed within the fixture, and during inflation the ball naturally found its centre position, due to the symmetrical nature of the ovoid balls about the centre plane (through the valve). The marks placed on the ball can be used to ensure reasonably accurate positioning.

Figure 4.25 Fixture used to measure unbalance about the equilateral axes

4.7.3 Fixture Calibration

Prior to the start of testing a tooling compensation needs to be performed by the balancing machine. The 'tooling' refers to all of the rotating parts within the system, other than the component that was being balanced e.g. the fixture. The tooling compensation measures the unbalance within the fixture, and compensates for this unbalance during the measurement procedure. During the tooling compensation the empty fixture is rotated to a known rotational velocity, 500rpm whilst the machine registers the vibrations produced around the spindle. This procedure needs to be repeated each time the position of the plates within the fixture are adjusted, or when the whole fixture was changed. The accuracy of the calibration was determined by attaching a known mass to the jig and completing a measurement cycle, with the value return $\pm$ 0.1g.

4.8 Procedure

The unbalance of ovoid balls was measured around three axes of rotation shown in Figure 4.26. In order to calculate an accurate value of unbalance, measurements were taken around the polar axis (xx) at four positions of 90° intervals, with the ball removed and re-positioned five times. Measurements were taken around the equilateral axes at four positions, chosen to measure the maximum and minimum out-of-balance within a ball spinning with tumble axis spin. Measurements were taken with the valve up and down (yy), left and right (zz), again with five repeats. Measurements for the valve up and down can be grouped together, along with measurements for the valve left and right, as they are measuring rotation about the same planes. Three balls per type were measured to allow an average unbalance value to be determined. The vertical balancing machine converts the magnitude of the vibration to a measurement of unbalance in grams. In order for this calculation to occur, the diameter of the ovoid ball, around the relevant rotation axis was inputted into the software.

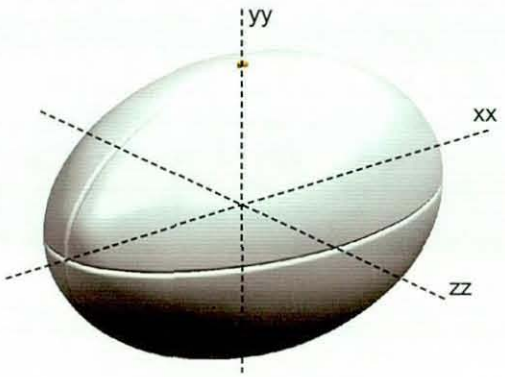

Figure 4.26 Axes of rotation

4.9 Results

Figure 4.27 depicts the unbalance measurement about the equilateral and polar axes.

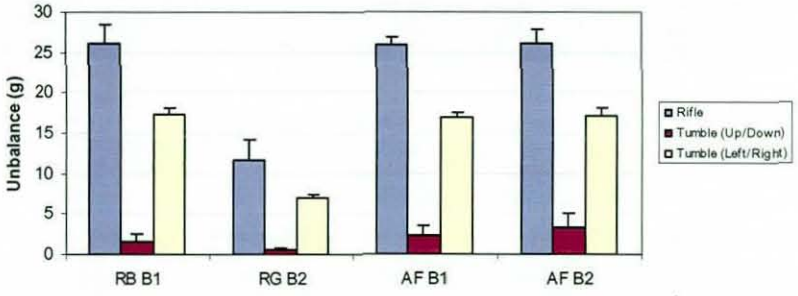

Figure 4.27 Unbalance measurements for ovoid balls.

The American Footballs tested produced similar values of unbalance for all comparative positions, unlike the rugby balls which produced lower values for the RGB 2 ball in comparison to the RGB 1 ball. All ovoid balls recorded a higher value of unbalance when the ball was rotated about the polar axis, with a maximum value of 29.1g and 28.4g for rugby and American football respectively. The unbalance was determined by converting the vibration measured into a mass value at a known distance from the centre of rotation. Due to the non spherical nature of the ovoid ball, the distance from the axis of rotation to the maximum tangential dimension of the ball, when rotating about the polar axis, was shorter than if rotated around the equilateral axes. When the ball was rotated about the equilateral axes, lower values of unbalance were recorded when the valve/laces were positioned up or down (yy). The inclusion of the valve and or laces within an ovoid ball creates a non uniform mass distribution causing an unbalance. When the ball was rotated with the valve/laces up or down, the centre of mass of the ball was likely to lie on or very close to the axis of rotation, reducing the unbalance.

4.10 Discussion

4.10.1 Ball Bounce Characterisation

The inclusion of a larger valve within the RGB 1 rugby ball has resulted in increased variability when measuring elevation angle, spin rate, and deviation angle, dependant upon the position of the valve at impact. The larger valve mass has been shown to significantly affect the mass distribution of the ball, moving the centre of mass away from the centroid. At the point of impact the gravitational force acts through the centre of mass of the ball, whilst the reaction force caused by the contact with the cylinder, acts in the opposite direction (Figure 4.28).

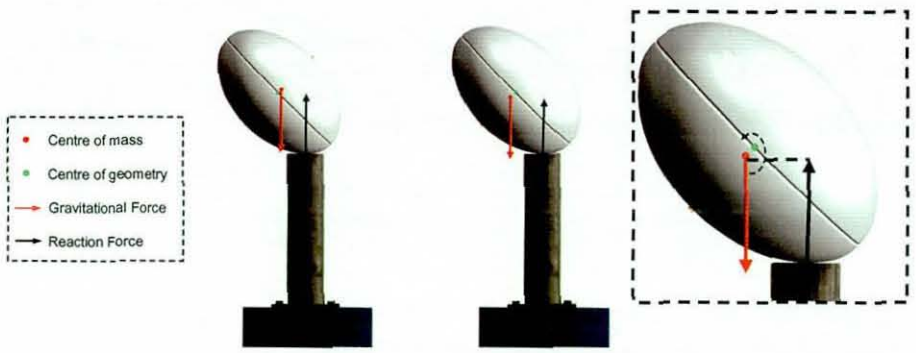

Figure 4.28 Normal and reaction force created during impact

The perpendicular distance from the centre of mass and reaction force creates a moment, calculated as a force multiplied by the acting distance between the centre of mass and reaction force. The placement of the valve at impact will affect the displacement of the centre of mass, creating a larger moment when the valve is in the downwards position. The moment's affect on the flight of the ball occurs during contact and causes a change in elevation angle and spin rate depending upon its magnitude. The moment produces rotation of the ball during contact, causing the ball's orientation angle to change, affecting the elevation angle. During an impact at a known ball orientation, the time that the ball was in contact with the plate was assumed to be constant irrespective of the valve position. The spin was created by the amount of rotation during the contact phase, hence a larger moment produces a higher magnitude of rotation during contact, resulting in a higher spin rate value.

The RGB 2 ball contained a valve with a smaller mass, which resulted in a smaller vertical displacement of the centre of mass when comparing valve upwards and downwards

impact positions. The lower level of displacement resulted in a reduced difference between the created moments, causing a reduction in the variation of elevation and spin rate, when comparing positions.

The orientation angle of the rugby ball immediately prior to impact caused the elevation angle and levels of spin imparted onto the ball to vary. It was shown that the elevation angle and spin rate values during impacts at different orientations created a U shaped curve and inverted curve respectively, with changing ball orientation depicted in Figures 4.9 and 4.10. Figure 4.29 depicts the centre of mass in relation to its centroid, and how this relationship changes with ball orientation angle. The variation of the centre of mass effects the moment created by the reaction force, which causes the variation in elevation angle and spin rate as described above.

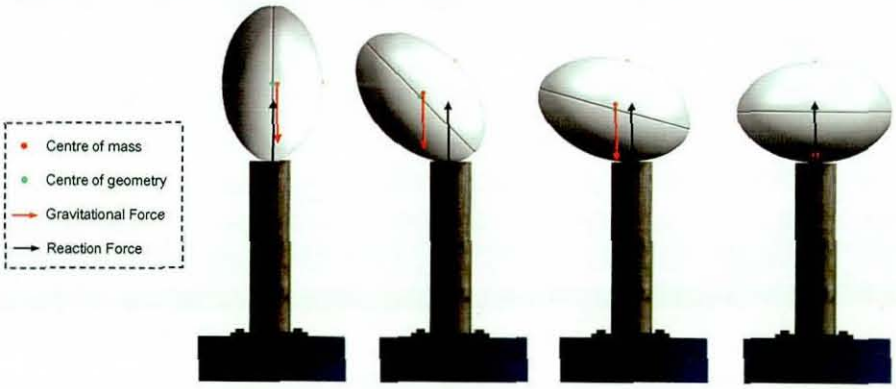

Figure 4.29 Elevation angle variations with the ball orientation

Figures 4.12 – 4.16 depicted the relationship between deviation angle and the position of the valve during impact. It was shown that placing the valve away from the theoretical centre plane of the motion (right or centre of the panel impact), caused the deviation angle to increase. This effect was amplified for the rugby ball with the larger valve mass. Positioning the valve to the right displaced the centre of mass from the centroid of the ball causing a moment to be created, which will result in lateral deviation of the ball after contact (Figure 4.30). During an impact with the valve in the upwards or downwards position, the reaction force and centre of mass are in the same plane causing no moment to be produced. Increasing the mass of the valve caused a greater displacement of the centre of mass from the centroid resulting in an increased lateral deviation.

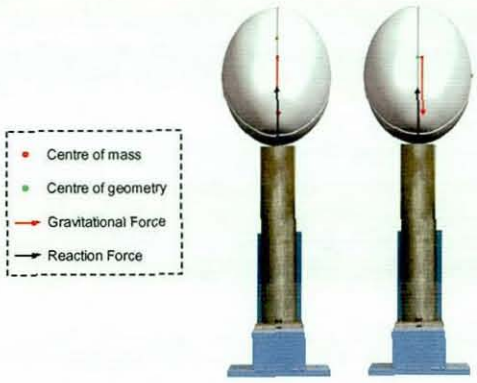

Figure 4.30 Deviation angle

4.10.2 Out-of-Balance Forces

The vertical balancing machine provided a method for assessing the unbalance within an ovoid ball caused by manufacturing variability, and the inclusion of the valve and or laces, which result in a non uniform distribution of mass. Results have shown that rugby balls with a larger valve mass created a greater level of unbalance when rotated around the polar axis and the equilateral axis when the valve left/right (zz). The increase in the valve weight, results in the centre of mass moving further away from the centroid, creating an out-of-balance force during rotation. The mean value of unbalance for the heavier valve rugby ball, when rotated about the zz-axis was 26.1g, which was a 122% increase in unbalance when compared to the rugby ball with the smaller valve.

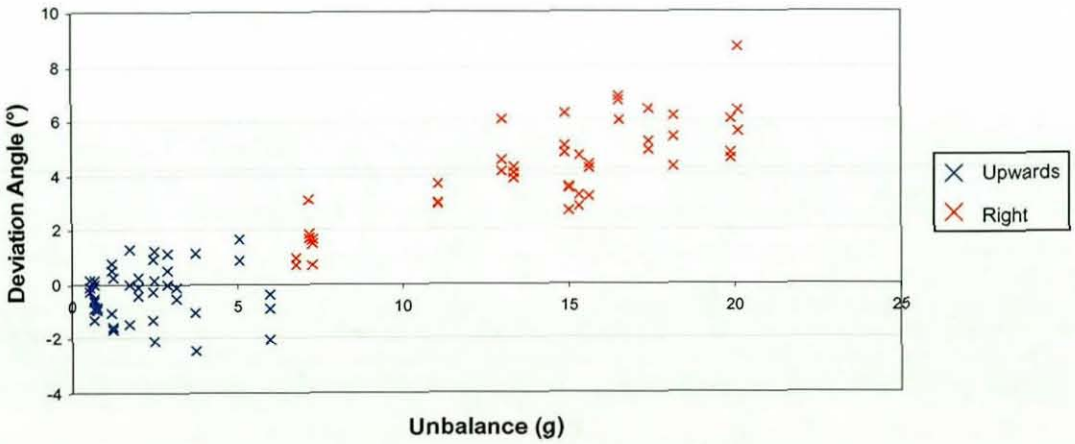

Figure 4.31 Unbalance plotted against deviation angle

Results from the bounce characterisation test showed that moving the valve away from the motion line of the ball caused an increase in the deviation angle post impact. The raw data for the deviation angle of both the RGB 1 and RGB 2 balls have been plotted against the unbalance measurement, when the valve was positioned upwards and to the

right. This allows a comparison of unbalance to deviation angle (Figure 4.31). The results demonstrate that increasing the unbalance within an ovoid ball causes the level of deviation to increase when the valve was positioned off centre. It is therefore important to reduce the displacement of the centre of mass, in order to create uniform bounce characteristics irrespective of impact position.

4.11 Conclusions

The measurement system developed allows the bounce characteristics of ovoid balls to be measured at a number of inbound orientation angles. It has been shown that the orientation angle of the ball pre impact affects the elevation angle and spin rate, with the maximum and minimum values occurring at 45°. Varying the position of the valve caused a variation in all measurement parameters. Impacts with the valve upwards and downwards resulted in a dramatic change in spin rate and elevation angle for the RGB 1 ball. Impacts with the valve off centre (right and centre of the panel) resulted in a lateral deviation during the ball's flight. The trajectory of the ball was calculated using MATLAB and showed an increase in horizontal, vertical and lateral variation during impact with the RGB 1 ball.

The use of the vertical balance machine allowed the unbalance within an ovoid ball to be measured to accuracies of ±0.1g. It was found that the maximum unbalance occurred during rotation around the polar axis, due to the reduction in the radius between the point of unbalance (valve and or laces) and the centre of rotation. A comparison between unbalance and deviation angle showed that an increase in the unbalance resulted in an increase in deviation angle.

Increasing the mass of the valve caused the tangential displacement of the centre of mass from the centroid to increase, which increases the unbalance and deviation angle during impacts with the valve off centre. It is therefore important to reduce the displacement of the centre of mass, in order to create uniform bounce characteristics irrespective of impact position.

The ball bounce characterisation and rebound tests could be implemented by a governing body as a means of experimentally testing the dynamic behaviour of an ovoid ball, ensuring that all balls behave in a similar way. The rebound test, described in Chapter 3,

would allow the dynamic variation of the ball to be measured, with the governing body defining a maximum variation in order for the ball to achieve accreditation. The ball bounce characterisation test should be performed at a 45° ball orientation angle, as this is the position of minimum elevation angle and maximum spin rate. Results showed that the 45° position defined the height and depth of the spin rate and elevation angle curves respectively, as measurement of this position would give an indication of the behaviour of the bounce at other ball orientation angles. Results also showed a relationship between deviation angle and out of balance measured within the balls. In order to reduce the digitisation process, the out-of-balance measurement could be used to define the lateral deviation of the ball when the valve is placed in an off-centre position.

Chapter 5

Determination of Ball Launch Characteristics

5 Introduction

The following chapter details the ball launch characteristics of elite rugby union players. The specification for an ovoid ball is defined by the sport's governing body, and generally falls into three main categories, the dimensions, weight and pressure of the ball at the start of play. The parameters defined are all static values, and dynamic ball performance is not measured. This is similar to the majority of other ball sports, however the ball's behaviour during play is of significant importance and other governing bodies are considering dynamic performance criteria. In order to develop dynamic ball assessment procedures it is necessary to appreciate the capabilities of elite players.

Rugby union players form the basis of the elite player study due to availability of players within the United Kingdom. This data can then be used to define the parameters for realistic dynamic ball tests. The aim of this study was to obtain the ball launch characteristics achieved by elite players, and following discussions with coaches, a spin pass and three different types of kick were assessed using professional players from senior English rugby union clubs. The three kick types selected are the place kick, drop kick and spiral kick.

5.1 Previous Investigations

It is apparent that little research has been conducted into the initial launch characteristics of a rugby ball during various types of kicks or passes. Macmillian (1975) used three skilled footballers to perform three different types of kicks seen in Australian Rules football. The drop punt and drop kick assessed are similar to the spiral and drop kick investigated during this study. A high speed camera operating at 400 frames per second with a shutter speed of 1/1200s was used during the testing. Ball velocities of 24.9 and 27.2m/s were stated for the drop kick and punt respectively. Hartschuh (2002) studied the ball launch characteristics during an American football punt. Punts were filmed using a 30 frames per second video camera and ball velocities of 24.5±0.6m/s and launch angles of 49.4±1.5° were stated. Cunningham et al (1975) carried out an analysis to determine the effect of air resistance on the flight of an American football for punt kicks.

The punt is a similar kick to the spiral kick often used in a game of rugby union and punts were divided into three distinct groups, Type I – long axis of the ball travels along the trajectory of the flight and the ball lands on the forward tip of the ball, Type II – similar trajectory to Type I except the ball lands parallel to the ground, and Type III – similar trajectory to Type I and II, except the ball lands on the rear tip. A Locan high speed camera operating at 200 frames per second with a shutter speed of 1/1200s was positioned perpendicular to the flight of the ball. The initial angle and velocity were calculated from the first five frames after the football left the foot, giving initial angles between 49.4 and 50.4°, and initial velocities between 35.87 and 37.92 m/s. No values for spin were given for either of the studies.

It is worth considering the number of studies that have examined ball velocities achieved during the kicking of a soccer ball. Neilson (2003) carried out a comprehensive study of 25 professional players, at five senior English football clubs. A high speed camera operating at 500 frames per second with a shutter speed set to 1/1000s captured the initial trajectory of the ball after impact. A maximum recorded velocity of 33.1m/s was stated for a full power kick, with a maximum ball spin of 833rpm achieved during an instep and outstep swerve kick. Asami and Nolte (1983) analysed six test subjects, including four professional players, performing a maximal velocity instep kick. The participants were filmed using a 500 frames per second high speed video camera and a mean ball velocity of 29.9m/s was reported. The maximum ball velocity was stated as 34.0 m/s, which is similar to the values reported by Neilson (2003). Studies by Roberts and Metcalfe (1968), Plangenhoef (1971) Isokawa and Lees (1988), Tsaousidis and Zatsiorsky (1996) and Nunome et al (2002) have all stated similar ball velocities ranging from 22 – 31m/s. Of significance is that the majority of studies do not include spin data. Asai and Akatsuka (1995) used a high speed camera operating at 4,500 frames per second to capture three amateur players performing a number of different kicks and measured ball spin rates in the range of 7- 10 rev/s during an instep swerve kick.

The study aimed to obtain comprehensive rugby ball launch data for a group of elite players, considered to represent the performance of leading players worldwide. The data from this study provides new knowledge on kicking capability and ball dynamics which can be used as a benchmark for scientific studies.

5.2 Participants

Player testing was carried out at six professional English rugby clubs, with data from fourteen players analysed and presented. All players were established kickers and had international representative honours, including four full internationals. The clubs consisted of five English Premiership clubs, Saracens RFC, Leicester Tigers RFC, London Irish RFC, Bristol RFC and Newcastle Falcons RFC and a national division one club, Nottingham RFC. The test players all wore their own boots and supplied their own kicking tees. Only one player analysed during the study kicked with their left foot. The player details are shown in Table 5.1

Table 5.1 Mean (±SD) test subject data (n=14)

Age (years)	25 ± 3.74
Body mass (kg)	88.06 ± 5.72
Body height (m)	1.78 ± 0.03
Boot size	9.71 ± 1.14

5.3 Testing Procedure

The subjects were requested to perform three different types of kick at full power, enabling maximum velocity to be achieved, at a distance 60m from a set of goal posts. The first kick was a place kick, the second a drop kick and the third a spiral kick. The subjects were asked to perform each skill until they had achieved five 'good' strikes or passes which were recorded. The test procedure was approved by the University Ethics Committee and players were informed of the test procedure and their rights prior to testing.

The testing procedure was carried out on five natural turf training pitch environments and a single artificial surface. Seven unbranded 'match balls' were used, to help negate any player brand bias that may exist. The balls were inflated to a recommended pressure of 9psi. The unbranded balls were marked with a series of constant and dashed lines to enable the accurate determination of spin during the digitising process, depicted in Figure 5.1.

Figure 5.1 Player performing place kick using an unbranded rugby ball

5.4 Equipment

The initial movement of the ball after impact or throw was captured using a NAC 500 high-speed camera operating at 500 frames per second with a shutter speed of 1/1000s to improve the clarity of the captured image. The camera resolution was defined as 640 x 480 pixels. The NAC 500 camera allows for high speed video recording directly onto a standard video home format (VHS) cassette. This video recording was later converted into digital format using MGI VideoWave 4 software. The camera was positioned perpendicular to the trajectory of the ball, 2m from the point of impact. The camera height varied from 1.4 – 1.8m depending upon kick type. A composite high-speed video image is depicted in Figure 5.2.

Figure 5.2 Composite image of place kick

5.5 Analysis

Throughout the study a total of two hundred and ten kicks and seventy passes were analysed. The high-speed camera recording was digitised using Image Pro Plus software, and the ball velocity and launch angle numerically calculated. The length of the ball about its long axis was measured, this process allowed the image to be calibrated using a known ball length measurement. This process was repeated for each image, to negate any possible errors due to the initial positioning of the ball before contact. The position of the ball was digitised by marking an enclosed rectangle around each image, allowing the 2D co-ordinates of the centre of the ball to be calculated. This process was repeated for each ball image, allowing the displacement of the centre of the ball to be calculated over a given time interval, depicted in Figure 5.3. The measurement of spin has been analysed by evaluating the number of frames required to measure a quarter rotation of the ball. The spin defined for the place and drop kick is tumble axis backspin, whilst rifle spin around the long axis is the main component of a spiral kick and spin pass. The distance to the first bounce of each of the kicks was measured using the Bushnell Yardage Pro 1000 laser range finder to an accuracy of ± 1m.

Figure 5.3 Analysis procedure using Image Pro Plus

Errors attributed to the ball flight not being perpendicular to the camera's focal plane, were difficult to measure and were controlled by accurate alignment of the camera's position, and requesting players to strike the ball along a given trajectory. The

repeatability of the analysis was calculated by analysing a single image a number of times (n=15). The repeatability of the velocity measurement was defined as ±1.33m/s (95% confidence), whilst the launch angle ±0.29° (95% confidence) and spin rate ± 6.35 rpm (95% confidence).

5.6 Results and Discussion

The test results are summarised in Table 5.2 and shown in graphical form in Figures 5.4 and 5.5.

Table 5.2. Mean (±SD) test results for rugby union kicking an passing data

Kick / Pass	Velocity (m/s)	Ball Spin (rpm)	Launch Angle (°)	Distance (m)
Place	26.44 ± 2.97	476.20 ± 89.84	30.22 ± 4.41	53.74 ± 5.72
Drop	25.60 ± 3.77	468.50 ± 133.14	35.76 ± 4.28	51.30 ± 5.70
Spiral	28.06 ± 3.70	432.82 ± 92.22	43.91 ± 4.55	55.42 ± 7.22
Spin Pass	13.79 ± 1.48	438.18 ± 65.96	12.19 ± 5.26	

The mean ball velocities achieved during the different types of kicks were similar, with the maximum recorded velocity of 38.1m/s achieved during a drop kick. Macmillan (1975) stated a mean velocity of 27.2m/s during an Australian rules drop kick. This lower value could be due to the differences between the types of balls investigated, an increase in player development and measurement differences. The maximum recorded velocity for the spiral and place kick were similar, 33.6 and 33.5 m/s respectively. Cunningham et al (1975) stated a mean velocity of 37.92m/s for an American football punt that has rifle spin, the long axis of the ball travelling along the trajectory of the flight and the ball landing on its forward tip, however the maximum velocity value was not stated. The mean velocity is considerably higher than the 28.06m/s measured during the rugby spiral kick. The difference in values is significant and could be due to the difference in technique, ball shape and aerodynamics and material properties or measurement technique. The maximum velocities recorded were also 5m/s higher than the full power soccer kick recorded by Neilson (2003). The mean velocity value for the spin pass was considerably lower than the kicking actions, but the low standard deviation illustrates the repeatability of the simple action. A maximum velocity of 18.3 m/s was recorded for the pass.

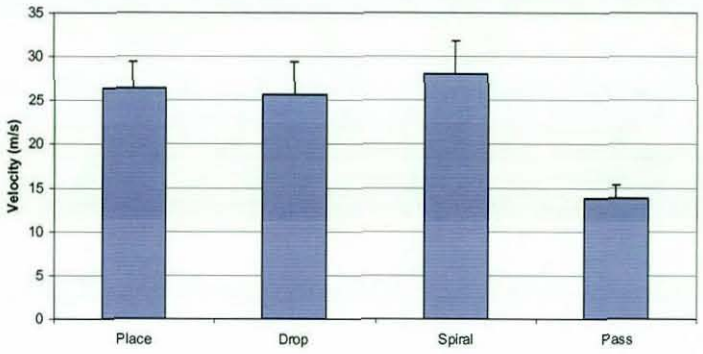

Figure 5.4.a) Graph depicting ball velocity data

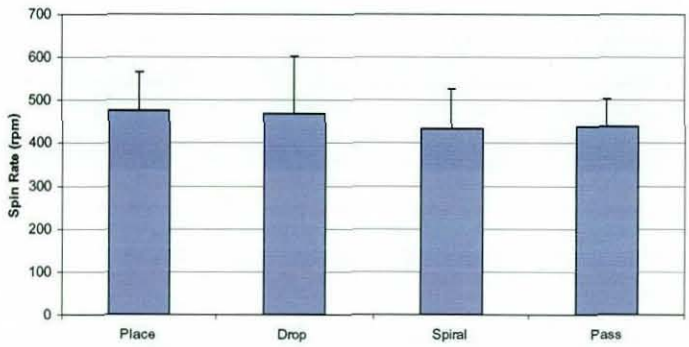

Figure 5.4.b) Box Graph depicting spin rate data

If is assumed that the energy imparted to the ball during a kick is constant then the resulting ball motion will be dependent on the ball characteristics and the kicking technique. In general it can be expected that low spin kicks will achieve a greater velocity and the kicks with high spin will have a lower velocity. This effect was noticeable during the measurement of the drop kick action. The maximum spin rate of 810 rpm was recorded during a drop kick, however this kick left the foot with a ball velocity lower than the mean. The ratio between spin and ball velocity is dependent upon the impact position in relation to the centre of mass of the ball. An increase in the distance from the centre of mass will reduce the ball velocity and increase the imparted spin. It was noted that the variation in measured spin rate for the drop kick was considerably greater than any of the other kick types and this effect was attributed to the difficult nature of the kick, as the ball has to make contact with the ground before it is struck.

During a spiral kick the mean spin rate was lower than the place and drop kick, although the difference was minimal and deemed insignificant. During the natural kicking motion of a drop or place kick, tumble axis spin is imparted onto the ball as it is struck below the centre of mass. It would be possible to impart a large amount of rifle spin during the spiral kick motion, however this would cause the player to strike across the ball, reducing

the velocity and overall distance. The maximum ball spin rates for a spiral kick and spin pass were 682 and 576 rpm respectively.

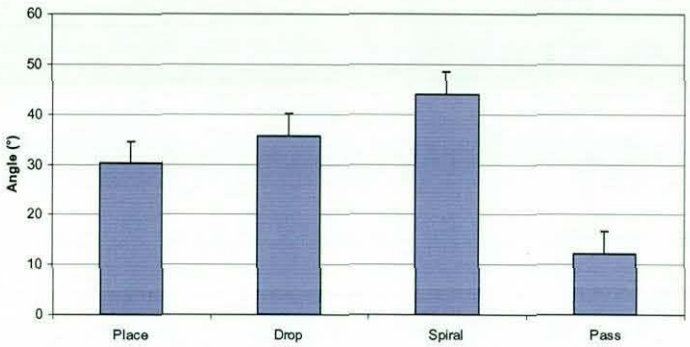

Figure 5.5a) Graph depicting elevation angle data

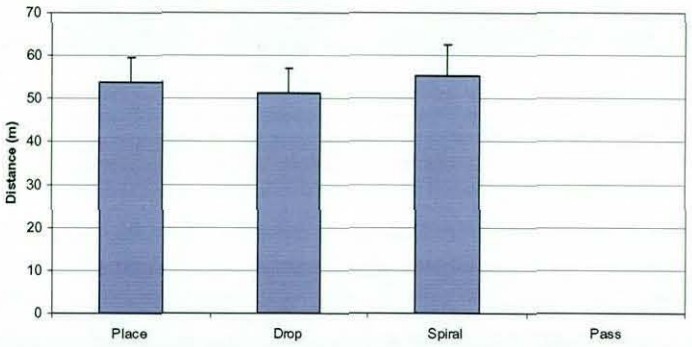

Figure 5.5 b) Graph depicting ball distance data

The lowest launch angle recorded was for the place kick, which might be expected as during a drop and spiral kick the ball is dropped before contact with the foot. The increase in launch angle between a spiral and drop kick was noted by Macmillan (1975) whose results state that the launch angle of a spiral kick was 7° greater than that of a drop kick. Cunningham et al (1975) stated a launch angle of 50.04° which is 6° higher than the value measured for the spiral kick. This difference could be attributed to the tactics used during an American football punt, as the offensive team try to increase the "hang time" of the kick.

The maximum distance achieved during any kicking action was 71m (spiral kick) which was considerably higher than the other kick actions, 63 and 60m for the place and drop kicks respectively. The mean distance for the spiral kick was similar to the other kick types, whilst the standard deviation was 26.7% higher than the other kick types. The spiral kick is a difficult motion to replicate and this could account for the high standard deviation measured for all the launch characteristics.

5.7 American Football Study

5.7.1 Introduction

Cunningham et al (1975) stated a mean velocity of 37.92m/s for an American football punt which was considerably higher than velocity measured during a rugby spiral kick. In order to determine ball launch characteristics of elite American football players, testing was carried out at the University of Tennessee. Data from four players was collected in an indoor testing environment, with the test players wearing their own boots and supplying their own kicking tees. Five American footballs, of the same brand used during college games, were marked with a series of constant and dashed lines to enable accurate determination of spin.

5.7.2 Procedure

Two quarterbacks were tested and asked to perform a maximal spin pass, whilst one punter and one field goal kicker were asked to perform their respective kick types at maximal velocity. During a game of American football the punter will vary the kick type depending upon tactics and field position, so the punter was asked to perform a series of kicks as if he was on the 20 yard line (maximum distance) or the 50 yard line (maximum hang time). The initial movement after the ball was thrown or impacted was captured using the Photron APX camera operating at 500 frames per second with a shutter speed of 1/1000s, in order to improve the clarity of the image. The resolution of the camera was defined as 1024 x 1024 pixels, with the image downloaded in between kicks. The distance to the first bounce was measured using the Bushnell laser range finder. The action of the player during their respective movement was also captured in order to allow the team's coaches to analyse their kicking and throwing action, depicted in Figure 5.6

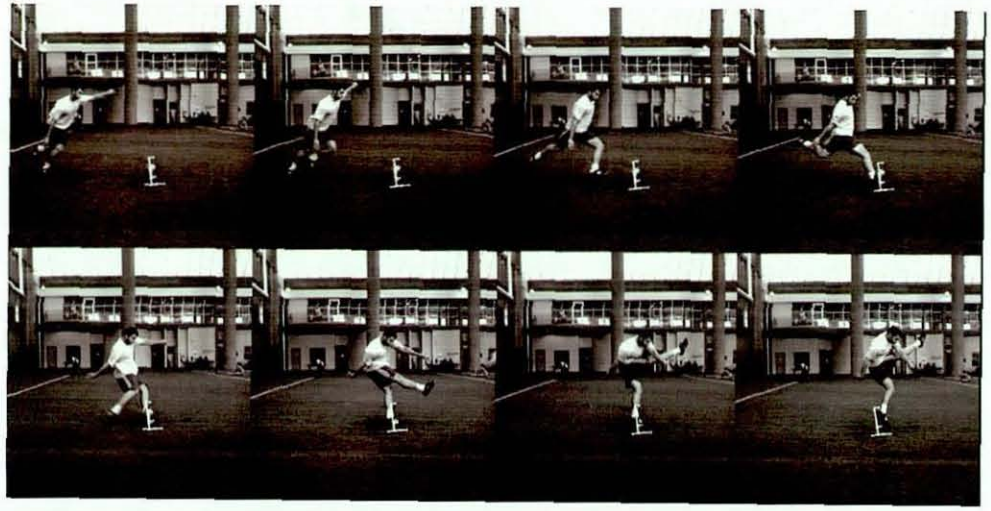

Figure 5.6a) American football field goal kicker

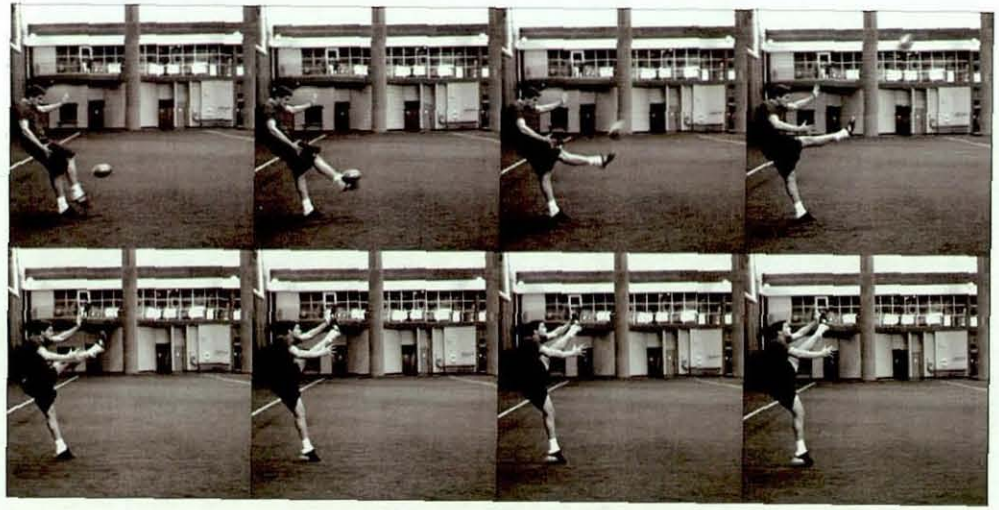

Figure 5.6b) American football punter

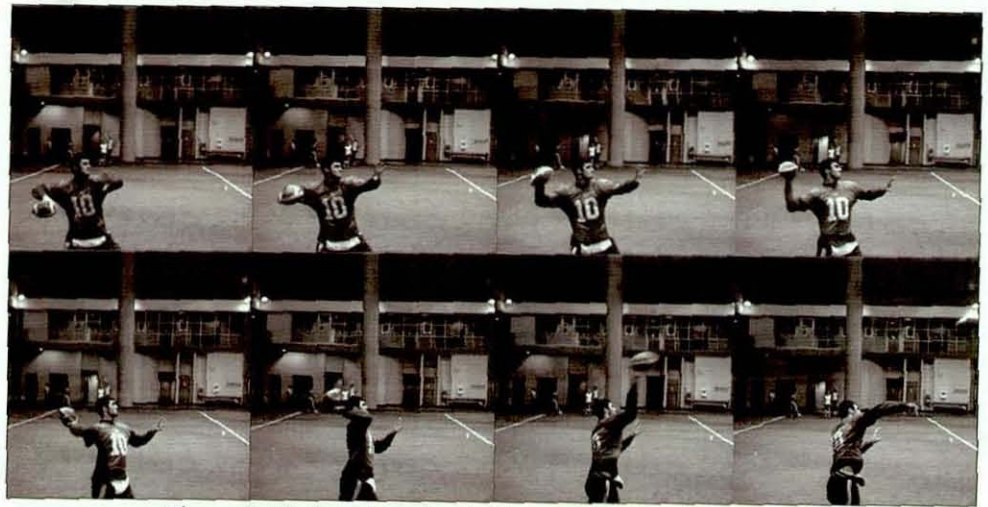

Figure 5.6c) American football quarterback – right handed

Figure 5.6d) American football quarterback – left handed

5.7.3 Results

The test results are summarised in Table 5.3 and a comparison to the rugby union player data is depicted in Figures 5.7 and 5.8. Data for the American football field goal was compared to the rugby place kick, whilst the spiral kick is compared to the American football punt, with spiral 1 representing the punt from the 20 yard line (maximum distance), and spiral 2 the punt from the 50 yard line (maximum hang time). No data is presented for an American football drop goal, as this is a rarely performed skill.

Table 5.3 Mean (±SD) test results for American football kicking and passing data

Kick / Pass	Velocity (m/s)	Ball Spin (rpm)	Launch Angle (°)	Distance (m)
Field Goal	28.4 ± 1.47	365.5 ± 76.2	27.3 ± 1.47	54.1 ± 2.7
Punt 1	27.6 ± 1.84	188.1 ± 29.0	57.0 ± 3.06	
Punt 2	29.3 ± 1.41	208.2 ± 22.8	65.5 ± 0.61	
Forward Pass	20.6 ± 1.25	618.0 ± 48.0	36.4 ± 2.24	50.1 ± 3.9

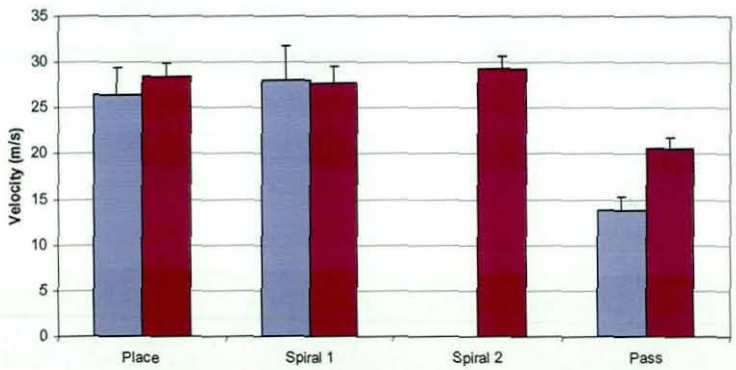

Figure 5.7a) Ovoid ball velocity comparison

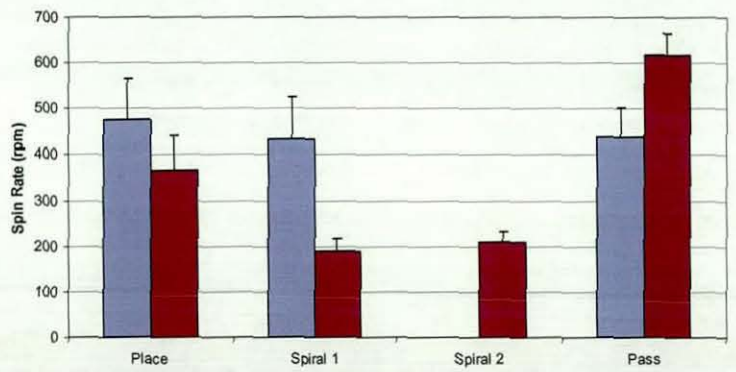

Figure 5.7 b) Ovoid ball spin rate comparison

Rugby American Football

The ball velocity achieved during the field goal and punts are similar to those achieved during the rugby place and spiral kick, with a maximum velocity of 30.6 and 30.3 m/s achieved for the field goal and punt respectively. The mean velocity during a punt, 28.3m/s, was considerably lower than the mean velocity stated by Cunningham et al (1975), 37.92m/s. The velocity of an American football pass was greater than the pass performed during the rugby action, with this difference possibly attributed to the difference in ball shape and aerodynamics, but was most likely due to the variation in technique.

The spin rates measured during the American football kicks were lower than those recorded during rugby player testing. The maximum difference occurred during a spiral/punt, with the punt recording 108% drop in spin (224.7rpm). The differences in spin could be attributed to the difference in technique, ball shape and aerodynamics and material properties of the ball. The spin imparted onto the ball during an American football pass was considerably higher than that measured during the rugby pass, which could be attributed to the difference in action, gripping method and shape and aerodynamics of the ball. The maximum spin rate of 681.8 rpm was measured, which was higher than the value of 600rpm stated by Nowark et al (2003). The study by Nowark et al carried out testing using an in flight recorder to measure flight dynamics of an American football, but used a foam rubber ball with two circuit boards mounted as an orthogonal pair. The standard of the player throwing the foam rubber ball was not stated, and this along with the difference between the ball types may result in the higher value measured during current player testing.

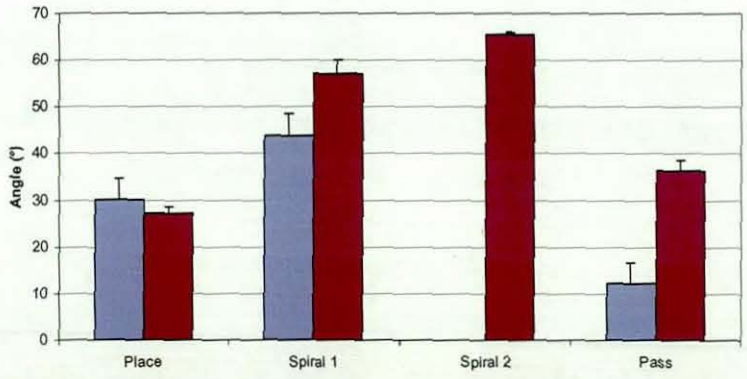

Figure 5.8a) Ovoid ball elevation angle comparison

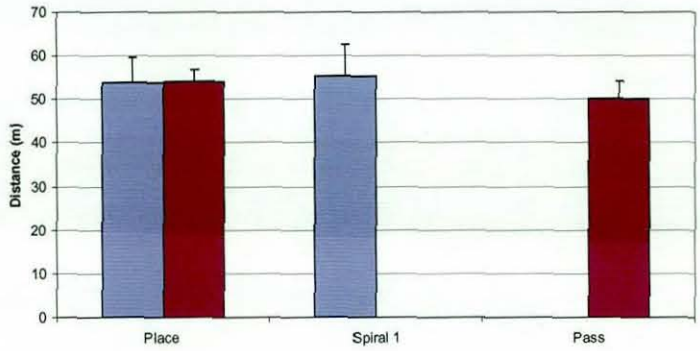

Figure 5.8b) Ovoid ball distance comparison

The elevation angle during a field goal was comparable to the rugby place kick, but the American football punts were kicked at a considerably higher angle. When performing a kick from the 50 yard line, the ball will leave the punter's foot with an average elevation angle of 65.5°, compared with 57.0° when punting for maximal distance. The differences between the rugby and American football values could be attributed to the tactics employed during the kick type, with the punter trying to keep the ball in field, unlike the rugby player performing a spiral kick to touch.

No distance data is presented for the American football punts, as the ball impacted the roof of the indoor testing facility due to the high elevation angle imparted onto the ball. The maximum forward pass distance of 55m was achieved by the right handed quarterback, which was comparable to the maximum distance achieved during the measured field goal attempts, 57m.

5.8 Summary of Ovoid Ball Lunch Characteristics

Tables 5.4 – 5.6 allow the comparison of ball launch data from a number of authors.

Table 5.4. Comparison of ball velocity data

Investigators	Ball Type	Kick Type	Velocity (m/s)
Neilson (2003)	Soccer	Power Kick	33.1 - max
Asami and Notle (1983)	Soccer	Power Kick	34.0 - max
Hartschuh (2002)	American Football	Punt	24.5 -mean
Cunnigham et al (1973)	American Football	Punt	37.7 - mean
Holmes (2006)	American Football	Punt	30.3 - max
Holmes (2006)	American Football	Field Goal	30.6 - max
Holmes (2006)	Rugby	Place Kick	33.5 - max
Holmes (2006)	Rugby	Drop Kick	38.1 - max
Holmes (2006)	Rugby	Spiral Kick	33.6 - max

The maximum ball velocity was measured during an American football punt by Cunningham et al (1973), and stated a mean velocity of 37.7m/s. This value is considerably higher than the maximal values stated by other authors.

Table 5.5. Comparison of spin rate data

Investigators	Ball Type	Kick Type	Spin Rate (rpm)
Neilson (2003)	Soccer	Instep Swerve	833 - max
Holmes (2006)	American Football	Punt	227 - max
Holmes (2006)	American Football	Field Goal	454 - max
Holmes (2006)	Rugby	Place Kick	652 - max
Holmes (2006)	Rugby	Drop Kick	810- max
Holmes (2006)	Rugby	Spiral Kick	682 - max

The maximal spin rate was measured at 810rpm during a rugby union drop kick, and the high spin rate was attributed to the shape of the ball and the kicking action.

Table 5.6. Comparison of elevation angle data

Investigators	Ball Type	Kick Type	Elevation Angle (°)
Hartschuh (2002)	American Football	Punt	49.4 -mean
Cunnigham et al (1973)	American Football	Punt	49.9 - mean
Holmes (2006)	American Football	Punt (max distance)	57.0 - mean
Holmes (2006)	American Football	Punt (max hang time)	65.5 - mean
Holmes (2006)	American Football	Field Goal	27.3 - mean
Holmes (2006)	Rugby	Place Kick	30.2 - mean
Holmes (2006)	Rugby	Drop Kick	35.8 - mean
Holmes (2006)	Rugby	Spiral Kick	43.9 - mean

The elevation angle measured during the American football punt was dependent upon the tactics employed by the punter, as they try to make a compromise between distance and hang time. A comparison could be made between a rugby union place kick and American football field goal due to the similar kicking action and ball launch characteristics.

5.9 Conclusion

The present study provides the first comprehensive data for launch characteristics for elite rugby players. The mean initial velocity for the three types of kicks ranges between 25.60 and 28.06m/s, depending upon kick type, with the mean velocity for the spin pass being significantly lower at 13.79m/s. Maximum velocities of 38.05 and 18.30m/s were recorded for a kicking action (drop kick) and spin pass respectively. The maximum spin rate obtained by a professional player in this study was 810 rpm (drop goal), which was considerably higher than data recorded for the pass (576 rpm). The launch angle increased during a drop goal kick to 43.91± 4.55°, in comparison to the other kicking actions, which compares to results stated by Macmillian (1975). The most difficult skill to replicate during the testing procedure was the drop kick, which accounts for the higher standard deviation when examining the spin rate and the distance measurement. The maximum distance measured was 71m (spiral kick) to the first bounce.

Cunningham et al (1975) stated a mean velocity of 37.92m/s for an American football punt which was considerably higher than velocity measured during a rugby spiral kick. The study carried out at the University of Tennessee, to measure the ball launch characteristics of an American football during a field goal, punt and forward pass, indicated a mean ball velocity of 28.4m/s, which was lower than the value stated by Cunningham et al. The elevation angle during a punt ranged from 53 – 66° depending upon the field position, which was higher than the value produced during a rugby spiral kick. The differences were attributed to the ball shape and aerodynamics, and tactics employed by the player.

The data from this study can be used to define the parameters of any dynamic simulations/tests that are to be developed in the future. The study used elite players, which ensures that the values obtained are close to the maximum achievable.

Chapter 6

High Speed Impact Measurement

6 Introduction

The following chapter details the method used to determine the dynamic properties of ovoid balls during high speed normal impacts. A description of the experimental testing equipment used will be given along with an analysis of the experimental errors.

6.1 Ovoid Ball Launch Facility

The normal impact described in the rebound test (Chapter 3), allowed the measurement of contact time and the coefficient of restitution (CoR), which can be used as a method of FE model validation. However Chapter 5 details a maximum ball velocity of 38m/s during a game related impact and it was important to examine the dynamic properties of ovoid balls at similar velocities. The ball launch facility used during the testing was initially created to allow the controlled launch of spherical balls at velocities up to 34m/s with balls launched towards a rigid steel plate (Figure 6.1). Various surfaces and instrumentation could be attached to the plate to record the reaction forces.

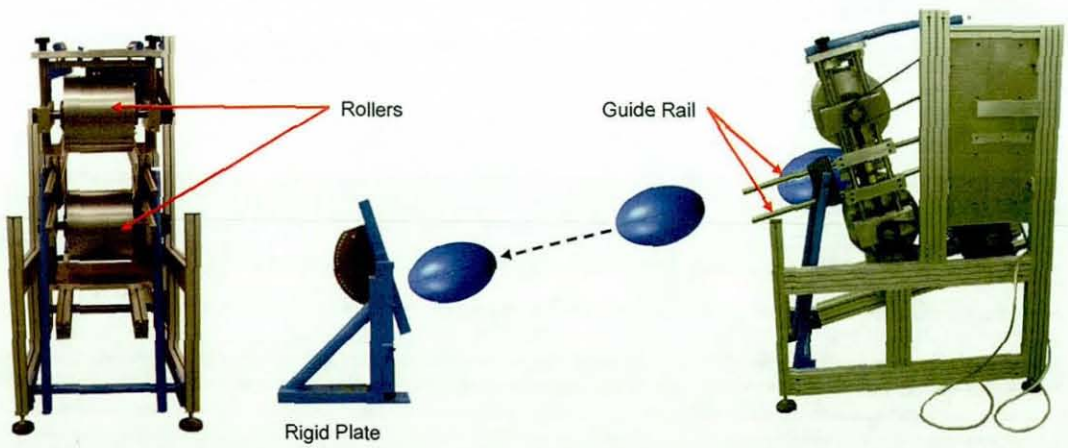

Figure 6.1 Ovoid ball launch facility

The machine consists of two independently driven rollers, 330mm in diameter, capable of rotating to a maximum velocity of 2800rpm. The rollers are mounted at a 15° orientation to allow the balls to return using a purpose built recycling system. The balls are constrained within a holding mechanism (Figure 6.2), allowing the orientation of impact to be defined pre impact, with location points which fit into the end of the ball to

allow accurate positioning. The holding mechanism is adjustable to allow ovoid balls of varying sizes to be launched at a high velocity. A guide rail system is used to support the holding mechanism allowing the ball's contact with the rollers to be consistent.

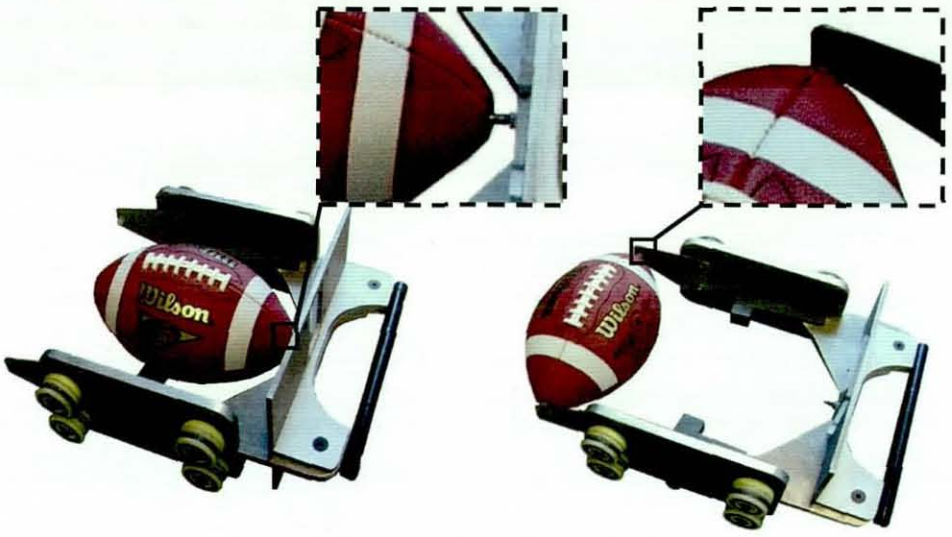

Figure 6.2 Ovoid ball holding mechanism

6.2 High Speed Normal Impacts

The high speed ball launcher produced a maximum ball velocity of 25m/s when projecting the ovoid balls onto their short circumference. Figure 6.3 depicts an American football deforming during contact with the rigid plate while impacting on the seam opposite the lace. Due to the smaller diameter of the American football, a number of polyethylene rings were manufactured in order to reduce the roller separation, depicted in Figure 6.4.

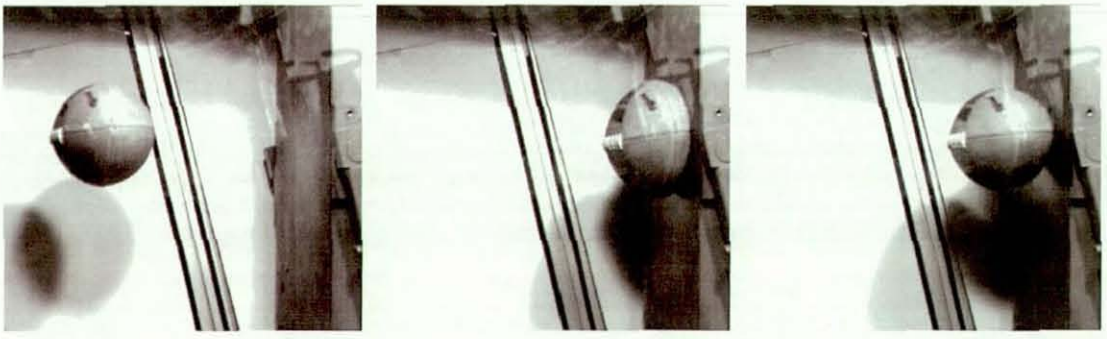

Figure 6.3 High speed seam impact

Whilst trying to recreate high speed impacts on the end of the ovoid balls it was noted that the ball would rotate 90° during its flight between the rollers and the rigid plate, causing variation in impact position. A high speed video camera was positioned behind

the rollers, allowing the ball to be filmed as it passed through the rollers towards the plate. The laces of an American football were positioned to the side to avoid contact with the rollers, as this would produce non uniform contact conditions. It was noted that the seam opposite the laces would always impact the rigid plate first, irrespective of whether the laces were initially placed to the left or right. The non uniform stiffness within the ball, caused by the inclusion of the laces and inflation valve, caused the ball to rotate due to the non-symmetrical deformation as the ball passes through the rollers (Figure 6.4). This effect occurred during end impacts with a rugby ball, with the rotation caused by the non uniform mass distribution created by the inclusion of the valve.

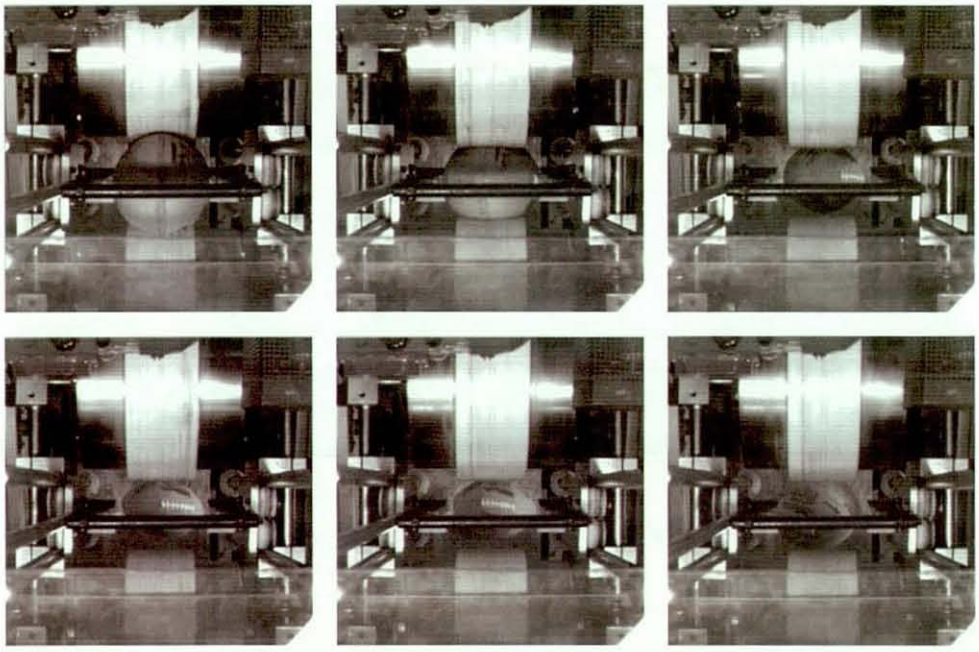

Figure 6.4 Rotation of an American football during an end impact

The roller separation can be adjusted using the double screw thread arrangement, allowing the contact pressure of the rollers on the ball to be managed. It was found that decreasing the roller separation increased the deformation of the ball as it passed through the rollers, which caused an increase the unwanted rotation during end impacts. The roller separation was increased in order to reduce the deformation, hence reducing the rotation, however this resulted in a dramatic reduction in velocity. Increasing the rotational speed of the rollers resulted in an increased ball velocity, but also resulted in a reduction in repeatability. The roller separation and rotational speed were adjusted in order to find a compromise and a maximal end impact velocity of 15m/s was achieved.

6.3 High Speed Camera Equipment

Throughout the research ball impacts were captured using high speed video cameras. The Photron Fastcam APX system was used during the vast majority of the testing procedures, and captured the motion of the ball in monochrome. This HSV camera was capable of recording at 100,000fps although the majority of the research involved capture rates of 2,000 – 10,000, with a capture resolution of 1024 x 1024 and 512 x 256 pixels respectively. The Photron SA-1 system was used during the ball flight characterisation testing (Chapter 9), with this system capable of capturing at full resolution, 1024 x 1024, at a high frame rate of 5,400 fps, whilst improvements in the light sensitivity of the system over its predecessor, allowed it to be used in an indoor environment. Photron conducted a testing procedure allowing the light sensitivity of the Photron APX RS camera to be calculated. The Photron APX RS camera was manufactured as a predecessor of the APX, whilst it has since be superseded by the SA-1. The camera was fitted with a 'half moon' back illuminated target (Figure 6.5), which allowed the level of luminance to be varied and compared to background levels (Photron 2007)

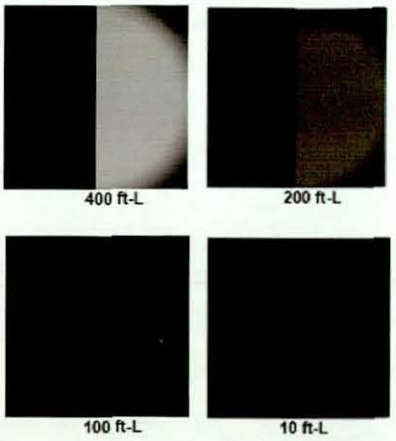

Figure 6.5 a) Camera integrated with 'half moon' b)Signal to Noise Ratio images

The average signal level and background level was calculated using a second order polynomial, and the difference between the background and the signal value was described as the signal to noise ratio (SNR), which was compared to the original luminance value (Figure 6.6).

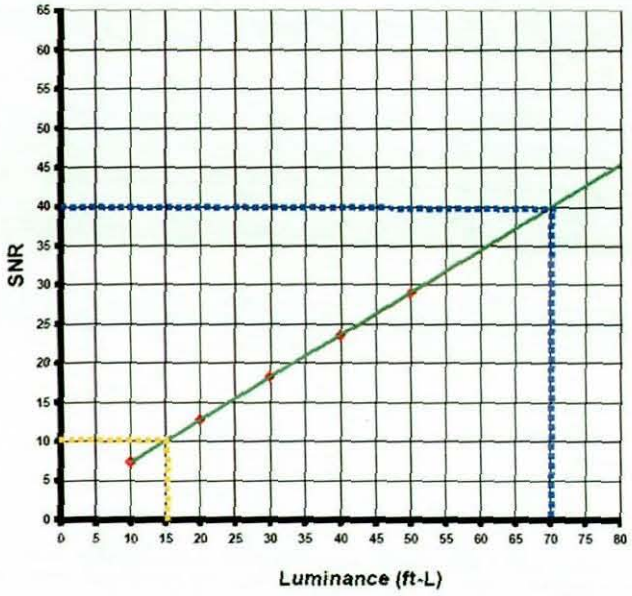

Figure 6.6 Signal to Noise Ratio (SNR) plotted against luminance (Photron 2007)

ISO 12232 specifies the method for assigning and reporting recommended exposure index values, for digital still cameras, and defines an SNR value of 40 as 'excellent' and 10 as 'acceptable'. The recommended exposure index can be used to define the frame rate at which the SNR is excellent and acceptable, and these frame rates are 5,000 and 25,000 respectively for the Photron APX RS camera.

The aperture is an opening through which light is received, with a larger aperture allowing the camera to function with less ambient illumination or at a higher shutter speed. Jain et al (1995) stated that there is a trade off between aperture size and depth of field, with a smaller aperture providing more depth of field but admitting less light. Figure 6.7 demonstrates the effect of reducing the depth of field by increasing the aperture.

Figure 6.7 F-stop effect on depth of field

The amount of light collected by the camera (ε) depends on the intensity of the light (E) and the duration of the exposure (t), ε = Et. The lens aperture will have a designated F-stop number which will create the same light intensity for different lenses at the same F-stop, and is proportional to the ratio of the focal length, (f) and diameter of the aperture (d) (Equation 6.1).

$$F-stop = \frac{f}{d}$$

Equation 6.1. Aperture F-stop

The F-stop is calculated in multiples of √2, as doubling the aperture area is the equivalent of increasing the aperture by a diameter of √2, which increases the light on the image plane by a factor of 2.

In house tests by Photron have shown that the APX and SA-1 cameras used throughout the research have different light sensitivity levels to the APX RS, tested in the above procedure. Results showed that in order to create the same image brightness, the aperture of the APX camera would have to be increased by one F-stop (increasing the light by a factor of 2), whilst the SA-1 camera could decrease the aperture by one F-stop, creating a factor of 4 difference between the Photron APX and SA-1 cameras.

6.4 Image Processing Software

A normal impact of an ovoid ball with a rigid plate resulted in a planar motion of the ball pre and post impact. The camera was always positioned perpendicular to the plane of motion, which allowed the motion of the object to be measured in 2-D. The software package Image Pro Plus, was used to enhance the image by modifying the brightness, contrast and gamma, allowing a darkened image to be artificially brightened to assist the digitisation process. Image Pro Plus was used to obtain the x and y pixel co-ordinate values for the centre of the ball pre and post impact, and the maximum deformation during contact with the rigid plate.

The velocity of the ball was calculated by determining the centre of the ball at two positions, a known time interval apart (Figure 6.8a). This procedure was completed pre and post impact, allowing the coefficient of restitution to be calculated. The centre co-ordinates of the ball were determined using the rectangle function which allowed the

circumference of the ball to be enveloped, whilst the length of the ball was used to calibrate the distance (m), of a pixel. The contact time was calculated by measuring the number of frames, for which the ball was in contact with the plate, and dividing this number by the frame rate. Maximum deformation during impact was calculated by measuring the length of the ball in pixels to determine the change in shape about the normal and tangential direction (Figure 6.8 b). Normal deformation was defined as the deformation in the direction of motion of the ball and is calculated by subtracting the measured value from the initial ball diameter. Tangential deformation was measured perpendicular to the motion of the ball, and is calculated by subtracting the diameter of the ball from the measured length.

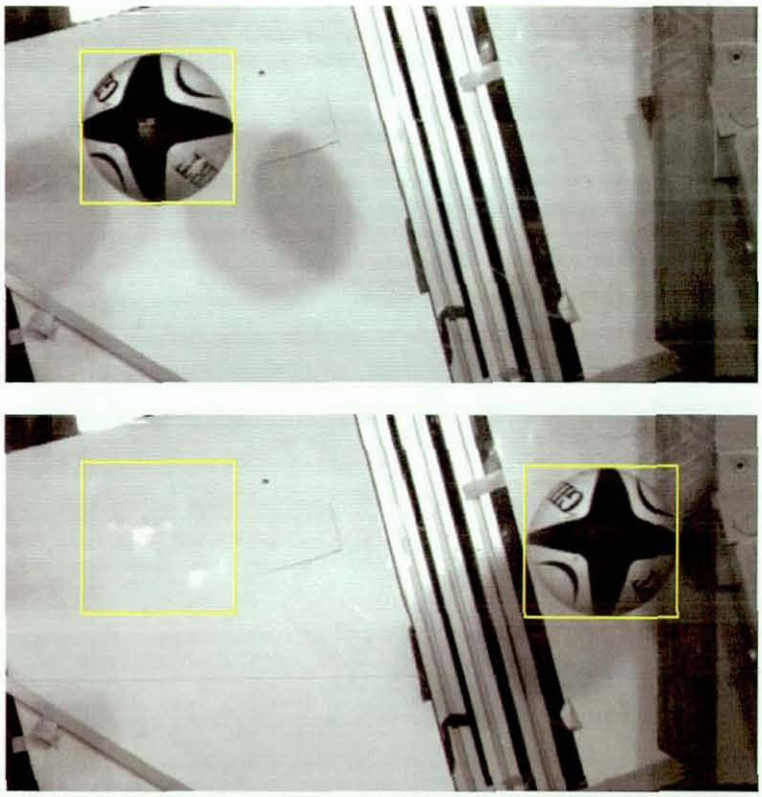

Figure 6.8a) Method for determining ball velocity pre impact

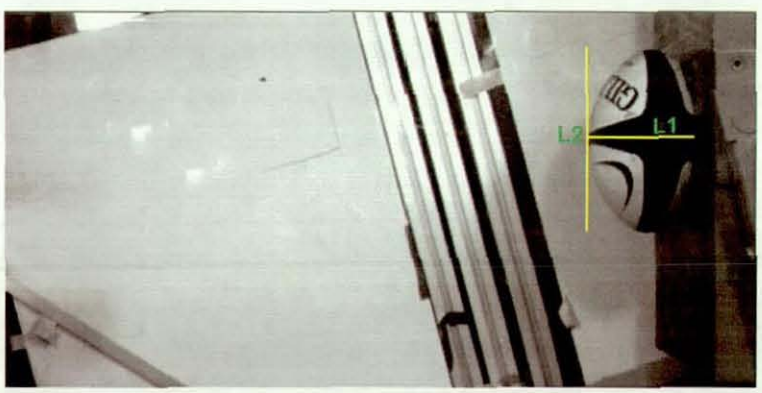

Figure 6.8b) Measurement of normal (L1) and tangential deformation (L2)

6.5 Measurement Errors

The high speed video camera creates a 2-D image which was used to identify the position of the ball with time from which the velocity of the ball pre and post impact was calculated. The total measurement error Q_{TOTAL} can be defined using Equation 6.2.

$$Q_{TOTAL} = Q_{SETUP} + Q_{DEVICE} + Q_{ANALYSIS}$$

Equation 6.2. Uncertainty of the measurement procedure

The uncertainty of the setup, Q_{SETUP}, was predominately attributed to the motion of the ball not being parallel to the camera focal plane. Q_{SETUP}, was difficult to measure, but was controlled by accurate alignment of the camera's position. The uncertainty of the device, Q_{DEVICE}, was largely attributed to the image distortion, caused by the lens. The two main types of radial lens distortion are pincushion and barrel (Figure 6.9).

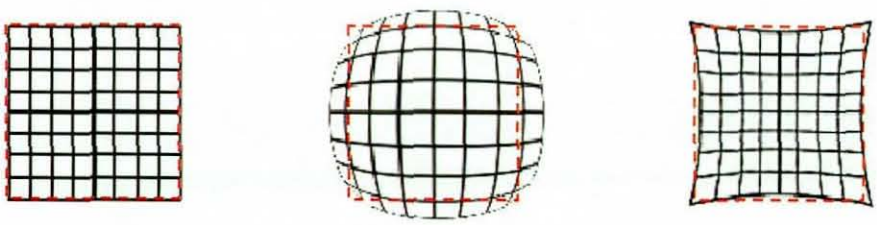

Figure 6.9 Image distortion a) Barrel b) Pin cushion

Barrel distortion generally occurs in wide-angle lenses when the image points are displaced closer to the centre as the image is distorted in order to fit into a smaller space (negative displacement). The pin-cushion distortion commonly occurs when using a telephoto lens, as the image points are displaced away from the optical centre as the image is stretched in order to fit the space (positive displacement). The distortions may not always be obvious but need to be examined and are most prominent at the outer extremities of the image. Symes (2006) measured the lens distortion using a Nikon 72mm diameter zoom lens, identical to the lens used throughout the experimental testing. A screen was created with five arrays positioned in the corners (position of maximum lens distortion) and the centre (minimum distortion) and an image was captured at the maximum resolution (1024 x 1024 pixels), depicted in Figure 6.10.

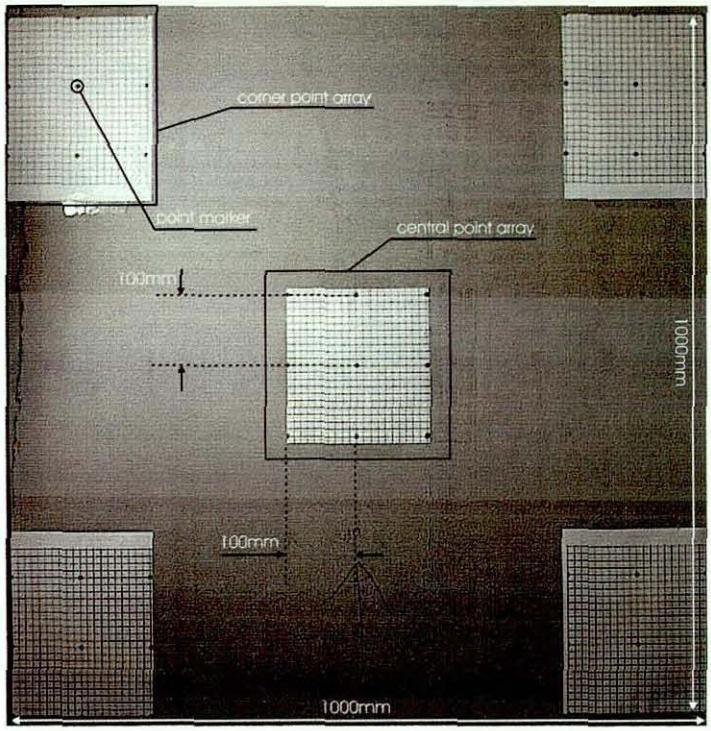

Figure 6.10 Image distortion test screen (Symes 2006)

Each of the arrays had nine markers positioned at 100mm intervals, and the manual digitisation of these markers, allowed the measured distance between the markers to be compared between the corner and centre arrays. The measurements of the centre array returned a distance of 100mm, identical to the actual distance, with the maximum deviation from this distance found in the bottom right array and measured to 98mm. It was therefore concluded that the maximum error incurred due to the lens distortion was 2%.

During the calculation of the maximum normal deformation, the measurement was taken at an area near the edge of the image rather than the central pixel. This induced an error due to lens distortion, which caused the face of the plate to be visible, rather than a single edge (Figure 6.8a). The deformation measurement was therefore taken at a point which was not in the centre of the ball, causing a reduction in determined value. The error was calculated as 6.9% the length of the ball at maximum deformation. This error was deemed to be consistent throughout the measurement procedure.

The uncertainty of the analysis, $Q_{ANALYSIS}$, can be described as a measure of repeatability of the human carrying out the digitisation process, and the measure of the accuracy of the digitisation software. The repeatability of the analysis will be calculated and defined

for each of the relevant experimental testing procedures. The accuracy of the image digitisation software was examined using images created in CAD, which consisted of two rugby balls, each with a black line to represent the seam, a known distance apart (Figure 6.11).

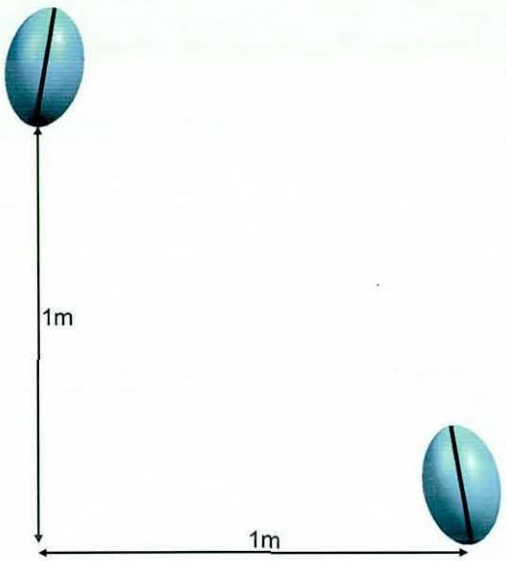

Figure 6.11 CAD image used to measure accuracy of image digitisation software

The resolution of the captured images during experimental testing did not remain constant throughout the research, as the resolution was affected by the frame rate and motion of the ball. During a normal impact the ball travelled with a 0° elevation angle. Therefore it was possible to zoom in and increase the number of pixels that represent the area of the ball, unlike the ball bounce characterisation test where the vertical and horizontal motion of the ball needed to be captured. During the digitisation of images with a lower resolution, it became increasingly difficult to ensure that only the ball was encompassed by the rectangle, resulting in an increase in human error. CAD images were created with the rugby ball length varying from 214 to 29 pixels (Figure 6.12), allowing the effect of the resolution to be examined.

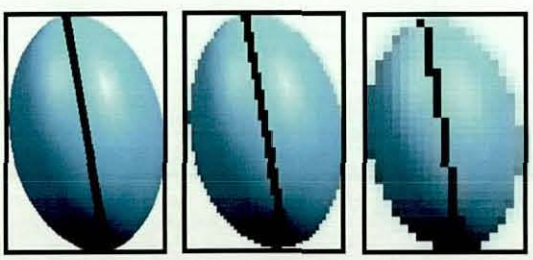

Figure 6.12 CAD images with a ball length of 214, 70 and 29 pixels

The x and y co-ordinates of the two rugby balls were measured ten times for each of the images at different resolutions, with no variation between the ten measurements. The distance between each of the CAD images was 1m in the horizontal and vertical direction and the difference between the real value and the measured value can be seen in Figure 6.13.

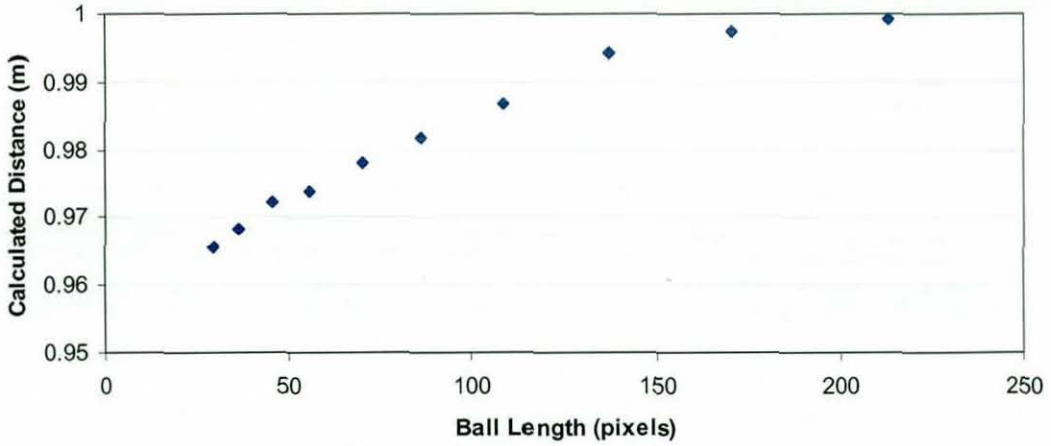

Figure 6.13 Calculated horizontal displacement

A ball velocity of 30m/s would be achieved if the time between the CAD images was 0.04714sec. The difference in velocity calculated and the real velocity is depicted in Figure 6.14, fitted with a fourth order polynomial trendline. The results showed that reducing the number of pixels to 29, caused a 3.5% error in the velocity calculation. In order to keep the error to below 1%, the equivalent ball length should be greater than 115 pixels. The elevation angle did not change with a decrease in resolution, and produced a measurement of 45° for each of the images.

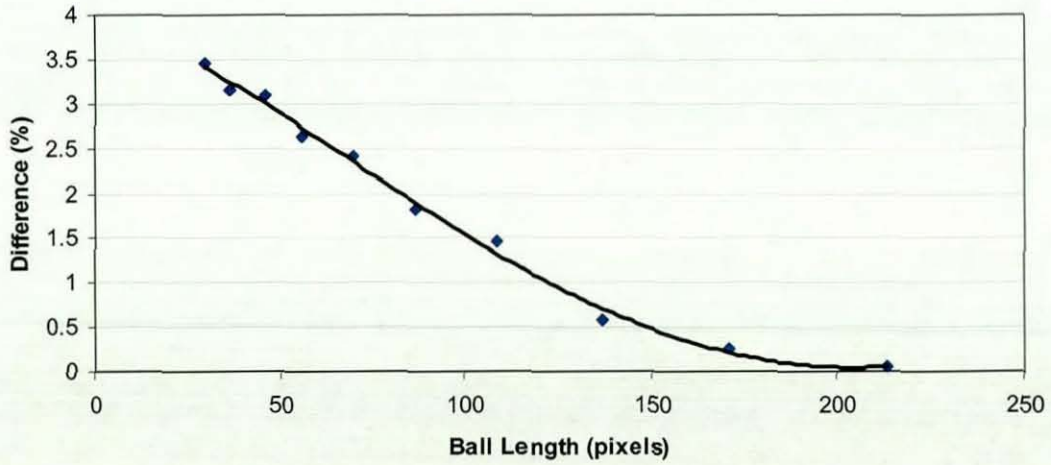

Figure 6.14 Percentage errors due to reduction in resolution

6.6 Conclusions

It is important to assess the dynamic properties of ovoid balls at game related velocities, and the high speed launcher is capable of producing ball velocities of 25m/s during short circumference impacts. A method for launching balls for end impacts at velocities higher than 15m/s has yet to be developed. Whilst trying to recreate end impacts with the rigid plate, the ovoid balls rotated resulting in a loss of control regarding impact orientation. This effect was caused by the varying stiffness of the ball, resulting in non uniform deformation whilst in contact with the rollers, causing rotation.

Throughout the research high speed video cameras were used to capture the motion of the ball, which can introduce errors within the measurements taken. The total error was established by analysing the error involved with the experimental setup, motion capture device and analysis procedure. It was found that the lens distortion created a maximum error of 2% when calculating a distance at the extremities of the image. The errors created from the analysis procedure were proportional to the resolution of the captured image. In order to keep the error to below 1%, $\geq$115pixels should be used to define a rugby ball's length.

Chapter 7

Development of Stitched Isotropic Ovoid Ball

7 Introduction

The following chapter details the development procedure for creating a finite element (FE) model of a stitched ovoid ball. The FE model provides a method of examining the dynamic behaviour of ovoid balls, whilst allowing the development of novel prototypes in a time-efficient manner. The initial part of the chapter describes the method for capturing the ball's shape, discretising the surface and mesh creation of a simple ovoid ball. The second part details the creation of an American football model, including the stitching and lace area, and the creation of a rugby ball model including the stitched seams and weighted valve. The dynamic performance of the rugby ball FE model was then validated against experimental data for normal and oblique impacts.

7.1 Finite Element Analysis

Finite element analysis (FEA) is a numerical method used to predict the solution of a physical problem by dividing a product shape into a number of small sections/elements. The term FEA was first used by Clough (1960), when numerical methods began to be widely used by the aerospace industry, however the theory dates back to the Ritz method of numerical analysis first introduced in 1909. Turner *et al* (1956) investigated the stiffness and deflection of complex structures which was considered to be a major contribution to the development of FEA. During the early 1970's FEA became an established numerical method for determining the solution of any physical system that could be described by differential equations. Initially the use of FEA was primarily in the aerospace, automotive, defence and nuclear industries to study the safety of structures. However FEA now has advanced to allow engineers to simulate the mechanical, electrical, and chemical forces that act on a part (Thilmany 2005). FEA is normally used when there are insufficient means to carry out practical testing or when the analytical solution is very complex.

For component analysis the shape is discretised into a number of elements (a mesh), connected by nodes. Each of the nodes within an element has a maximum of six spatial degrees of freedom, which are illustrated in Figure 7.1. Each element is then analysed

using relatively simple mathematical calculations, which will have linear or quadratic variation of the desired property with length. Due to the large number of calculations required within a FEA solution, the analyses are generally processed using computers. Advances in computer technology are helping to increase the availability and use of FEA packages, and decrease the computational time of analysis. Mechanical properties such as density and stiffness are assigned to each of the elements within the model and boundary conditions are applied to the nodes or elements to detail the external loads, fixings and contact conditions that they will experience during the analysis. The number of elements and their relative degrees of freedom, as well as the complexity of the boundary conditions are the main factors in determining the computational time of the analysis.

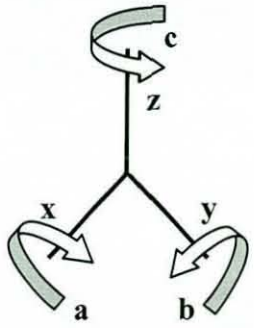

Figure 7.1 Six degrees of freedom

The FEA package ABAQUS has been used throughout the research programme. ABAQUS is a well established, commercially available FEA software package. It has been used previously for sports ball analysis and is compatible with the project collaborator's computer based systems.

7.2 Ball Shape Measurement

In order to create a surface model of an ovoid ball, a co-ordinate measuring machine (CMM) was used to capture 3D co-ordinates of the ball's surface, whilst inflated to the standard pressure. A Ferranti Metrology Systems Merlin co-ordinate measuring machine, fitted with a Renishaw probe system, was used in this instance. The Renishaw probe system allows different ruby tipped probes to be utilised, however the outer surface of most ovoid balls is generally constructed from a material which has been embossed with small pimples. The height of these pimples has been measured using a laser based surface scanner and values between 220 μm to 440 μm have been recorded (Figure 7.2). The possibility of errors from touching on or off a pimple are apparent and these have been

reduced by using a probe diameter significantly larger than the pimple size, in this case 5mm, ensuring contact with pimples, irrespective of surface position. The measurements taken therefore represent the outer envelope of the ball, which was not scaled down due to the small height of the pimples.

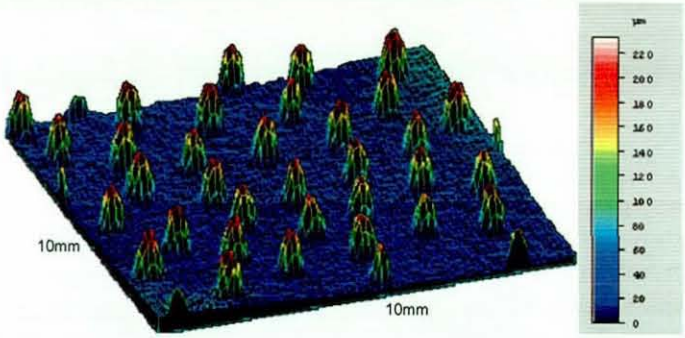

Figure 7.2 Surface scan of embossed outer panel material

The ball was mounted in a measurement jig with either end of the ovoid ball fixed between centres. During the measurement procedure the ball was held stationary using a jig, with the probe utilizing a touch force of less than 1g, allowing ball deflection to be deemed negligible. It was assumed that the ball shape was essentially uniform so only one panel was measured. This information was then instanced four times to create the ball shape. The shape of the panel was defined using the seams and three vertical splines at equal increments along the length of the ball, with measurements taken at 10mm intervals, depicted in Figure 7.3. The origin of the x, y and z axis were defined, using the axes of the centres, and the probe was manually positioned on the touch points allowing its 3D co-ordinate position to be recorded.

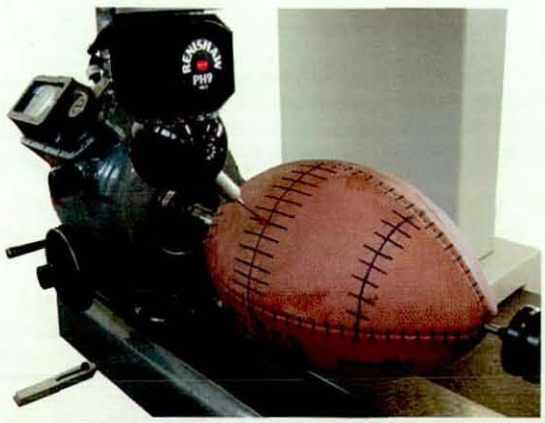

Figure 7.3 CMM geometry measurement procedure

7.3 Mesh Production

The geometry of the majority of ovoid balls is constructed from four panels arranged longitudinally around the ball. In order to simplify the model and the number of elements, the seams or laces shape were not modelled, as they could be represented by appropriate material properties. During previous modelling of spherical balls, the initial sphere has been discretised into a number of smaller regular polyhedra shapes. Polyhedra were developed by the early Greek mathematicians and are three-dimensional shapes consisting of an arrangement of vertices, faces and edges. Each face represents a polygon, whose constituent edge length and angles are equal (Figure 7.4). Previous work by Cordingley (2002) and Price (2005) found that the spherical icosahedron exhibited rotational symmetry and could be combined with a triangular element base to produce an FE model with uniform impact characteristics.

	Tetrahedron	Hexahedron	Octahedron	Dodecahedron	Icosahedron
Planar Polyhedra		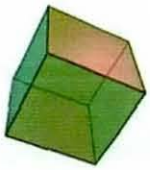	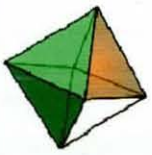		

Figure 7.4 Five regular polyhedrons

The octahedron was considered the most appropriate to represent an ovoid ball, with eight identical triangles arranged so that there was a single vertex at each end of the shape. Each single triangle was then discretised into a further series of four triangles (Figure 7.5), in order to allow greater control during the mesh construction.

Figure 7.5 Discretisation of surface for meshing

The surface of the model was discretised into thirty two faces exhibiting rotational symmetry and simple geometric definition well suited to mesh generation.

7.4 Element Selection

Elements are categorised into families (Figure 7.6), which are commonly used within FEA, with each element tailored for use in a specific problem. The family of elements used during an analysis will be dependent on the shape and the application of the model, e.g. solid (or continuum) elements can be used for linear analysis and for complex nonlinear analyses involving contact, plasticity and large deformations (ABAQUS 2005a).

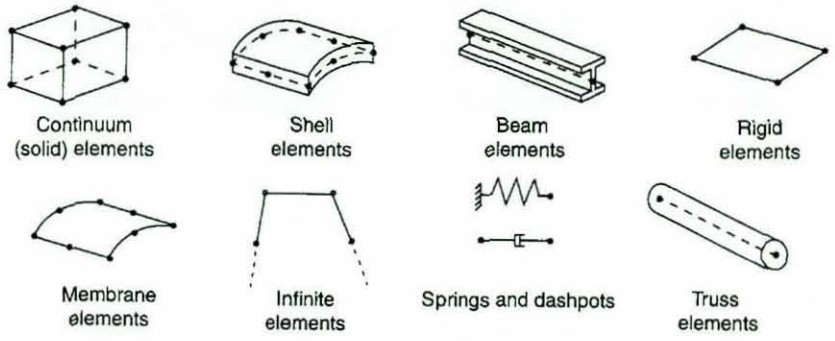

Figure 7.6 Commonly used element families (ABAQUS 2005a)

An ovoid ball represents a thin hollow prolate spheroid and it is recommended that shell elements are used for this type of analysis. Cordingley (2002) stated that shell elements are suitable when the thickness is no more than 10% of the other dimensions. For an ovoid ball, with width approximately 185mm and panel thickness 3mm, giving a thickness to diameter ratio of 1/62, makes shell elements an appropriate choice for this application.

Shell elements are also desirable as they are computationally efficient in comparison to solid elements. Shell elements are defined as either triangles (three nodes) or quadrilaterals (four nodes), and can be given a defined thickness parameter which acts as a third dimension (Figure 7.7). Shell elements are suitable for large strain analyses, and allow for changes in shell thickness produced during high velocity impacts. Previous modelling of high velocity sports impacts by Hocknell et al (1998a, 1998b), Cordingley (2002) and Price (2005) for golf, tennis and soccer respectively have found that due to

their geometry, triangular elements are notoriously stiffer. However with appropriate mesh refinement, three node triangular shell elements have produced acceptable results.

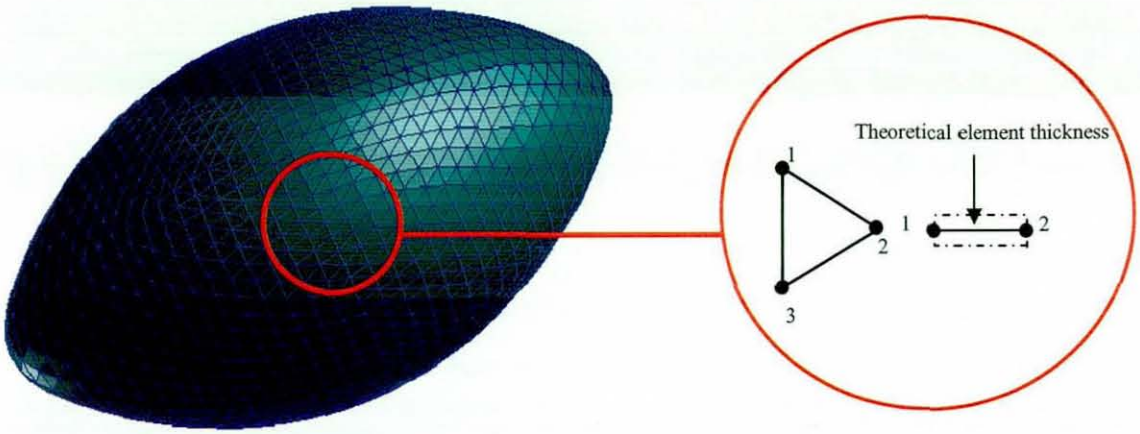

Figure 7.7 Triangular shell elements

During high speed analyses involving large levels of deformation, first order reduced integration elements must be used (Figure 7.8a). These elements have a single integration point in the geometric centre of the element, at which the stresses are calculated. During the bending of a single element it is possible for the outer surface tensile load to be equal to the inner surface compressive load. A reduced integration element, with a single integration point, may predict a zero strain in such a situation. This problem is known as hourglassing (Figure 7.8b). During this type of deformation the element has zero stiffness in this mode causing inaccuracies. Fortunately ABAQUS allows an artificial hourglass stiffness to be defined, reducing the negative effect of hourglassing.

Figure 7.8 a) First order reduced integration element b) Hourglassing effect

7.5 Material Model Production

A detailed description of the manufacture and materials used in ovoid balls can be found in Chapter 1. An ovoid ball is generally constructed from a bladder, to allow pressurisation, and a number of outer panels which are stitched together surrounding the bladder. The outer panel of the modelled rugby ball consists of a composite layer of rubber outer panel and woven fabric panel, whilst the outer panel of an American football consists of a woven fabric stitched to a leather outer panel. The woven fabric in both ovoid ball types consist of a number of layers of woven fabric, which are fed through a series of rollers and bonded together using liquid resin. This process allows the sheets of woven fabric to be aligned at different angles in order to achieve desirable material properties. The specific alignment of the woven fabric layers produces material anisotropy which will be discussed in Chapter 8. The basic ovoid ball models will assume material isotropy, throughout the construction materials. Tensile test data was produced for the outer panel material and bladder materials in order to create a hyperelastic strain energy potential model within the ABAQUS software.

7.5.1 FE Material Model

Materials with rubber-like properties are well suited to modelling using the hyperelastic material model. The material model is isotropic, nonlinear and is valid for materials that exhibit instantaneous elastic response up to large strains (ABAQUS 2005b). The materials are defined as isotropic due to the initial random orientation of the long chain molecules in elastomer materials. During stretching, the molecules re-orientate themselves, producing anisotropy. However, the directionality of this re-orientation follows the direction of straining, allowing the material to be considered isotropic. Rubber-like materials have very little compressibility in comparison to their shear flexibility. The relative compressibility of the material can be defined as the ratio of its initial bulk modulus to its initial shear modulus. This ratio is generally expressed in terms of its Poison's ratio, approximately 0.5 for hyperelastic materials.

The energy stored in the material per unit volume, as a function of the strain at that point in the material, is described as the strain energy potential, U (ABAQUS 2005b). There are several forms of strain energy potential available in ABAQUS to model the approximately incompressible elastomers, including the Arruda-Boyce form, the Marlow

form, the neo-Hookean form, the Orgen form, the polynomial form and the reduced polynomial form.

The strain energy potential, U, is defined as a function of the deviatoric strain variants I_1, I_2 and the total volume ratio J. The deviatoric strain variants are expressed in Equation 7.1, in terms of the principle stretches λ_i, which define the deformation along the three principle material axes.

$$I_1 = \lambda_1{}^2 + \lambda_2{}^2 + \lambda_3{}^2$$

Equation 7.1 First deviatoric strain invariant, I_1

As previously mentioned there are a large number of strain energy potentials, which are defined to capture the behaviour of rubber-like material properties within the hyperelastic material model. Experimental stress-strain data can be used to define the material coefficients of the hyperelastic material models, and the different models capture the non linear behaviour of the rubber-like material to different levels of accuracy. For instance the neo-Hookean model provides a good approximation for rubber-like materials undergoing low levels of strain, but cannot capture the second inflexion point associated with higher levels of strain (Price 2005). Some of the models require data from several different kinds of deformation over a range of strain rates, and use all of the data to determine the required co-efficients. These models are termed phenomenological models with the Ogden and polynomial form being two examples.

The reduced polynomial strain energy potential defined in Equation 7.2, was used during the formation of models by Cordingley (2002) and Price (2005). The model allows the prediction of complex deformation states when test data for only one deformation state is available. C_i and D_i are temperature dependent material properties, proportional to the shear and bulk moduli respectively, whilst J_{el} is the Elastic volume ratio.

$$U = \sum_{i=1}^{N} C_{i0}(\overline{I}_1 - 3)^i + \sum_{i=1}^{N} \frac{1}{D_i}(J_{el} - 1)^{2i}$$

Equation 7.2 Reduced polynomial strain energy potential

7.5.2 Material Testing

Material samples representing the bladder and the outer panel of an American football and rugby ball were uniaxially tested to a strain of 0.6. Cordingley (2002) and Price (2005) stated that the maximum strain exhibited throughout tennis ball and soccer ball impacts to be equal to or less than 0.5. The direction of the tension was aligned with the principle material direction for the outer panel. Strain rates of 100 and 500mm/min were used, with each test repeated five times. Figure 7.9 depicts the strain rate response of the rugby ball outer panel material samples during the tensile test. The results show strain rate dependence above a strain of 0.1, with a minimal increase in elastic modulus during measurement at the 500mm/min. During game related impacts an ovoid ball will experience high velocity deformation. Therefore future material samples will be subjected to the maximum strain rate of the tensometer, 500mm/min, as this will provide a good first approximation of the material's behaviour.

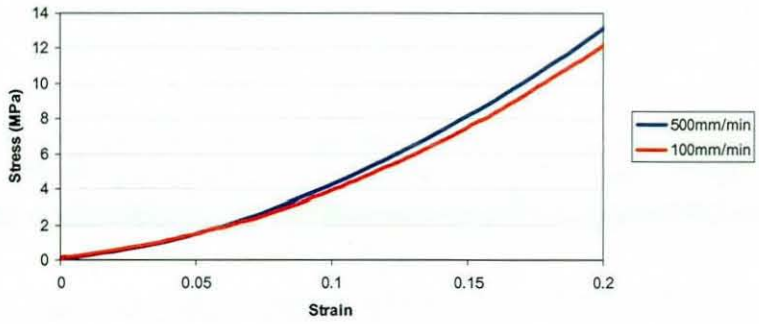

Figure 7.9 Strain rate response of rugby ball outer panel material

7.5.2.1 American Football

Figure 7.10 depicts the stress strain response of the American Football woven fabric and leather outer panel when strained to a value of 0.6.

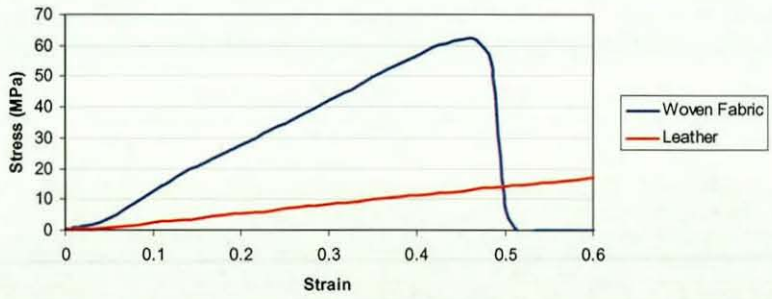

Figure 7.10 Strain rate responses of American Football woven fabric and leather material

Failure was observed within the woven fabric at a strain of 0.47, although a failure noise occurred towards a higher level of strain. This noise could indicate the failure of individual yarns and account for the non-linearity throughout extension, although this value was below the maximum strain stated by Cordingley (2002) and Price (2005) when examining tennis ball and soccer ball impacts. The stiffness of the leather was considerably lower than that of the woven fabric, and the leather did not fail at the maximum strain of 0.6.

7.5.2.2 Rugby Ball

Figure 7.11 depicts the stress strain response of the latex bladder and composite outer panel material when strained to a value of 0.6.

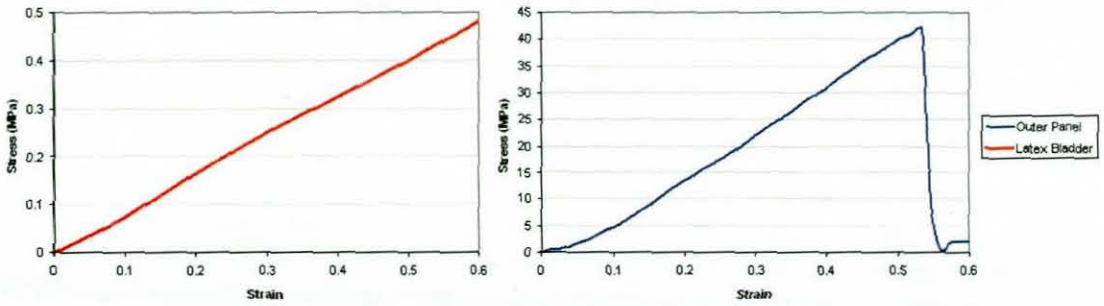

Figure 7.11 Stress strain response for rugby ball bladder and outer panel

The latex bladder did not fail at a strain of 0.6 and produced a lower stress strain response in comparison to the outer panel material. During the straining of the outer panel, failure occurred at a 0.55, although a failure noise occurred towards the higher strain levels indicating failure of individual yarns.

7.5.2.3 FE Material Model

As previously stated the reduced polynomial strain energy potential allows the prediction of complex deformation when only a single deformation state was available. The reduced polynomial strain energy potential with a material parameter of N=2 provided good agreement with the stress-strain test data, depicted for the latex bladder stress strain data in Figure 7.12, and was used to define the material within the model.

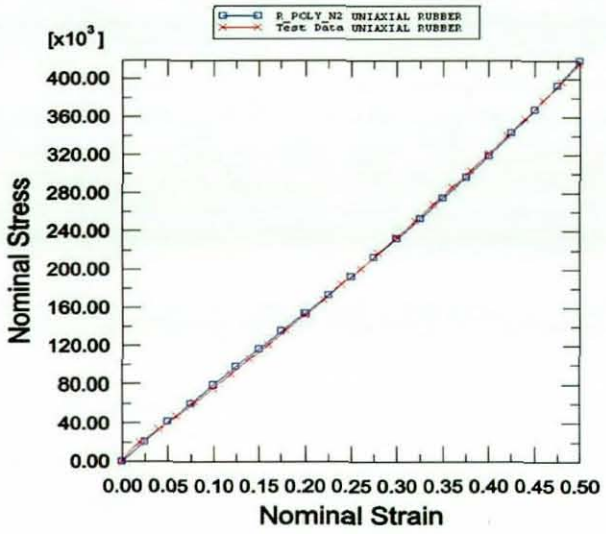

Figure 7.12 Stress-strain data and reduced polynomial strain energy potential material model

7.6 Inflation

The internal pressure within the bladder of the FE model must be modelled, as without this ABAQUS would interpret the hollow within the ball to be a vacuum which would cause a number of inaccuracies. During impact the deformation would be greatly exaggerated, and the ball would not return to its original shape as the surface of the model would invert. Pressurisation of the model was accomplished by creating a set of hydrostatic fluid elements on the internal surface of the model. These elements share coincident nodes with the shell elements, allowing the pressurisation of the model to be combined with the material response of the shell elements. A single reference node, coupled with the hydrostatic fluid element nodes, represents the pressure within the fluid cavity. A mass flow rate of a specific density fluid was used to inflate the model to the correct pressure which resulted in an induced stress within the cavity wall. The stress within the material produced straining of the model, resulting in a volumetric increase. The non spherical nature of an ovoid ball's geometry resulted in non uniform stress during inflation (Figure 7.13). Price (2005) and Cordingley (2002) stated that the stress value across the surface of the pressurised model would be constant due to the spherical nature of the soccer bladders and tennis ball cores respectively. In order to overcome the volumetric increase, the initial surface geometry was scaled.

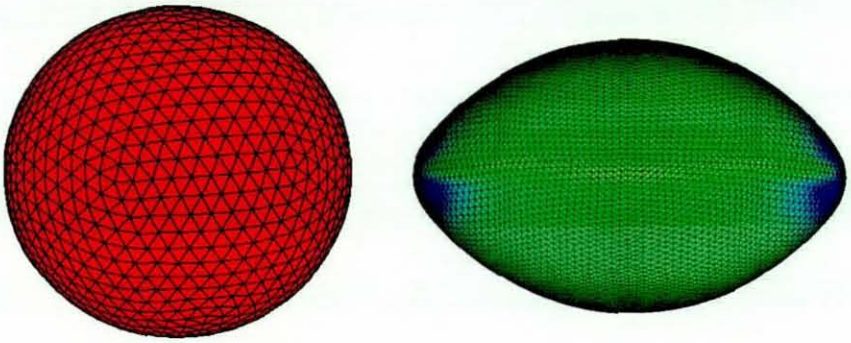

Figure 7.13 Stress contour plots for a spherical soccer ball and an ovoid ball

The effect of non uniform stress during inflation was analysed during inflation of an American football and it was noted that the greatest volumetric increase occured at the centre of the panel, with an increase of 11.9mm. Figure 7.14 depicts an overlay of an ovoid ball before and after inflation

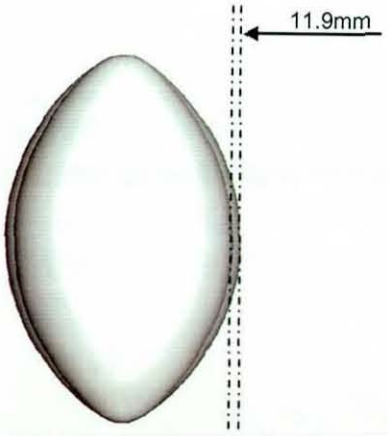

Figure 7.14 Volumetric increase due to inflation

7.7 Seam Assessment

7.7.1 Stitching Region

Price (2005) demonstrated that the ball stitching provides a rigid framework similar to a skeletal structure. It was important to include the stitched region within the ball model as it is likely to vary the global stiffness, affecting the deformation and contact time. In order to determine the material properties of the stitching seam, a jig was manufactured to replicate the two panel edges. The jig was manufactured from two pieces of mild steel plate 2mm thick, and was T-shaped to allow clamping within the tensometer (Figure 7.15). Twelve evenly spaced, 1mm diameter holes were drilled at a distance of 5mm from

the bottom edge of the plate and the jig was stitched in an identical way to the panels of the ovoid ball. Eight evenly spaced 5mm holes were also drilled at a distance 10mm from the bottom edge of the plate allowing the material properties of the lacing region of an American football to be examined.

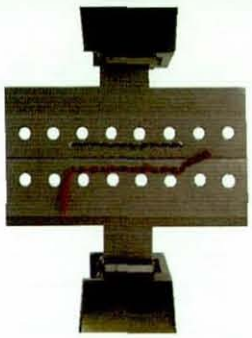

Figure 7.15 T shaped stitching seam tensile jig

Testing was carried out to a strain of 0.2, with a crosshead speed of 500mm/min. Tensile tests were conducted with 4, 8 and 12 stitches, with five repeat tests. Figure 7.16 depicts the average force extension curves for the stitching seam assembly tensile tests with 4, 8 and 12 stitches. The number of stitches directly affected the stiffness resulting in an increase of 259KNm^{-1} to 939KNm^{-1} for 4 and 12 stitches respectively, at an extension of 2mm.

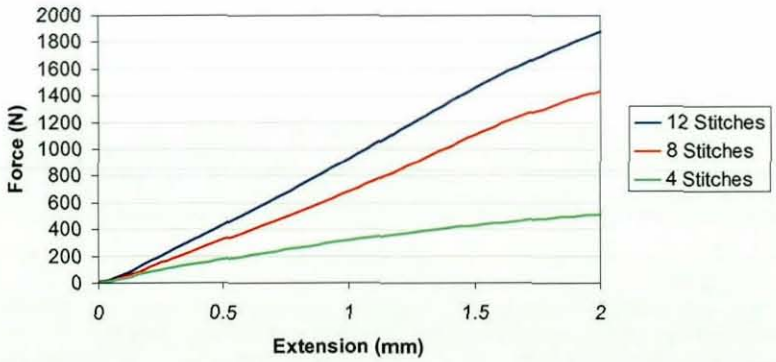

Figure 7.16 Force-extensions curve for the American football stitching

Figure 7.17 allows a comparison between the stitching region and the panel materials that are used in the construction of a rugby ball. The elastic modulus for the various material properties are 0.75, 77.6 and 304 MPa for the bladder, outer panel and stitching region respectively. This verifies the hypothesis stated by Price (2005) that the stitching provides a skeletal structure for the ball. In the case of rugby the outer panel gives an elastic

modulus of 78MPa, whilst the stitching region gives an elastic modulus of 304MPa, a factor of 3.9 larger.

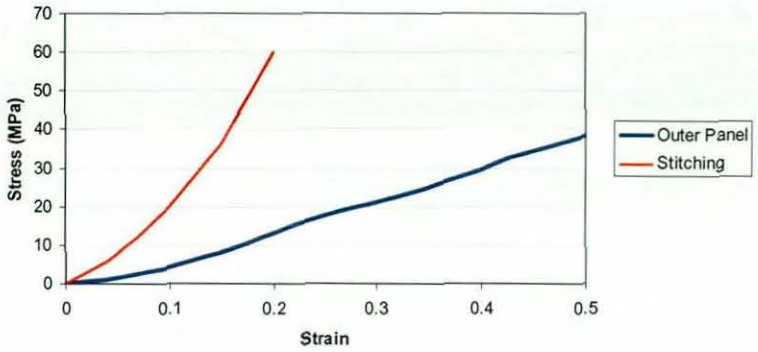

Figure 7.17 Comparison of stress-strain data for a rugby ball (outer panel and stitching region)

7.7.2 Lace Region

The lace region of an American football exists within one of the seams, and is the final process in the manufacture of the ball, joining the final two panels together, once the ball has been turned the "right way out". As well as being a key stage in the manufacturing procedure, the laces also provide an area of grip to the players. The region consists of a single gridcord material, 4.5mm in width and 1.4mm thick, which is laced by the most skilled workers with the ball deflated. Eight evenly spaced holes were inserted into the stitching seam jig to allow the properties of this region to be determined. The lacing region was recreated (Figure 7.18), and testing was carried out to a strain of 0.2, with a crosshead speed of 500mm/min.

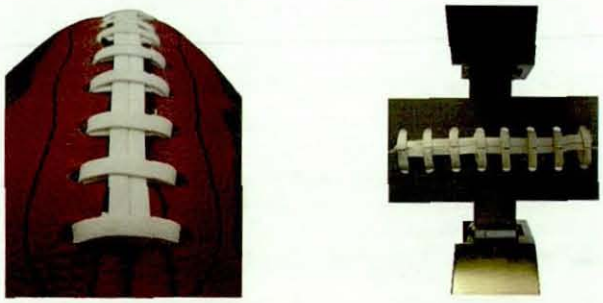

Figure 7.18 a) American football lace region b) Material testing jig

Figure 7.19 depicts the stress strain response of the lace region and allowed comparison with the stitching region within an American football. Results showed that the lace did not fail at a strain of 0.2 and produced a lower stress than the stitching region, 32MPa and 108MPa respectively.

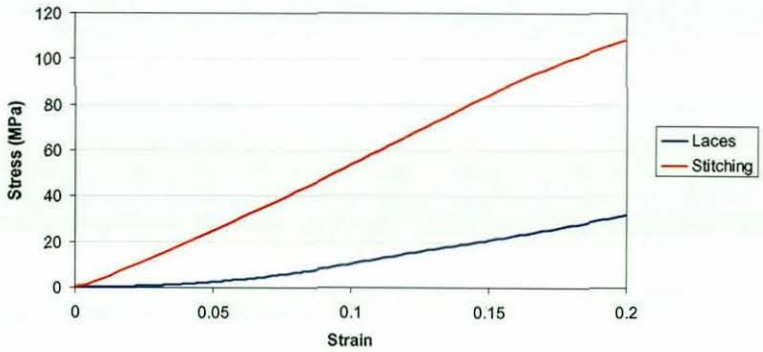

Figure 7.19 Stress strain response of the lace region

Although the lace region produced a lower stress, it also contains a strengthening region with similar stitching to the rest of the ball, which in combination with the laces produced an area of increased stiffness (Figure 7.20).

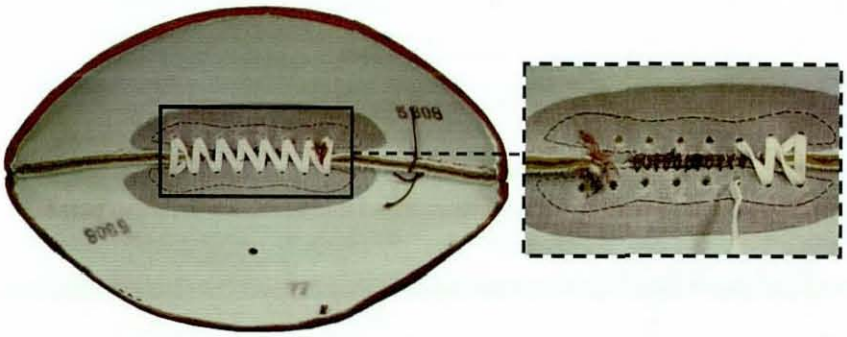

Figure 7.20 Lace region highlighting hidden stitching

7.8 Ovoid Ball Model Production

The discretisation of the surface geometry was based around the octahedron, with the eight faces further discretised into four triangular facets. The simple geometric definition allows a uniform three node triangular shell element mesh to be created. The basic rugby ball model also includes the stitching region defined using four node quadrilateral shell elements.

The four material models for the bladder, outer panel, stitching and laces (American football only) were applied to the ovoid ball models (Figure 7.21), in order to allow correct material definition.

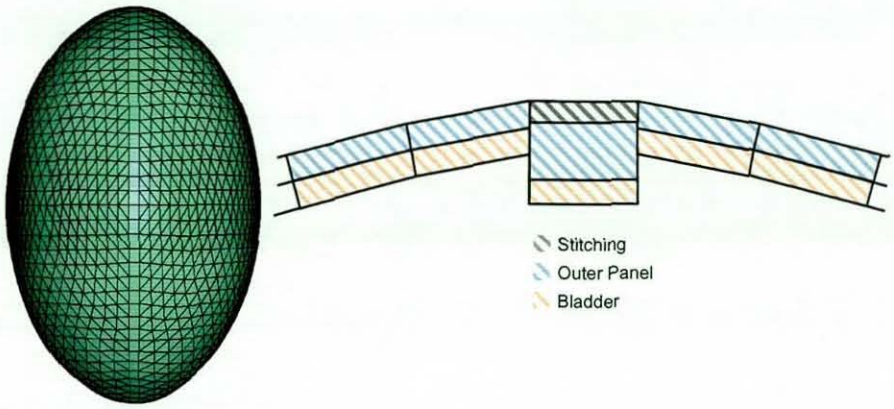

Figure7.21 a) Rugby ball mesh b) Material definition

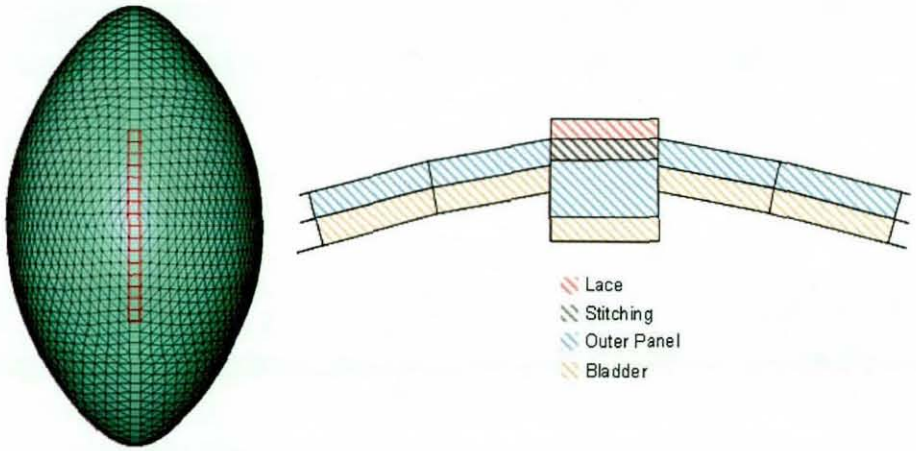

Figure7.21 b) American Football mesh (laces highlighted) b) Material definition

7.8.1 Rugby Ball Valve Modelling

The rugby ball replicated during the FE modelling has a large inflation valve weighing 25g positioned within the seam. It is that stated the increased mass of the valve will improve the flight of the ball, when kicked at a point opposite the valve and on the opposing seam (Webb 1998) (Figure 7.22a). The position and size of the valve was included as it will cause a non-uniform mass distribution within the model. The valve was modelled using a series of triangular and quadrilateral shell elements to represent its size and mass. The valve is constructed from latex and its material properties were defined using the bladder material model. Figure 7.22b) depicts the modelled valve as a series of solid elements in order to portray its size and shape.

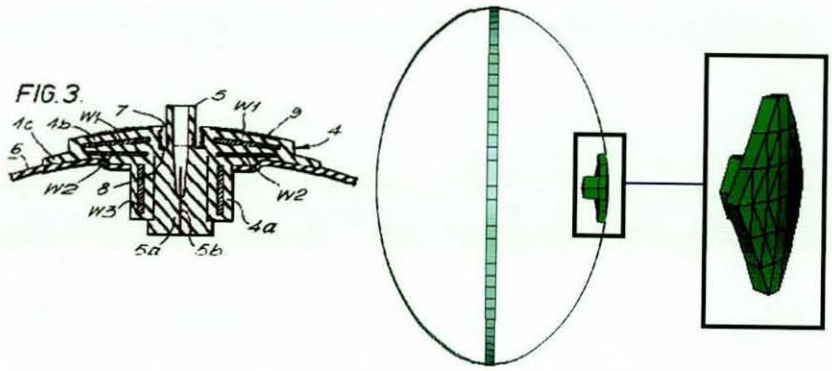

Figure 7.22 a) Over weighted inflation valve b) Mesh representation of valve

7.8.2 Ovoid Ball Model Inflation

It has been shown that inflation of an ovoid ball results in non uniform stress and a volumetric increase, with the introduction of the stitching to the ball producing a higher level of stress in the seam regions (Figure 7.23a). The area representing the valve indicates higher stress levels due to the incorporation of the extra material volume. Lower levels of stress are seen at the end of the ball in comparison to the centre of the panel, which experiences three times the level of stress. Figure 7.23 b) depicts the non uniform volumetric expansion occurring, with the maximum value at the centre of the panel, whilst the minimum occurred at the stitching region. The larger volumetric increase at the centre of the panel was possibly due to the lower stiffness of this region, as well as the non uniform expansion caused by the ovoid geometry.

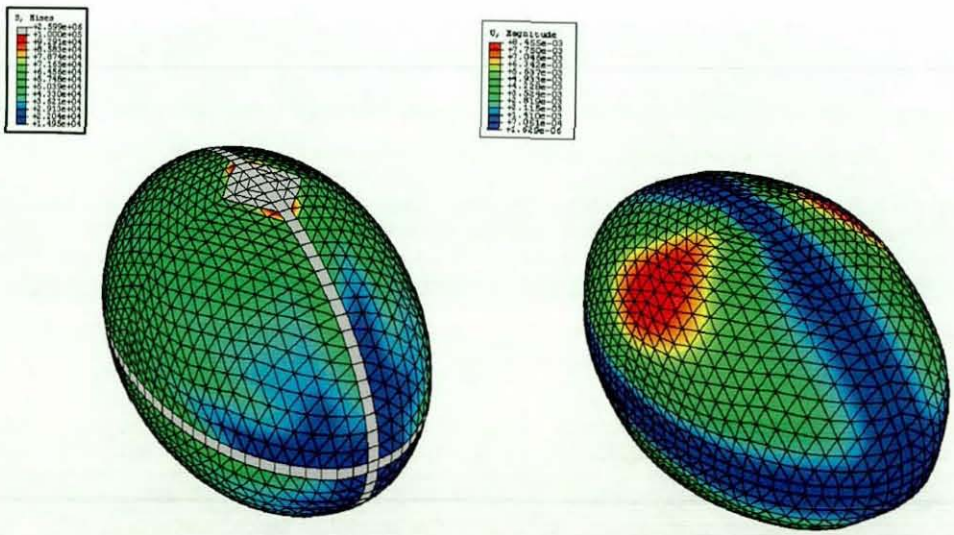

Figure 7.23 a) Stress distribution during inflation b) Volumetric increase

During the inflation of an American football it was noted that the inclusion of the lace and stitching region caused an increased level of stress in these regions, in comparison to the centre of the panel. Previously it was noted that the stitching region also produced non uniform volumetric increase within the rugby ball model, however all seams would show a similar level of increase during inflation as well as stress. An American football has a single set of laces placed within one of the stitching seams, and it was noted that during inflation the lace region would demonstrate a reduction in volumetric increase. The other panels adjacent to the one with the lace region also showed a variation in volumetric increase at the seams, with the seam opposite the lace region demonstrating a greater increase during inflation (Figure 7.24).

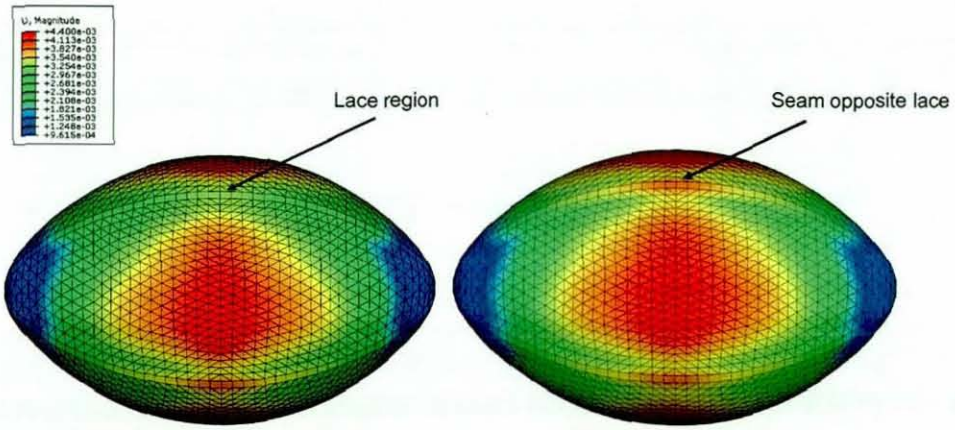

Figure 7.24 Non uniform volumetric increase of the seams during inflation

An experimental procedure was developed to allow the effect of the lace region during inflation to be determined, using the CMM. An American football was mounted in a measurement jig in a similar manner to the procedure used to capture the ball's surface, and the panel opposite the lace region was measured using a grid of forty five points (Figure 7.25). A program was created allowing the points to be automatically measured, with the probe positioned normal to the panel's surface. The ball was inflated to 10, 15, 20, 25, 30, 40 and 50psi and measurements of the surface were taken at each pressure interval. The process was repeated five times, with the ball deflated in between tests to allowed sufficient time for material recovery.

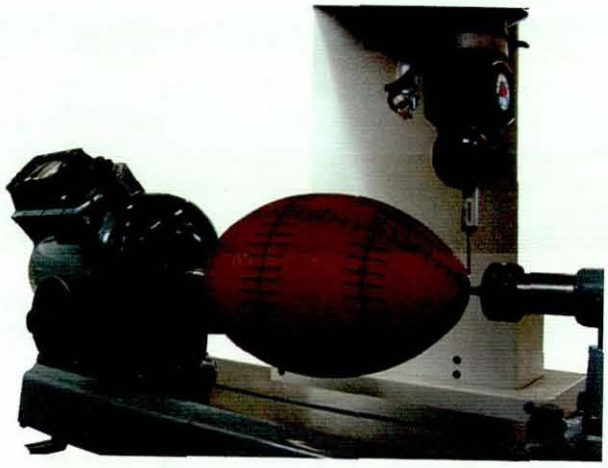

Figure 7.25 CMM used to measure surface change during inflation

The 3D co-ordinates were used to calculate the change in the surface during inflation and Figure 7.26 depicts the measurements taken across the centre of the panel, with the increase calculated relative to the 10psi measurement. The results showed that the maximum increase did not occur at the centre of the panel, but was skewed towards the seam opposite the lace, demonstrated by the FE simulation. The seam opposite the laces increased by 2.5mm when the ball was inflated to 50psi, which was 100% greater than the 1.25mm measured at the seam adjacent to the laces.

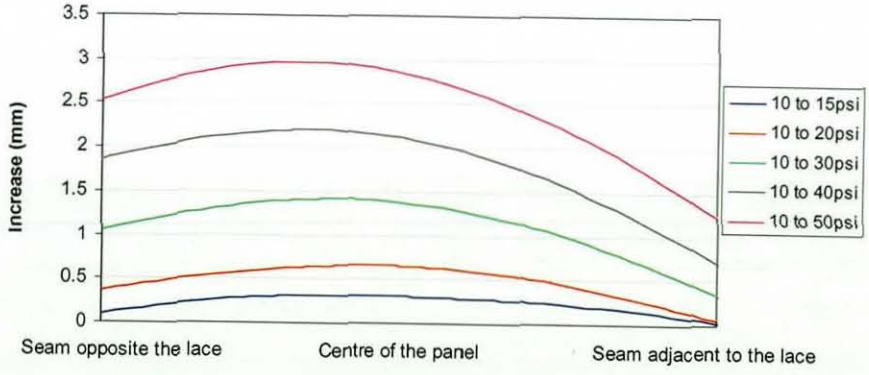

Figure 7.26 Non-symmetrical increase during inflation of an American football

When manufacturing an American football each of the panels are cut to the same size and shape, so that a symmetrical ball can be produced, assuming manufacturing errors are kept to a minimum. Experimental and FE simulation results showed a non uniform volumetric increase due to the lace region, which will cause asymmetry within the ball about the polar axis.

7.8.3 FE Impact Simulations

The rugby ball model was validated using experimental data measured from the rebound, bounce characterisation and high speed impact testing procedures developed in Chapters 3, 4 and 6. The validation is divided into two sections, normal impacts (rebound and high speed impacts) and the oblique impacts (bounce characterisation test)

7.8.3.1 Normal Impacts

Experimental data obtained during the rebound test equates to an inbound velocity of 6m/s, whilst the high speed impact testing relates to an 11 and 25m/s inbound velocity. FE impacts were simulated for end, seam, valve and centre of panel impact positions, and CoR and contact time analysed. As stated in Chapter 6, the non uniform mass and stiffness distribution of the rugby ball does not allow end impacts to be experimentally measured at 25m/s. A maximum velocity of 15m/s was measured during end impacts, and this data will be included in the 11m/s graphs.

Figure 7.27 a) - c) depicts a comparison between experimental and FE simulation contact time and CoR. Contact time decreases with an increase in velocity during experimental testing and was confirmed by FE simulations, which is normal for all sports balls. The FE simulations predict an increase in contact time during end impacts, which agreed with experimental findings. However the simulated contact time was higher than that measured experimentally at 15m/s. An increase in inbound velocity produced little variation in contact time between impact positions, shown during both experimental and FE simulations. The contact time measured during centre of the panel and seam impacts at 25m/s was greater than that measured experimentally, indicating an area of future work.

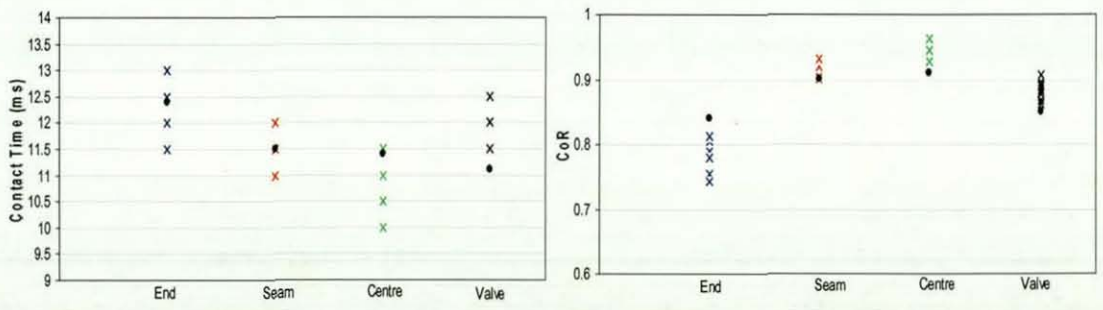

Figure 7.27a) Contact Time and CoR at 6m/s inbound velocity

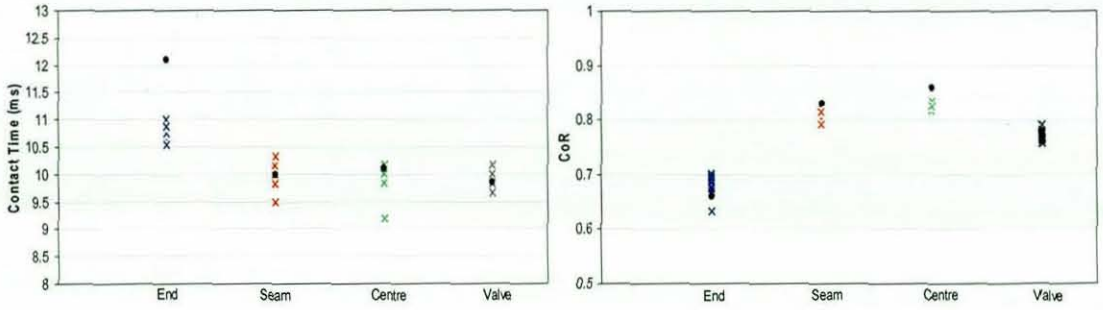

Figure 7.27b) Contact Time and CoR at 11m/s inbound velocity (15m/s – end impact)

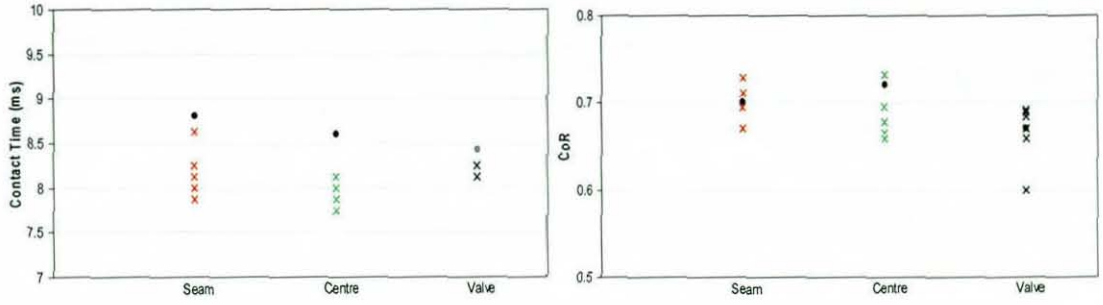

Figure 7.27c) Contact Time and CoR at 25m/s inbound velocity

Impacts involving the end of the ball demonstrate a dramatic reduction in CoR, seen in both FE simulations and experimentally, however the simulated value under estimates the experimental reduction in CoR. At the end of the ball, four seams converge to a single point creating a region of increased stiffness, and possibly damping, causing a reduction in CoR. The introduction of the seam and the valve produced a reduction in CoR irrespective of inbound velocity. The experimental data and FE simulations showed good agreement in this respect, <5% difference. An increased inbound velocity resulted in a reduction in CoR, irrespective of impact position. This may be attributed to the increase in deformation experienced at higher inbound velocities.

Figure 7.28 depicts the increase in deformation with respect to velocity for centre panel impacts. Experimental data and FE simulations showed good agreement, that normal deformation increases with inbound velocity. The level of deformation increased with impact velocity and this was attributed to the higher levels of energy within the ball prior to contact with the plate. Higher levels of deformation were experienced during seam impacts for both experimental and FE simulation data, irrespective of velocity. Lower

contact times measured during centre of the panel impacts may be attributed to the lower levels of deformation.

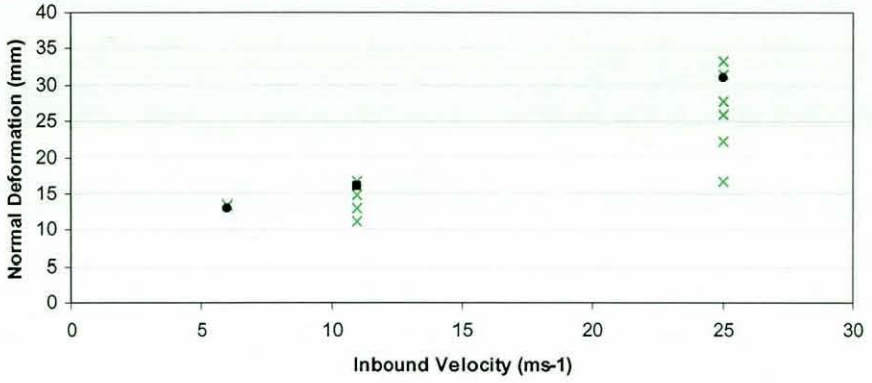

Figure 7.28 Comparison between experimental and FE simulation deformation data

The effect of valve weight can clearly be seen during a high speed impact, where the increased mass of the valve almost acts as a separate body during the impact phase. During a seam impact, the ball contacts the rigid plate directly opposite the valve. As the ball begins to leave the plate, the valve briefly travels in the opposite direction to the rest of the ball, causing an inversion within the panel. The asymmetrical deformation is depicted in Figure 7.29a). The valve then accelerates to a velocity higher than the rest of the ball, resulting in an elongation, producing visible ball oscillations.

Asymmetrical deformation was also produced during centre of the panel impact at high velocities, as the valve causes an inversion within the panel. Depending upon its position, the valve will produce an upwards or downwards deformation, during a centre of the panel impact. The level of deformation was lower than that experienced during a seam impact, due to the off-centre position of the valve, Figure 7.29 b). During a valve impact the ball elongates as the ball leaves the plate caused by the lower acceleration of the valve in comparison to the rest of the ball, Figure 7.29 b).

A comparison between qualitative deformation seen during a 25m/s impact for experimental and FE simulations is depicted in Figure 7.29. FE simulation and experimental results showed a good agreement with similar modes of deformation visible during the various impact positions.

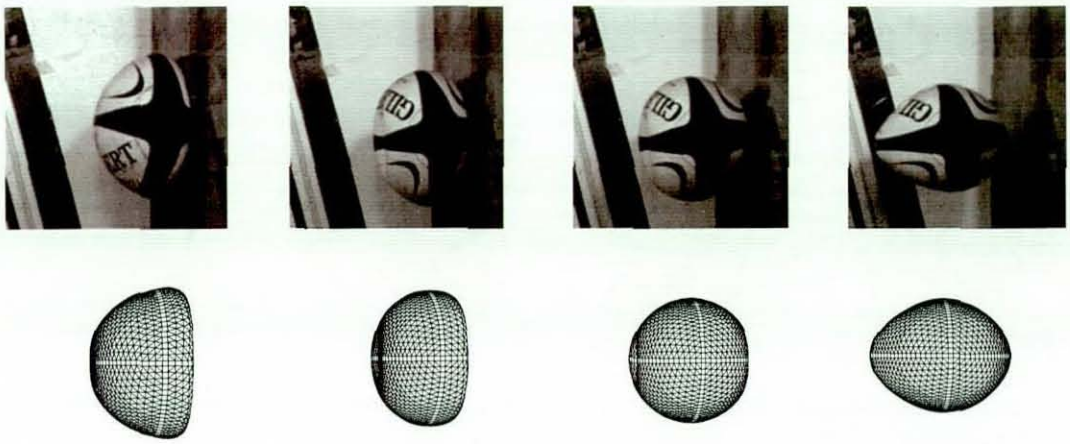

Figure 7.29 a) Qualitative comparison of a seam impact at 25m/s

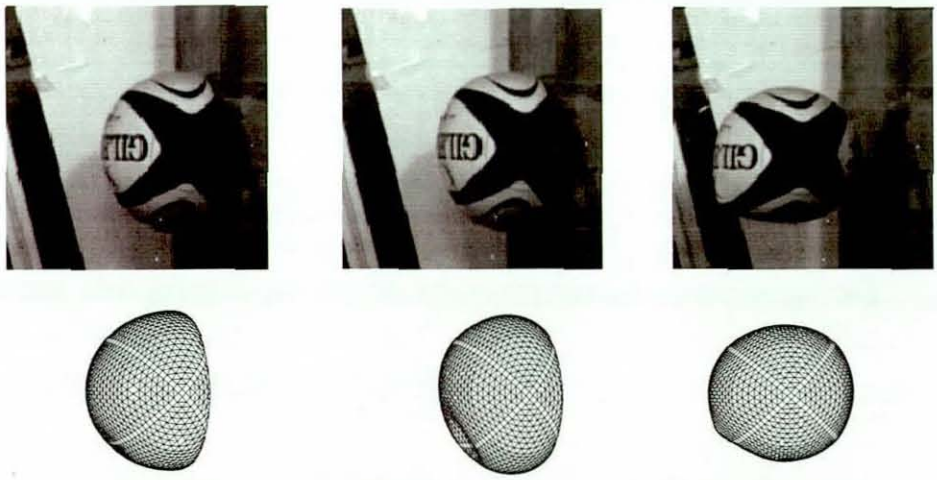

Figure 7.29 b) Qualitative comparison of a centre of the panel impact at 25m/s

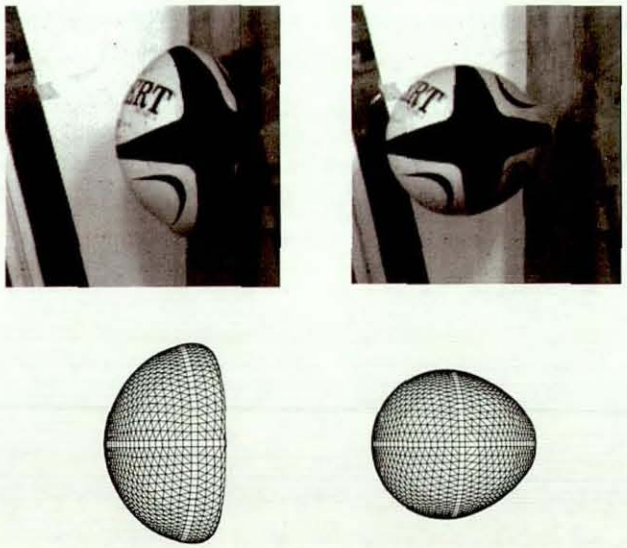

Figure 7.29 c) Qualitative comparison of a valve impact at 25m/s

The ball oscillations visible during testing and FE simulations have been measured in order to allow a direct comparison. Image Pro Plus was used to measure the position of the leading edge of the ball after contact with the plate during a seam and valve impact. The data was used to calculate the velocity of this part of the ball. Measurements were taken at 1.25ms time intervals.

The velocity of the relative node within the ball mesh was exported from the simulation allowing direct comparison between experimental and simulation testing (Figure 7.30). It can be seen that the simulation and experimental measurements show good agreement both for frequency and magnitude.

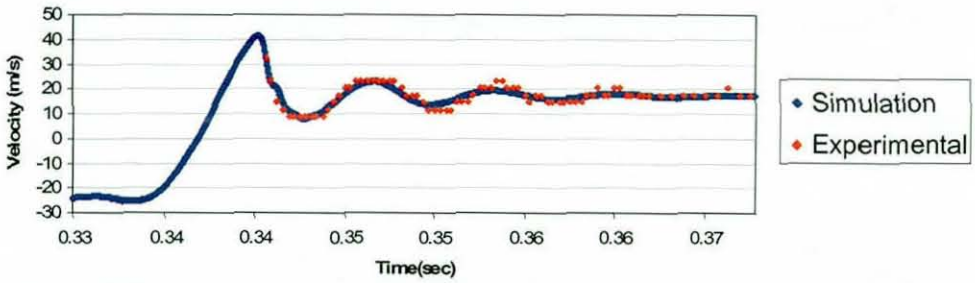

Figure 7.30 a) Comparison of leading edge velocities during valve impact (25m/s)

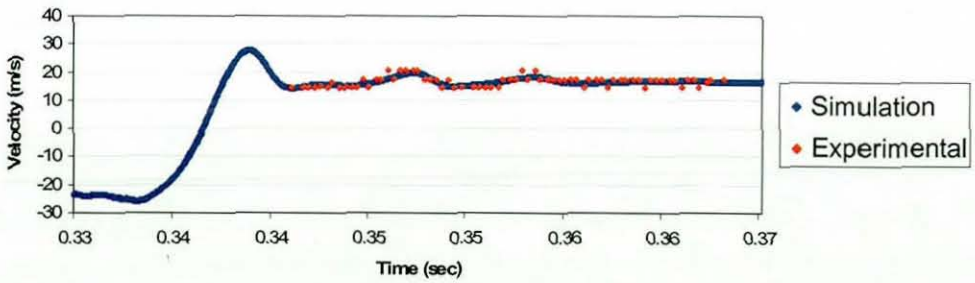

Figure 7.30 b) Comparison of leading edge velocities during seam impact (25m/s)

7.8.3.2 Increase in End Damping

End impact simulations shown in Figures 7.27 a – b) do not demonstrate good agreement with the experimental data for the measured value of CoR and contact time at 6 and 15m/s respectively. It has been noted that the meeting of four panels at a single vertex produces an area of increased stiffness and damping. An area of increased damping was applied to a number of elements within the end of the ball, highlighted in Figure 7.31 and the simulations repeated.

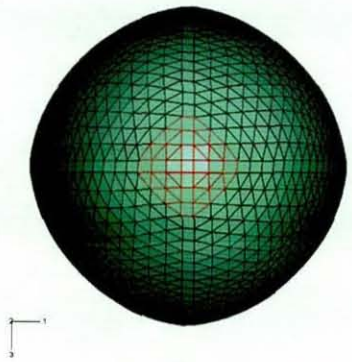

Figure 7.31 Area of increased damping

Results for the simulations with increased damping are shown in Figure 7.32.

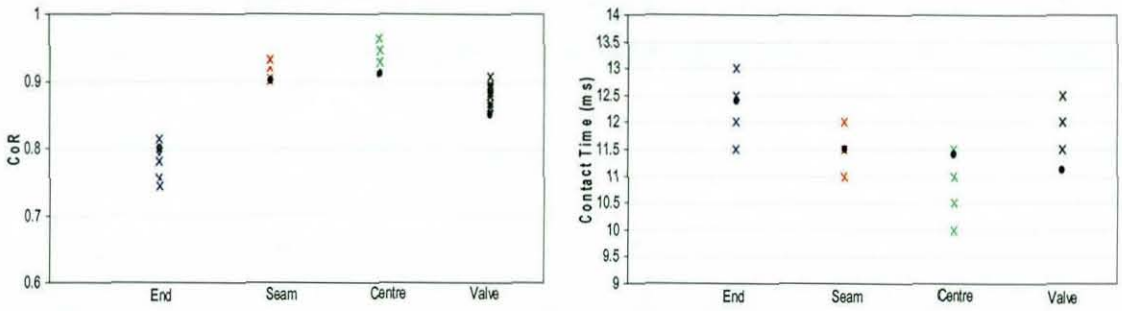

Figure 7.32a) Contact Time and CoR at 6m/s inbound velocity (end damping)

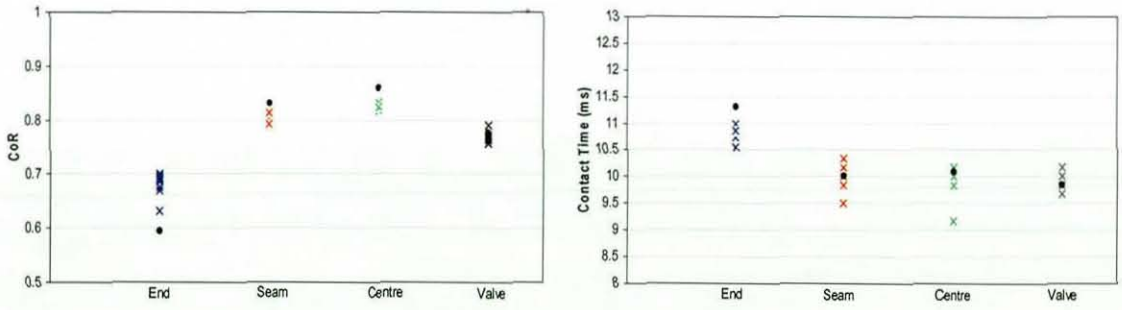

Figure 7.32) Contact Time and CoR at 15m/s inbound velocity (end damping)

The end impact simulation with increased end damping at 6m/s, showed a good agreement with the experimental results. However the CoR measured during the 15m/s end impact was underestimated, whilst the contact time at 15m/s was overestimated. The inclusion of the area with an increased level of damping also has a dramatic effect on the computational time. Gibbs (2007) stated that the time taken to process a job is roughly dependant upon the number of degrees of freedom to be solved in each increment and the number of increments to be solved. The solver automatically limits the size of the

time increment, based on the stable time (Δt) of the model. This is fundamentally the shortest time taken for a stress wave to propagate across any of the elements, and is based on the stiffness, size and damping (Equation 7.3).

$$\Delta t = \min\left(Le\sqrt{\frac{\rho}{\hat{\lambda} + 2\hat{\mu}}} \right)$$

$$\hat{\lambda} = \lambda_0 = \frac{\upsilon E}{(1+\upsilon)(1-2\upsilon)}$$

$$\hat{\mu} = \mu_0 \frac{E}{(1+\upsilon)}$$

Equation 7.3 Equation to calculate stable time (Δt)

Le is defined as the characteristic length associated with an element (in an un-damped material this is the shortest side), ρ is the density, υ is the Poisson's ratio, E is the Elastic modulus, whilst $\hat{\lambda}$ and $\hat{\mu}$ are the Lamé's constants.

In order to avoid a dramatic drop in the stable time increment, the stiffness proportional damping factor, β_R, should be less than or of the same order of magnitude as the initial stable time increment without damping (ABAQUS 2005b). The introduction of the area of increased damping has resulted in a reduction in the stable time increment ($9.946e^{-7}$ to $1.115e^{-7}$), and hence a greater time for the simulation.

The deformation visible during testing and simulation of an end impact at 15m/s is depicted in Figure 7.33. During experimental testing the ball exhibits 'concertina' buckling, with a reduction in diameter at the point of contact, in comparison to the simulation, which demonstrates a softer response. The concertina buckling is likely to be caused by the effects of anisotropy within the woven fabric, and highlights the need for an anisotropic FE model.

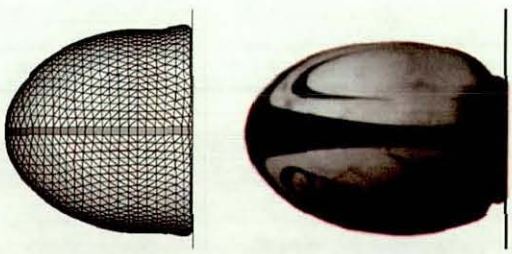

Figure 7.33 Deformations at 15m/s

7.8.3.3 Oblique Impacts

The bounce of a rugby ball was examined in Chapter 4, using the developed ball bounce characterisation test, and simulations recreating the effect of valve position and ball orientation have been developed (Figure 7.34). The effect of changing the original ball orientation pre-impact is detailed in Figure 7.35, and compares measurements for the spin rate, elevation angle and CoR.

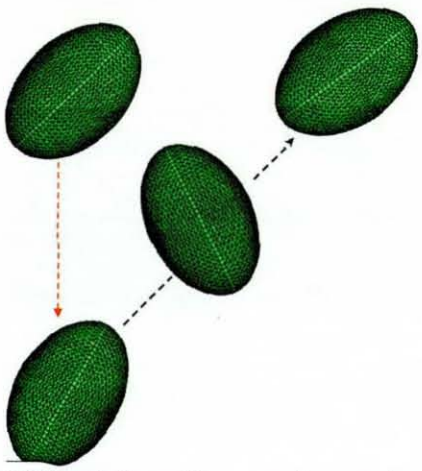

Figure 7.34 Simulation of bounce characterisation test

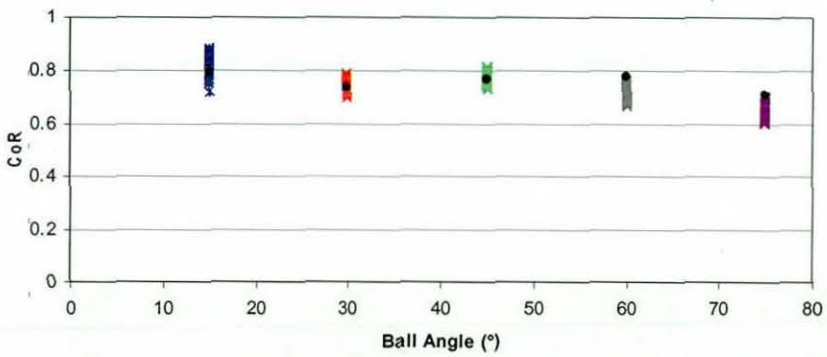

Figure 7.35a) CoR

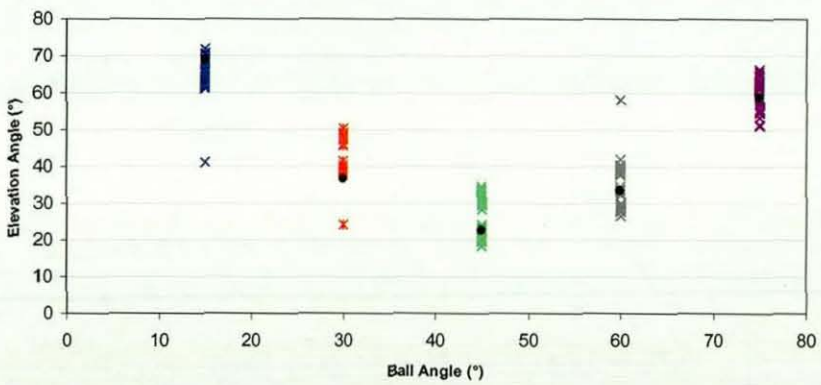

Figure 7.35b) Elevation angle

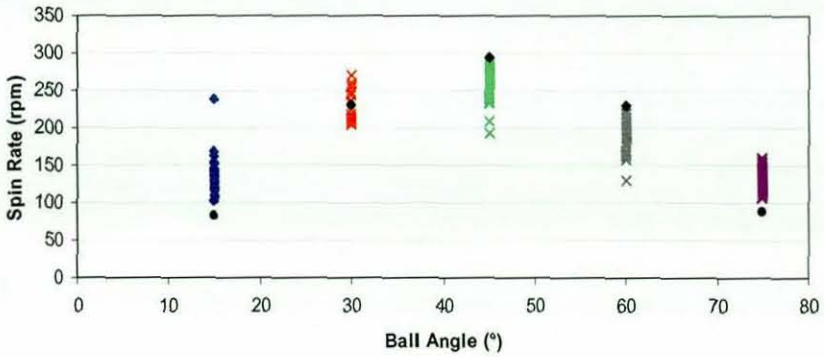

Figure 7.35c) Spin rate

Experimental and simulation results showed good agreement for elevation angle, spin rate and CoR. The elevation angle after impact showed the U shaped trend measured during experimental testing, whilst the simulations confirmed an inverted U shaped trend when measuring spin rate.

Experimental findings in Chapter 4 showed that off-centre valve impacts, (right and centre of the panel impacts) result in an increased deviation angle. Simulations were computed with a 45° ball orientation angle pre-impact (Figure 7.36)

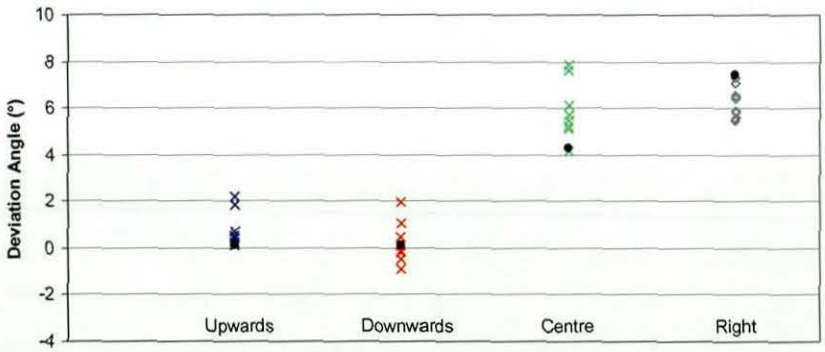

Figure 7.36 Simulation and experimental deviation during bounce characterisation test

Again simulation results showed good agreement with the experimental data with the deviation angle increasing during centre of the panel and valve right impacts. The measurement of deviation angle during a centre of the panel impact was half the value measured during a valve right impact.

Experimental results showed that the elevation angle and the spin imparted onto the ball varied when the valve was placed upwards or downwards pre impact. This effect was also

demonstrated within the simulation with an increase of 20.7% (7.0°) in elevation angle, and a decrease of 20.3% (40rpm) during a valve upwards impact.

7.9 Conclusions

This chapter has detailed the procedure for creating a FE model of a manually stitched ovoid ball. A procedure has been established to capture the geometry of the ball, discretise the surface and create a mesh that exhibits rotational symmetry and simple geometric definition. Three node triangular shell elements have been used in the creation of the FE model as they are computationally efficient in comparison to solid elements. Shell elements are applicable where the thickness is no more than 10% of other dimensions, and as the ratio of ball width to panel thickness is 1/62, making shell elements an appropriate choice for ovoid ball modelling. Hydrostatic fluid elements have been coupled with the shell elements to allow for pressurisation in the model.

The non spherical nature of an ovoid ball resulted in a non-uniform stress and volumetric increase during the process of inflation, and it was shown that the greatest volumetric increase occurs at the centre of the panel. Experimental assessment of the stitching region showed that the stitching seam was around four times stiffer than the outer panel material. Inclusion of the stitching region in the FE model resulted in an increase in stress levels within this region during inflation. After the inclusion of the stitching region and the valve a reduction in volumetric increase was noted, although the expansion now had a non-uniform distribution, which was attributed to the non uniform stiffness.

The inclusion of the lace region within an American football results in a non-uniform stiffness within the four seams, causing a non-uniform volumetric increase. FE simulation and experimental results showed that the laces affected the expansion of every seam during inflation, with the seam opposite the laces demonstrating the maximum increase. The non-uniform expansion results in an asymmetric American football.

The inclusion of the weighted valve and stitching region within the FE rugby ball model has increased stiffness in comparison to the centre of the panel. This resulted in a reduction in CoR during impacts irrespective of inbound velocity. It was also noted that impacting the stiffer regions of the ball resulted in an increase in contact time during low

velocity impacts. Non uniform deformation was experienced during high speed impacts irrespective of impact position, due to the over weighted valve.

FE simulations and experimental data showed good agreement for CoR, contact time and deformation for all impact positions and inbound velocities, although an increase in damping was needed to accurately predict the CoR measurement during low speed end impacts. This increase in damping dramatically affected the stable time increment.

Simulation of the ball bounce characterisation test in Chapter 4 showed good agreement with the experimental findings. Simulation results confirmed the U shaped trend for elevation angle, and inverted U trend for spin rate, dependant upon ball orientation angle pre impact. Simulations with the valve placed off-centre (centre of the panel and valve right) indicated an increase in deviation angle shown in experimental results. Adjusting the centre of mass of the ball, by placing the valve upwards or downwards, resulted in variation of elevation angle and spin rate measured during experimental testing.

The 'concertina' buckling effect visible during high speed end impacts was not apparent within the isotropic FE model. The nature of this deformation is believed to occur due to the anisotropic nature of the woven fabric within the outer panel. This, along with the need for applying extra damping within the end of the ball, highlights the need for an accurate anisotropic rugby ball FE model.

Chapter 8

Development of Anisotropic Stitched Ovoid Ball

8 Introduction

The following chapter details the development of an anisotropic FE stitched ball model, consisting of a latex bladder, outer panels and stitching regions to represent the seams. Since the 'concertina' buckling effect visible during high speed end impacts was not apparent within the isotropic FE model, Chapter 7, it was decided to investigate if the nature of this deformation was due to the anisotropic nature of the woven fabric within the outer panel. Material anisotropy was determined through a series of directional tensile tests at various incremental stages from the principle material orientation to the bias (45°).

8.1 Material Model Production

8.1.1 Material Testing

The woven fabric incorporated into the construction of the outer panel has material properties dependent upon the direction of strain. The outer panel was subjected to a series of directional tensile tests in order to enable the effect of the material anisotropy to be determined. Specimens were prepared at 15° increments from 0 to 90°, as depicted in Figure 8.1, and tensile tests were carried out at a strain rate of 500mm/min, to a maximum strain of 0.6 with five repeats per material orientation.

Figure 8.1 Material samples allowing anisotropic effect of woven fabric to be analysed

Figure 8.2 depicts the average strain-strain response of the outer panel material at the different material orientations.

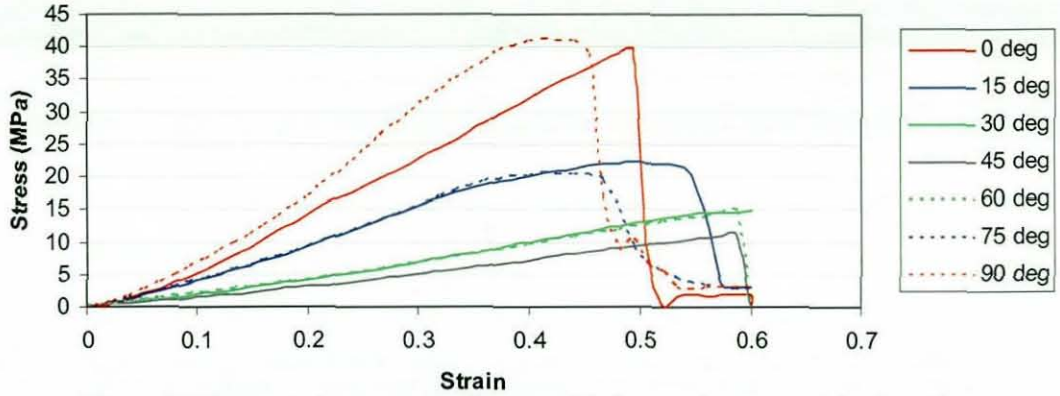

Figure 8.2 Stress-strain response of woven fabric at various material orientations

Results showed a maximum stiffness of the outer panel during straining of the material at 0 and 90°, whilst the greatest reduction in stiffness was measured at a 45° fibre orientation. Material failure was noted during the straining of samples at 0, 15, 75 and 90°, whilst samples at 30, 45 and 60° did not fail when strained to a maximum value of 0.6. The stiffness values measured at 30 and 15° were similar to those measured at 60 and 75° respectively, which was attributed to the fact that they are at the same angle relative to one of the two principle fibre orientations.

8.1.2 FE Material Model

The results from the tensile tests were used to calculate the Elastic Modulus of the material at the various fibre orientations. In order to simplify the production of the material model, it was assumed that the material stiffness was similar at 0 and 90°, and the ABAQUS Lamina material model was used to define the anisotropic material behaviour (Figure 8.3).

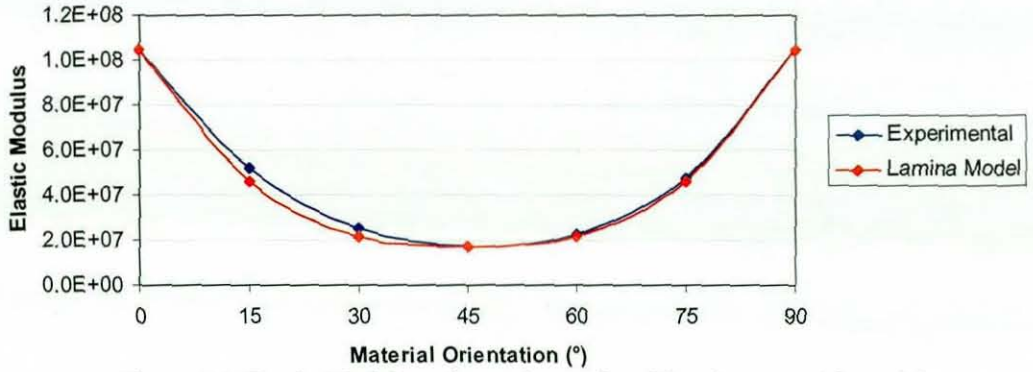

Figure 8.3 Elastic Modulus of experimental and Lamina material model

8.2 Model Production

The anisotropic FE model was created using the same discretised surface used for the creation of the isotropic model in Chapter 7. The simple geometric definition allowed a uniform three node triangular shell element mesh to be created, which included the stitching region defined using four node quadrilateral shell elements. Isotropic material models were defined for the bladder, valve and stitching region, whilst the outer panel was defined using the anisotropic Lamina material (Figure 8.4).

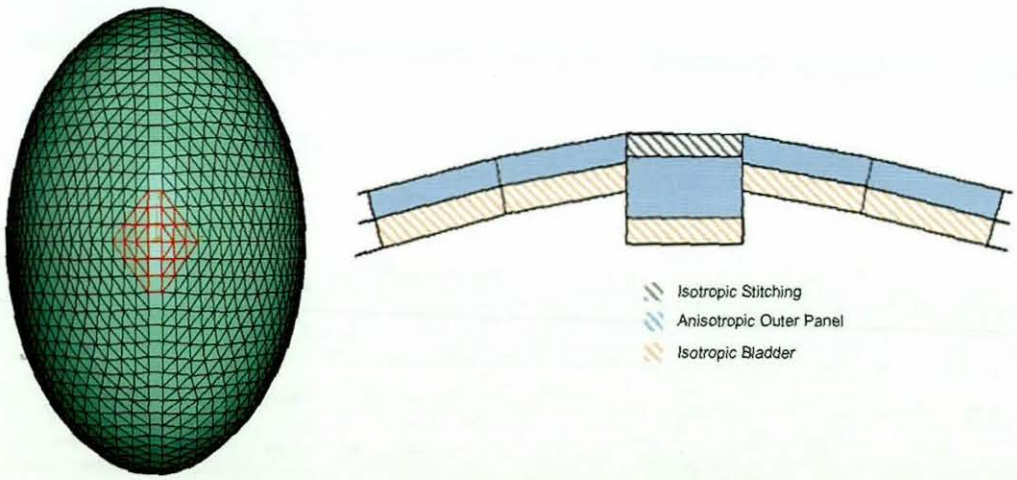

Figure 8.4 Mesh with highlighted valve region and material definition

8.3 FE Impact Simulations

The dynamic characteristics of the model were validated using experimental data measured from normal impacts at velocities from 6 – 25m/s. The validation examined the CoR and contact time for impacts on the end, centre of panel, valve and seam (Figure 8.5 a – c). No data was provided for end impacts at 25m/s as the non-uniform stiffness within the RGB 1 ball caused rotation prior to impact with the plate, resulting in an inconsistent impact position.

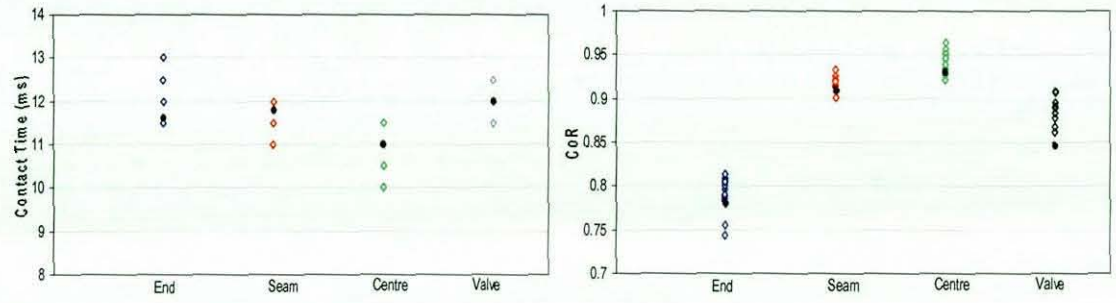

Figure 8.5a) Contact Time and CoR at 6m/s inbound velocity

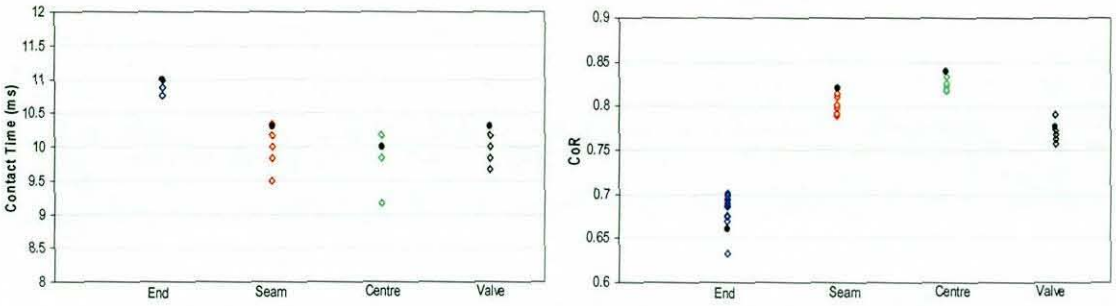

Figure 8.5b) Contact Time and CoR at 11m/s inbound velocity (15m/s – end impact)

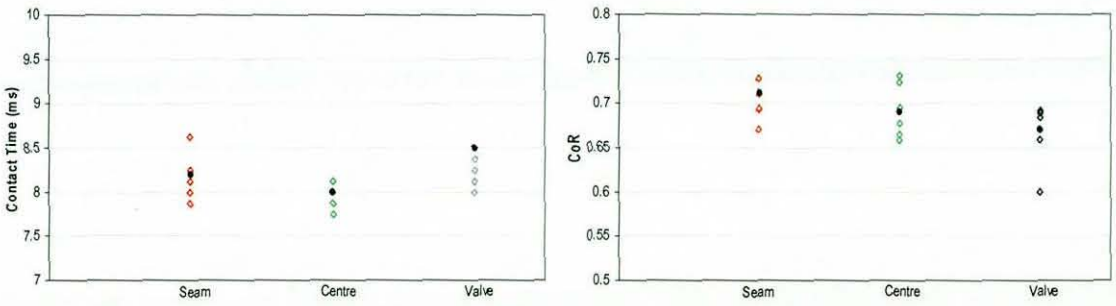

Figure 8.5c) Contact Time and CoR at 25m/s inbound velocity

X Experimental ● Simulation

Figures 8.5 a - c) depict that contact time decreases with an increase in velocity during experimental testing and this effect was also demonstrated by the anisotropic FE simulations. The regions with a high level of stiffness, the end and seam, showed an increased contact time in comparison to the centre of the panel impact.

Impacts involving the end of the ball resulted in a dramatic reduction in CoR, seen in both FE simulations and experimentally. The introduction of the seam and the valve produced a reduction in CoR irrespective of inbound velocity. The experimental data and FE simulations showed good agreement in this respect, <5% difference. An increased inbound velocity resulted in a reduction in CoR, irrespective of impact position. This

may be attributed to the increase in deformation and energy losses experienced at higher inbound velocities.

During Chapter 7 the non-uniform deformation caused by the valve was demonstrated during high speed impacts. During a seam impact as the ball begins to leave the rigid plate, the valve briefly travels in the opposite direction to the rest of the ball, depicted in Figure 8.6. This effect is also demonstrated in the anisotropic FE model.

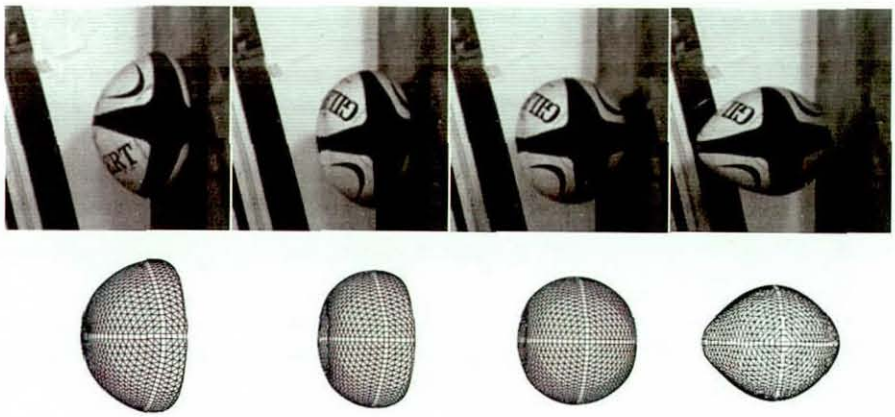

Figure 8.6 Qualitative comparison of a seam impact at 25m/s

Asymmetrical deformation was also produced during centre of the panel and valve impacts at high velocities (Figure 8.7). The anisotropic simulation showed good agreement with the experimental testing, with the valve producing increased deformation. During a valve impact, the valve leaves the plate with a lower acceleration, due to its increased mass, causing an elongation. This effect was demonstrated by the anisotropic model (Figure 8.7 b)

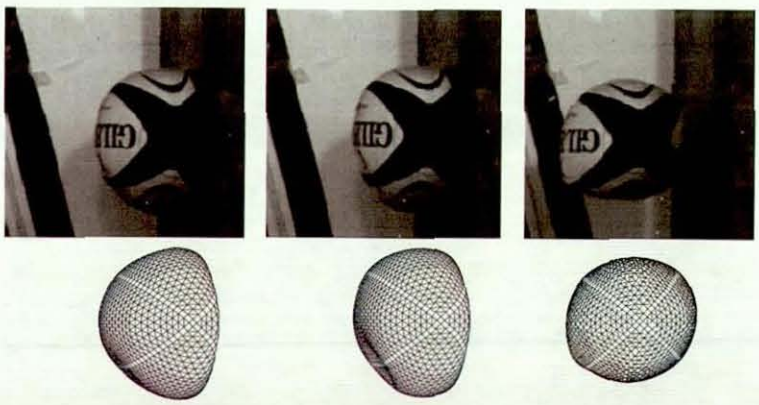

Figure 8.7a) Qualitative comparison of a centre of the panel impact at 25m/s

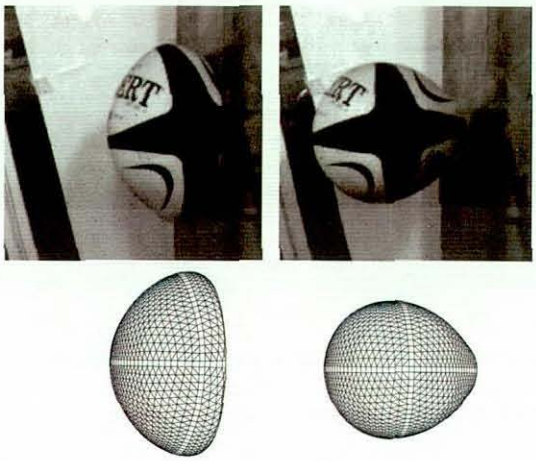

Figure 8.7b) Qualitative comparison of a valve impact at 25m/s

Chapter 7 detailed the 'concertina' buckling effect visible during high speed end impacts, which was not apparent within the isotropic FE model. This deformation was believed to occur due to the anisotropic nature of the woven fabric within the outer panel. The use of the Lamina material model within the anisotropic FE model allowed the directionality of the material to be defined, and Figure 8.8 depicts the concertina buckling effect visible during high speed end impacts. The levels of deformation demonstrated by the FE simulation are similar to those seen experimentally.

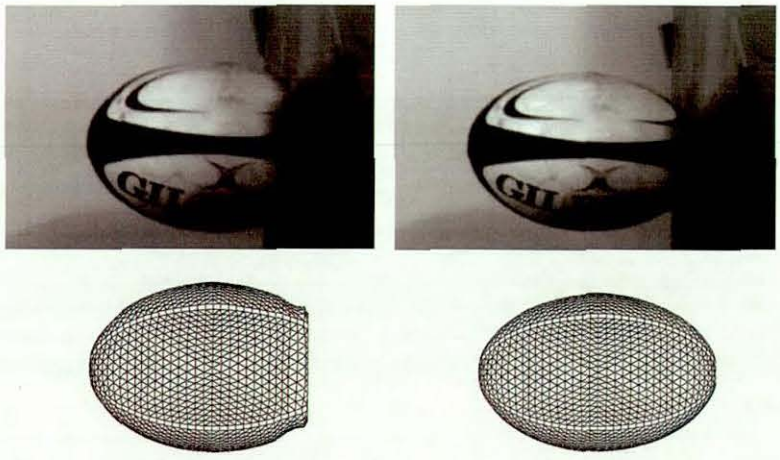

Figure 8.8 Qualitative comparison of an end impact at 15m/s

Figures 8.9 a - b) depict the deformation measured in the normal and tangential directions during high speed impacts. The centre impact produced a lower level of normal and tangential deformation during impacts at 11 and 25m/s, and the FE simulation showed good agreement with the experimental data. The increase in velocity

produced a greater amount of normal and tangential deformation for all impact positions.

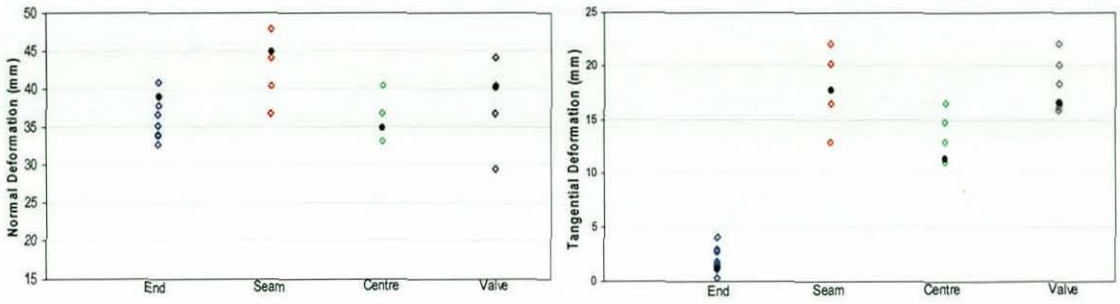

Figure 8.9a) Normal and tangential deformation at 11m/s inbound velocity (15m/s – end impact)

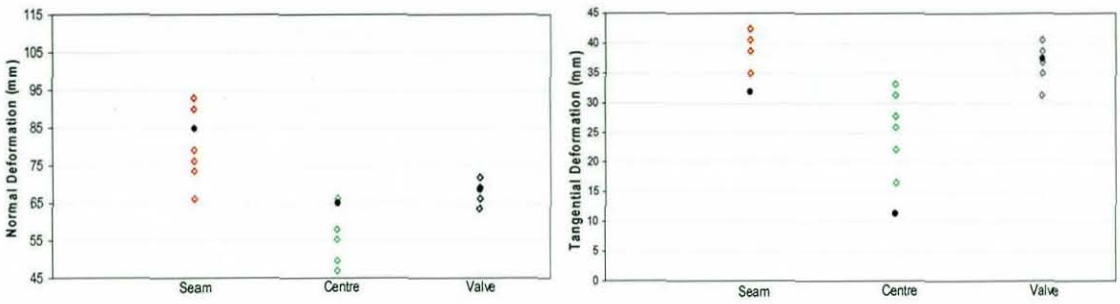

Figure 8.9b) Normal and tangential deformation at 25m/s inbound velocity

◇ Experimental ● Simulation

During an end impact at 15m/s the ball produced a high level of normal deformation, 36mm, whilst the tangential deformation was minimal, 2mm. This effect was also demonstrated by the FE simulation. The minimal expansion tangentially suggests that the ball was buckling, snapping through and inverting (Figure 8.10).

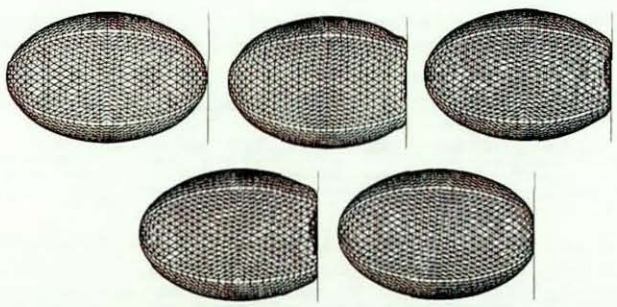

Figure 8.10 Deformation during end impact at 15m/s

The ball surface oscillations visible during experimental testing were measured in order to allow a direct comparison between experimental and FE simulations. Figure 8.11 a) depicts the velocity of the point opposite the contact point during a seam impact at 25m/s, and shows good agreement with the experimental data. It was noted from experimental results that oscillations would occur during all impact positions except for an end impact, during which the ball would deform and recover quickly with very little oscillation. A comparison between the experimental and simulation oscillations during end impacts can be depicted in Figure 8.11b).

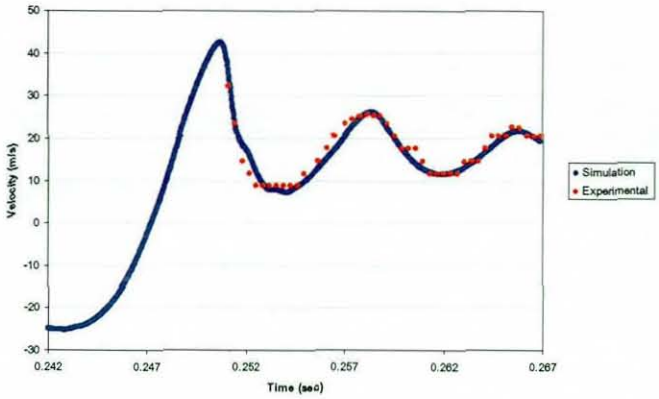

Figure 8.11a) Oscillation during a seam impact at 25m/s

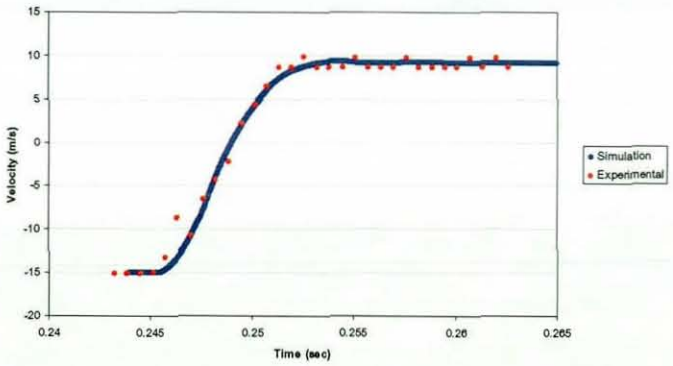

Figure 8.11b) Simulation and experimental oscillation during end impact at 11m/s

Figure 8.12 compares the ball oscillations during the FE simulation of a seam, valve and end impact. The pre impact velocity was 11m/s for the seam and valve impacts, and 15m/s for the end impact, with the maximum and minimum oscillations post impact measured during seam and end impacts respectively. The oscillations during the seam impact were caused by the movement of the valve positioned opposite the point of impact.

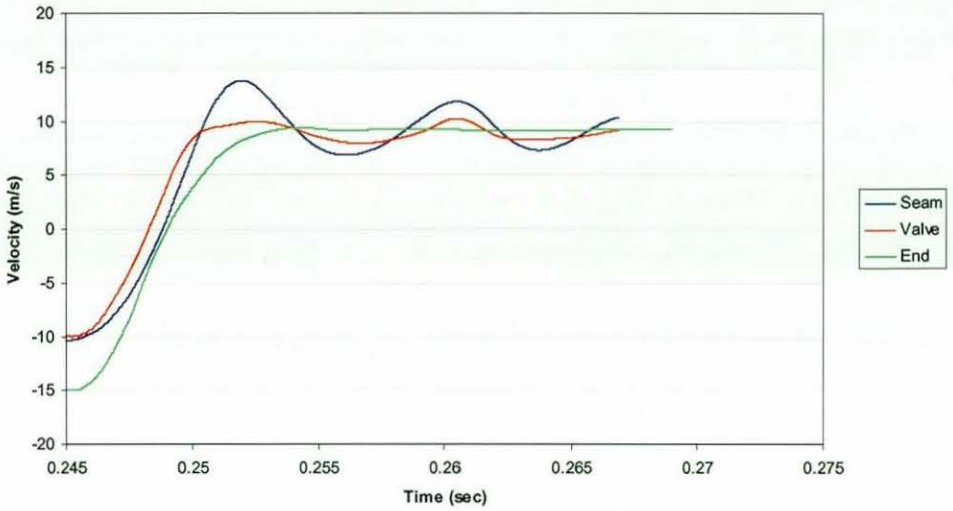

Figure 8.12 Oscillations during high speed impacts

A Fast Fourier Transform (FFT) was used to determine the frequency of the oscillations within the ball during the different impact positions, at 11m/s. It was found that the seam and valve impacts are oscillating at 125Hz with a 16% increase in magnitude for the seam impact in comparison to the valve. The increase in magnitude may be attributed to the higher levels of deformation, caused by the movement of the valve, during the seam impact, or the increased levels of damping in the valve region. Analysis of high velocity impacts, 25m/s, noted a frequency of 130Hz which was similar to that value determined at 11m/s, which suggests that the natural vibration of the ball occurs at a frequency of 125 – 130Hz. Ronkainen and Harland (2007) analysed the dynamic response to two soccer balls using a Scanning Laser Doppler Vibrometer. The authors noted that the first model frequency of the soccer balls occurred at 150Hz which is a similar frequency to those measured during the rugby ball oscillations.

8.4 Conclusions

FE simulations and experimental data showed good agreement for CoR and contact time for all impact positions and inbound velocities. The inclusion of the material anisotropy caused by the woven fabric used in the outer panel caused a reduction in CoR during FE simulated end impacts, without having to increase the level of damping.

It was possible to model the 'concertina' buckling effect visible during high speed end impacts with the inclusion of the material anisotropy within the woven fabric. The normal and tangential deformation measured during FE simulations showed good agreement with experimental findings. Tangential deformation was minimal during a high

speed end impact and this effect was demonstrated within the FE simulations, which suggests that the ball was "snapping through" and inverting, visible within the FE simulation. Once the ball had left the plate, there was minimal oscillation, unlike seam, valve and centre of panel impacts.

Analysis of the oscillations occurring post impact demonstrated a good agreement between experimental and FE simulation data. Results show that during an end impact, the deformation seen in the ball will recover very quickly with little oscillation. Analysis of the oscillations, using an FFT, determined that the ball oscillates at a frequency of 125-130Hz irrespective of impact position and inbound velocity, with the magnitude of the oscillations during a seam impact increasing by 16% in comparison to a valve impact. The increased magnitude may be attributed to the increased deformation, caused by the movement of the valve, during the seam impact, or the higher damping levels within the impact region during a valve impact.

The anisotropic FE simulation accurately predicts the CoR, contact time and deformation visible during experimental testing. As a result it can be used to predict the dynamic behaviour of a rugby ball during various impact scenarios.

Chapter 9

Ovoid Ball Rotation

9 Introduction

It has been demonstrated in Chapter 5 that players are capable of imparting high levels of spin onto the ovoid ball during a number of game related situations. Due to the non-spherical nature of the ball, different types of spin can be imparted depending upon the principal axis of rotation, with rifle axis spin imparted about the polar axis, and tumble axis spin about an equilateral axes. This chapter details the procedures created to determine the moment of inertia of an ovoid ball about each of its principal axes, and details the effect of rotation on the performance of the ball.

9.1 Moment of Inertia

The moment of inertia of a body determines its angular acceleration when it is subjected to a moment, defined by Equation 9.1, where r is the perpendicular distance of the mass dm from the axis of rotation.

$$I = \int r^2 dm$$

Equation 9.1 Moment of inertia

During rotation the moment of inertia can be described as a body's resistance to change in rotational velocity due to the radial distribution of mass around an axis of rotation.

An object will have different moments of inertia for each of its axes of rotation, unless the object is symmetric about all axes. The moment of inertia tensor describing all moments of inertia of an object with one quantity, can be defined by Equation 9.2.

$$I = \begin{bmatrix} I_{xx} & I_{xy} & I_{xz} \\ I_{yx} & I_{yy} & I_{yz} \\ I_{zx} & I_{zy} & I_{zz} \end{bmatrix}$$

Equation 9.2 Moment of inertia tensor

During rotation about the principle axes the moments of inertia are defined as I_{xx}, I_{yy} and I_{zz}. A rigid body with two and three identical moments are defined as a symmetrical top and a spherical top respectively. The principle axes of a prolate spheroid are illustrated in Figure 9.1.

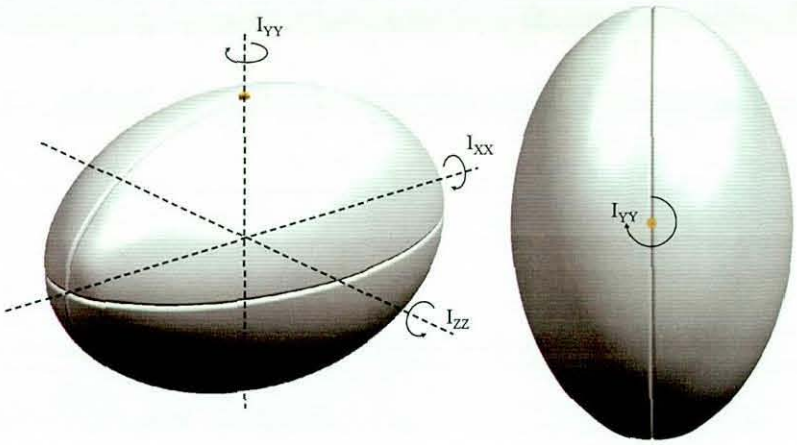

Figure 9.1 Principle axes of rotation

I_{yy} and I_{zz} define the moments of inertia of the prolate spheroid for a rotation about an equilateral axes which should be equal, similar to a symmetrical top. However the majority of ovoid balls have a non uniform distribution of mass due to the inclusion of an inflation valve and laces (American football and Australian Rules football), causing an increase in I_{zz}. During play, rotation about the equatorial axis is most commonly seen during a place, drop or end over end kick and is described as tumble axis spin.

I_{xx} defines the moment of inertia of the prolate spheroid about its polar axis. Due to the geometric properties of a prolate spheroid, the moment of inertia is considerably lower than I_{yy} or I_{zz}. During play, rotation about the polar axis will be seen during a spin pass or spiral kick and is described as rifle spin.

Brancazio (1987) assumed that the shape of an American football was similar to that of a prolate spheroid, with uniform mass distribution meaning that I_{yy} was equal to I_{zz}. Using the equations for a solid homogenous ellipsoid, the author derived equations to represent the moments of inertia about the polar and equilateral axes for a thin walled ellipsoid (Equations 9.3 and 9.4).

$$I_{xx} = \frac{8\pi\rho b^3 t(4a+b)}{15}$$

ρ – density
a – radius of equilateral axis
b – radius of polar axis
t – wall thickness

Equation 9.3 Moment of inertia about the polar axis (Brancazio 1987)

$$I_{yy} = I_{zz} = \frac{4\pi\rho bt[(a+b)^3 + a(a^2+b^2)]}{15}$$

9.4 Moment of inertia about an equilateral axes (Brancazio 1987)

The author used average values for an official American football to calculate that moments of inertia about the polar and equilateral axes were 0.00212 and 0.00343 kg/m^2 respectively.

9.1.1 Measurement Procedure

A machine manufactured by Inertia Dynamics, was used to measure the moment of inertia of an ovoid ball around the three principal axes of rotation. The machine consisted of an oscillating torsional pendulum onto which an object could be mounted (Figure 9.2).

Figure 9.2 Moment of inertia measurement machine

The period of the oscillation of the torsional pendulum was measured and the relationship between the period of oscillation and moment of inertia was defined by Equation 9.5, where T was the time for a single period of oscillation and C was a calibration constant for the instrument, which accounted for the torsional stiffness of the complete system.

$$I = CT^2$$

Equation 9.5 Moment of inertia calculation

An adjustable custom fixture was created to allow ovoid balls of varying sizes to be securely mounted to the measurement device, allowing the moment of inertia to be measured about the principal axes I_{xx}, I_{yy} and I_{zz} (Figure 9.3).

Figure 9.3 Moment of inertia custom fixtures,

The moment of inertia of the empty fixture was measured in order to determine the tare value for the machine, which was removed from measurements with a ball installed. A series of custom built calibration devices were used to determine the difference between the experimental and theoretical values of moment of inertia. Negligible differences, (<1%) were found, allowing measurements to be taken from the machine with confidence. The moments of inertia of three rugby balls and three American footballs were measured about the three axes depicted in Figure 9.1, in order to assess typical values for both ovoid ball types.

In order to accommodate for any misalignments, measurements were taken about the polar axis (I_{xx}) at four positions of 90° intervals, with the ball removed and re-positioned five times in each position. Measurements were taken about the equatorial axis at four positions, chosen to measure moment of inertia about the two principle axes within a ball spinning with tumble axis spin. Measurements were taken with the valve/laces facing upwards and downwards (I_{yy}), and left and right (I_{zz}), again with five repeats. Measurements made with the valve/laces facing forward and backwards were grouped together, as were measurements made with the valve facing left and right, as the set up represented rotation about the same axis, 180° out of plane, for each measurement pair. Three balls of each type were measured to allow an average moment of inertia value to be determined.

9.1.2 Results

Figure 9.4 depicts the mean (+1SD) moment of inertia of the ovoid balls, experimentally measured about the principal axes of rotation.

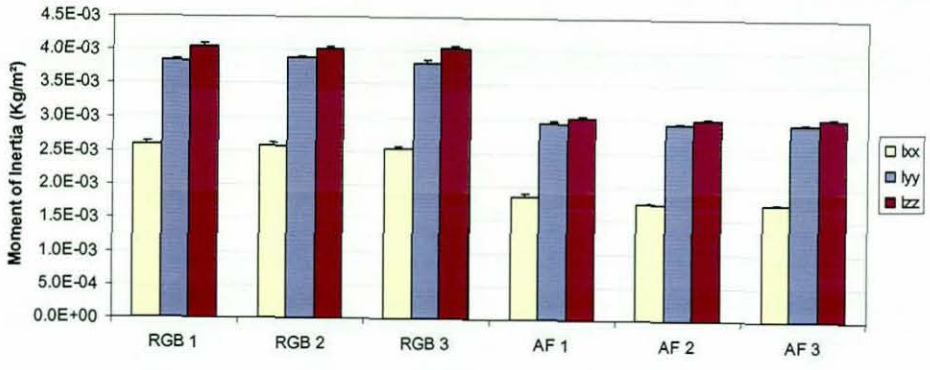

Figure 9.4 Moment of inertia measurements

Rotation about the polar axis (xx), resulted in the lowest moment of inertia for all of the ovoid balls measured, which was anticipated due to their non spherical shape. The moment of inertia measured during rotation of the American footballs about all principal axes was lower than that of the rugby balls, due to the reduced dimensions and mass of this type of ovoid ball. The measurement about the equatorial tumble axes of rotation resulted in a difference between the two orientations, due to the non uniform mass distribution, created by the inclusion of the valve and/or lace. The intermediate moment of inertia was measured when the balls were rotated about an axis through the valve/laces. The difference between the largest and intermediate moment of inertia was smallest for the RGB 2 ball in comparison to the other rugby balls, due to the smaller valve mass included in this particular design, which was 15g in comparison to the 25g for the RGB 1 and RGB 3 rugby balls.

9.2 Unstable Axis of Rotation

9.2.1 Theory

A rigid body that is rotating can either be stable or unstable depending upon the axis of rotation. Rotation about the axis with the largest and the smallest moments of inertia are stable, unlike the intermediate axis (Marion 1965). This principal can be demonstrated with the rotation of a book wrapped with a rubber band (to stop the book opening) depicted in Figure 9.5. I_{zz} is the maximum moment of inertia, whilst I_{xx} and I_{yy} are the

minimum and intermediate moments respectively. When the book is rotated about I_{yy} a rotation about the x axis will also be induced albeit with a lower angular velocity, this is described as unstable rotation.

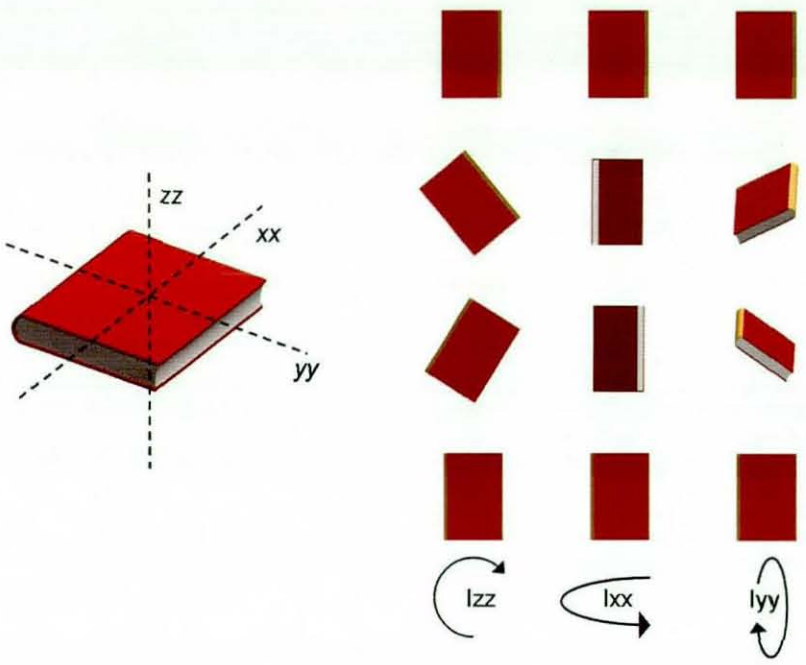

Figure 9.5 Unstable rotation of a book

Euler defined a number of equations which can be used to examine the rotation of a rigid body, Equations 9.6 – 9.8

$$I_1 \frac{d\omega_1}{dt} + (I_3 - I_2)\omega_2 \omega_3 = 0 \qquad (9.6)$$

$$I_2 \frac{d\omega_2}{dt} + (I_1 - I_3)\omega_1 \omega_3 = 0 \qquad (9.7)$$

$$I_3 \frac{d\omega_{31}}{dt} + (I_2 - I_1)\omega_1 \omega_2 = 0 \qquad (9.8)$$

Numerous mechanists have used Euler's equations to explain the unstable rotation of a rigid body (Kleppner and Kolenkow (1973), Marion (1965) and Barger and Olsson (1938)). Barger and Olsson (1938) described the unstable rotation using the example of a rotating tennis racket, as this phenomenon can often be seen when a player tosses their racket into the air after wining or loosing a point during a match. The method of deriving the stability of the rotation about the three principal axes can be found in Appendix B. The authors state that when the racket was rotated about the axis perpendicular to the

handle in the plane of the strings, the racket will perform unstable rotation, causing rotation about more than one principal axis, making it difficult to catch.

9.2.2 Gymnastics

The principle of unstable axes of rotation has been examined during a number of investigations, in particular detailing the effect on a human who is somersaulting during a gymnastic movement. The principal axes of a human body are depicted in Figure 9.6, with the moments of inertia $I_{xx}<I_{yy}<I_{zz}$, and during a somersault the gymnast will rotate about the axis with the intermediate moment of inertia, I_{yy}. This rotation will induce an unstable rotation, creating a twisting movement about I_{xx}.

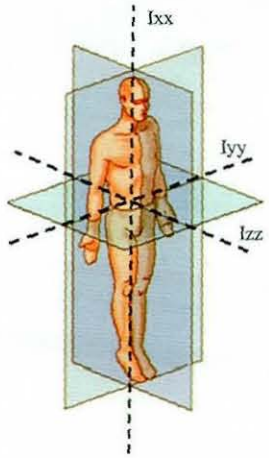

Figure 9.6 Axes of rotation of a human

Yeadon (1993a-d) has investigated the biomechanics of twisting somersaults, and examined the effect of twist during a somersault in gymnastics. The theoretical approach used a rigid body 11-segment computer simulation model, linked together with 10 joints. Yeadon showed that the twist angle would vary during the somersault and defined the movement in three specific phases; 1) somersault with no twist, 2) somersault during which a half twist occurs, 3) somersault with no twist. The model would complete a full twist during four complete somersaults, although the twisting motion would occur in two distinct half twists, depicted in Figure 9.7.

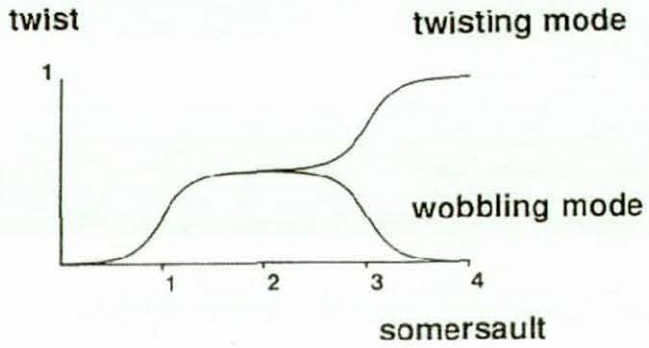

Figure 9.7 Twisting and wobbling modes (Yeadon 1993a)

The nature of the second half twist defines whether the rotation is about the twisting or the wobbling mode. The twisting mode occurs when both half twists are in the same direction, whilst during the wobbling mode the half twists are in opposite directions. During the wobbling mode the twist angle oscillates about a mean value with amplitude less than a quarter twist, and will occur if an initial twist angle exists within the model. The principle moments of inertia defined in the rigid body simulation were I_{xx} – 0.70, I_{yy} – 10.56 and I_{zz} – 11.01 kg/m^2 (Yeadon 1993a). The difference between the moments of inertia of the principal axes will define the number of rotations needed in order to produce a half twist.

9.3 Rotation of a Rugby Ball

The inclusion of the valve within a rugby ball creates non uniform mass distribution, creating a difference in moment of inertia when rotated about I_{yy} and I_{zz}. Rotation about the intermediate axis, I_{yy}, should result in unstable rotation similar to that of a theoretical gymnast when somersaulting. A rigid body FE model was created in order to analyse this effect.

9.3.1 Rigid Body Model

The rigid body FE model was created using the same discretised surface created during the FE modelling. A rigid body constraint was applied to the three node triangular and four node quadrilateral shell elements, which allowed the model to be rotated without deformation. The material properties of the panel, stitching and valve regions were defined, creating a model with a non uniform mass distribution, resulting in the intermediate moment of inertia about one of the equilateral axes. All of the nodes within the model were coupled to a single node, located at the centroid of the model, and by

applying a rotational velocity to this centroid node, tumble axis spin could be created within the model. Rotations about the intermediate and largest moments of inertia were simulated.

9.3.2 Results

Figure 9.8 depicts the unstable rotation of a rugby ball when rotated about its intermediate axis, I_{yy}. A vertical velocity was applied to the simulation, to recreate throwing a ball in the air, with images taken from a plan view at a constant time interval, with the simulation completing eight rotations between frames one and twenty.

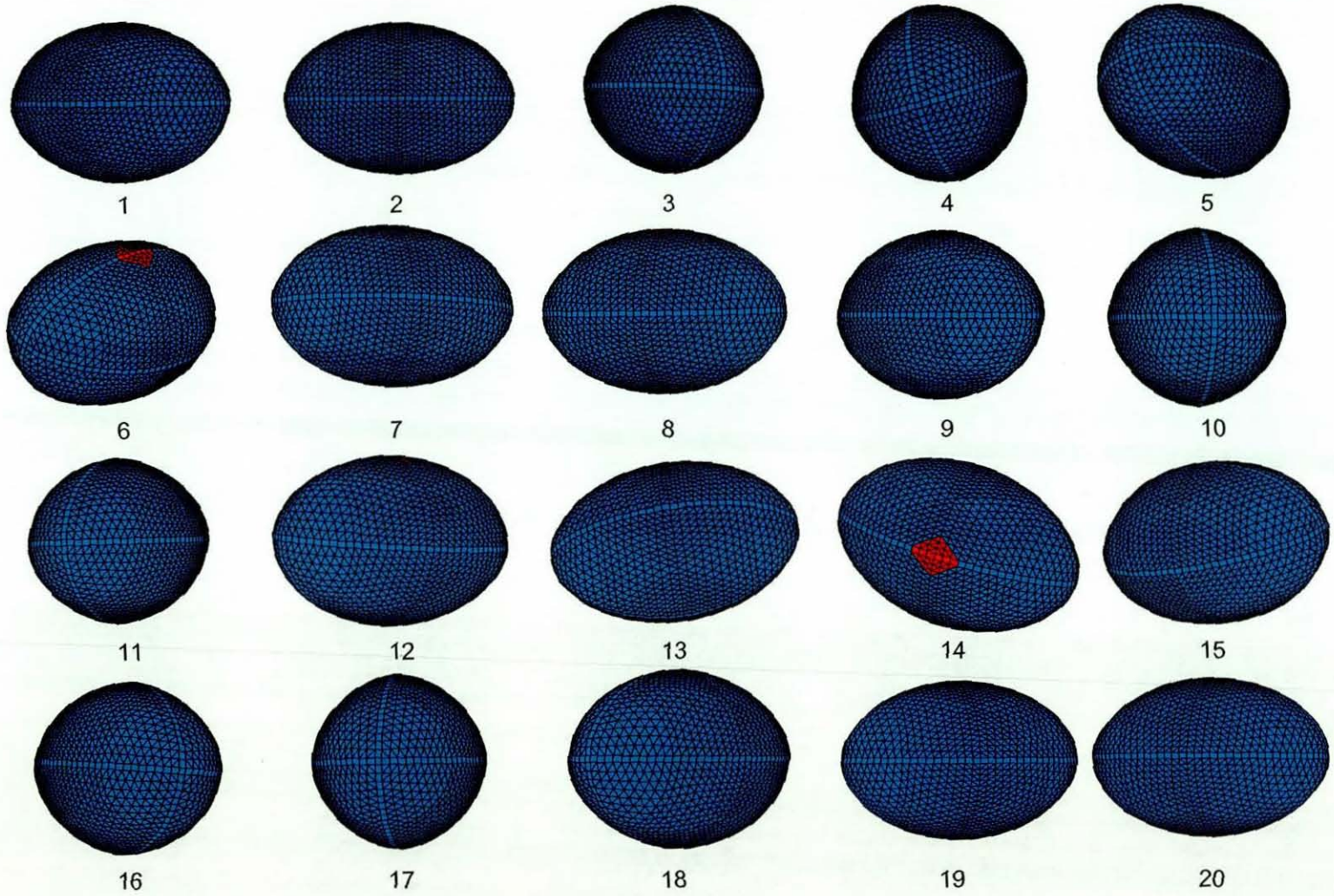

Figure 9.8 Unstable axis of rotation during a FE simulation

The valve, highlighted in red, initially starts at the bottom of the image, then after a number of rotations the ball performs a half twist, moving the valve to the top of the image, images four to six. The ball then continued to rotate with the valve in this position, before performing a second half twist, moving back to the initial starting position, images thirteen to sixteen.

Figure 9.9 depicts the movement of the valve during rotation about the equilateral axes with the intermediate, I_{yy} and largest moments of inertia, I_{xx}. The twisting of the valve did not occur during the simulation rotated about the axis with the largest moment of inertia, I_{zz}.

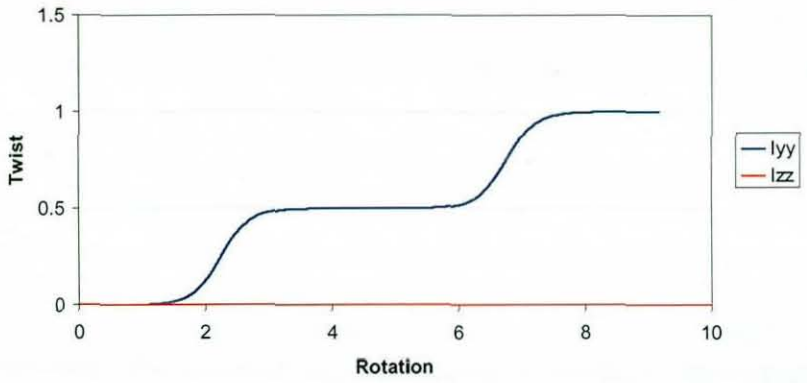

Figure 9.9 Twisting of the valve during rotation about the equilateral axes

In order to examine the relationship between rotation and the half twist rate, the single valve FE simulations were completed with a rotational velocity of 300, 600 and 900 rpm. Results showed that the time taken to commence and complete a half twist was dependent upon the number of completed rotations, and not the rate at which these rotations occurred.

The inclusion of an initial twist within the model resulted in the wobbling mode occurring during rotation of the model around the intermediate axis (Figure 9.10). The increased initial twist results in a reduction in the time taken to commence and complete the half and full twists, with the time taken to complete the full twist decreasing from 7.7 rotations to 5.4 and 4.8 for an initial twist of 10° and 15° respectively.

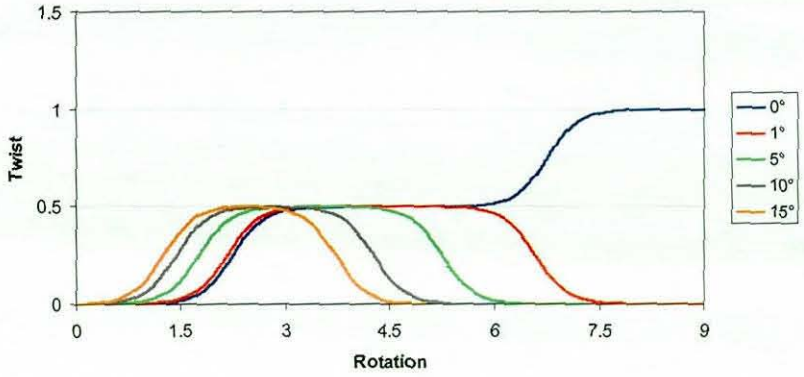

Figure 9.10 Wobbling mode caused by initial twist before rotation

9.3.3 Effect of Valve Configuration

The number of rotations taken to complete a half twist is dependent upon the difference between the intermediate and the largest moments of inertia. In order to examine the effects of varying the mass distribution within the ball, FE models were created with different valve configurations. The configurations were a single side valve (a valve within the middle of the ball), a double side valve (2^{nd} valve opposite the first), a quadruple side valve (four valves positioned at 90° intervals) a single end valve (a valve in the end of the ball), and a double end valve (2^{nd} end valve, opposite the first). Each of the valves within the model had identical geometric and material characteristics. The effect on the moment of inertia about the principal axes was determined from the model, and is summarised in Table 9.1.

Table 9.1 Moment of inertia – different valve configurations

Valve Configuration	Ixx (Kg/m^2)	Iyy (Kg/m^2)	Izz (Kg/m^2)
Single side valve	$3.09e^{-3}$	$4.65e^{-3}$	$4.88e^{-3}$
Double side valve	$3.36e^{-3}$	$4.65e^{-3}$	$5.16e^{-3}$
Quadruple side valve	$3.88e^{-3}$	$5.17e^{-3}$	$5.17e^{-3}$
Single end valve	$2.86e^{-3}$	$5.53e^{-3}$	$5.53e^{-3}$
Double end valve	$2.87e^{-3}$	$6.45e^{-3}$	$6.45e^{-3}$

The inclusion of a second side valve opposite the first caused an increase in the moment of inertia, when rotated about I_{zz}, which increased the difference between the largest and intermediate moments of inertia. The models with end valves, single or double, and quadruple side valves have identical moments of inertia about the equilateral axes of rotation. The effect of the different valve configurations depicted in Figure 9.11.

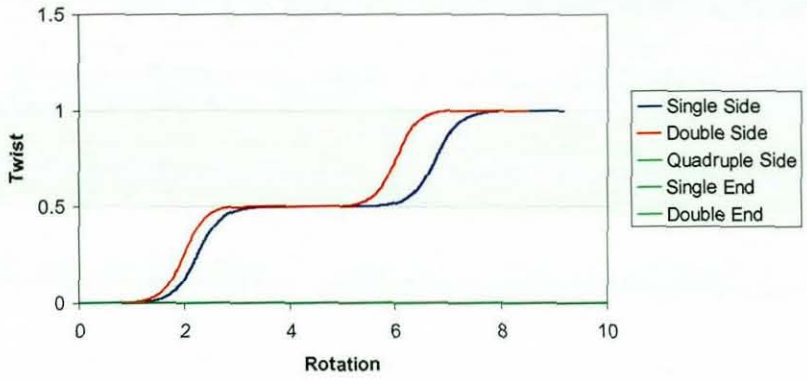

Figure 9.11 Valve configurations effect on unstable axis of rotation

During rotation about the unstable axis, the time taken for the twisting motion to commence and complete a half twist reduces with the inclusion of the second side valve, due to the increased difference between the intermediate and largest moments of inertia. The double valve configuration will begin to twist after a single rotation, and complete the first half twist in just two rotations. The second half twist does not commence until the fifth rotation and again takes two rotations to complete. The quadruple side valve, and end valve configurations result in zero twist during rotation and hence stable rotation.

9.4 Experimental Testing

Results from the FE simulation indicate that rotation about the intermediate axis, I_{yy}, results in twist about the polar axis, I_{xx}, with two distinct half twists. In order to experimentally validate the theory demonstrated within the FE simulations, a motion tracking system, Vicon, was used to capture the flight of a rugby ball when rotated about the two tumble axes.

9.4.1 Vicon

The Vicon system provides a means of capturing the movement of an object, within a defined volume, using reflective markers and high resolution cameras, each with a ring of LED strobes fixed around the lens (Figure 9.12). As the object moves through the capture volume, light from the strobe is reflected back into the camera lens and strikes a light sensitive plate creating a signal (Vicon 2002). The infrared reflective markers consist of a small polymer ball, of varying size, covered in 3M reflective tape, which is attached to a small circular disc and can be mounted onto any physical object. The size of the

marker used depends upon the distance from cameras, the size of movement and capture volume.

The MX-13 cameras have a maximum capture rate of 2000fps, and are capable of operating at full resolution (1280 × 1024pixels) at 480fps. The cameras, strobes and any other equipment being used to record data, i.e. a force plate, are controlled using the 'datastation'. The data is then passed to the 'workstation' which collects and processes the raw data, and combines the two dimensional data with calibration data, in order to construct three dimensional motions. This allows x, y and z co-ordinate data of the markers to be viewed as a virtual three dimension model, for analysis by the Vicon software or exported for use in other software packages.

9.4.2 Procedure

The Vicon system was used to capture the flight of the RGB 1 rugby ball when manually rotated about the two principle tumble axes of spin. 14mm diameter markers were placed at the valve and either end of the ball (Figure 9.12), allowing the position of the valve to be measured throughout the rotation. The rugby balls were manually launched upwards within a volume, 2×2×5m, and captured using a fourteen camera system, operating at 480fps. A calibration procedure was completed allowing the system to capture the volume, and position and orientation of each of the cameras. The calibration procedure was two fold, firstly a static calibration using an L-frame which allows the orientation of the axes to be defined, and secondly a dynamic calibration using a 'wand', which calculated the orientation and position of the relative cameras.

Figure 9.12 Vicon setup and marker placement

9.4.3 Results

Figures 9.14 and 9.15 depict the rotation about the equilateral axes with the intermediate and largest moments of inertia (plan view), with the ball completing seven rotations. The Vicon Nexus software allows lines to be placed between markers to aid visualisation, depicted in Figure 9.13.

Figure 9.13 Nexus visualisation of marker position overlaid onto a rugby ball

It can be seen that the rugby ball rotating about I_{yy}, produces two distinct half twists (Figure 9.14), whilst the rotation about I_{zz} was stable (Figure 9.15). The images were taken from the plan view at regular time intervals, with the ball completing seven rotations between frame one and fifteen. The valve is highlighted in order to enable identification of the twist.

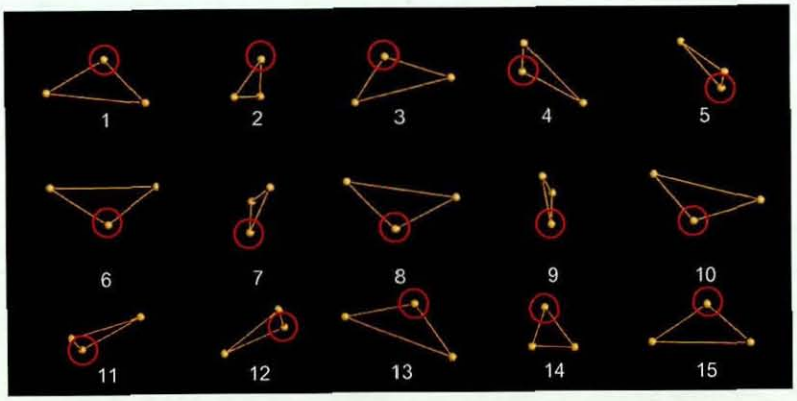

Figure 9.14 Plan view – rotation about I_{yy}

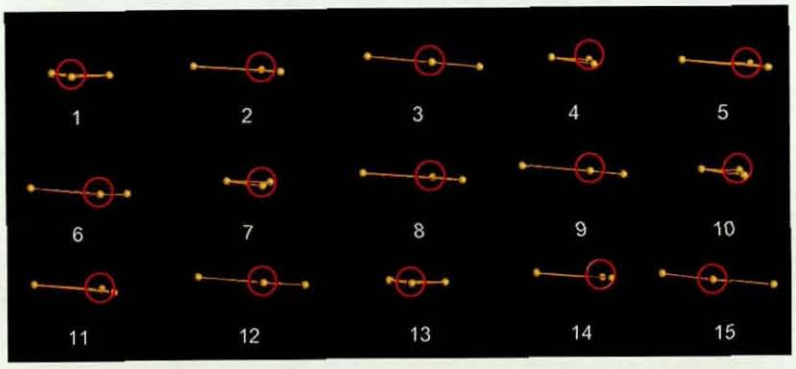

Figure 9.15 Plan view – rotation about I_{zz}

The x, y, z co-ordinate data for each of the markers was extracted from Vicon, allowing the results to be analysed using MATLAB. The centre of the ball was calculated, allowing a line to be created from the centre of the ball to the third marker at the valve. Figure 9.16 depicts trials with the ball rotated around the intermediate and largest moments of inertia. The results show that the valve does not move from the line of rotation when rotating about I_{zz}, whilst rotation about I_{yy} causes the valve to move from the left side to the right and then back again. The half twist occurs just before the ball reaches the apex of its trajectory, where it holds its position before beginning to perform a second half twist.

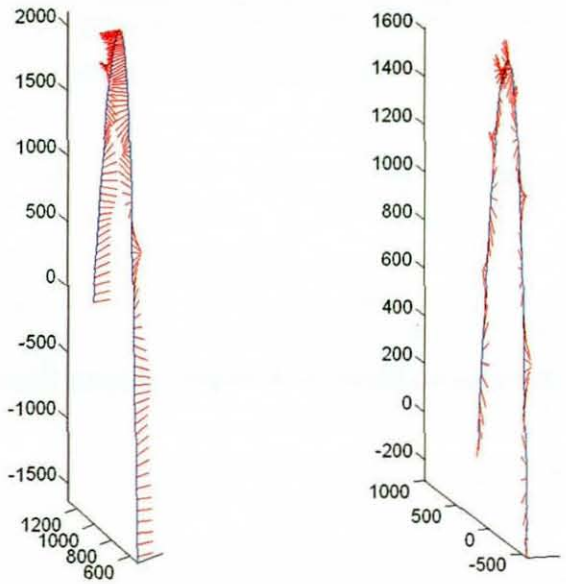

Figure 9.16 Rotation about a) I_{yy} and b) I_{zz}

Figure 9.17 depicts the rotation about the unstable axis I_{yy}. The oscillations within the experimental data coincide with the rotation about the tumble axis, and are possibly due to the ball not rotating about the same axis to which the marker was positioned. It was noted that the magnitude of the oscillations, were at a maximum during the twisting motion. This suggests that the valve marker may be moving as it tries to resists the force created during the twisting motion, which was possible as they are only attached to the ball using double sided tape. The examination of the visualisation, with the Vicon software, showed that the twisting occurs within the wobbling mode, caused by an initial twist angle. Figure 9.10 demonstrated the effect of an initial tilt angle, and results from a rigid body FE simulation with a 5° initial twist angle shows good agreement. The rugby balls were launched manually, which may have caused a small initial twist angle.

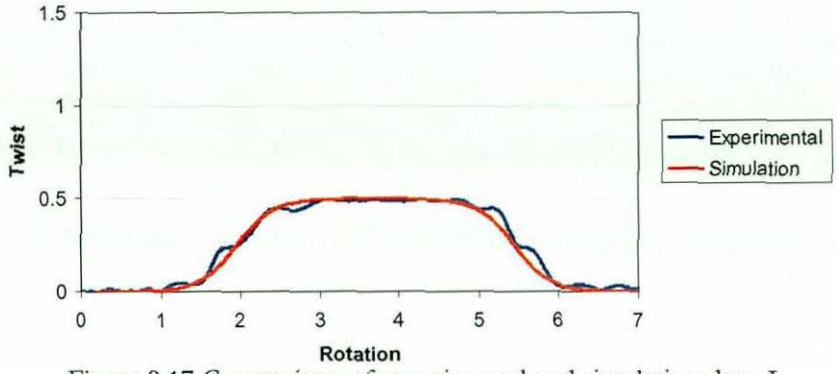

Figure 9.17 Comparison of experimental and simulation data, I_{yy}

9.5 Aerodynamic Effects

Experimental and FE simulations have shown that the non-uniform mass distribution of a rugby ball results in unstable motion when rotating about one of its principle equilateral axes. It is also important to examine any detrimental effects that this phenomenon may have on the flight of a rugby ball. It was noted that as the rugby ball performs a half twist, the tilt angle of the ball would increase, depicted in Figure 9.18.

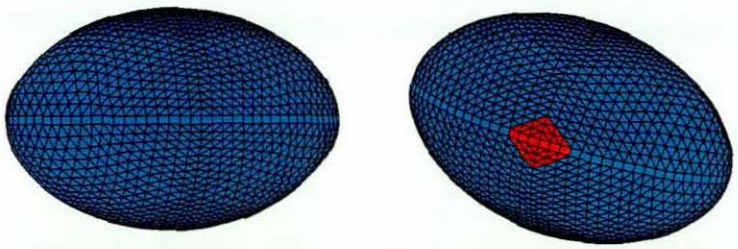

Figure 9.18 Variation in tilt angle during half twist (plan view)

The drag force, F_D, generated during the flight of a projectile is calculated using Equation 2.8. The increase in the tilt angle that occurred during the half twists will affect the drag force of the rugby ball, as it changes the cross sectional area and drag coefficient. Each of these factors will be examined separately.

9.5.1 Cross Sectional Area

During the twisting sequence the tilt angle of the ball will increase resulting in an increase in the cross sectional area of the rugby ball facing the upstream flow. When the ball was positioned with the equilateral axis parallel to the upstream flow (Figure 9.19a), the increase in tilt angle does not increase the cross sectional area. When the polar axis of the

ball was parallel to the upstream flow (Figure 9.19b), the increase in tilt angle resulted in an increase in cross sectional area, which in turn will increase the drag force.

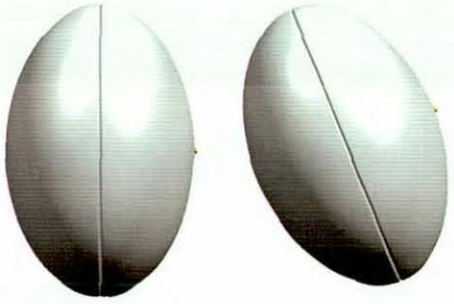

Figure 9.19a) Identical cross sectional area, with increase in tilt angle (air flow into the page)

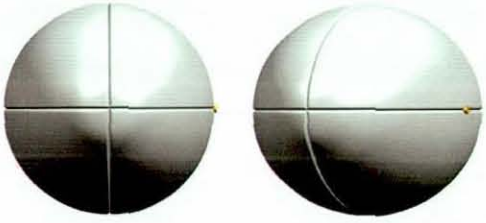

Figure 9.19b) Change in cross sectional area, with increase in tilt angle (air flow into the page)

In order to examine the change in cross sectional area, the blob analysis function within Image Pro Plus was utilised, which allowed the cross sectional area parallel to the upstream flow to be calculated at 15° increments. A blob (binary large object) is an area of touching pixels with the same logical state having non-zero values. These pixels are said to be in the foreground, where as the background consists of pixels with a zero state. During a blob analysis, the software will calculate the number of pixels contained within the foreground and background. The rigid body FE model with a single valve was rotated about the equilateral axes, allowing direct comparison of the cross sectional area of a rugby ball rotating with and without twisting motion.

Results showed a maximum increase in cross sectional area of 8% when the polar axis was parallel to the air flow, during rotation about the intermediate axis, as depicted in Figure 9.19b), whilst the average increase during two half twists was measured at 2.9%.

The increase in the difference between the intermediate and largest moments of inertia affects the tilt angle of the ball during the half twist motion, with the inclusion of a second valve within the FE model producing an increase in tilt angle, in comparison to a

single valve. In order to examine the effect of increasing the difference between the intermediate and largest moments of inertia, the density of the single valve within the FE model was varied, and simulations completed with rotation about the intermediate axis. Table 9.2 shows the maximum tilt angle during the various simulations.

Table 9.2 Effect of changing valve density within a single valve FE model

Iyy	Izz	% Difference	Max Tilt	Max % Increase Area	Rotations per Twist
3.77e-3	3.90e-3	3.4	13.8	2.9	9.6
3.77e-3	4.00e-3	5.9	18.9	5.9	8.2
3.78e-3	4.09e-3	8.4	23.3	8.7	7.7
3.78e-3	4.18e-3	10.7	26.0	10.8	7.4
3.78e-3	4.27e-3	12.8	28.5	12.8	7.2
3.79e-3	4.35e-3	14.8	31.0	14.8	7.0
3.79e-3	4.42e-3	16.7	33.5	16.9	6.9
3.79e-3	4.50e-3	18.6	36.8	19.9	6.8
3.80e-3	4.56e-3	20.3	39.4	22.3	6.7
3.80e-3	4.63e-3	22.0	42.3	24.9	6.6

The increase in cross sectional area, in comparison to a ball with 0° tilt angle, can be found in Table 9.2. Results showed that during a maximum 42° tilt angle, the cross-sectional area increased by 22%. The increase in difference between the intermediate and largest moments of inertia, also reduced the time taken to commence and complete a half or full twist, resulting in the twist motion action occurring at a higher frequency during the ball's flight. This resulted in the average tilt angle of the ball increasing during a number of known rotations, causing an increase in the average cross sectional area during the ball's flight, which in turn will result in a higher drag force.

9.5.2 Coefficient of Drag

The coefficient of drag of a rugby ball was measured by Alam et al (2006), described in Chapter 2. Alam et al showed that the coefficient of drag would increase depending upon the position of the ball relative to the upstream flow, with the maximum and minimum drag coefficients measured with the equilateral and polar axes facing the upstream flow respectively. As the tilt angle of the ball changes during the half twist motion, the area of the ball parallel to the airflow increases, causing an increase in the drag coefficient. It was

shown during simulations with the single valve FE model that the tilt angle would increase to a maximum of 42°, with a 22% difference between the intermediate and largest moments of inertia. Alam stated that the coefficient of drag would vary from 0.18 to 0.67 when measured experimentally in a wind tunnel at 140kph, with the minimum value found when the polar axis was facing the airflow. The increase in tilt angle, during the twisting motion, would result in an increase in the coefficient of drag, causing the drag force to increase.

The flow structures around a rugby ball are very complex, and the results stated by Alam were measured during quasi-static testing. Experimental aerodynamicist, Newnham (2007), stated that the twisting motion of the rugby ball, during unstable rotation, would result in an increase in the coefficient of drag. In order to accurately predict the increase, further wind tunnel experimental testing needs to be completed, with the variation in tilt angle measured, and if possible the examination of spinning balls.

9.6 Conclusions

The inclusion of the valve within a rugby ball creates a non uniform mass distribution resulting in a difference in the moments of inertia about the principal equilateral axes. During rotation about the axis with the intermediate moment of inertia, unstable rotation will occur, resulting in an object performing rotations about both of the other principle axes. During the rotation of a rugby ball about the intermediate axis, the ball will perform a series of half twists whose frequency are dependent upon the difference in moments of inertia of the principal axes.

A rigid body FE simulation allowed the mass distribution of the ball to be varied and its effect on the unstable rotation analysed. The experimental and simulations for the RGB 1 rugby ball showed good agreement, with the ball performing two distinct half twists during seven rotations. Results showed that the inclusion of a second valve, opposite the first, resulted in an increase in the difference between the moments of inertia of the equilateral axes. This reduced the time taken for the twisting motion to commence and complete a half twist, whilst the quadruple side valve, and end valve configurations resulted in zero twist during rotation and hence stable rotation.

During the twisting motion an increase in tilt angle was demonstrated which resulted in an increase in drag force. The magnitude of the tilt angle was governed by the difference between the principle moments of inertia. The inclusion of four valves, placed at 90° intervals, resulted in similar moments of inertia about both equilateral axes, creating a dynamically balanced ball with stable rotation about both equilateral axes.

Chapter 10

Prototype Rugby Balls

10 Introduction

It has been demonstrated that the manufacture of current rugby balls creates a product that has non uniform mass distribution, resulting in lateral deviation during impacts when the valve is positioned off centre (Chapter 4). The inclusion of a single valve also results in unstable rotation about one of the principle equilateral axes, causing an increase in the drag force during flight (Chapter 9). A number of manually stitched rugby balls were manufactured to allow the examination of some of the phenomenon visible during previous chapters.

10.1 Novel Ball Designs

Several manually stitched four panel rugby balls were manufactured by the collaborating company with varying mass distributions in order to examine some of the theories developed throughout the research. The prototypes had similar outer panel shape, material and construction and varied only depending upon the valve configuration within the bladder. The prototypes were split into two groups, firstly rugby balls with a single valve, CHS1a – c, and then those which are statically and dynamically balanced, CHS2 and CHS4 respectively (Figure 10.1). The individual valve weight of the CHS1 rugby balls was 12, 24 and 48g for the 1a, 1b and 1c respectively, allowing the effect of the displacement of the centre of mass from the centroid, with increasing valve mass, to be analysed. The statically balanced ball, CHS2, was created using two 24g valves positioned at a 180° interval, aligning the centre of mass with the centroid of the ball. Introducing a second valve within the ball effects the ball's rotation about the equilateral axes, causing an increased difference between the intermediate and largest moments of inertia resulting in the unstable rotation previously described in Chapter 9. The development of the CHS4 rugby ball, with four 12g valves at 90° intervals, created a ball with the centre of mass located at the centroid of the ball, whilst the moments of inertia about the equilateral axes are equal, allowing stable rotation about all principle axes. The CHS1c, CHS2 and CHS4 rugby balls have a combined valve mass of 48g, which allowed the analysis of the mass distribution within the ball. It was not possible to create a prototype

rugby ball with a valve positioned in the end of the bladder, due to the difficulties associated with the current manufacturing procedure.

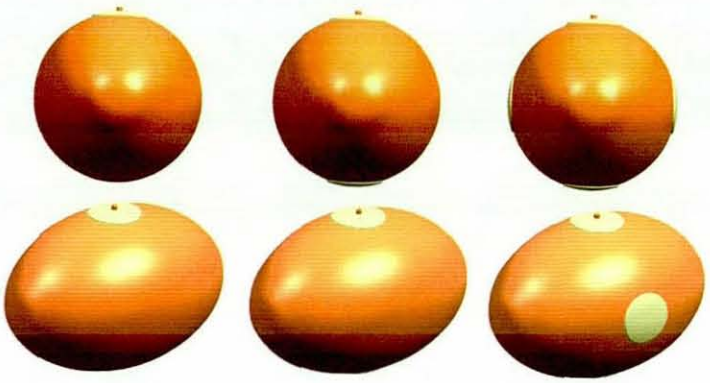

Figure 10.1 a) CHS1 b)CHS2 c)CHS4

10.2 Experimental Testing

10.2.1 Moment of Inertia

The moments of inertia of the prototype rugby balls and bladders were measured about three principal axes of rotation. The same measurement procedure was employed as previously described in Chapter 9. Three bladders/balls per type were measured to enable an average moment of inertia value to be determined.

Figure 10.2 Measurement of CHS4 bladder's moment of inertia

Figures 10.3 and 10.4 depict the mean moment of inertia (+1SD) of the prototype rugby balls and bladders respectively, measured about the principle axes of rotation.

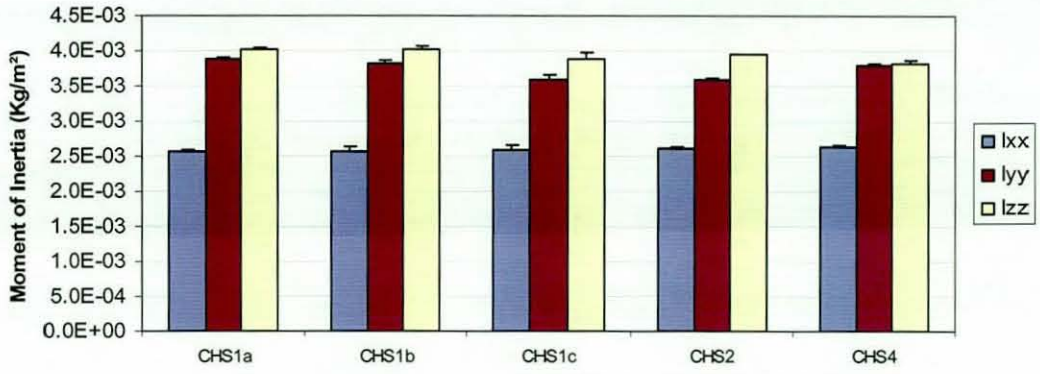

Figure 10.3 Prototype rugby balls' moment of inertia

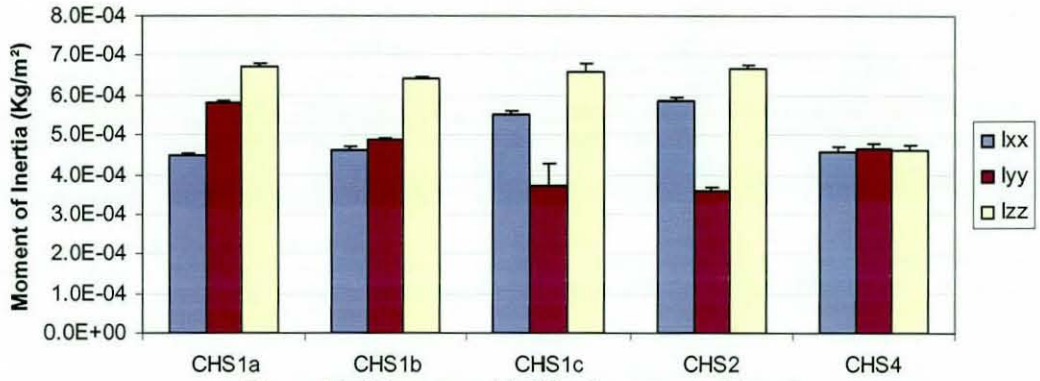

Figure 10.4 Prototype bladders' moment of inertia

Results for the prototype rugby balls showed that the minimum moment of inertia occurred during rotation about the polar axes, whilst the intermediate and largest moments of inertia occurred about the equilateral axes. Increasing the mass of the valve contained within the CHS1 prototype balls increased the difference between the intermediate and largest moments of inertia when rotated about I_{yy} and I_{zz}. The CHS1c and CHS2 have similar moments of inertia about all axes, with the maximum difference between the largest and intermediate moments of inertia. However the inclusion of the extra valves within the CHS4 ball resulted in little difference between the moments of inertia about I_{yy} and I_{zz}.

Results for the testing of the bladders showed that the minimum moment of inertia did not always occur during rotation about the polar axis, I_{xx}. During rotation of the CHS1c and CHS2 bladders it was found that the minimum moment of inertia occurred around the I_{yy} axis, whilst the intermediate axis was located around I_{xx}. This effect resulted in the bladders performing a half tumble axis rotation, when the ball was spun with rifle spin, and was captured using a high speed video camera operating at 500fps, with the ball being manually thrown towards the camera lens (Figure 10.5).

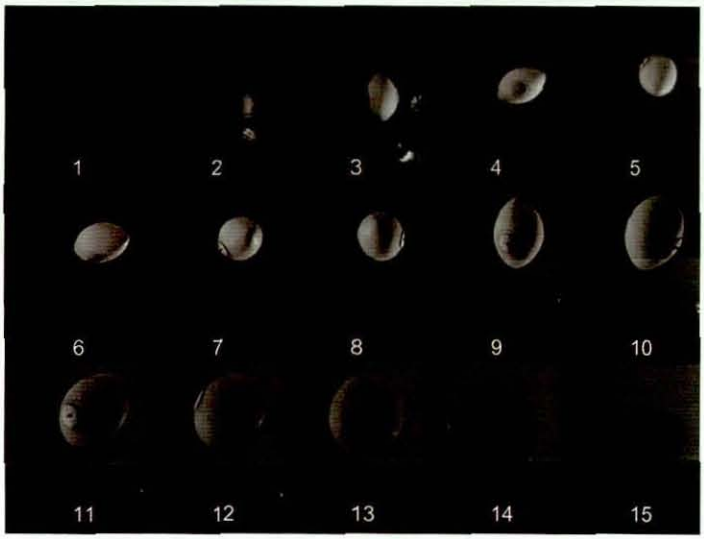

Figure 10.5 Rifle axis rotation about the polar axis

The rigid body FE model described within Chapter 9 was used to examine the effect of a bladder with two valves, similar to the CHS2. The material properties for the bladder and valve regions were defined, creating a model with a non-uniform mass distribution, resulting in the intermediate moment of inertia occurring about the polar axis (I_{xx}). A rotational velocity was applied to the centroid node allowing the model to rotate with rifle spin. The model would complete two distinct half rotations about the tumble axis, whilst spinning about the polar axis. Figure 10.6 depicts a sequence of images taken at a constant time interval from a plan view.

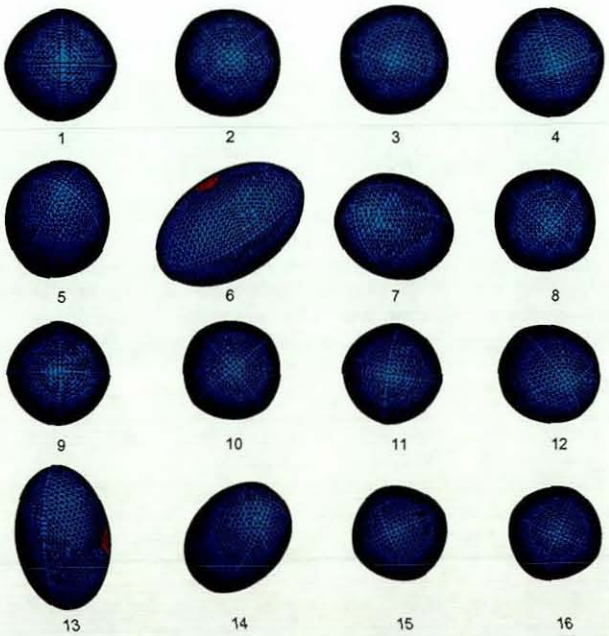

Figure 10.6 FE simulation of rifle axis rotation about the polar axis

10.2.2 Unstable axis of rotation

The Vicon setup, described in Chapter 9, was used to measure the flight of the prototype rugby balls when manually rotated about the principal equilateral axes. It was noted that the CHS4 rugby balls would exhibit stable rotation about I_{yy}, unlike the CHS2 and CHS1c rugby balls which would perform two distinct half twists. Figures 10.7 and 10.8 depict the rotation about I_{yy} for the CHS2 and CHS4 rugby balls. The images were taken from the plan view at regular time intervals, with the ball completing five complete rotations. The valve is highlighted in order to enable identification of the twist.

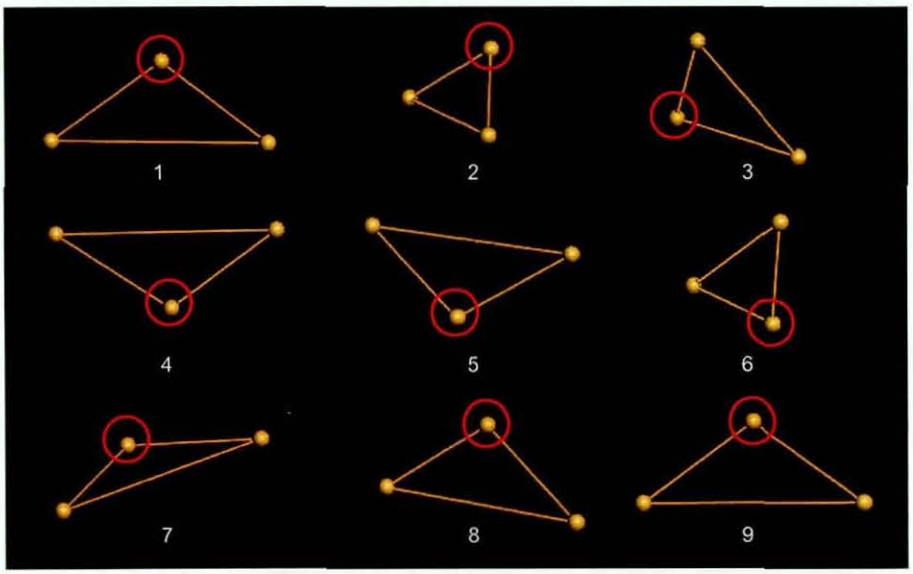

Figure 10.7 Rotation about I_{yy} – CHS2 (plan view)

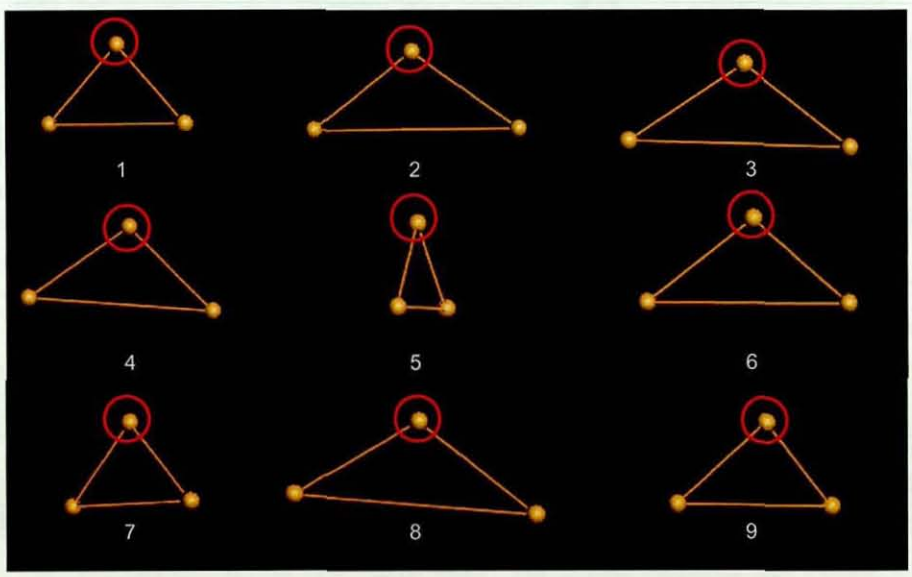

Figure 10.8 Rotation about I_{yy} – CHS4 (plan view)

Figure 10.9 depicts the rotation of the CHS1c, CHS2 and CHS4 rugby balls about the intermediate axis I_{yy}.

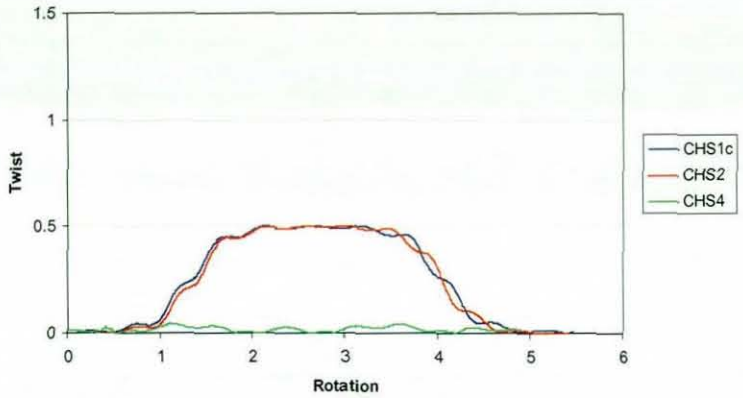

Figure 10.9 Simulation results for rotation about I_{yy}

Results showed that the CHS2 and CHS1c rugby balls both commence and complete the half and full twists after a similar number of rotations. The time taken to complete a full twist was reduced in comparison to the RGB 1 ball, due to the increase in difference between the largest and intermediate moments of inertia.

The experimental moment of inertia measurement of the CHS4 prototype balls showed a small difference between the two equilateral axes, possibly due to manufacturing tolerances. During the capture of the flight motion it was noted that certain CHS4 balls would produce a half twist during rotation about I_{yy}. The time taken to commence and complete the half twist (eight rotations) was greater than the non-dynamically balanced balls. The tilt angle created during the twisting motion was calculated to 8.4° which was lower than the 40.4° measured during the twist of the CHS2 rugby ball. The reduction in tilt angle should result in minimal changes in the aerodynamic properties of the ball during flight.

10.2.3 Rebound and Bounce Characterisation

It was suggested in Chapter 4, that the rebound test and the bounce characterisation test, at a 45° ball orientation angle, could be implemented by a governing body in order to assess the dynamic behaviour of ovoid balls. These testing procedures were used to analyse the performance of the CHS1c, CHS2 and CHS4 prototype rugby balls. Figures 10.10 and 10.11 depict the contact time and CoR during the rebound test.

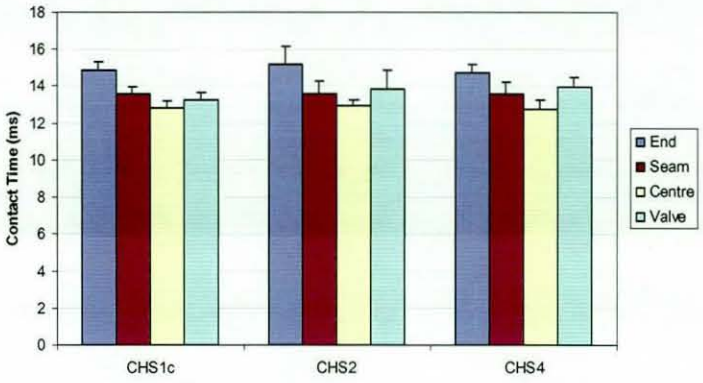

Figure 10.10 Rebound test – contact time

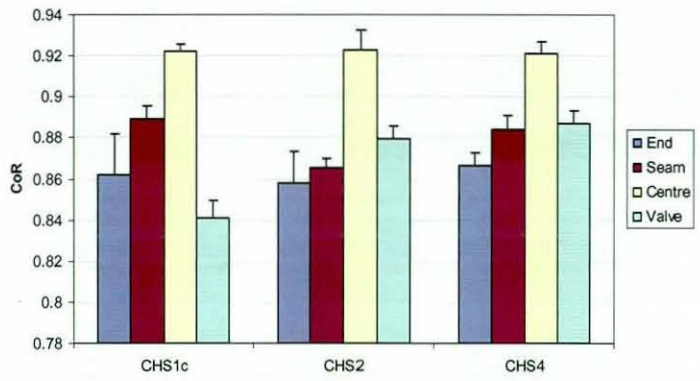

Figure 10.11 Rebound test – CoR

Results showed that the maximum CoR was measured for a centre of the panel impact for all prototype rugby balls. The CHS4 demonstrated uniform contact time and CoR characteristics when impacted on the valve and seam, unlike the CHS1c ball which produced a reduction in CoR when impacted on the 48g valve. During previous rebound testing of ovoid balls (Chapter 3), a dramatic reduction in CoR was noted during end impacts. Although the CoR was lowest during an end impact for the CHS2 and CHS4 balls, a large reduction in CoR was not apparent.

Figures 10.12 – 10.15 depict the CoR, elevation angle, spin rate and deviation angle during the ball bounce characterisation. The position of the valve at impact was varied to allow the effect of the mass distribution to be analysed.

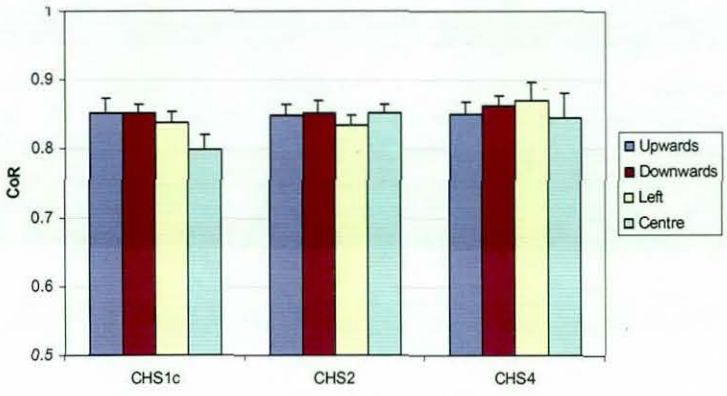

Figure 10.12 Bounce characterisation - CoR

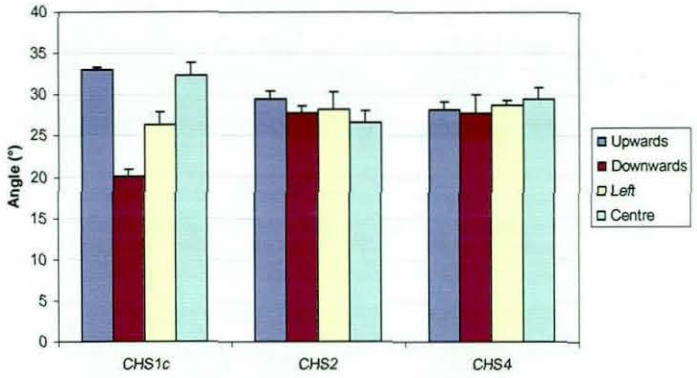

Figure 10.13 Bounce characterisation – elevation angle

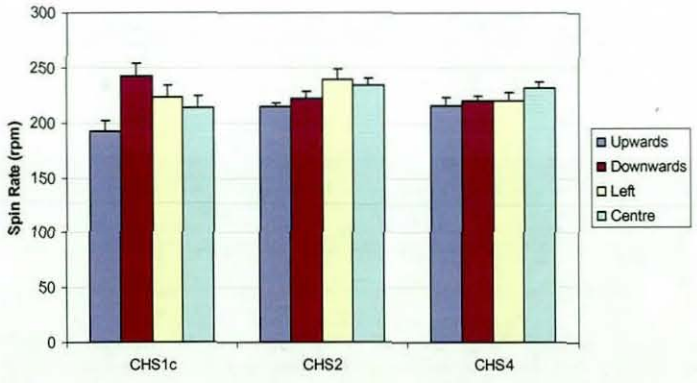

Figure 10.14 Bounce characterisation – spin rate

Results demonstrate maximum variation in elevation angle and spin rate when the CHS1c ball was impacted with the valve in the upwards and downwards position, whilst the CHS2 and CHS4 balls showed minimal variation across all impact positions. The minimal variation was due to the centroid of the ball coinciding with the centre of mass, producing little or no torque during the impact phase.

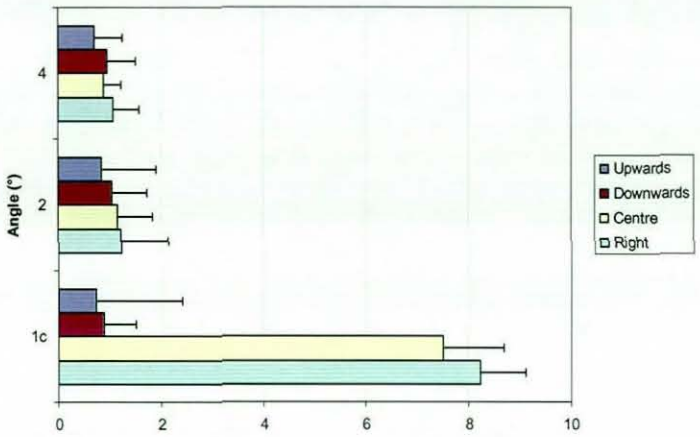

Figure 10.15 Bounce characterisation – deviation angle

The maximum deviation angle was measured for the centre of the panel and valve right impacts for the CHS1c ball, however the deviation angle for the CHS2 and CHS4 ball was minimal irrespective of valve position. Figures 10.16 and 10.17 depict a series of images with the valve positioned to the right, for the CHS1c and CHS4 balls respectively.

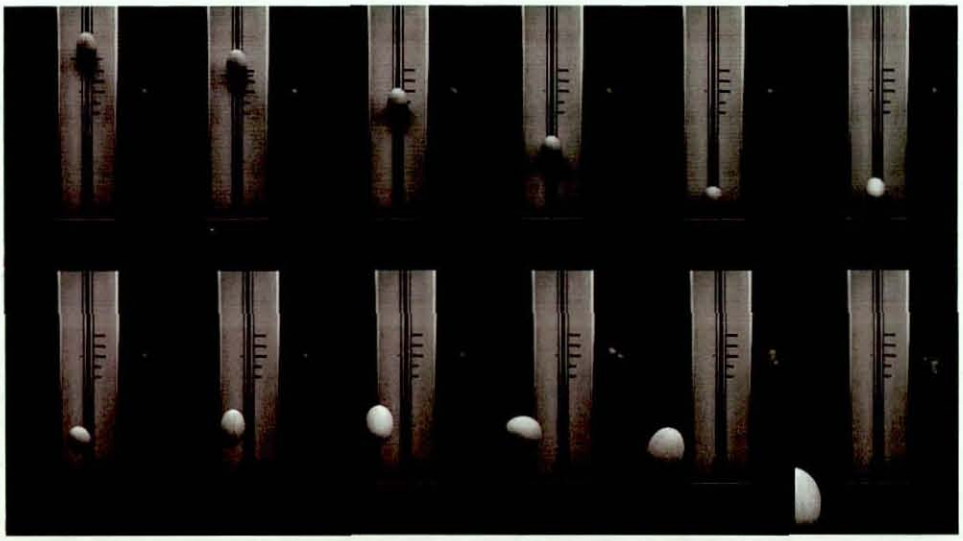

Figure 10.16 CHS1c – valve right impact

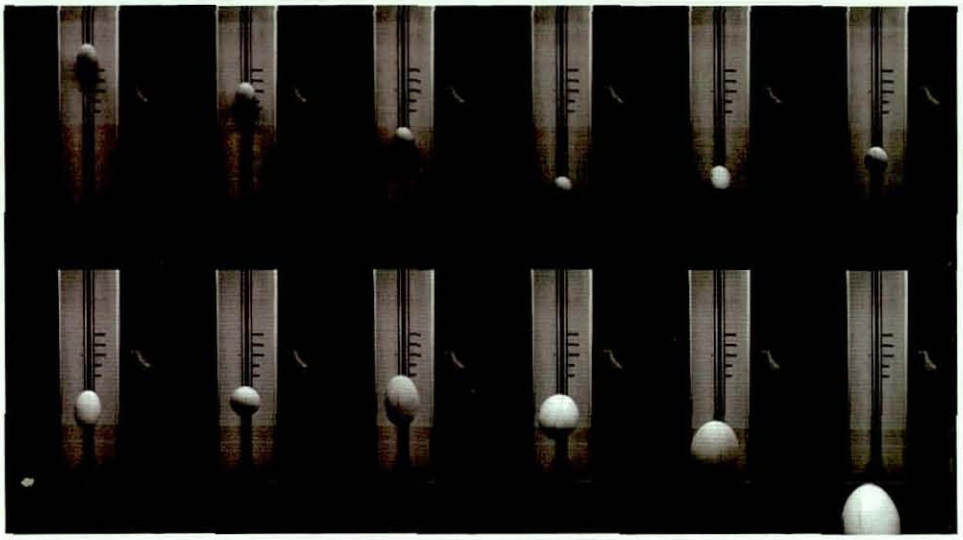

Figure 10.17 CHS4 – valve right impact

During a centre of the panel impact, or the valve positioned to the right, it was noted that the CHS2 ball would begin to perform a half twist causing an increase in tilt angle, attributed to the unstable rotation about these axes. Figure 10.18 depicts the increase in tilt angle as the CHS2 rugby ball performs a half twist during a centre of the panel impact. The valve is highlighted to enable identification of the twist.

Figure 10.18 CHS2 – centre of the panel impact

10.3 Conclusions

Results from previous chapters noted that the displacement of the centre of mass from the centroid resulted in an increase in non uniform dynamic characteristics, and unstable rotation about one of the equilateral axes. A number of prototypes were created in order to experimentally examine the effect of variation in mass distribution. The inclusion of a second valve, opposite the first, resulted in the centroid coinciding with the centre of mass, improving the dynamic performance of the ball during the ball bounce characterisation test. However this valve configuration resulted in a greater difference between the intermediate and largest moments of inertia, resulting in an increased frequency of half twist motion during rotation about the axis with the intermediate moment of inertia.

The inclusion of four valves, placed at a 90° orientation, resulted in uniform behaviour during the dynamic testing, as the centroid coincided with the centre of mass. The mass distribution of the CHS4 rugby ball resulted in similar moments of inertia about the equilateral axes, creating a dynamically balanced ball with stable rotation about both equilateral axes.

Chapter 11

Ball Flight Characterisation

11 Introduction

Ball sports equipment has utilised mechanical impact simulators or 'robots' for experimental verification of prototypes and computer models. In the case of soccer, kicking machines are used during ball development as they provide repeatable impact conditions unobtainable for human testing procedures. This chapter details the development of a mechanical kicking simulator which enables accurate and repeatable creation of the ball launch characteristics that exist for the various kicks in the game of rugby. A mechanical simulator was used to determine the launch and flight characteristics of a rugby ball when experimentally tested under wind free conditions.

11.1 Mechanical Kicking Simulators

Athletes have been extensively used by manufacturers during the development and testing of sporting equipment. However athletes will tire during testing and therefore provide inconsistent performance. During the human evaluation of golf club performance, Suzuki and Ozaki (2004) found that this evaluation technique requires many trials because weather conditions and physical condition of the golfer at the time of testing greatly affect the distance of the hit ball. Mechanical simulators have been developed to overcome the issue of athlete fatigue and have been used since the early 1920's, particularly in golf. Harper (2007) noted that smart structures have been used increasingly over the last four decades to re-create consistent athlete/sports motions which offer increased repeatability. Mechanical simulators are now used by manufacturers, governing bodies and academic institutes to provide accurate and repeatable simulations.

Mechanical simulators are designed to either replicate an athlete's motion or the launch conditions of the projectile. Mechanical simulators developed by Hatze (1992) and Schempf (1995) aimed to replicate an athlete's motion during the game of tennis and football respectively. Hatze developed a device capable of replicating the human forehand tennis stroke, dubbed the 'manusimulator', which aimed to exhibit all degrees of freedom in the shoulder, elbow and wrist joints, and used adjustable spring dampening

combinations to account for the muscular actions at impact. The device was used to objectively analyse tennis racket performance, but was unable to achieve the racket impact speeds measured during game related studies. It was a complex device which was also costly and inconsistent.

Schempf (1995) developed the kicking robot ('roboleg') as a tool to evaluate existing and future soccer balls and boot designs, whilst removing the statistical variance associated with human testing (Figure 11.1). The complex design was manufactured at a significant cost and was designed to approximate, as closely as possible, the human kinematics and dynamics during the action of kicking a soccer ball. Spring loaded actuators were used to replicate the thigh rotation and swing of the shank, whilst linear actuators were used to simulate the Achilles tendon. This allowed for a toe up and toe down motion, whilst a small gearing system allowed for toe rotation. During the replicated motion, the individual joints are sequentially actuated using user-defined delays. These delays were determined through analysis of human motions. During preliminary testing the roboleg achieved ball velocities of 40m/s, with good repeatability, which was comparable to that of a human kick. However due to the complex nature of the simulator, the roboleg experienced multiple problems including gear mesh failure and over heating. As a result this machine is no longer used.

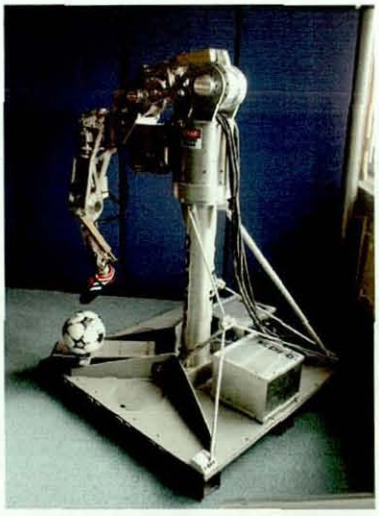

Figure 11.1 Athlete motion simulator; 'roboleg' (Schempf 1995)

The main issue concerned with mechanical simulators is their increased complexity, as they try to re-create human movements using mechanical parts. In order to reduce the complexity of the machine, a number of mechanical simulators aim to reproduce the

launch characteristics of the projectiles' motion. Kotze (2002) in conjunction with the International Tennis Federation developed a high speed tennis serve device (Figure 11.2). The device consists of a drive arm, which rotates the constrained racket through the throat. The servo driven arm accelerates the racket to the correct service speed, where it makes contact with a dropped ball at the desired impact location. The device is capable of producing impact velocities of up to 60m/s.

A simplified mechanical simulator was used to extensively test the +Teamgeist™ soccer ball used in the 2006 World Cup (Figure 11.2). adidas (2006) stated that their football laboratory in Scheinfeld features a high-tech robotic leg which is used for a variety of ball tests. The machine is able to repeat an identical kick in the exact same angle and with exactly the same speed and power. The device consists of a pneumatically driven kicking leg which operates as a mechanical pendulum. The pendulum is attached to a simple rack and pinion system. Price (2005) noted that the two pistons are attached to either side of the rack, such that the push-pull arrangement is formed which generates the required linear motion of the pinion to drive the leg. However the kicking robot is only capable of achieving 25m/s ball velocity, which is lower than velocities measured during player testing studies. This, along with the inconsistency of air pressure, associated with pneumatically driven machines, are its main limitations.

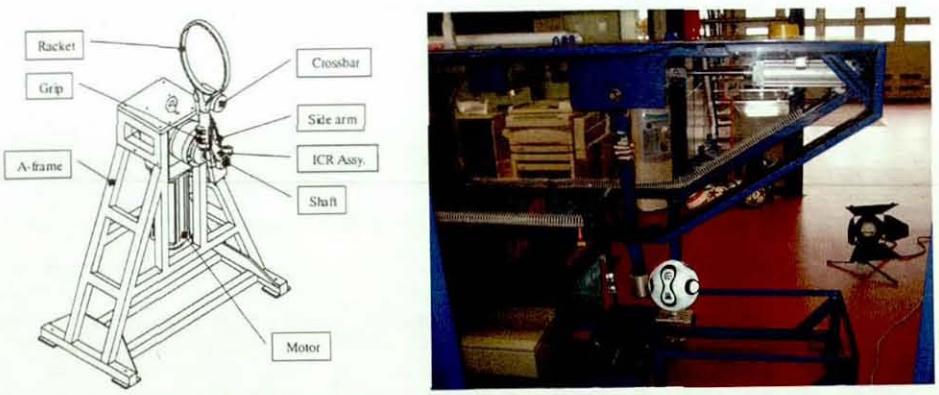

Figure 11.2 Launch characteristics simulators; high speed tennis serve device (Kotze 2002) and kicking robot (adidas 2006)

11.2 Design of Mechanical Simulator

Athlete motion simulators have generally been proven to be unreliable due to their complex nature. In order to produce soccer and rugby ball impact conditions accurately and reliably, the simulator was designed around a simple leg rotation device. As previously stated in Chapter 5, elite rugby players are capable of producing launch

velocities of 38m/s and in order to allow for future gains in player performance, the simulator was designed to produce ball velocities of 45m/s, with a repeatability of 1%.

The mechanical simulator was designed around a rigid A-frame design, manufactured from 50x50mm steel box section. The tee cage at the front of the welded structure provided a substantial frame on which to base the adjustable ball teeing system, capable of manipulation about three axes. The velocity of the end effector was calculated using Equation 11.1 defined by Plagenhoef (1971). The reflected mass of the foot was calculated as 3.489kg, based on the 50th percentile male (Hay 1993), with the coefficient of restitution defined as 0.5 (Lees and Nolan 1998), and the mass of the ball 0.453kg (FIFA 2006).

$$V_{Ball} = V_{Foot}\left(\frac{M(1+e)}{M+m}\right)$$

V_{Ball} - Ball velocity after impact
V_{Foot} - Foot velocity prior to impact
M - Relative mass of foot
m - Mass of ball
e - Coefficient of restitution

Equation 11.1 End effector velocity calculation (Plagenhoef 1971)

The drive system uses a Lenze 6.9kW asynchronous geared servo motor to rotate the kicking leg, and is capable of accelerating to a maximum velocity of 2300deg/sec in 270°. The machine's software allows the length and rate of acceleration and deceleration to be specified, allowing different impact conditions to be achieved.

The counterbalanced kicking leg consists of two aerospace grade aluminium plates, connected by a number of cross members (Figure 11.3). This achieved the desired strength to weight ratio, whilst maintaining a safety factor of 5.4 under impact loading conditions at 45m/s. In order to achieve the variety of different impact conditions, the kicking leg is designed with an interchangeable end effector.

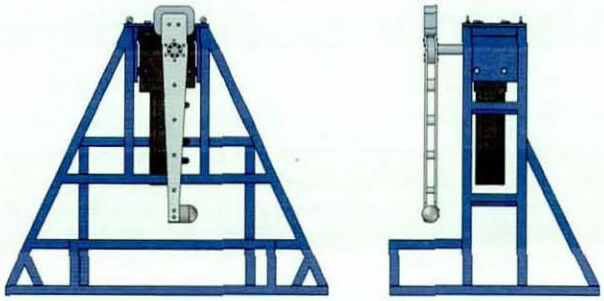

Figure 11.3 CAD images depicting assembled mechanical kicking simulator

11.3 Preliminary Testing

The leg motion software was defined to achieve a constant velocity throughout impact, and during the total rotational movement (1080°), the leg accelerates for 270° and decelerates for 720°. This creates a smooth profile and minimises stress within the leg. High speed video of soccer and rugby ball impacts at 10,000 fps, enabled a detailed analysis of launch conditions and ball deformation. A maximum ball speed of 50m/s was achieved, with the repeatability of the leg velocity calculated to ±0.032m/s (95% confidence). The repeatability measure was calculated using a series of light gates to measure the time interval for a known displacement.

11.4 Re-creation of a Rugby Place Kick

In order to validate the design, the place kick was first simulated, using player testing data which provided the launch conditions to be achieved whilst performing the kick. The key variables were the launch angle (30.22°), spin rate (476 rpm) and ball velocity (33.6m/s). The variables to be optimised were ball placement angle, ball position with respect to the machine's centre of rotation, impact position with respect to ball centre and impact velocity. The significant difference between the mechanical kicking simulator and the human kick are the centre of rotation is displaced, the human leg movement is a double pendulum and the impactor is an 85mm diameter hemisphere compared to a foot. The launch angle was manipulated by adjusting the position of impact using the teeing mechanism, whilst the ball velocity was achieved by varying the leg velocity during the impact (19.9m/s). The flight of the ball was captured using high speed video (10,000 fps), which was digitised using Image Pro Plus software, and the ball velocity, spin rate and launch angle numerically calculated. The software allows the displacement of the centre of the ball to be calculated over a given time interval.

The digitised high speed video recording established that the mechanical kicking simulator was able to accurately repeat the rugby place kick with the correct elevation angle and ball velocity. Experimental testing showed that the spin rate values produced by the mechanical kicking simulator were 194rpm, which was considerably less than the 476rpm measured during elite player testing. The mechanical simulator impacts the rugby ball with a leg velocity of 19.9m/s, which stays constant throughout the impact, in order to produce a ball velocity of 33m/s. Asami and Nolte (1983) stated that the foot velocity decelerates during contact with a soccer ball, with the maximum foot velocity prior to impact measured at 31.1m/s in comparison to the 18.6m/s after contact. The natural deceleration of the foot is not simulated with the rotating leg and this could explain the difference in measured spin rates, as well as the differences between the end effectors.

11.5 Ball Flight Characterisation

The mechanical kicking simulator was used to re-create a place kick with similar launch characteristics to those described in the previous section. The prototype rugby balls described in Chapter 10 were used to examine the effect of varying mass distribution when a rugby ball undergoes a kick with tumble axis spin. It was important to examine this effect in an environment in which no wind conditions could affect the flight of the ball. An indoor testing environment was required with sufficient headroom to allow a place kick to be re-created, the required dimensions were at least 75m in length and 35m high.

11.6 Indoor Testing Environment

The identification of an indoor facility with the required dimensions provided a considerable challenge. A number of possible venues were examined, and eventually the old RAF base at Cardington, Bedfordshire provided the most suitable location. Hanger one at RAF Cardington was built in 1915 for the manufacture of airships for the Admiralty and was initially 700ft in length. In 1926 the hanger was extended to 812 feet (247m) in length and the height was raised to 180ft (55m) in preparation for the manufacture of the R101 airship. The R101 was built as the result of the British Government initiative (the Imperial Airship Scheme) to develop an airship that was capable of carrying two hundred troops or five fighter aircraft. The R101 was manufactured between 1926 and 1929 under the British Government's Air Ministry, and was 777feet (237m) in length with a diameter of 131feet (40m). The R101's maiden

voyage departed for Karachi (British India) on the 4th October 1930, with a total of fifty four passengers and crew on board. Myddelton (2007) noted that the thirty seven 'crew members' luggage totalled 468lbs, whilst the Secretary for Air, Lord Thompson, included a large roll of carpet and two cases of champagne, bringing the total of his personal luggage to 254lbs, which was regarded as extremely heavy as carrying extra weight naturally causes a problem. On the 5th October 1930 the R101 encountered gusting winds near Beauvais (north of Paris), which tore the outer cover of the ship rupturing the first gas bag. The R101 crashed into a hillside causing the leaking hydrogen to ignite killing forty eight of the fifty four passengers and crew. The crash of the R101 caused the British Government to abandon the airship schemes and the hanger was subsequently used as a storage base.

The site at RAF Cardington consists of two hangers of similar size (247m long, 83m wide and 55m high). Hanger two has been renovated with all of the sheet steel cladding replaced (55,000m^2) and is currently used as a film set, whilst hanger one is in need of repair with a number of holes developing in the roof due to corrosion. Despite the degrading nature of hanger one, it provided a suitable testing environment due to its large volume (750,000m^3), and was available for rental (Figure 11.4). It was estimated that a period of seven days would be required to perform over2000 impacts.

Figure 11.4 Image of hanger one and two at RAF Cardington

Within the RAF Cardington site, the Meteorological Office (Met Office) operate a weather measurement station which allowed the wind speed values to be measured during the testing week, with the average wind speed measured over a one minute interval (Figure 11.5). A maximum wind speed value of 12m/s was measured during testing hours on the 8/12/07. The wind speed inside the hanger was measured at a number of positions of varying height, using an anemometer which contained a small

electronic rotating vane. The vanes of the anemometer did not rotate due to the wind speed inside the hanger being lower than the minimum recordable value, 0.5m/s.

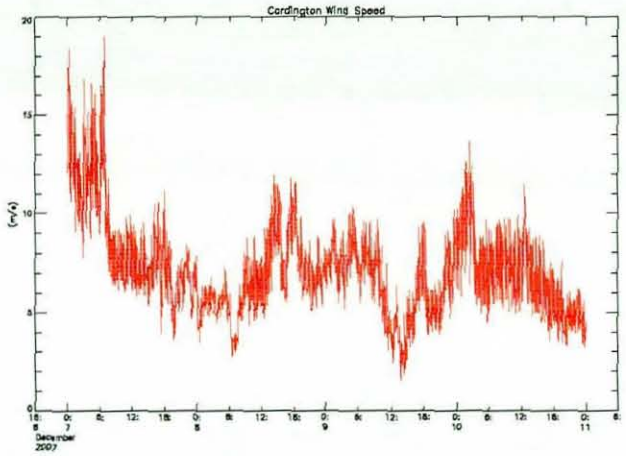

Figure 11.5 Wind speed measurement (met office)

11.7 Equipment

Hanger one contained minimal internal lighting therefore an external source was needed. Eight 1.6kVa link tower lighting stands were used, each fitted with four metal halide lamps, providing sufficient lighting to allow the use of HSV cameras. The geared servo motor of the mechanical kicking simulator requires a 3 phase voltage supply in order to create the leg rotation. This supply must conform to the International Electrotechnical Commission (IEC) standard IEC 61000-2-4:1994. The standard is concerned with the conducted disturbances in the frequency range from 0 to 9 kHz, and specifies the levels of electromagnetic disturbance expected. The disturbances considered include voltage dips/interruptions, harmonics up to order fifty and interharmonics up to the 50th harmonic. A 100kVa generator, conforming to the relevant IEC standards, along with 950m of cable was hired to provide power to the HSV, lighting towers and mechanical kicking simulator.

11.8 Testing Procedure

A number of prototype rugby balls as well as the RGB 1 rugby ball were selected for the flight characterisation testing. Prototypes CHS1a, CHS1b and CHS1c were tested as this allowed the effect of the mass of the valve to be examined. Prototypes CHS2 and CHS4 were also used as they have the same overall mass as CHS1c, yet have different valve configurations, allowing the effect of mass distribution to be analysed. Five rugby balls per type were examined with a total of ten impacts per impact position. The mechanical

kicking simulator was used to perform a series of place kicks with a leg velocity of 19.9m/s, which created a kick with tumble axis spin. The ball teeing system was adjusted in order to achieve the correct impact position calculated within this chapter, re-creating the launch characteristics measured during player testing. The rugby ball was positioned upon a kicking tee and orientated to a 55° ball angle, depicted in Figure 11.6. Laser levels were used to aid the placement of the ball so that the angle of the ball could remain constant throughout the testing, irrespective of impact position. The position of the ball was captured a number of times in the various impact positions to allow the variation in ball angle to be calculated.

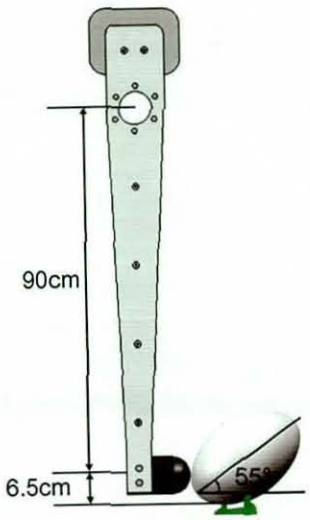

Figure 11.6 Mechanical simulator impact position

Each of the rugby balls were impacted at 4 different locations to enable the effect of the valve position to be determined. The ball was positioned with the valve facing upwards, downwards, right and finally an impact in the centre of the panel (valve facing right and upwards) (Figure 11.7). The design of the safety guarding surrounding the mechanical kicking simulator, meant that it was not possible to launch balls left of the normal direction (i.e. with the valve facing left), as the ball would impact with the guarding. However it can reasonably be assumed that ball launch characteristics with the valve to the left would be a 'mirror' of those with the valve placed to the right. The variation in impact position allowed the effect of the mass and placement of the valve to be determined during the balls' flight.

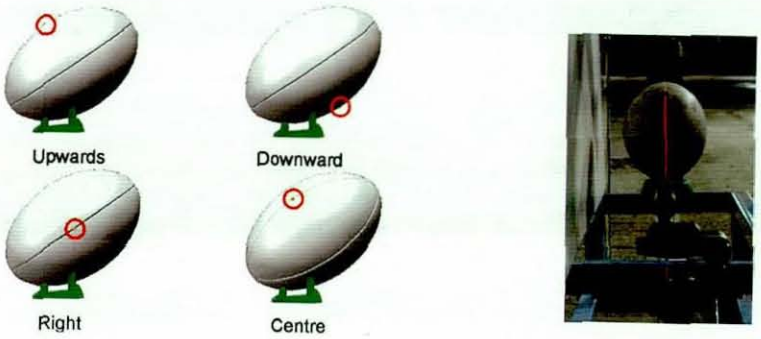

Figure 11.7 Ball valve positions and laser alignment aids

Two Photron SA 1 HSV cameras operating at 500 frames per second, with a shutter speed of 1/4000s, were used to capture the flight of the ball at a maximum resolution of 1024×1024 pixels. The two cameras were synchronised using a voltage output from the mechanical kicking simulator produced when constant velocity was achieved. Figure 11.9 shows a simplified diagram of the testing setup.

Figure 11.8 Photographs of the experimental setup

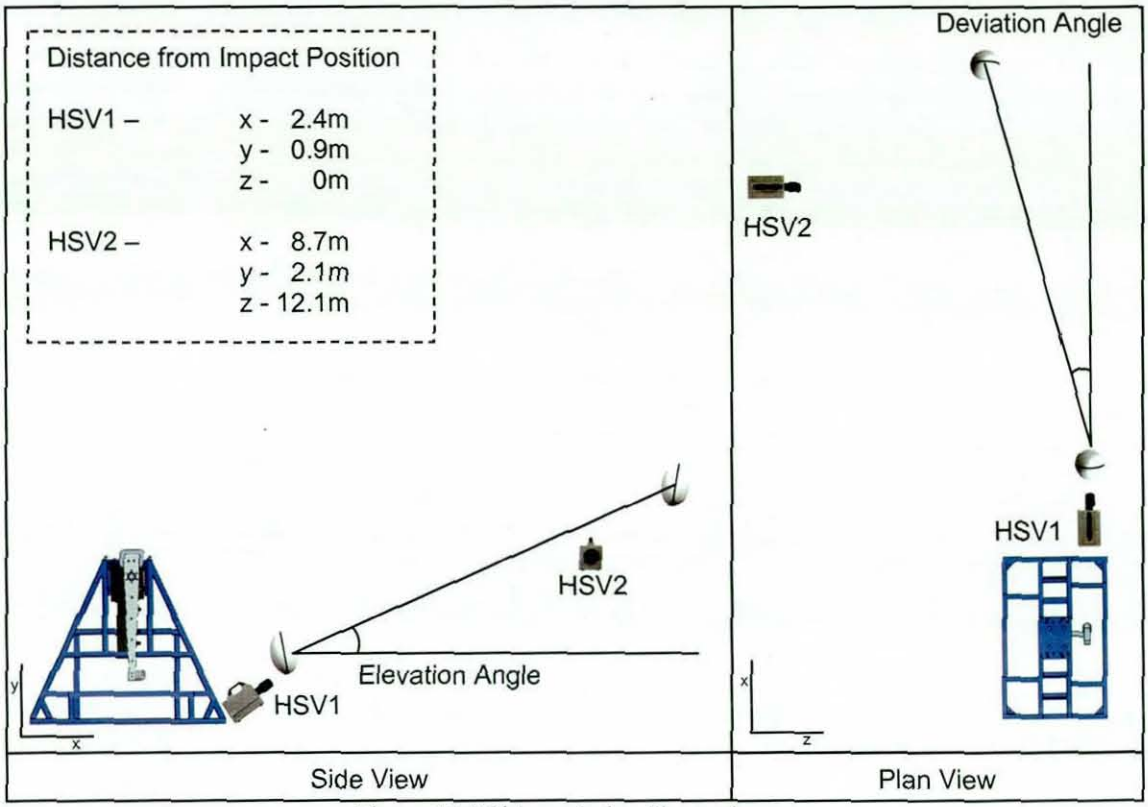

Figure 11.9 Side and plan illustrations

11.9 Analysis

Images captured using HSV 2 were digitised allowing the x and y pixel co-ordinate positions to be obtained at two positions, a known time interval apart. The co-ordinate values were then used to calculate the ball velocity and elevation angle in a direction normal to the camera. The angle of the ball at the two positions was measured and used to calculate the change in angle during the known time interval, allowing the spin rate to be determined. The digitisation of the images captured using HSV 1 allowed the x and y pixel co-ordinate of the ball position to be determined at a known distance, 8m from the mechanical kicking simulator. This measurement allowed the ball deviation from the line of the leg's rotation to be determined. The synchronisation of the two HSV cameras, allowed the rugby ball's global position in space to be calculated, which in turn allowed the deviation angle of the ball to be determined.

The still images of the ball on the kicking tee were analysed and the mean ball orientation angle was measured at 55.9°±1.05° (1SD) from the horizontal. In order to minimise measurement error attributed to the ball movement not being perpendicular to the camera, the camera was carefully aligned using a digital inclinometer. The repeatability of

the analysis was determined by digitising the same impact a number of times. The uncertainty of the ball velocity was calculated to be ±0.03m/s, elevation angle ±0.02° and the spin rate ±3.6rpm all to 95% confidence.

11.10 Results

11.10.1 Ball Launch Characteristics

Figures 11.10 - 11.12 depict the ball velocity, elevation angle and spin rate for impacts with 19.9m/s leg velocity. The graphs depict the mean values (+1SD). The discussion of the results will be divided into two sections comparing the effect of increasing the mass of the valve and the effect of the mass distribution.

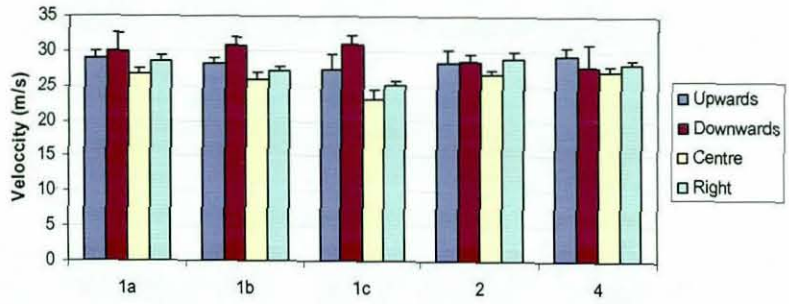

Figure 11.10 Ball velocity

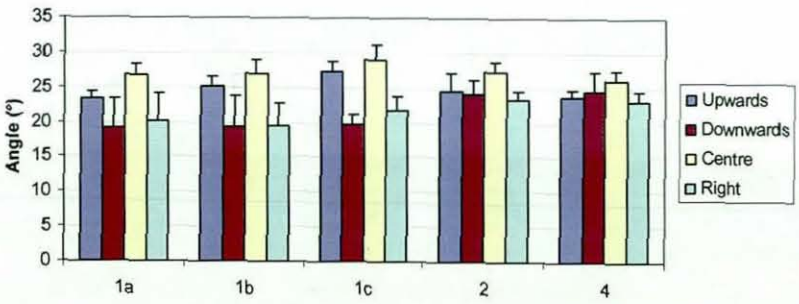

Figure 11.11 Elevation angle

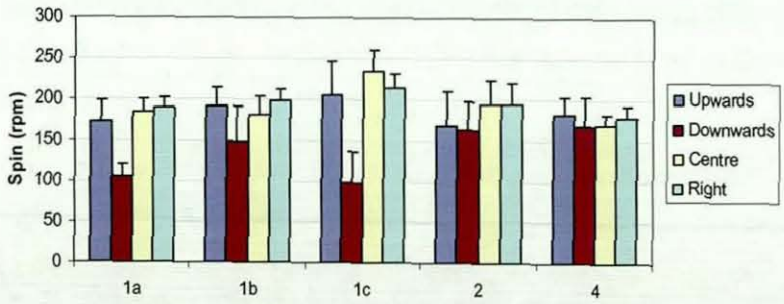

Figure 11.12 Spin rate

11.10.1.1 Valve Mass

The CHS1a, 1b and 1b rugby balls all have a single valve and results indicated that increasing the mass of the single valve increases the variability of all the measured parameters when varying the impact location. Ball velocity remained reasonably consistent during impacts with the valve facing upwards and downwards, however the velocity dramatically reduced when impacting the CHS1c ball with the valve off centre (position right and centre). The ball velocity was measured in a plane normal to the HSV camera and a reduction in ball velocity could be due to an increase in the ball velocity out of the plane of the camera. This could be that the impact motion was not through the centre of mass, which was offset from the centroid due to the mass of the valve.

The increase in valve mass also had a significant effect on the variation of elevation angle. The larger mass resulted in an increase in elevation angle when the valve was in a upwards and central position. Impacting the CHS1c ball in a downwards position resulted in a 7.7 and 9.2° reduction in elevation angle in comparison to impacting in the upwards and central positions respectively.

Increasing the mass of the valve resulted in a maximum variation between impact positions occurring in the CHS1c prototype. Increasing the mass of the valve also resulted in a 140% (134rpm) increase in spin between the downwards and central position. This value was significantly larger than the 82% (66rpm) increase measured for balls with the smaller mass.

11.10.1.2 Mass Distribution

The inclusion of a number of valves within the CHS2 and CHS4 ball has reduced the inconsistency measured from impacts with a single valve (CHS1c). Rugby balls CHS2 and CHS4 resulted in more uniform measured flight characteristics irrespective of impact location. During impacts with the valve in the central position, the CHS1c ball measured a 140% increase in spin rate compared with the downwards position. The CHS2 and CHS4 ball measured a variation of 19% and 8% respectively.

11.10.2 Deviation Measurement

Figures 11.13 depict the x and y pixel co-ordinates of ball position normal to the kicking direction measured using HSV1 at a known distance of 8m from the mechanical kicking simulator.

11.10.2.1 Valve Mass

A larger valve mass resulted in an increase in the dispersion of the ball position data, at the known distance, both horizontally and vertically (Figure 11.13a). Figure 11.13b) demonstrates the effect of impacting the CHS1c rugby ball in different valve positions, with each position forming a cluster of points. Impacting the ball with the valve in the downwards position created a lower position on the screen in comparison to the upwards position. This was validated by the reduction in elevation angle recorded by the side on camera. Impacting the ball with the valve positioned to the right resulted in the ball laterally deviating towards the right, whilst its vertical position was located in between the upwards and downwards positions, as the valve was positioned centrally. The results for the centre of the panel impact demonstrated a smaller lateral deviation then the right position, yet a larger deviation than the upwards or downwards position. The effect occurred as the valve was positioned at a mid point between the two extremes.

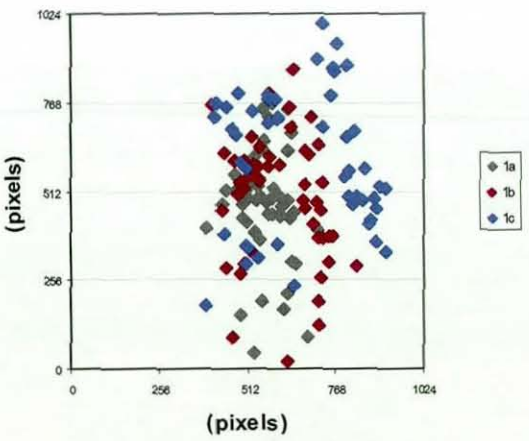

Figure 11.13a) Ball position at 8m

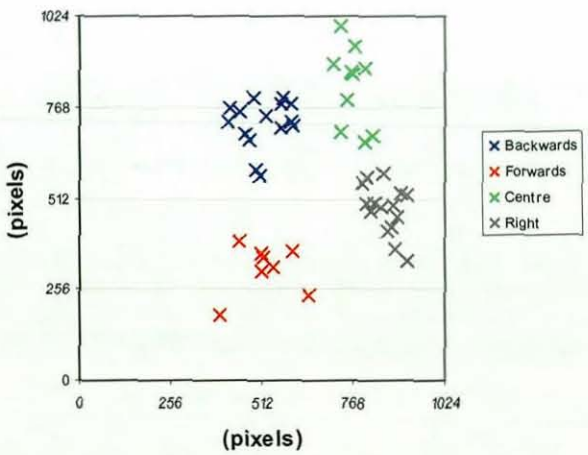

b) Ball position relative to impact position (CHS1c)

11.10.2.2 Mass Distribution

The inclusion of a number of valves within the CHS2 and CHS4 ball has reduced the spread of the points indicating the ball's position at the known distance. Although each of the positions still creates a cluster of points, there was minimal difference between the

clusters. Figure 11.14a) depicts the position of the CHS1c, CHS2 and CHS4 ball for all impact position, whilst Figure 11.14b) depicts the CHS4 balls position relative to impact position.

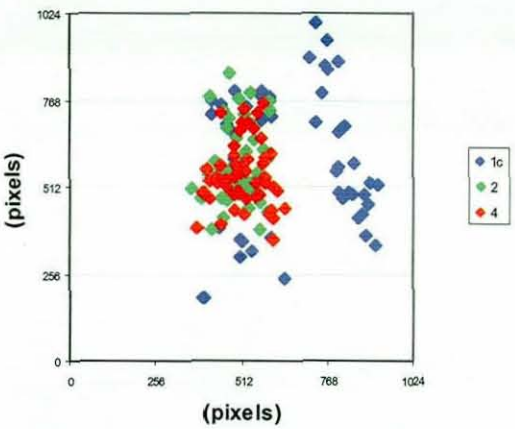

Figure 11.14a) Ball position at 8m

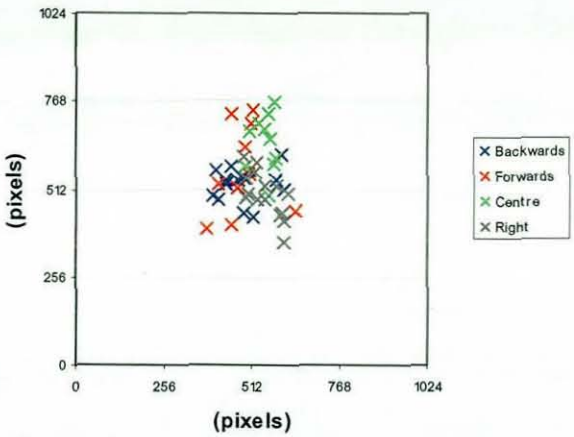

b) Ball position relative to impact position (CHS4)

11.10.2.3 Mean Ball Position Relative to Kicking Line

The mechanical kicking simulator was aligned with a calibrated grid on the floor of the airship hanger, which allowed the HSV1 to be accurately placed in the line of the kicking motion. In order to calibrate the line of the kicking motion, with respect to HSV1, an image was taken of a calibration pole 8m from the mechanical kicking simulator (Figure 11.15 a). This image allowed each of the x and y pixel co-ordinates measured to be converted into a height and lateral measurement. During a game a player may impact the ball in any orientation, therefore a set of data points was created for the theoretical left position, by mirroring the valve right data about the average x co-ordinate position, calculated using the upwards and downwards impact data,(Figure 11.15 b).

Fig 11.15a) Calibration image

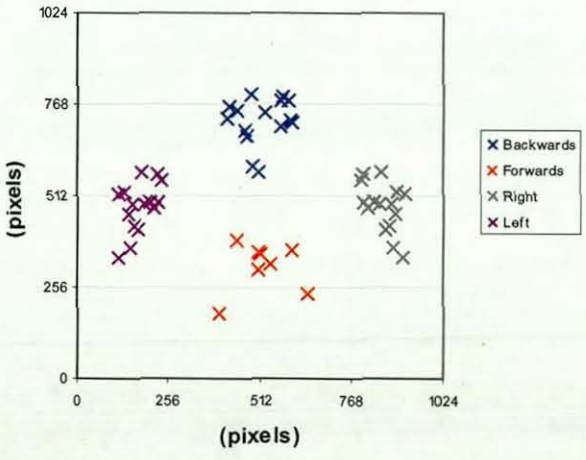

b) Ball position including 'theoretical' left (CH1c)

Analysis of the upwards, downwards, right and theoretical left positions allowed the mean, standard deviation and distance from theoretical kicking line to be calculated (Figure 11.16).

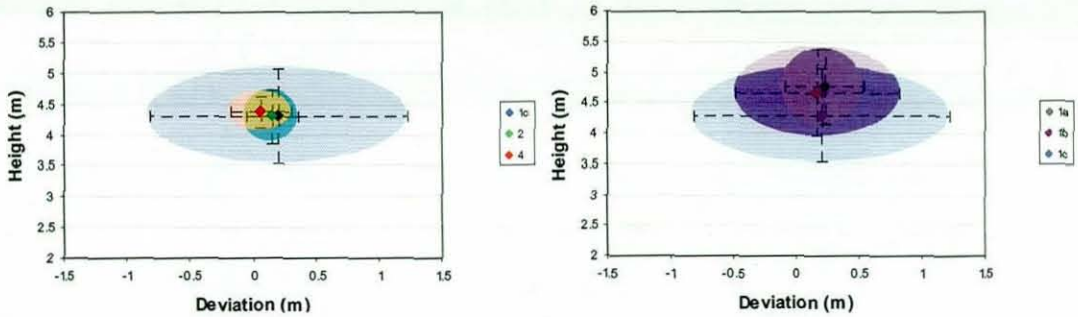

Figure 11.16a) Average ball position ±1SD b) Average ball position ±1SD

The average x co-ordinate position for the CHS1c rugby ball was only 0.20m from the theoretical kicking line, which was a similar value to the ball with the light valve (CHS1a). The increase in mass has had a negative effect by increasing standard deviation from 0.32 to 1.02m. The inclusion of the extra valves resulted in the smallest horizontal standard deviation, 0.21 and 0.31m for CHS2 and CHS4 respectively.

11.10.3 Unstable Axis of Rotation

Launch and flight characteristics measured within this chapter demonstrated that the rugby balls with multiple valves produced uniform characteristics irrespective of impact position. Figures 11.17 and 11.18 depict composite images of the CHS2 and CHS4 when impacted with the valve facing upwards and to the right, at a time interval of 0.1s. During rotation about the unstable axis it has been demonstrated that the rugby ball produced an increase in tilt angle as it twisted around the rifle axis, which can be seen during a valve right impact with the CHS2 ball. Chapter 8 details the aerodynamic effects of the wobbling mode, as the cross-sectional area of the ball increases along with the drag coefficient, creating a larger drag force. The wobbling mode was not visible during impacts with the CHS4 rugby ball in any valve orientation, due to the minimal difference between the intermediate and largest moments of inertia, when rotating about the equilateral axes.

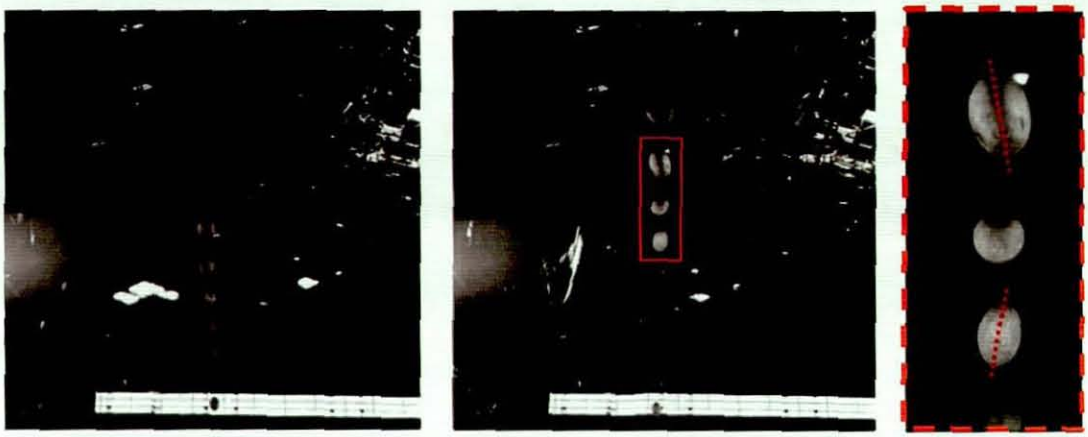

Figure 11.17a) Composite image CHS2 (upwards) b) Composite image CHS2 (right)

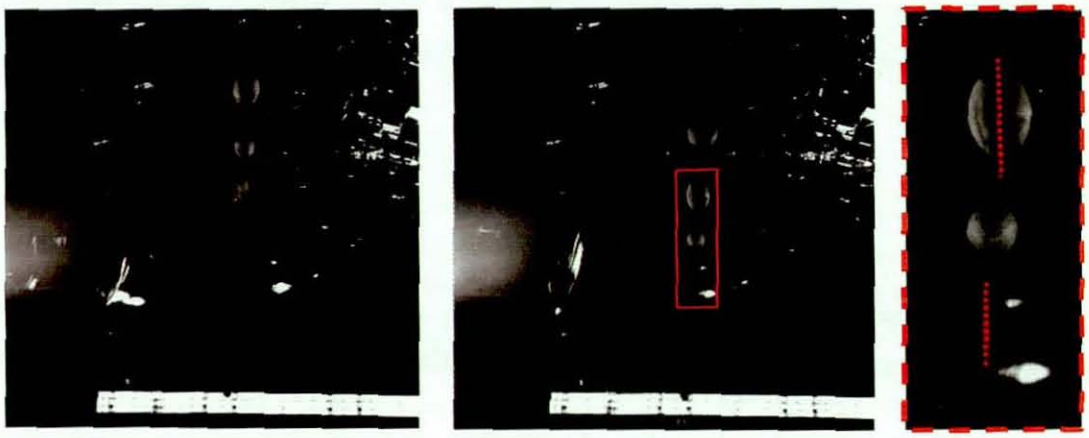

Figure 11.18a) Composite image CHS4 (upwards) b) Composite image CHS4 (right)

11.10.4 Kick Distance and Flight Time

In order to determine the balls' position of impact with the ground, at first bounce, a video camera operating at 25fps was positioned on one of the hanger's staircases at a height of 14m. A number of markers were placed within the camera's field of view at 5m intervals creating a calibration grid, allowing the point of impact with the ground to be digitised and the distance from the mechanical simulator calculated.

At the point of impact the mechanical kicking simulator produces a voltage which could be outputted to power a bright LED, placed within the field of view of the video camera using an extension cable. The flight time of the rugby balls could then be calculated by determining the number of frames between the lighting of the LED and impact with the ground. Figure 11.19 depicts a series of images from the impact video camera.

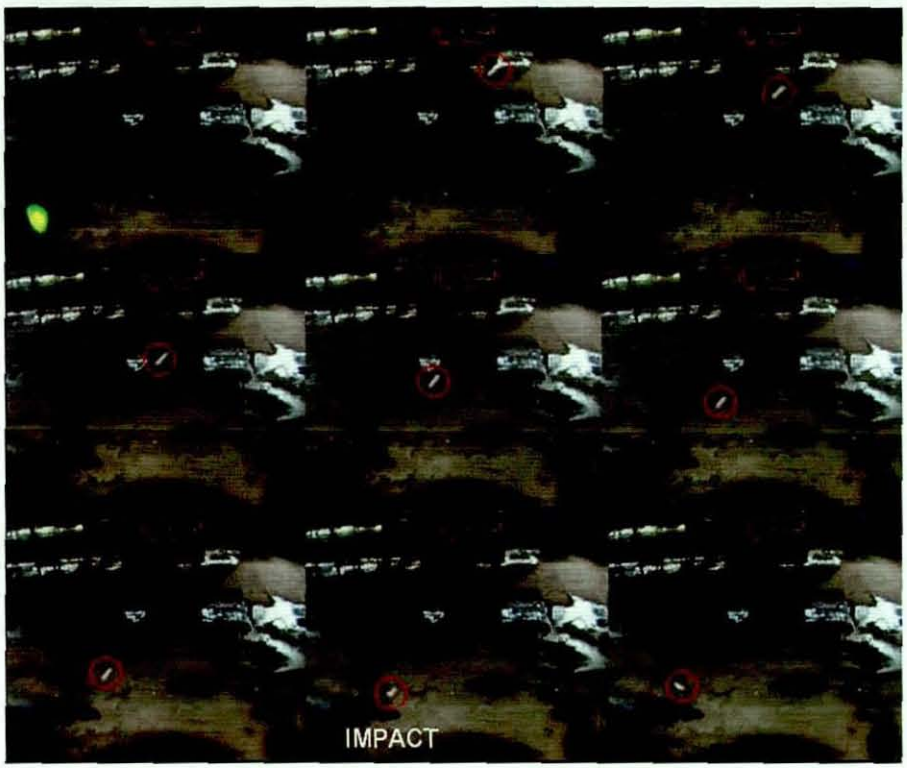

Figure 11.19 Series of images depicting the LED and point of impact with ground

Table 11.1 mean impact distance and flight time, ±1SD

Ball Type	Impact Position	Impact Distance (m)	Hang Time (s)
CHS1c	Upwards	56.7 ± 0.9	4.06 ± 0.14
CHS1c	Downwards	51.9 ± 1.7	3.29 ± 0.27
CHS2	Upwards	58.3 ± 1.7	3.86 ± 0.16
CHS2	Right	56.1 ± 1.1	3.60 ± 0.08
CHS4	Upwards	58.7 ± 0.9	3.89 ± 0.10
CHS4	Right	59.1 ± 0.5	3.81 ± 0.08

Figures 11.10 – 11.12 demonstrated a maximum variation in spin rate, velocity and elevation angle during impacts with the CHS1c rugby ball. Results showed that the mean impact distance and flight time decreased by 4.8m and 0.77sec when impacting the ball with the valve downwards, in comparison to an upwards impact. Figure 11.20 shows a composite image depicting the flight of the CHS1c rugby ball with the valve placed upwards and downwards. The reduction in distance and variation in angle of attack can clearly be seen.

Figure 11.20 Composite image of CHS1c a) valve upwards b) valve downwards

Results have shown that the CHS2 and CHS4 rugby balls had very similar launch characteristics irrespective of impact position, however the CHS2 ball produced an unstable rotation during flight with the valve to the right. The impact distance and flight time for the CHS4 rugby ball was very similar with the valve in the upwards and right positions. However the CHS2 ball showed a reduction in impact distance and flight time when the valve was placed to the right. This effect may be attributed to the unstable rotation discussed in Chapter 9, which will cause an increase in tilt angle during the twisting motion and may result in an increased drag force during the flight.

The number of half twists performed by the CHS2 rugby ball can be calculated using the moment of inertia valves, the flight time and the spin rate at launch. The difference between the I_{yy} and I_{zz} was calculated at 9.77%, which results in the ball performing a full twist every 7.5 rotations. When the valve was placed to the right, a spin rate of 194rpm was measured, resulting in the ball performing twenty five full twists and a single half twist before the point of impact with the ground.

11.11 Wear Effects

Previous studies have noted that the wear of sporting equipment may change the dynamic properties of the product during game related situations. The 'knocking-in' of cricket bats is common practice as it compresses and hardens the fibres of the wood. Sayers et al (2000) noted that the hardness of the bat face can double with only 4-6hours of knocking-in, whilst the core of the bat is left unhardened producing a more elastic response during ball bat impacts. Steele (2006) examined the degradation of tennis balls, and noted that the properties of the ball would change after repeated impacts with the racket and court. Changes in the ball's cloth and loss of ball pressure were identified as

areas of degradation, and their effect on the dynamic behaviour of the ball examined. It was noted that the natural ageing of a ball resulted in a lower stiffness and increased damping, whilst the variation in cloth condition had an important role in determining the impact and rebound characteristics of the tennis ball.

Results from the rebound test in Chapter 10 noted that the prototype rugby balls did not demonstrate a significant reduction in CoR during an end impact, normal to ovoid balls. The ball flight characterisation test was carried out prior to the laboratory based measurement procedures described in Chapter 10, which may have resulted in a wear effect occurring. In order to gain an understanding of the effect of repeated impacts, five match rugby balls were subjected to a wear simulation protocol, with repeated impacts using the mechanical kicking simulator. Their dynamic characteristics were established using the rebound test, pre and post wear simulation, to allow comparison. Each ball was subjected to one hundred and fifty impacts at a leg velocity of 20m/s, with the indentor impacting the ball as depicted in Figure 11.6.

Comparison of the rebound test data for pre and post wear simulation noted that the maximum variation in results occurred during end impacts. This effect was attributed to the impact position of the indentor during the wear simulation. Figure 11.21 depicts the pre and post CoR measured during the rebound testing.

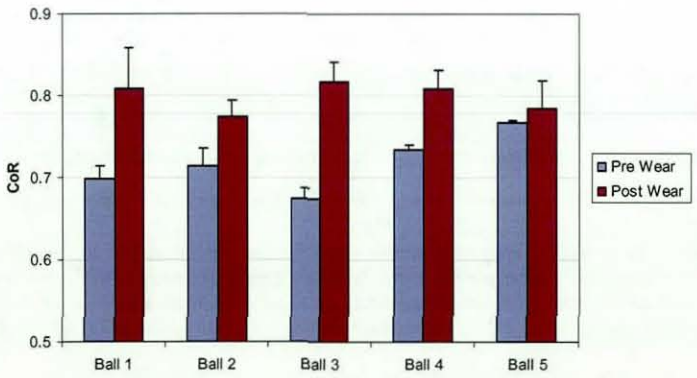

Figure 11.21 Rebound test – CoR for an end impact

Results show an increase in CoR post wear, possibly due to changes in the outer panel material properties and relaxation of the stiffness within the seams. In order to gain a better understanding of the mechanisms evolved further work needs to be conducted.

11.12 FE Comparison

The anisotropic FE rugby ball model developed in Chapter 8 was used to re-create the impact conditions measured in the airship hanger. The model was impacted with a rigid body indentor created to replicate the nylon end effector used on the mechanical kicking simulator. The leg rotation of the mechanical kicking simulator was created by rotating the indenter at a constant velocity about a reference point 0.9m from its centre line (Figure 11.22). The angle of the ball and position of the impact were generated using measurements taken from the experimental tests.

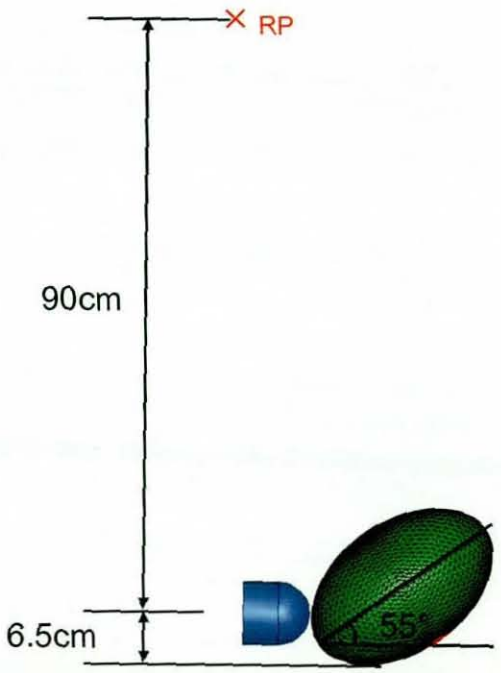

Figure 11.22 FE mechanical kicking simulation

Figures 11.23 – 11.25 depict the experimental ball launch characteristics of the RGB 1 rugby ball when tested under the wind free conditions, and the anisotropic FE rugby ball rotating impactor simulations.

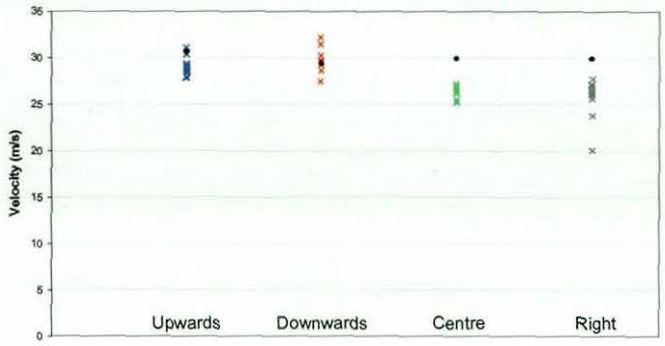

Figure 11.23 Ball velocity

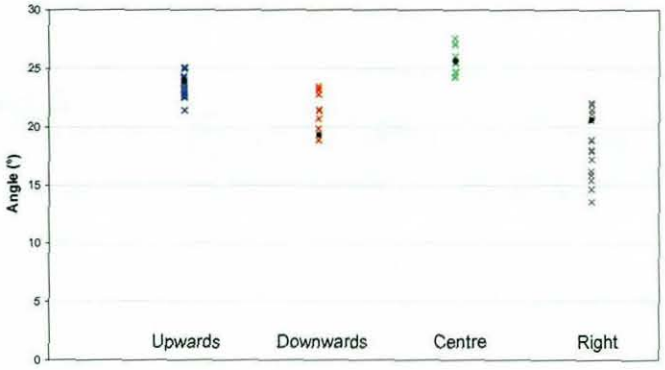

Figure 11.24 Elevation angle

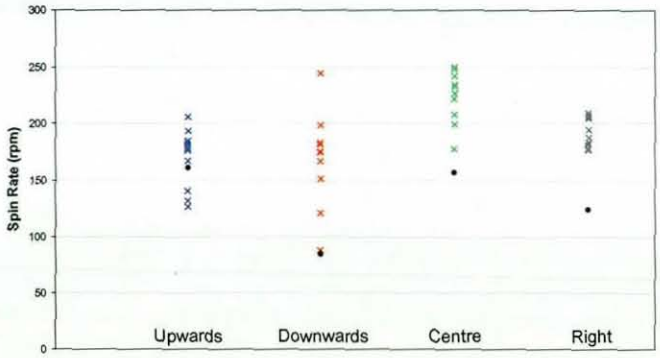

Figure 11.25 Spin rate

The experimental results for the RGB 1 rugby ball demonstrate a similar trend to those recorded for the prototype rugby ball with the single valve. The ball velocity measured during FE simulations demonstrated minimum variation with valve impact position. Changing impact position caused a variation in the results for elevation angle and spin rate, due to the large mass of the valve and its placement. FE simulations showed good agreement with the experimental results with the minimum elevation angle recorded when the valve is placed downwards, and the maximum recorded during centre impacts. The elevation angle for the right valve position lies between the angles for the upwards

and downwards positions. FE simulations underestimated the spin rate values measured experimentally, although the positional trend demonstrates good agreement with the experimental results.

Figure 11.26 depicts the RGB 1 and FE simulation deviation data. It can be seen that generally the experimental results validate the FE simulations. The vertical height, at a horizontal distance 8m from the mechanical kicking simulator, demonstrates good agreement with the experimental data, which validates the agreement with the elevation angle. The lateral deviation when the valve was placed to the right and centre position demonstrates a similar trend to the experimental data, although the experimental data demonstrates a greater deviation. The ball velocity measured during FE simulations (Figure 11.23), demonstrated minimum variation with valve impact position, unlike the experimental data. The measurement of the 2D ball velocity did not take into account any out of camera plane velocity, and the increased lateral deviation measured experimentally may explain the variation between experimental and FE simulation results. During impacts with the valve upwards and backwards, FE simulations calculate a deviation of 0m, however the experimental results range from -0.52 to 0.4m. The increase in experimental deviation could be attributed to human error when aligning the ball on the kicking tee, or errors in the alignment of the robot.

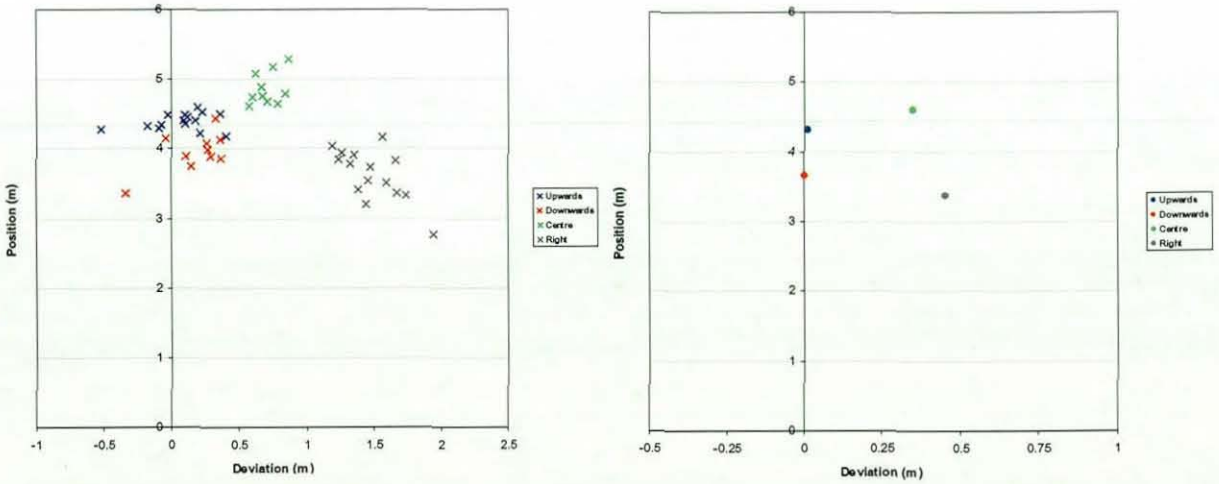

Figure 11.26a) Experimental ball position at 8m b) FE simulations of ball position at 8m

11.13 Discussion

11.13.1 Valve's Effect on Launch Parameters

For single valve balls, adjusting the valve position relative to the impact position caused a significant variation in the elevation angle and spin rate of the rugby ball. The change in launch parameters could be attributed to either the stiffness variation caused by the valve, or the effect of the valve displacing the centre of mass of the ball from the centroid. Non-uniform stiffness would affect the deformation of the ball, causing the area with lower stiffness to deform at a higher rate producing rotation within the ball. FE simulations allowed these theories to be examined using two separate models. The first model, used to examine the effect of the stiffness, incorporated a second valve with identical dimensions and density (Figure 11.27), similar to the CHS2 ball, but assigned a material with a higher stiffness. The Elastic Modulus of the bladder and higher stiffness material were 0.84 MPa and 564 MPa respectively, creating a FE model with a non uniform stiffness but a coincident centre of mass and centroid. Simulations were completed with the stiffer valve facing upwards and downwards.

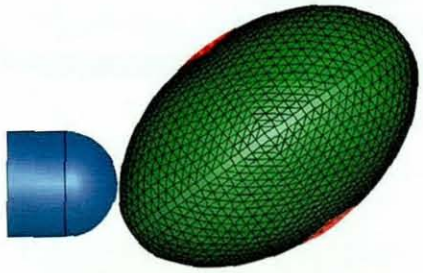

Figure 11.27 FE model with two valves of different stiffness

The incorporation of the over weighted valve within the RGB 1 rugby ball resulted in the centre of mass no longer coinciding with the centroid. The inclusion of the valve region created an offset between the centroid and the centre of mass, calculated to be 17.98mm. The force created by the impactor during contact with the ball creates a moment about the centre of mass, similar to that described in the bounce characterisation test (Chapter 4). Figure 11.28 depicts the angle of the force, created by the moving impactor throughout the contact with the ball during impact with a deformable FE model.

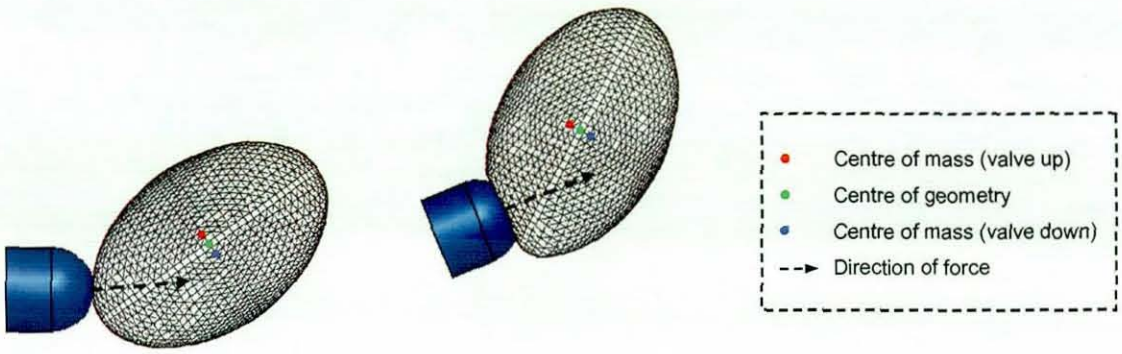

Figure 11.28 Image depicting the valve's effect on the centre of mass

A rigid body constraint was applied to the elements representing the ball within the FE model, creating a rigid body model in which stiffness variation could not have an effect. FE simulations with the rigid body constraint produced higher elevation angle, due to zero deformation during the contact period. As a result simulations were carried out with an initial ball angle of 55° and 30°, in order to allow fair comparison.

Results indicated that the position of the stiffer valve region, upwards or downwards, within the deformable model resulted in minimal change in elevation angle (<1°). Adjusting the centre of mass of the rigid model, by varying the position of the valve, relative to the centroid produced a variation in elevation angle of 21.3 and 18.6% for ball angles 30 and 55° respectively, with the higher elevation angle measured with the valve in the upwards position. Variation in stiffness produced an increase in spin rate of 12% (47.2rpm) when the stiffer valve was placed in the upwards position. This increase in spin rate was attributed to the lower levels of deformation in the stiffer valve, hence creating an increase in rotation. Adjusting the position of the centre of mass within the rigid model caused an 80% increase in spin measured (302.2rpm) when the valve was facing upwards.

11.14 Conclusions

The mechanical kicking simulator developed was capable of reproducing the launch conditions experienced during rugby and soccer game related impacts in an accurate and repeatable manner, with the exception of spin. A maximum velocity of 50m/s was achieved, with the repeatability of the leg velocity calculated to ±0.032m/s (95% confidence). This velocity is currently greater than those measured during player testing.

The adjustable teeing mechanism and velocity profile software allows for the initial launch angle and ball velocity of a rugby place kick to be accurately replicated. However the tumble axis spin produced during simulation is lower than that recorded experimentally. This is possibly due to the current differences between the end effector and the leg motion of the simulator in comparison to the players' kicking action, as currently the natural deceleration of the foot is not simulated with the rotating leg.

The re-creation of the place kick in wind free conditions allowed the effect of the valve mass and the mass distribution to be measured. Results showed that increasing the mass of a single valve within the rugby ball created inconsistent flight characteristics when impacting the ball in a number of different positions. The significant variations were measured for elevation angle and spin rate. Increasing the mass of a single valve resulted in a greater deviation from the kicking line when the valve was placed in the centre and right positions. The results for all of the rugby balls with a single valve showed that the ball's deviation from the centre line was dependent upon impact position, and a distinct cluster was produced for each of the impact positions. The introduction of multiple valves within the ball's bladder, created rugby balls (CHS2 and CSH4) that had uniform ball velocity, elevation angle and spin rate irrespective of impact position. The position of the x and y co-ordinates of the balanced balls was independent of impact position with no distinct clusters forming. The average co-ordinate position of the CHS4 rugby ball was 5.9cm from the theoretical kicking line and having a horizontal standard deviation of 0.31, in comparison to the 1.02m for the CHS1c rugby ball.

The anisotropic FE model was used to re-create the impact conditions measured under wind free conditions. The simulations and experimental data showed good agreement for ball velocity and elevation angle. The spin rate showed a similar trend to the experimental results, although the values were underestimated. The deviation from the kicking line demonstrated a similar trend to the experimental data although the values were underestimated. The increase in experimental deviation could be attributed to human error when aligning the ball on the kicking tee, or errors in the alignment of the robot.

The anisotropic FE model allowed the variation in elevation angle and spin rate to be explored. It is suggested that the variation in elevation angle measured during the experimental testing can be attributed to the effect of displacing the centre of mass from

the centroid, causing a 20% increase in elevation angle when the valve was facing upwards. The variation in spin rate was found to be affected by both a non uniform stiffness in the ball, and a displacement of the centre of mass. It was noted that a considerable difference in stiffness between the valves only resulted in a 12% increase in spin, when the stiffer valve was facing upwards. However the effect of moving the centre of mass away from the centroid, by placing the valve upwards resulted in an 80% increase in spin.

Chapter 12

Novel Rugby Ball Design

12 Introduction

The following chapter details the development of a novel rugby ball design that will be constructed from a latex bladder, panelled carcass (to provide the structure) and thermo-bonded outer panels. The thermo bonded technology provides significant design opportunity for different outer panel shapes, whilst the inner carcass can have an increased number of inner panels, in various configurations, which will improve its performance. Each one of the designs will try to alleviate some of the current problems that exist within a four panel manually stitched rugby ball.

12.1 Soccer Ball Manufacture

12.1.1 Manually Stitched

The majority of manufactured soccer balls consist of a number of composite panels manually stitched together, around a bladder which allows the ball to be pressurised. The bladder would typically be manufactured from a rubber latex or thermoplastic polyurethane (TPU). The composite panels consist of three layers, an outer PU film to provide waterproofing, PU foam layer to increase damping and feel between the ball and foot, and a number of woven fabric layers consisting of polyester/cotton fibre yarn. The majority of the designs are based around a thirty two or eighteen panel design (Figure 12.1). The thirty two panel design has been based up a truncated icosahedron consisting of twelve pentagons and twenty hexagons, whilst the eighteen panel design is based upon a spherical hexahedral polyhedron.

Figure 12.1 Panel configurations of manually stitched soccer balls

12.1.2 Thermo-bonded Construction

In 2004 adidas released the 'Roterio' soccer ball used for the European Championships, which was revolutionary due to its thermo-bonded construction. The manufacturing procedure was developed to increase consistency of products, whilst reducing production time and cost. The thermo-bonded ball depicted in Figure 12.2, consists of a latex bladder, around which a twelve panel dodecahedron machine stitched fabric carcass provides the integral structure of the ball, onto which the outer panels are adhered. The outer panels consist of a ethylene-propylene-diene-monomer (EPDM) foam and an outer PU layer, and these panels are moulded and have an appropriate surface curvature.

Figure 12.2 Thermo-bonded ball exploded view

The carcass panels consist of two layers of polyester and cotton yarn based woven fabric, orthogonally bonded with latex glue. These panels are stamped from a sheet of material and machine stitched in order to form the dodecahedron structure. The orientation of the stamped panels defines the stiffness and the uniformity of deformation during impact. Price (2005) demonstrated the effect of impacting the carcass in various orientations, and its effect on contact time, CoR and deformation. The outer and foam layers are stamped and thermoformed in order to produce outer panels with the desired shape. The edges of these panels are glued and inserted into a double hemisphere mould (Figure 12.3). The inflated carcass is then inserted and the mould is closed and heated to allow the adhesion between the carcass and outer panels.

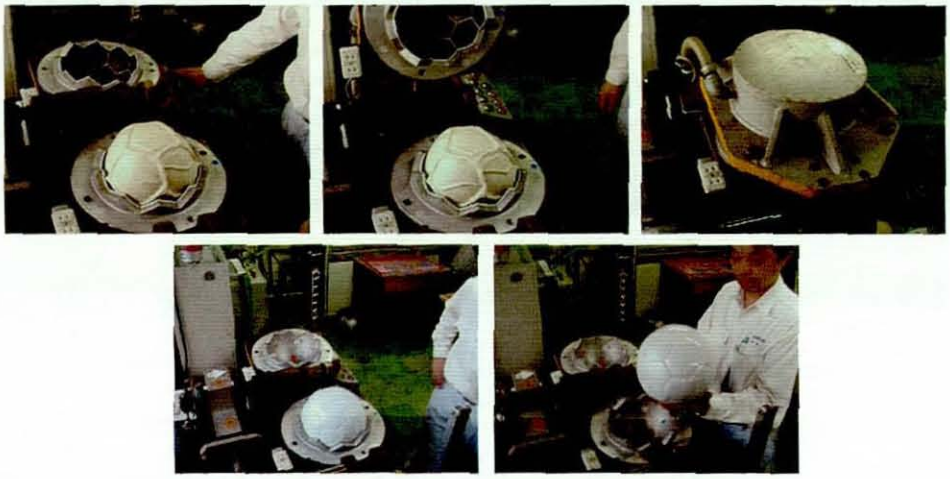

Figure 12.3 Thermo-bonded ball manufacture

One of the major advantages of the thermo-bonded manufacturing technique is the increased design flexibility. The Roterio soccer ball had a thirty two outer panel construction based upon the truncated icosahedron, however the ball released by adidas for the 2006 soccer World Cup, (Teamgeist), only had fourteen outer panels. The Teamgeist outer panels consisted of six 'propeller' and eight 'turbine' panels (Figure 12.4), and reduced the number of points where three panels joined together by 60%, from sixty to twenty four, improving the measured sphericity of the ball. Prior to the Teamgeist soccer ball, the largest ball sales based on a conventional stitched ball was four million for the 2002 World Wup Fevernova ball. To date, sales for the Teamgeist have exceeded twenty million emphasising the ball's inherent quality based on the new technology. Rugby ball's have been, and are currently produced using conventional stitched methods, and the success of the thermo bonded technology provides an opportunity for increased design flexibility and improved performance. This chapter investigates the possibility of using the new technology for ovoid balls.

Figure 12.4 Teamgeist outer panel construction

12.2 Novel Designs

Analysis of the stitching region within a rugby ball showed an increase in the Elastic Modulus, by a factor of 3.9, in comparison to the centre of the panel. This increase in stiffness causes non uniform stress and volumetric increase during inflation (Figure 12.5). The non uniform stiffness affects the dynamic behaviour of the ball, as the CoR, contact time and deformation measured during impacts varied depending upon the ball position pre impact. During a game players would expect the ball to produce similar characteristics whether the ball is impacted on the seam or the centre of the panel, and currently this is not the case.

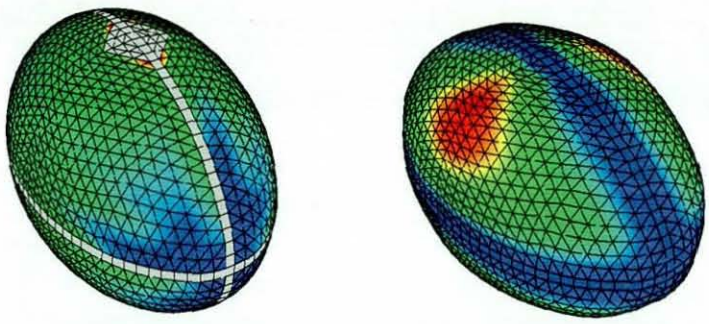

Figure 12.5a) Non uniform stress b) volumetric increase

It is anticipated that the introduction of carcass and formed panel construction methods will achieve consistent ball behaviour. The IRB rules state that a rugby ball must consist of four panels, and because of the traditional manufacturing methods this has tended to be of four petal shaped stitched panels. However the introduction of the thermo bonded manufacturing technique provides significant design opportunity for different outer panel shapes, whilst the inner carcass can have an increased number of inner panels in a configuration which may improve performance. Clearly there is a balance between performance improvement and manufacturing efficiency to be considered, and the next section considers several design possibilities. The optimisation of material anisotropy analysed by Price (2005) may not be considered to be so significant for ovoid ball design. The shape of the ovoid ball will result in symmetrical deformation during a normal impact, only occurring during an end or centre of the panel impact. The important factor for ovoid balls is that there is symmetry for impacts either side of the centre line. This needs to be considered when creating future designs.

12.3 Rhombic Dodecahedron

The carcass creates the integral structure of a thermo-bonded ball and controls the dynamic behaviour of the ball during impact scenarios. In order to create a more uniform stiffness throughout the ball, it is important to discretise the shape of a rugby ball into a number of smaller panels. A polyhedron is a three dimensional mathematical shape constructed from a number of polygons or faces, with their origin attributed to early Greek mathematicians Shenitzer and Stillwell (2002) state that the five regular polyhedra were known to the Greeks and Etruscans around 500_{BC}. The naming system of the polyhedron is based upon the Greek alphabet and with the name detailing the number of faces within the shape. For example a tetrahedron has three faces, whilst a dodecahedron has eight. The suitability of the different polyhedron was analysed and it was found that the rhombic dodecahedron, with twelve rhombic faces and fourteen vertices (Figure 12.6), would allow the shape of a rugby ball to be discritised into a series of smaller panels. The increased number of identically shaped panels and non parallel nature of the seams is likely to result in a more uniform distribution of stress within the ball. This construction has the advantage that it consists of only two panel shapes.

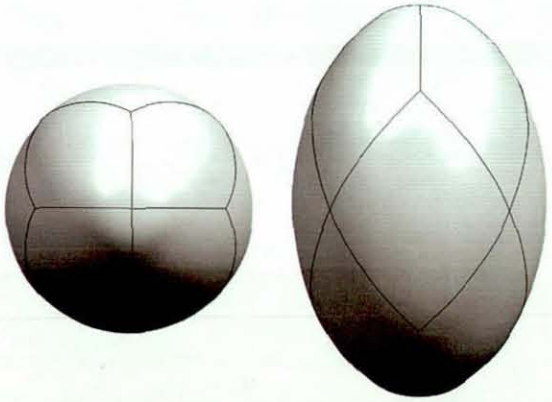

Figure 12.6 Rhombic Dodecahedron

12.3.1 Unigraphics Flat Pattern Function

The shape of the novel ball panels were constructed using the CAD package Unigraphics, which allowed the polyhedra to be re-constructed using the 3D co-ordinates of the vertices, and the edges of the faces projected onto the surface of the rugby ball. The projected lines could then be used to discretise the surface model into the correct panel shapes and using the 'Flat Panel' function the 3D surface was converted to a set of 2D panel shapes. The 'Flat Pattern' function used did not take into account the directionality of the woven fabric, which may stretch in a non uniform manner, but

assumed isotropy within the material. Figure 12.7 depicts the flattened 2D shape of the centre panel M1, created using the 'Flat Pattern' function of a rhombic dodecahedron. The 2D shape can then be used to create a cutting pattern, or an input drawing for a carbon dioxide laser cutting device.

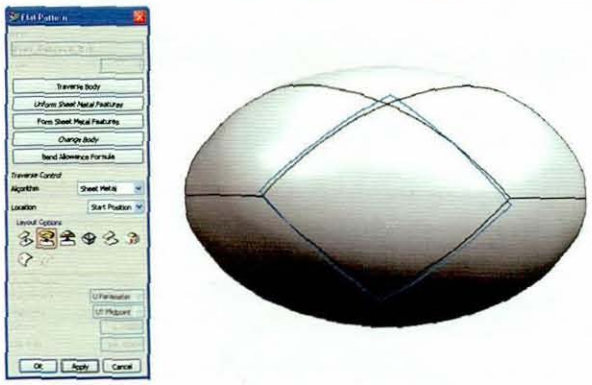

Figure 12.7 'Flat Pattern' function used to create 2D shape of middle panel

12.3.2 Sewing Machine Specification

The layered carcass material and thread used during the manufacture of thermo-bonded soccer balls was used in the creation of prototype novel rugby ball designs. The carcass material required a heavy duty industrial sewing machine due to the stiffness and the thickness of the proposed seams. A Durkopp single needle walking foot lockstitch machine, with under bed trimmer, was used in the manufacturing process, as the walking foot allows the unified feed of material from above and below, helping to keep the heavy duty material in the correct position. The density of the stitching was calculated by measuring the average distance between stitches on a carcass soccer ball. The sewing machine allowed the stitch length to be programmed, along with the back tacking at either end of each seam, to secure the seam ends, and the final trimming of the thread.

12.3.3 Assembly

The panels were joined together "inside out", in a devised sequence to aid the final assembly process. Figure 12.8 depicts the net diagram of a rhombic dodecahedron, with eight end panels (E1-E8) and four middle panels (M1-M4), and indicates the areas of machine and hand stitching.

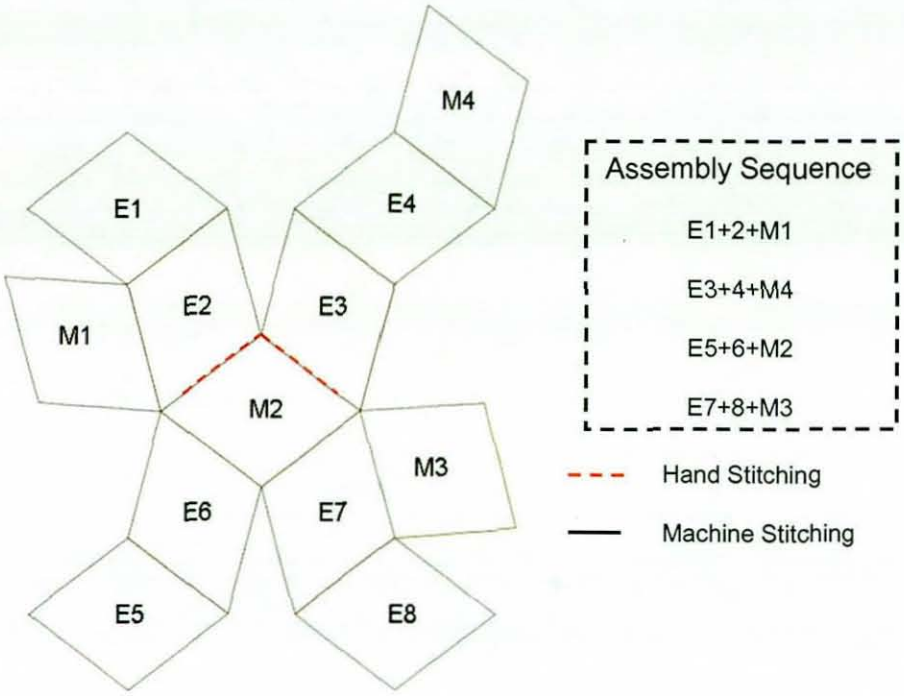

Figure 12.8 Rhombic dodecahedron net pattern

The assembly involved joining two end panels together, then attaching a middle panel, repeated four times.

Figure 12.9 Joining of one middle and two end panels

These three panel combinations were joined together leaving a small opening to allow the ball to be turned the "right side" out. In order to aid the final hand stitching, the sewing machine was used to punch holes through the fabric to provide a guide for the hand stitches. Heat was used to increase the flexibility of the material to aid the process of turning the ball the "right side" out.

Figure 12.10 Construction of fourteen panels still inside out

The bladder was inserted through a small hole, and the ball completed by hand stitching the final seams.

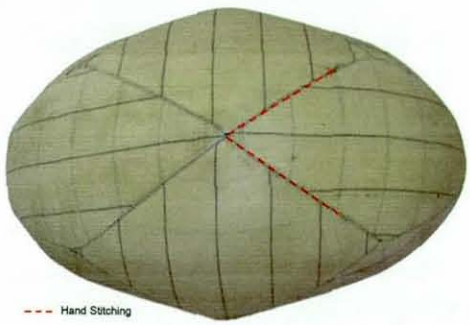

Figure 12.11 Complete construction of rhombic dodecahedron

12.3.4 Problems with the Rhombic Dodecahedron

The rhombic dodecahedron consists of twelve rhombic faces and fourteen vertices, with four panels converging at six of the vertices. The four vertices around the middle of the ball create an irregular shape due to the overlap of each panel creating a volume of excess seam material (Figure 12.12).

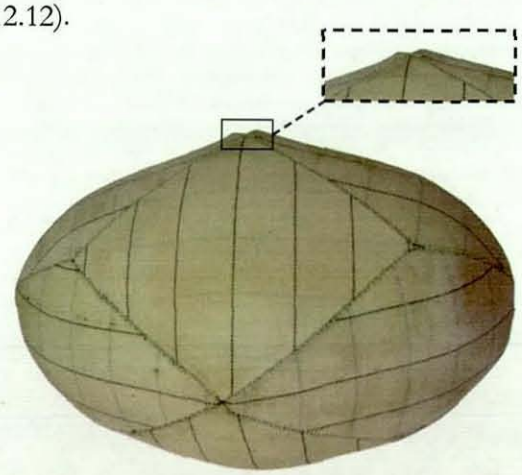

Figure 12.12 Material bulge caused by four panels converging at a vertex

The eighteen or thirty two panel soccer balls only have a maximum of three panels meeting as a single vertex, as this produces adequate room for the volume of excess material to lie flat causing a ridge-less seam. In order to overcome this issue with the rhombic dodecahedron, an alternate solution with only three panels meeting at the middle vertices was required.

12.4 Other Possible Geometric Shapes

12.4.1 Rhombo-Hexagonal Dodecahedron

The rhombo hexagonal dodecahedron or extended rhombic dodecahedron is a convex polyhedron with eight rhombic and four equilateral hexagonal faces (Figure 12.13). The twelve panel design only has three panels meeting at the middle vertices, which will remove the irregular shape caused by the excess volume of material. The design did not consist of uniform panel shapes due to the inclusion of the hexagonal faces, which are likely to result in a non uniform stress throughout the ball. Unfortunately the design also included two end vertices which have four panels converging at a single point.

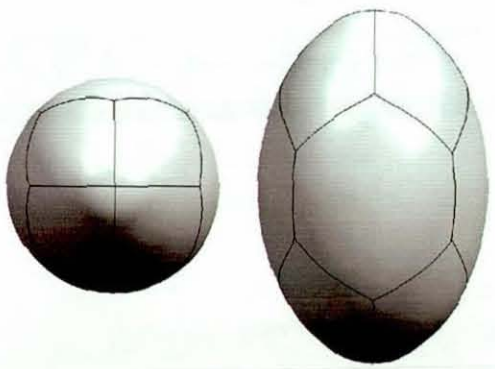

Figure 12.13 Rhombo hexagonal dodecahedron or extended rhombic dodecahedron

12.4.2 Tetragonal Trapezohedron

The tetragonal trapezohedron has eight faces which are congruent "kites" (Figure 12.14). Each of the panels within the tetragonal trapezohedron are identical in shape resulting in a more uniform stress distribution throughout the ball, which also reduces the cost of production as only a single panel shape needs to be stamped, in addition to a smaller number of panels. Unfortunately the design still features four panels meeting at the end vertices.

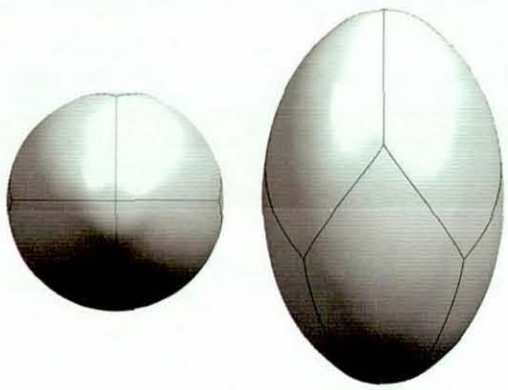

Figure 12.14 Tetragonal trapezohedron

12.4.3 Trigonal Trapezohedron

The trigonal trapezohedron has six faces which are congruent rhombi (Figure 12.15). Each of the panels are identical in shape, resulting in a more uniform stress distribution and a reduction in production costs. There are only three panels converging on a single vertex, creating a regular shape, due to the reduction in volume caused by the panel overlap. Only six panels are used in the construction of the trigonal trapezohedron resulting in a significant reduction in production time for prototypes (60mins for the rhombic dodecahedron to 35mins).

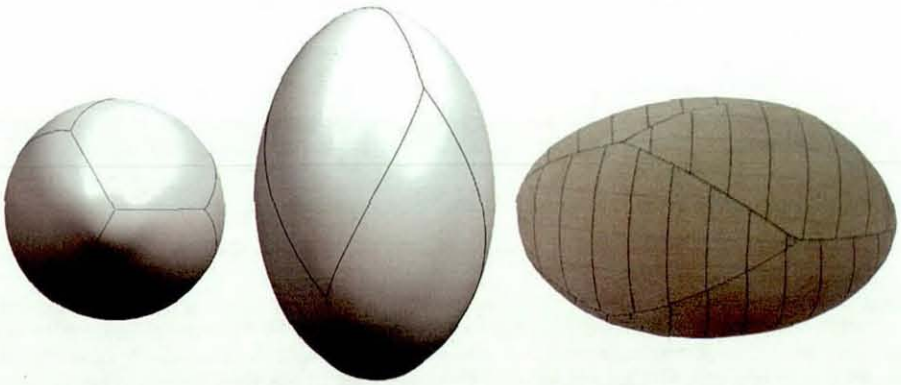

Figure 12.15 Trigonal trapezohedron model and prototype

12.4.4 Dodecahedron

The dodecahedron consists of twelve regular pentagonal faces, with three meeting at each vertex, with thirty vertices in total (Figure 12.16). The dodecahedron forms the carcass used in the thermo-bonded soccer ball and each of the pentagons are of identical shape. Increasing the number of panels within the carcass will increase production costs, but may allow a greater amount of freedom when assigning the material orientation of each of the carcass panels, allowing its dynamic properties to be optimized.

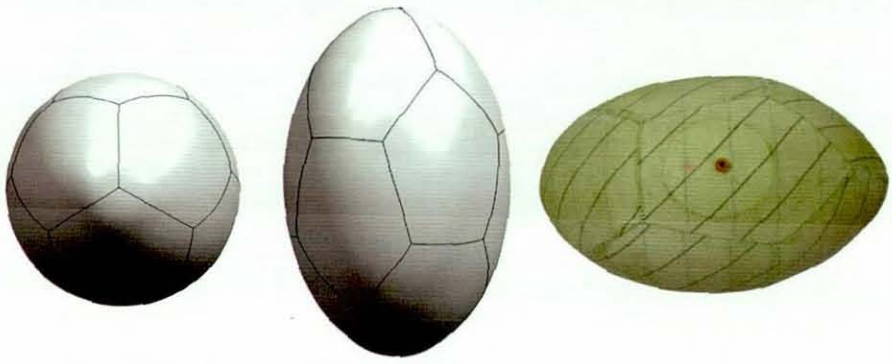

Figure 12.16 Dodecahedron model and prototype

12.5 FE Carcass Models

The trigonal trapezohedron and dodecahedron models were chosen for further evaluation as both desigsn provide a more uniform stress distribution due to the similar panel shapes within each design, and the non parallel nature of the seams. FE modelling will be used as a tool to evaluate the effectiveness of the different designs, allowing the effect of panel arrangement and material orientation to be analysed. Unfortunately due to confidentially conflicts with our collaborators we were unable to obtain enough carcass material to experimentally validate the FE models, therefore only simulated results are presented.

The geometric shape was projected onto the surface of the rugby ball geometry, allowing the surface to be divided into a number of smaller surfaces. Each of the surfaces used to create a carcass design were then discretised into a series of smaller surfaces to allow greater control during the mesh production (Figure 12.17).

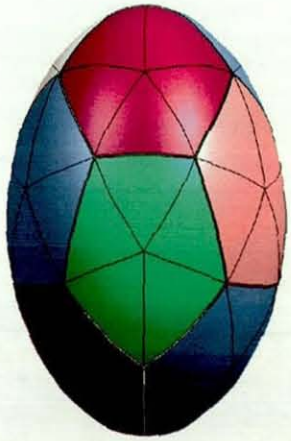

Figure 12.17 Dodecahedron surface discretised for meshing

The surface geometry allowed a uniform three node triangular shell element mesh to be created, coupled with hydrostatic elements in order to pressurise the model. The stitching region was defined with 4 node quadrilateral shell elements, and material models were created for the bladder, carcass and stitching material, and applied to the FE model.

12.6 Material Model Production

12.6.1 Carcass Material Assessment

The woven fabric used in the construction of the carcass has material properties dependent upon the direction of strain. The material was subjected to a series of directional tensile tests in order to allow the effect of the material anisotropy to be determined. Specimens were prepared at 15° increments from 0 to 90°, as depicted in Figure 12.18, and tensile tests were carried out at a strain rate of 500mm/min, to a maximum strain of 0.6 with five repeats per material orientation.

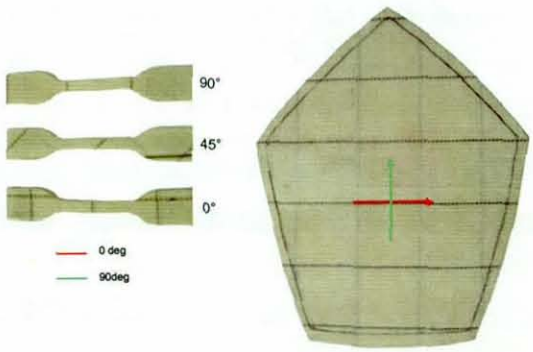

Figure 12.18 Carcass material samples and dodecahedron panel

Figure 12.19 depicts the average strain-strain response of the carcass material at the different material orientations.

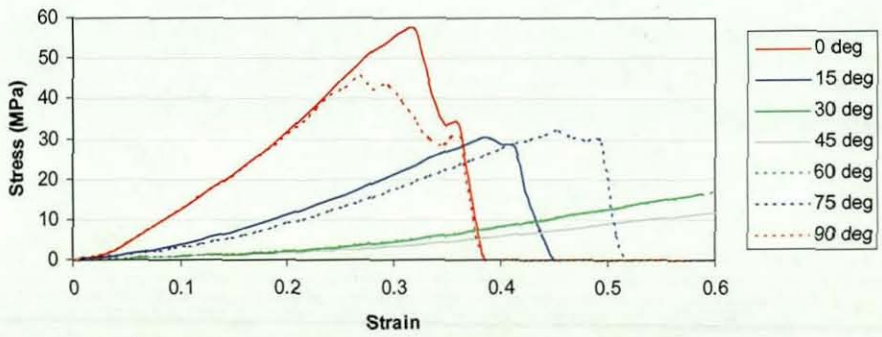

Figure 12.19 Stress strain response of the carcass material

The maximum stiffness was measured when the carcass material was strained in line with the fibre orientation, 0 and 90°, whilst the greatest reduction in stiffness was measured at

a 45° fibre orientation. Material failure was noted during the straining of samples at 0, 15, 75 and 90°, whilst samples at 30, 45 and 60° did not fail when strained to a maximum value of 0.6. The stiffness values measured at 30 and 15° were very similar to those measured at 60 and 75° respectively, which was attributed to the fact that they are at the same angle relative to one of the two principle fibre orientations.

12.6.2 Stitching Assessment

A jig, similar to that developed in Chapter 7, was used to measure the stiffness of the stitching region in a carcass ball (Figure 12.20).

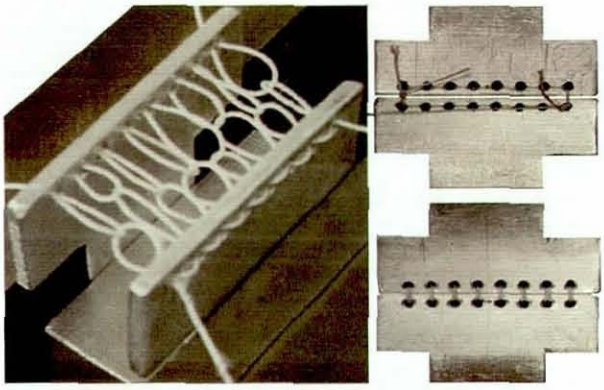

Figure 12.20 Caracas stitching seam assessment

The stitching was strained to a value of 0.4 at 100mm/min and the results can be seen in Figure 12.21, which also depicts the stress strain response of the outer panel material at 90 and 45° material orientation.

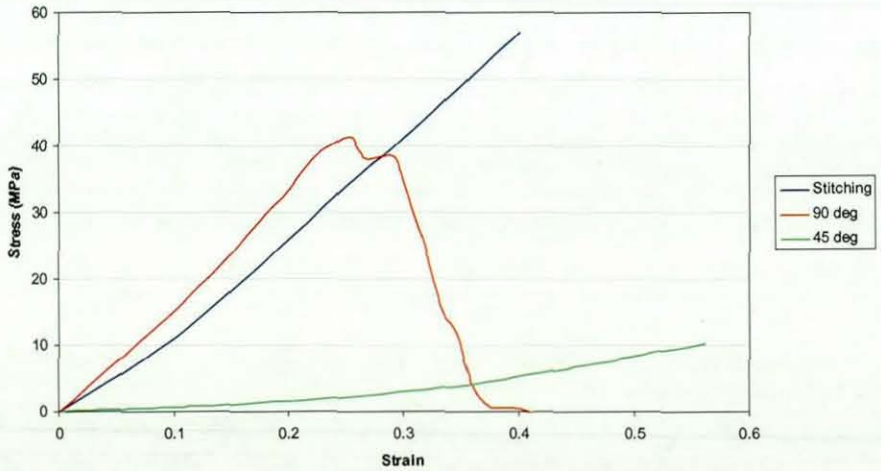

Figure 12.21 Stress strain response of carcass stitching

Results showed that the stress strain response of the carcass stitching material was softer than the carcass at 90° material orientation, which was considerably lower than the

material values used in a manually stitched ball. The carcass stitching material consisted of a yarn with similar dimensions and material properties to the carcass material, which would explain the comparable stiffness.

12.6.3 FE Material Model

The results from the tensile tests were used to calculate the Elastic Modulus of the material at the various fibre orientations. In order to simplify the production of the material model, it was assumed that the material stiffness was similar at 0 and 90°, and the ABAQUS Lamina material model was used to define the anisotropic material behaviour (Figure 12.22).

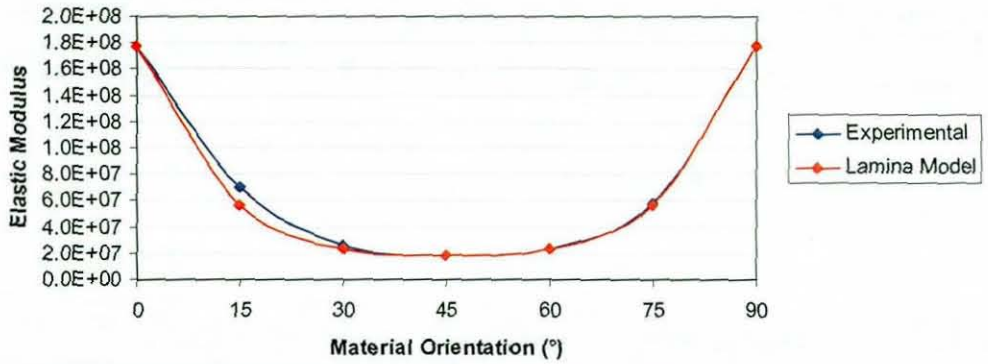

Figure 12.22 Elastic Modulus of experimental and Lamina material model

12.7 Inflation

It has be previously shown that the inclusion of the stitching region within a rugby ball results in a non uniform stress and volumetric increase across the ball, with the stitching region producing higher levels of stress in comparison to the centre of the panel. The non uniform stiffness within the ball affects the dynamic behaviour of the ball, as experimental and FE simulations have shown a change in measured parameters depending upon impact position. The dodecahedron and trigonal trapezohedron FE models were inflated to a standard pressure, 9psi, in order to allow the uniformity of ball stiffness to be evaluated. Figure 12.23, depicts the stress within a four panel stitched ball, a dodecahedron and trigonal trapezohedron carcass model.

It has been demonstrated during experimental normal impacts, Chapters 3 and 6, that impacting the ball on the seam and centre of the panel resulted in a variation of measured parameters. The inclusion of the non-parallel seams within the trigonal trapezohedron and dodecahedron carcass models has resulted in a uniform stress distribution across the

surface of the ball, which will result in an increased uniformity of the dynamic behaviour of the ball during impacts.

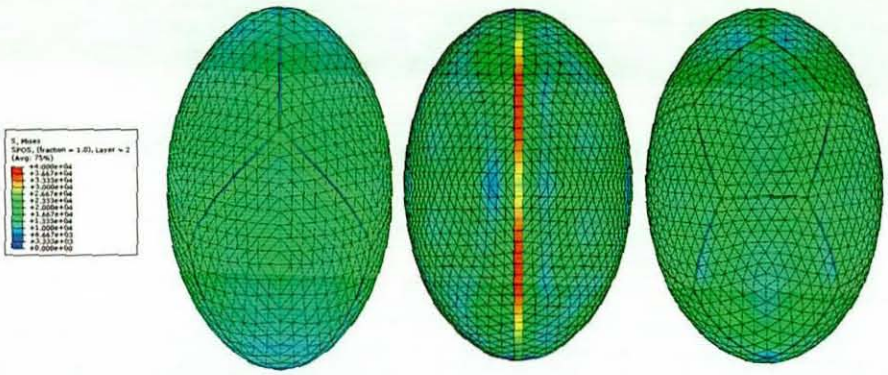

Figure 12.23 Inflation Stress a) Trigonal trapezohedron b) 4 panel c) Dodecahedron

12.8 Effect of Material Orientation

12.8.1 Stress and Volumetric Increase

The dodecahedron has an increased number of panels in comparison to the trigonal trapezohedron, and a FE model was used to examine the effect of the material orientation within the carcass. Models were created with 0° and 45° material orientation and a combination of both (Figure 12.24).

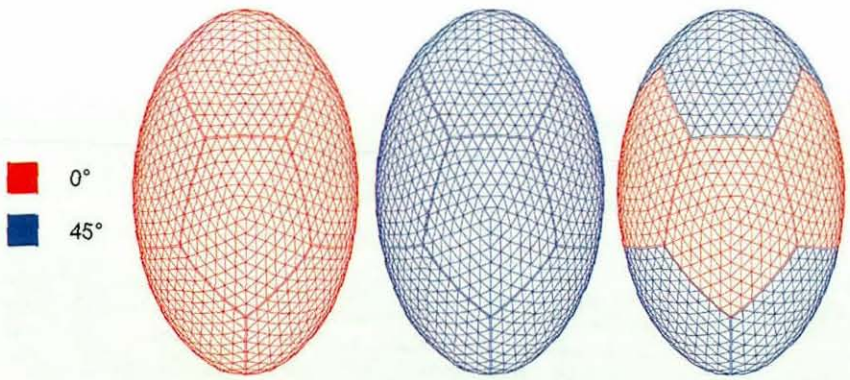

Figure 12.24 Dodecahedron model with different material orientation

The variation in material orientation affected the shape and the stress of the carcass during inflation to 9psi (Figure 12.25), with the 0° carcass showing the minimal volumetric increase and stress within the panels, which was symmetrically distributed. The 45° carcass demonstrated high levels of stress due to the reduction in stiffness of the material at this orientation, and resulted in the significant volumetric change. The carcass with a combination of material orientations showed an increase in stress in panels at the

top and the bottom of the ball, as these panels had a 45° orientation. The combination of different material orientations resulted in a non uniform volumetric increase, as the bottom and top panels increased at a greater rate.

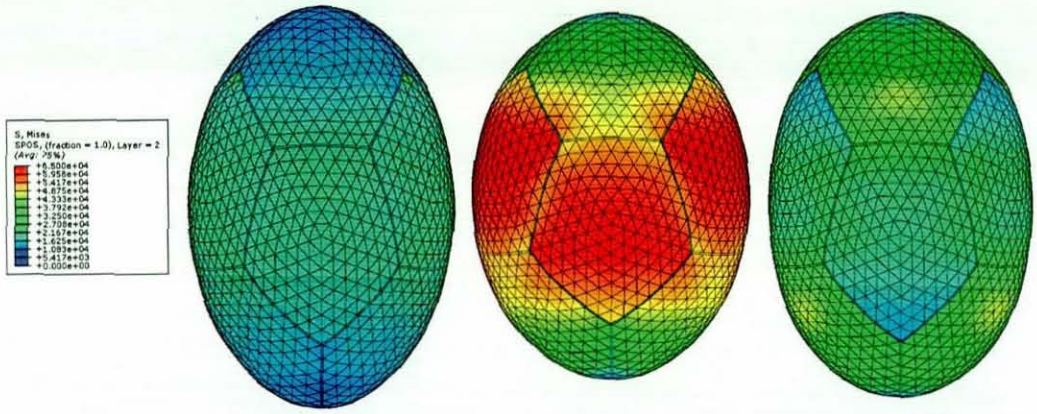

Figure 12.25 Stress during inflation a) 0° b) 45° c) Combination

12.8.2 Dynamic Properties

The variation in material orientation also affected the dynamic behaviour of the carcass during the simulation of a normal impact, and the CoR, contact time and deformation were measured. Table 12.1 details the dynamic parameters measured during the FE simulations at 6, 11 and 25m/s for end impacts. The material orientation within the carcass is represented by the following colours, 0°, 45° and combination.

Table 12.1 Dynamic behaviour of dodecahedron carcass – end impact

Velocity (m/s)	CoR	Contact Time (ms)	Deformation (mm)	
			Normal	Tangential
6	0.80	7.5	14	0.9
11	0.69	8.0	24	0.8
25	0.53	7.5	46	2.7
6	0.93	12.0	48	4.5
11	0.91	10.8	67	12.2
25	0.82	9.3	110	30.1
6	0.94	10.5	33	0.9
11	0.91	9.3	47	1.4
25	0.81	7.3	78	3.6

Results show that, as expected, for all material orientations, increasing the velocity resulted in a decrease in CoR and an increase in deformation. Impacts involving a 0°

material orientation produced a similar contact time irrespective of inbound velocity, but showed a dramatic reduction in CoR at higher velocities, whilst a 45° material orientation resulted in an increased contact time, but a higher CoR for all impact velocities. The carcass with both 0 and 45° material orientation demonstrated an increase in contact time at lower velocities, in comparison to the 0° carcass, but showed a similar CoR to the 45° carcass.

Figure 12.26 depicts the maximum deformation during a 25m/s impact. It was noted that the 0° carcass deforms with the 'concertina' style buckling demonstrated during experimental end impacts with the stitched rugby ball and the anisotropic FE model.

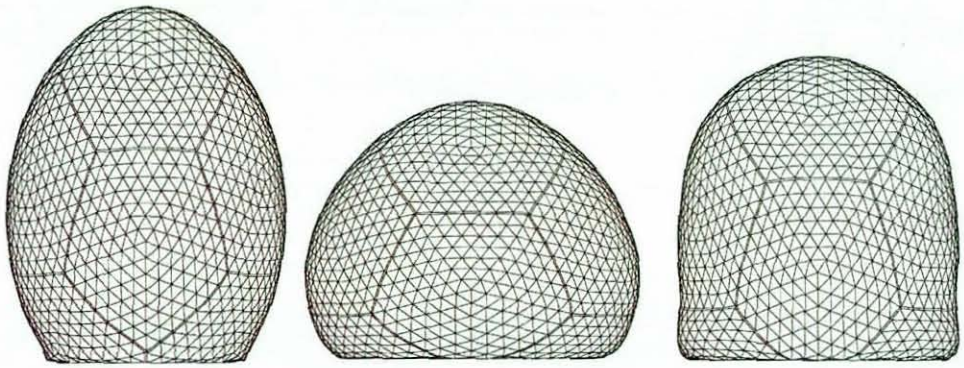

Figure 12.26 Maximum deformation a) 0° b) 45° c) Combination carcass

The normal deformation measured during an impact with the 45° carcass was considerably higher than the 0° and the combination carcass, probably due to the lower stiffness at this material orientation. The combination carcass exhibited an increased level of normal deformation in comparison to the 0° carcass due to the inclusion of the 45° material orientation in the panels which make contact with the plate. The tangential deformation in the 0° carcass impacts was <1mm, whilst the softer response of the 45° carcass produced a 30mm increase during a 25m/s impact. The combination carcass demonstrated a low measure of tangential deformation, which was attributed to the fact that the panels around the centre of the carcass, which exhibit the maximum tangential deformation, have a 0° material orientation. This produced a bulging effect where the 0 and 45° panels meet, depicted in Figure 12.26.

Table 12.2 details the dynamic parameters measured during the FE simulations at 6, 11 and 25m/s for centre of the panel impacts. The material orientation within the carcass is represented by the following colours, 0°, 45° and combination.

Table 12.2 Dynamic behaviour of dodecahedron carcass – centre impact

Velocity (m/s)	CoR	Contact Time (ms)	Deformation (mm)	
			Normal	Tangential
6	0.95	8.5	14	7
11	0.94	7.5	25	13
25	0.82	6.5	51	30
6	0.94	9.3	9	2
11	0.92	8.3	23	6
25	0.82	7.3	57	23
6	0.94	7.8	14	7
11	0.91	7.0	25	14
25	0.80	6.0	51	31

The introduction of the 45° material orientation within the end panels of the combination carcass has resulted in similar levels of CoR and deformation to the 0° carcass for centre of the panel impacts at all inbound velocities. The maximum difference between the measured value of CoR for end and centre impacts was demonstrated by the 0° carcass, whilst the 45° and combination carcass demonstrated similar CoR values at all inbound velocities. The 45° carcass produced a very soft response during impact, resulting in higher levels of deformation than were measured for the combination carcass (Figure 12.27). Adjustment of the material orientation within certain panels of the carcass resulted in a uniform CoR during all impact positions, without the high levels of deformation visible in the 45° carcass.

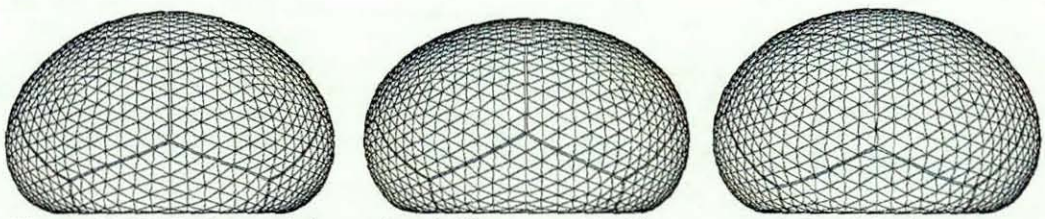

Figure 12.27 Maximum deformation a) 0° b) 45° c) Combination carcass

12.9 Final Design

12.9.1 Bladder

The inclusion of a single valve within a rugby ball's bladder has a detrimental effect on the dynamic characteristics of the ball in game related situations. A single valve moves the centre of mass away from the centroid of the ball, causing a lateral deviation demonstrated in the ball bounce characterisation test (Chapter 4) and the ball flight characterisation (Chapter 11). The non-uniform distribution of mass within the rugby ball also affects the flight of the ball, by causing unstable rotation about its axis with the intermediate moment of inertia, (Chapter 9). The inclusion of a second valve will statically balance the bladder and result in the centre of mass coinciding with the centroid of the ball, but this will increase the difference between the intermediate and largest moment of inertia. This effect was demonstrated in Chapter 11, as the statically balanced CHS2 rugby ball produced minimal lateral deviation during impacts with the mechanical kicking simulator, but demonstrated an increase in tilt angle caused by unstable rotation, which results in an increase in cross-sectional area, hence an increase in drag force.

Results from the ball flight characterisation (Chapter 11), clearly show that the dynamically balanced CHS4 rugby ball produces uniform flight characteristics irrespective of impact position. The novel rugby ball will therefore include a dynamically balanced bladder with a single inflation valve, and three volumes of material with an identical mass to the valve, placed at 90°increments (Figure 12.28).

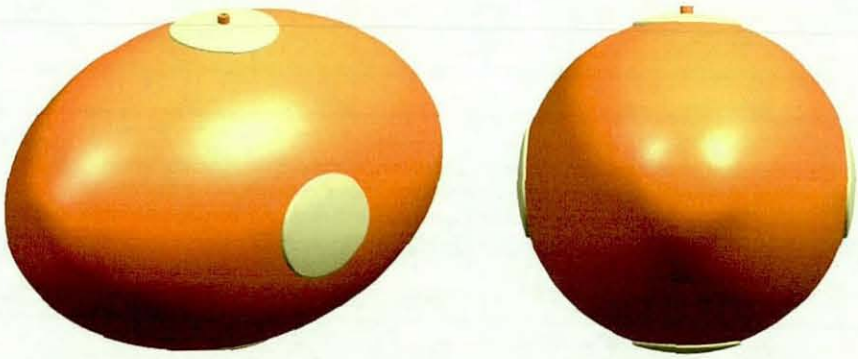

Figure 12.28 Dynamically balanced bladder

12.9.2 Carcass

The carcass will provide the integral structure of the novel rugby ball, with the panel configuration and material orientation depending upon the desired dynamic behaviour. Material testing has shown that the stitching region in a manually stitched rugby ball is

considerably stiffer than the panel region, creating a non uniform stiffness around the ball. The non uniform stiffness results in changes to the dynamic properties depending upon impact position. The inclusion of non parallel panel joins within the carcass demonstrated a uniform stress across the surface of the ball reducing the variation in dynamic performance. Prototype manufacture showed that more than three seams converging on a single vertex caused an irregular shape due to the excess volume of material caused by the panel overlap.

The trigonal trapezohedron and dodecahedron have six and fourteen panels respectively, with three panels meeting at every vertex, resulting in a uniform shape. The trigonal trapezohedron can be used as a basis for the carcass if it is desirable to reduce production time and cost due to fewer panels. However the reduction in panels limits the scope for varying the material orientation to tune the dynamic properties of the carcass. The dodecahedron has fourteen panels, resulting in an increase in production time and costs, but it has been demonstrated throughout the research that end impacts produced a reduction in CoR, at all inbound velocities, in comparison to centre of the panel impacts. The FE simulation results have shown that the material orientation of the end panels of a dodecahedron carcass can be adjusted to reduce the drop in CoR associated with end impact in a 0° stitched ball and carcass.

12.9.3 Outer Panels

Manufacturing a rugby ball using the thermo-bonded technique, results in increased design flexibility when constructing the outer panels. The outer panels no longer need to be stitched as they can be adhered to the inner carcass, allowing the designer to create panel shapes that could not be used in a stitched ball. This increased design flexibility was highlighted in the production of the Teamgeist soccer ball for the 2006 World Cup. Currently stitched balls have four panels converging on a single vertex, often resulting in a non symmetrical ball due to manufacturing errors. The outer panel configurations depicted in Figure 12.29 are an example of how to reduce this problem by incorporating a single panel at the end of the ball. FE models of the outer panel designs have not been created, as the models will not demonstrate the manufacturing improvements associated with the new construction technique, as these imperfections are not included within an FE model.

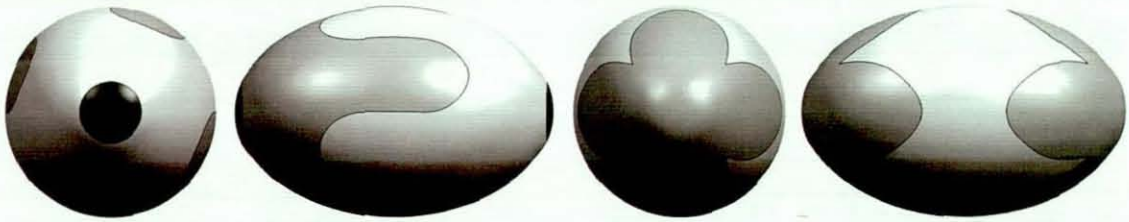

Figure 12.29 Outer panel designs

Law 2 detailed by the IRB states that the rugby ball must be oval and made from four panels, however if a law change allowed for a greater number of panels then it would be possible to design outer panels with increased freedom. An example of a fourteen panel design, based upon the Teamgeist soccer ball is depicted in Figure 12.30.

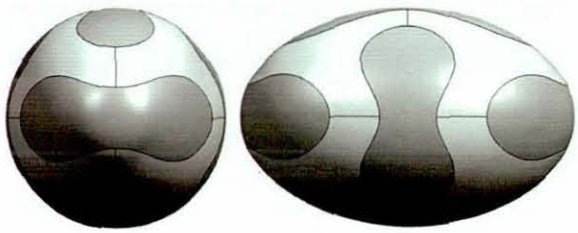

Figure 12.30 Teamgeist outer panel design

The novel rugby ball could consist of a dynamically balanced bladder which produces uniform flight characteristics irrespective of impact position, a carcass to provide the integral structure, which allows the material orientation of each panel to be defined in order to tune the dynamic behaviour, and outer panels which are adhered to the carcass, allowing increased design flexibility (Figure 12.31)

Figure 12.31 Exploded view of a novel rugby ball

12.10 Conclusions

The inclusion of the stitching region within a rugby ball created a non uniform stress distribution affecting the dynamic behaviour of the ball. During a game players would expect the ball to produce similar characteristics whether the ball is impacted on the seam of the centre of the panel, and currently this is not the case. Elite competition soccer balls manufactured by adidas are now made using a thermo-bonded construction which was developed to increase consistency of products, whilst reducing production time and cost. The thermo-bonded ball consists of a latex bladder, around which a twelve panel dodecahedron machine stitched fabric carcass provides the integral structure of the ball, to which the outer panels are adhered. Using this technique it is possible to develop a novel rugby ball with a unique carcass configuration and outer panels with increased design flexibility.

A number of carcass designs, based upon mathematical shapes, were created to increase the consistency of the dynamic behaviour of the ball when impacted at different locations. The manufacture of a prototype rhombic dodecahedron demonstrated the irregular shape caused by four panels joining at a single vertex, due to the excess panel overlap material. The trigonal trapezohedron and dodecahedron are mathematical shapes with six and fourteen faces respectively. The non parallel seams within the trigonal trapezohedron and dodecahedron carcass models resulted in a uniform stress distribution across the surface of the ball, which will increase the consistency of the dynamic behaviour of the ball during impacts.

Adjustment of the material orientation within certain panels of the carcass allows the dynamic behaviour to the ball during impact scenarios to be tuned. Applying a 45° material orientation to the top and bottom panels of the dodecahedron carcass resulted in a uniform CoR during all impact positions, without the high levels of deformation visible in a purely 45° carcass.

The manufacturing of a rugby ball using the thermo-bonded technique, should result in increased design flexibility when constructing the outer panels, allowing the designer to create panel shapes that could not be used in a stitched ball.

Chapter 13

Conclusions and Future Work

13 Conclusions

The research represents a first investigation into the dynamic behaviour of ovoid balls and develops an understanding of how they behave during game related situations. With the development of this knowledge, new ball assessment procedures and design concepts were investigated to improve consistency of dynamic performance. This will allow manufacturers to create balls with improved physical characteristics.

Experimental procedures were created which allowed the dynamic behaviour of an ovoid ball to be characterised. A rebound test was devised which enables accurate determination of the coefficient of restitution. It was found that the coefficient of restitution varies depending upon the position of impact, irrespective of ball type. The rebound test could be used by a governing body to specify and measure the dynamic variation of balls bounce in order for a ball to achieve official accreditation. The ball bounce characterisation test should be performed at a 45° ball orientation angle, as this is the position of minimum elevation angle and maximum spin rate, whilst placing the valve in an off-centre position would indicate the level of lateral deviation that will occur. Results showed that the orientation angle of the ball pre impact affects the elevation angle and spin rate, whilst varying the position of the valve at impact caused a variation in all measurement parameters.

An experimental procedure has been developed to measure the moment of inertia of ovoid balls about their principle axes. The inclusion of the valve within a rugby ball creates a non-uniform mass distribution resulting in a difference in the moments of inertia about the principle equilateral axes. During flight rotation about the axis with the intermediate moment of inertia, unstable rotation will occur, resulting in the ball performing a series of half twists at a frequency dependant upon the difference in moment of inertia of the principle axes.

Prototype rugby balls were manufactured with various mass distributions, which allowed the effect of the unstable rotation to be analysed. Results showed that the inclusion of a

second valve, opposite the first, reduced the time taken for the twisting motion to commence and complete a half twist, whilst the quadruple side valve produced zero twist during rotation and hence resulted in stable rotation. During the twisting motion, an increase in tilt angle was demonstrated, which resulted in an increase in drag force. A model to predict the unstable rotation of a ball in flight with tumble spin has been developed.

An assessment of elite player kicking was performed to enable test procedures that replicated play conditions. A novel mechanical kicking simulator has been designed and manufactured to simulate player kicks. The machine was used to validate theoretical predictions. The re-creation of the place kick in wind free conditions allowed the effect of the valve mass and the mass distribution to be measured. Results showed that increasing the mass of a single valve within the rugby ball created inconsistent flight characteristics when impacting the ball in a number of different positions, with significant variation in elevation angle and spin rate. Increasing the mass of a single valve also resulted in a greater lateral deviation from the kicking line when the valve was placed in the centre and right positions. The introduction of multiple valves within the ball's bladder, created rugby balls (CHS2 and CSH4) that demonstrated uniform ball velocity, elevation angle and spin rate irrespective of impact position. The effect of ball balancing by using valves at the ends of the ball requires further study.

The procedure for creating a FE model of a manually stitched ovoid ball has been developed, which allowed the capture of the ball's shape, discretisation of the surface, and the creation of a mesh that exhibits rotational symmetry and simple geometric definition. Hydrostatic fluid elements were coupled with shell elements to allow the pressurisation of the model. The non-spherical nature of an ovoid ball resulted in a non-uniform stress and volumetric increase during the process of inflation, whilst the experimental assessment of the stitching region showed that the stitching seam was four times stiffer than the outer panel material.

FE simulations and experimental data showed good agreement for CoR and contact time for all impact positions and inbound velocities, with the inclusion of the material anisotropy exhibited in the woven fabric, along with the 'concertina' buckling effect

visible during high speed end impacts. Analysis of the oscillations occurring post impact demonstrated good agreement between experimental and FE simulation data. Results showed that during an end impact, the deformation seen in the ball will recover very quickly with little oscillation. Analysis of the oscillations, using an FFT, determined that the ball oscillates at a frequency of 125-130Hz irrespective of impact position and inbound velocity.

The anisotropic FE simulation accurately predicted the CoR, contact time and deformation visible during experimental testing. As a result it can be used to predict the dynamic behaviour of a rugby ball during various impact scenarios.

The thermo-bonded soccer ball consists of a latex bladder, around which a machine stitched fabric carcass in the shape of a twelve panel dodecahedron, provides the integral structure of the ball, to which the outer panels are adhered. Using this technique it is possible to develop a novel rugby ball with a unique carcass configuration and outer panels with increased design flexibility. A number of carcass designs, based upon mathematical shapes, were created to increase the consistency of the dynamic behaviour of the ball when impacted at different locations. The trigonal trapezohedron and dodecahedron are mathematical shapes with six and fourteen faces respectively. The non-parallel seams within the trigonal trapezohedron and dodecahedron carcass models resulted in a uniform stress distribution across the surface of the ball, which will increase the consistency of the dynamic behaviour of the ball during impacts.

Adjustment of the material orientation within certain panels of the carcass allows the dynamic behaviour of the ball during impact scenarios to be tuned. The manufacture of a rugby ball using the thermo-bonded technique, should result in increased design flexibility when constructing the outer panels, allowing the creation of panel shapes that could not be used in a stitched ball.

13.1 Future Work

Areas of future work which have been identified from the current research have been sub-categorised and described below.

During the characterisation of the dynamic properties of an ovoid ball, the effect of mass distribution was examined in detail. The rules defined by the relative governing bodies specify a number of static dimensions, allowing considerable scope for varying the shape and performance of the ball. Using the procedures developed within this research it would be worthwhile examining the dynamic properties of ovoid balls whilst varying the shape of the panels.

The effect of variation in the dynamic properties of an ovoid ball, due to impacts, was demonstrated within this research. Further investigation needs to be conducted in order to determine the mechanics behind this variation in properties, and the amount of impacts needed in order to obtain optimum performance. The practice of 'wearing in' is worthy of consideration by manufacturers as it affects the dynamic properties of the ball. The number of impacts needed to experience significant differences requires further investigation along with the effects of surface wear/degradation, as customers may not appreciate worn products.

The research has presented experimental data which demonstrates the improved consistency of the prototype rugby balls, however this information could be combined with subjective data ascertained from a player perception study. Roberts (2002) established a method of interviewing elite players to determine the perceived characteristics of a golf shot. This method could be employed to understand players' perception and requirements of ovoid balls.

Grip plays an important part in determining the dynamic properties of an ovoid ball, due to the amount of time the ball spends in the hands of the players. Cotton (2008) examined the ball surface interaction during a soccer impact, during wet and dry conditions. A number of experimental procedures have been established to allow the frictional properties of different soccer balls to be characterised. Using similar experimental procedures it should be possible to determine the effect of optimising the outer panel texture, in order to improve consistency during game related situations. FE

modelling of ball surface interactions in wet and dry conditions presents an exciting area of research.

The research simulated a number of novel rugby ball designs, which were not validated due to a lack of carcass material. In order to examine the validity of the proposed designs, inner carcasses need to be constructed and validated using experimental procedures established during this research. Current outer panels consist of four petal shaped panels, but the thermo bonded construction method allows the designer to create panel shapes that could not be used in a stitched ball, which provides a key area for future work.

At present no theoretical flight models to predict ovoid ball flight exist and wind tunnel procedures for spinning ovoid ball present considerable problems. This is an interesting area of future work.

All sport governing bodies are concerned about maintaining the traditions of their sports. They want to emphasise the importance of skill and are concerned that the introduction of technology does not diminish the fundamental qualities of the sport. The research and methods developed throughout the thesis will enable more consistent, innovative and better performing balls to be created. Coupled with the progressive improvement in player capability, particularly in a lucrative professional sport, ovoid balls will continue to be kicked further. It is important that sport governing bodies understand the science relating to their equipment in order to introduce rules to maintain the balance between tradition and technology in the sport. A research programme to benchmark acceptable ball performance for ovoid ball games would be worthwhile.

References

Abaqus (2005a). Abaqus version 6.5 users manual volume IV: Element. *Abaqus INC*

Abaqus (2005b). Abaqus version 6.5 users manual volume III: Materials. *Abaqus INC*

adidas (2006). Testing and development of the adidas +Teamgeist. *http://www.press.adidas.com*

Alam, F., Subic, A and Watkins, S. (2005). Measurements of aerodynamic drag forces of a rugby ball and Australian football. *Asia Pacific Congress on Sports Technology:* pp.276-279.

Alam, F., We, P., Subic, A and Watkins, S. (2006). A comparison of aerodynamic drag of a rugby ball using EFD and CFD. *Engineering of Sport 6*: pp.145-149.

Aoki, A. O., M. Nonaka, K and Yamaguchi, K. (2002). The effect of dimple number on the flying characteristics of a golf ball. *Sports Engineering 5:* pp.330-336.

Armstrong, C., Levendusky, T, Eck, J, Spyropoulos,P, Kugler, L. (1988). Influence of inflation pressure and ball wetness on the impact characteristics of two types of soccer balls. *Science and Football: Proceedings of the first World Congress of Science and Football:* pp.394-398.

Asai, T., Carre, M, Akatsuka, T and Haake, S. (2002). The curve kick of a football I; Impact with the foot. *Sports Engineering 5:* pp.183-192.

Asai, T. and Akatsuka., T. (1995). Computer simulation of curve-ball kicking in soccer. *XVth Congress of the International Society of Biomechanics*: pp.433-430

Asami, T., and Notle, V. (1983). Analysis of powerful ball kicking. *Biomechanics. VIII* pp.675-700

Association, A. F. C. (2005). Complete guide to special teams. *Human Kinetics.*

Barger, V. and Olsson, M (1938). Classical mechanics: A modern perspective. *McGraw-Hill.*

Bernstein, A. (1977). Listening to the coefficient of restitution. *American Association of Physics Teachers* 45: pp.41-44.

Brancazio, P. (1985a). The physics of kicking a football. *American Association of Physics Teachers* 23: pp.403-407.

Brancazio, P. (1985b). Why does a football keep its axis pointing along its trajectory. *American Association of Physics Teachers* 23: pp.571-573.

Brancazio, P. (1987). Rigid body dynamics of a football. *American Journal of Physics* 55: pp.415-420.

Bridge, J. (1998a). The way balls bounce. *Physics Education* 33: pp.174-181.

Bridge, J. (1998b). The way balls really bounce. *Physics Education* 33: pp.236-241.

Brody, H. (1990). The tennis ball bounce test. American *Association of Physics Teachers* 28: pp.407-409.

Carré, M., Goodwill, S. and Haake, S. (2005).Understanding the effect of seams on the aerodynamics of an association football. *Journal of Mechanical Engineering Science* 219: pp.657-666.

Ciesielske, A (1999). An introduction to rubber technology. *RAPRA Technology Ltd.*

Clough, R, W. (1960). The finite element method in plane stress analysis. *Proceedings, 2nd Conference on Electronic Computation, A.S.C.E. Structural Division,* Pittsburgh, Pennsylvania, Sept.

Cochran, A and Stobbs, J(1968). The search for the perfect swing. *Heinemann, London..*

Cotton, R. (2008). Surface interactions of soccer balls. *Wolfson School of Mechanical and Manufacturing Engineering, Loughborough University.*

Cordingley, L. (2002). Advanced modelling of hollow sports ball impacts. *Wolfson School of Mechanical and Manufacturing Engineering, Loughborough University.*

Coriolis, G. (1835). Théorie mathématique des effets du jeu de billiard .

Cross, R. (1999). The bounce of a ball. *American Association of Physics Teachers* 67: pp.222-227.

Cunningham, J. and Dowell, L. (1976). The effect of air resistance on three types of football trajectories. *Research Quarterly* 47: pp.852-854.

Daish, C. (1972). The physics of ball games. *The English University Press.*

Daniel, I. and Ishai, O. (2006). Engineering mechanics of composite materials. *Oxford University Press.*

Dowell, L., Snowden, S and Powell, S. (1991). A comparison of force of impact compression area and velocity of selected balls. *Journal of Human Movement Studies* 20: pp.279-289.

Drane, P. and Sherwood, J. (2004). Characterization of the effect of temperature on baseball CoR performance. *Sports Engineering 4.*

Falcon, E., Laroche, C, Fauve, S and Coste, C. (1998). Behaviour of one inelastic ball bouncing repeatedly off the ground. *The European Physics Journal* 3: pp.45-57.

FIFA (2006). Footballs - Test Criteria.
http://www.fifa.com/en/development/pitchsection/0,1245,2,00.html
Gent, A. (2001). Engineering with rubber. *Hanser Publishers, Munich.*

Gibbs, P. (2005). Virtual testing of footwear. Wolfson School of Mechanical and Manufacturing Engineering, Loughborough University.

Gugan, D. (2000). Inelastic collision and the Hertz theory of impact. American *Association of Physics Teachers* 68: pp.920-924.

Harper, T. (2007). Robotic simulation of golf swings. Wolfson School of Mechanical and Manufacturing Engineering, Loughborough University.

Hartschuh, R. (2002). Physics of punting a football. *http://www.wooster.edu/physics/JrIS/Files/Ryan.pdf*

Hatze, H. (1992). The effectiveness of grip bands in reducing racket vibration transfer and slipping. *Medicine and Science in Sports and Exercise.* 24: pp.226-330

Hay, J. (1993). The biomechanics of sports techniques. *Prentice Hall*

Hearle, J., Grosberg, P. and Backer, s. (1969). Structural mechanics of fibres, yarns and fabrics. *John Wiley and sons, New York.*

Hocknell, A., Jones, R, and Rothberg, S. (1996). Experimental analysis of impacts with large elastic deformation; I. Linear motion. *Measurement Science Technology* 7: pp.1247-1254.

Hocknell, A., Jones, R and Rothberg, S. (1998a). Computational and experimental analysis of the golf impact. *Third World Scientific Congress of Golf.* pp.37-47

Hocknell, A., Mitchell,S, Jones, R, and Rothberg, S. (1998b). Hollow golf club head modal characteristics; Determination and impact applications. *Experimental Mechanics* 38: pp.140-146.

Holmes, C., Jones, R. and Harland, A (2006). Ball launch characteristics of elite rugby union players. *Engineering of Sport. 6:* pp.211-216

Holmes, G. and Bell, M. (1985). The effect of football type and inflation pressure on rebound resilience. Journal *of the Sports Turf Research Institute* 61: pp.132-135.

Horton, J., Tupholme, G. and Gover, M. (2002). Axial loading of bonded rubber blocks, *Journal of Applied Mechanics, ASME* 69: pp.836–843.

Hubbard, M. and Stronge, W. (2001). Bounce of hollow balls on flat surfaces. *Sports Engineering 4*: pp.49–61.

International Rugby Board (IRB). (2005). Pick your union. *http://www.irb.com*

Isokawa, M and Lees, A. (1988). A biomechanical analysis of the instep kicking motion in soccer. *Science and Football Proceedings of the First World Congress of Science and Football,* pp 449-455

Jain, R., Kasluri, R. and Schunck, B. (1995). Machine vision. *McGraw-Hill, Inc, US.*

Johnson, W., Reid, S. and Trembaczowski-Ryder, R. (1972). Impact, rebound and flight of a well inflated pellicle as exemplified in association football. *The Manchester Association of Engineers,* Session 5: pp.1-25.

Jones, I. (2002). Is the impact of a golf ball Hertzian. *Science and Golf IV: Proceedings of the World Scientific Congress of Golf.* pp.920-924

Kleppner, D. and Kolenkow, R. (1973). An introduction to mechanics. *McGraw-Hill.*

Kong, h., Mouritz, A. and Paton, R. (2004). Tensile extension properties and deformation mechanisms of multiaxial non-crimp fabrics. *Composite Structures,* 66, pp.249-259.

Kotze, J. (2002). A tennis serve impact simulation machine. *Engineering of Sport. 4th* pp.477-483

Lees, A., and Nolan, L. (1998). The biomechanics of soccer; A review. *Journal of Sports Sciences.* 16: pp.221-234

Levendusky, T., Armstrong, C, Eck, J, Jeziorwski, J and Kugler, L. (1988). Impact characteristics of two types of soccer balls. *Science and Football : Proceedings of the First World Congress of Science and Football* : pp.384-393

Luthander, S. and Ryberg, A. (1935). Experimentelle Untersuchungen uber den uftwiderstand bei einer um ein mit der Windrichtung parallelen Achse roteirenden Kugel. *Phys. Z.* 36: pp.552–558

Macmillian, M. (1975). Determinants of the flight of the kicked football. *Research Quartley* 46: pp.48–57.

Marion, J. (1965). Classical dynamics of particles and systems. *Academic Press.*

Myddelton, D. (2007). They meant well: Government project disasters. *The institute of economic affairs.*

Neilson, P. (2003). The dynamic testing of soccer balls. *Wolfson School of Mechanical and Manufacturing Engineering, Loughborough University.*

Newnham, P. (2007). Discussions with Dr P Newnham, experimental aerodynamicist.

NFL (2005). History of NFL. *http://www.nfl.com/history.*

Nowak, C. (2003). Flight data recorder for an American football. *Masters of Engineering Project Report, University of Buffalo.*

Nunome, H, Asai, T, ikegami, Y and Sakurai, S. (2002). Three-dimensional kinetic analysis of side-foot and instep soccer kicks. *Medicine and Science in Sports and Exercise,* 34: pp.2028-2036

Percival, A. (1977). The impact and rebound of a football. *The Manchester Association of Engineers 5:* pp.17-28

Photron (2007). Equivalent ISO/ASA Light Sensitivity FASTCAM APX-RS.

Plagenhoef, S. (1971). Patterns of human movement. *Prentice Hall.*

Price, D. (2005). Advanced modelling of soccer balls. *Wolfson School of Mechanical and Manufacturing Engineering, Loughborough University.*

Price, A., Cohen, A. and Johnson, I. (2005). Pizzuto's fabric Science. *Fairchild, New York.*

Rae, W. (2003). Flight dynamics of an American football in a forward pass. *Sports Engineering 6:* pp.149-162.

Rae, W. and Streit., R (2002). Wind tunnel measurements of the aerodynamic loads on an American football. *Sports Engineering 6:* pp.165-172.

RFU (2005). Rugby history.
http://www.rfu.com/index.cfm/fuseaction/RFUHome.Simple_Detail/storyID/10232/storytypeID/96/.

Roberts, E. and Metcalf, A. (1968). Mechanical analysis of Kicking. *Biomechanics I:* pp.315-319.

Roberts, J., Jones, R and Rothberg, S. (2001). Measurement of contact time in short duration sports ball impacts; An experimental method and correlation with the perception of elite golfers. *Sports Engineering 4:* pp.191-203.

Roberts, J. (2002). Mechanical and physiological influences on the feel of a golf shot. *Wolfson School of Mechanical and Manufacturing Engineering, Loughborough University.*

Ronkanien, J. and Harland, A. (2007) Soccer ball modal analysis using a scanning laser doppler vibrometer (SLDV). *Journal of Sports Engineering,* 10: pp.49-55

Rutgers (2005). History of American football.
http://www.scarletknights.com/football/history/first_game.htm

Sayers, A., Koumbarakis, M. and Sobey, S. (2000). Surface hardness of cricket bats following 'knocking in'. *Department of Mechanical Engineering, University of Cape Town*

Schempf, H. (1995). Roboleg: A robotic soccer-ball kicking leg. *IEEE international conference on robotics and automation.* pp.1314-1319

Shenitzer, A. and Stillwell, J. (2002). Mathematics and its history. *Springer, New York*

Sidhu, R., Averill, R., Riaz, M. and Pourbograt, F. (2001). Finite element analysis of textile composite perform stamping. *Composite Structures,* 52: pp.483-497.

Sporting Goods Manufacturing Association (SGMA) (2007a). The State of the Market.
http://www.sgma.com

Sporting Goods Manufacturing Association (SGMA) (2007b). Manufacturers sales by category report, US wholesale value of annual manufacturers' shipments ($million). *http://www.sgma.com*

Stensgaard, I. and Laegsgaard, E. (2001). Listening to the coefficient of restitution - revisited. *American Journal of Physics Teachers* 69: pp.301-305.

Steele, C. (2006). Tennis ball degradation. *Wolfson School of Mechanical and Manufacturing Engineering, Loughborough University.*

Sun, H., Ning, P. and Postle, R. (2004). The Poisson's ratio of a woven fabric. *Composite Structures*, 68: pp.505-510.

Suzuki, M. and Ozaki, Y. (2002). Three dimensional analysis of a new golf swing robot emulating skilful golfers. *Engineering of Sport 4:* pp.450-455.

Symes, A. (2007). The effect of mass distribution on cricket bats playing properties. *Wolfson School of Mechanical and Manufacturing Engineering, Loughborough University.*

Tatara, Y. (1993). Large deformations of a rubber sphere under diametral compression. *JSME International Journal* 36: pp.195-203.

Thilmany, J. (2005). FEA finds its place. Mechanical Engineer Magazine.
Townsend, M. (1984). *Mathematics in Sport, Ellis Horwood Ltd.*

Turner, M. J. Clough, R. W, Martin, H.C. and Topp, L.J. (1956). Stiffness and deflection analysis of complex structures. *Journal of the Aeronautical Sciences*, Vol. 23, No. 9, pp.805-823.

Updike, D. and Kalnins, A. (1970). Axisymmetric behaviour of an elastic spherical shell compressed between rigid plates. *ASME Journal of Applied Mechanics*, 92, pp.635-640.

Vicon (2002). Vicon motion systems manual.

Watanabe, K. (1982). The hysteresis of the drag of a sphere in the critical Reynolds number range. *Japan Society Mechanical Engineers.* 25: pp.203-206.

Watts, R. and Moore, G. (2003). The drag force on an American football. *American Association of Physics Teachers* 71: pp.791-793.

Watts, R. and Sawyer, E. (1974). Aerodynamics of a knuckleball. *American Association of Physics Teachers* 43: pp.960-963.

Webb, J. (1998). Inflatable footballs such as rugby: EP0837719.
http://www.freepatentsonline.com/EP0837719B1.html

Wilson (2005). Why do college footballs have half stripes?. www.wilson.com

Yeadon, M. (1993a). The biomechanics of twisting somersaults Part I: Rigid body motions. *Journal of Sports Sciences.* 11: pp.187-198.

Yeadon, M. (1993b). The biomechanics of twisting somersaults Part II: Contact twist. *Journal of Sports Sciences.* 11: pp.199-208.

Yeadon, M. (1993c). The biomechanics of twisting somersaults Part III: Ariel twist. *Journal of Sports Sciences.* 11: pp.209-218.

Yeadon, M. (1993d). The biomechanics of twisting somersaults Part IV: Partitioning performances using the tilt angle. Journal *of Sports Sciences.* 11: pp.219-225.

Appendix A

Ovoid Ball Specification

The specifications for ovoid balls are established by the relative governing body, with the specification for a rugby ball defined by the International Rugby Board (IRB). American football has a number of governing bodies, the National Football League (NFL), the National Collegiate Athletic Association (NCAA) and the National Federation of State High School Association (NFHS). The differences between the governing bodies' specifications are detailed below, along with the specification for a Canadian football and Australian Rules football.

Rugby Ball Specification

Figure A.1 Rugby ball dimensions

Shape

The ball must be oval and made of four panels.

Dimensions

Length - 280 to 300 mm

Equilateral axis circumference - 740 to 770 mm

Polar axis circumference - 580 to 620 mm

Materials

Leather or suitable synthetic material. It may be treated to make it water resistant and easier to grip.

Pressure

65.71-68.75 kilopascals, or 0.67-0.70 kilograms per square centimetre, or 9.5-10.0 lbs per square inch.

Weight

410 - 460 grams

Spare balls

Spare balls may be available during a match, but a team must not gain or attempt to gain an unfair advantage by using them or changing them.

Smaller balls

Balls of different sizes may be used for matches between young players.

American Football Specification

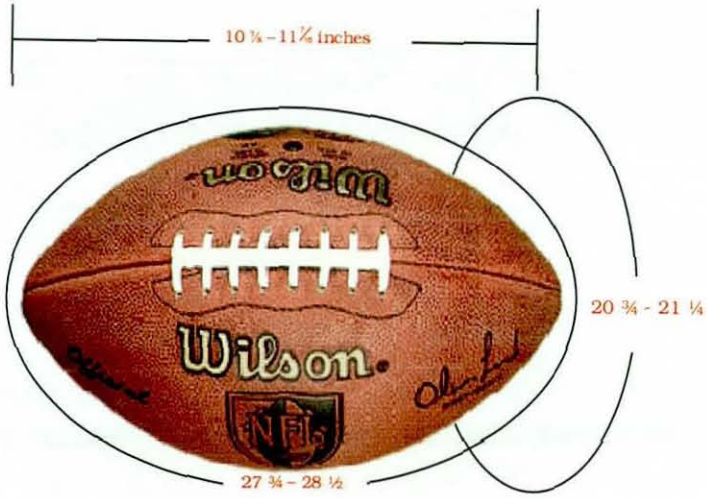

Figure A.2 American football dimensions

Dimensions

Length – 10 7/8 to 11 7/16 inches

Equilateral axis circumference - 27 3/4 to 28 1/2 inches.

Polar axis circumference - 20 3/4 to 21 1/4 inches.

Materials

New or nearly new. (A nearly new ball is a ball that has not been altered and retains the properties and qualities of a new ball.)

Cover consisting of four panels of pebble-grained leather without corrugations other than seams.

Natural tan colour.

Pressure

Inflated to the pressure of 12.5 to 13.5 pounds per square inch (psi).

Weight

Weight of 14 to 15 ounces.

Laces

One set of eight equally spaced lacings.

Stripe

Two 1-inch white stripes located only on the two panels adjacent to the laces, which are 3 to 3 ¼ inches from the end of the ball.

General

The ball may not be altered. This includes the use of any ball-drying substance. Mechanical ball-drying devices are not permitted near the sidelines or in the team area. Advertising is prohibited on the ball [Exceptions: (1) Ball manufacturer's name or logo, and (2) Governing body's logo].

Variations between governing bodies

Panel Restrictions

NHFS define that there are no panel restrictions as stated by the NFL

Stripe

All American footballs used to have a single complete horizontal stripe, a set distance from the end of the ball, however NFL players began to complain that their thumbs were slipping on the paint of the stripe (Wilson 2005), which resulted in the removal of the stripe. The half stripe is now only used for college and high school balls as its placement, on the top two quarters of the ball, does not affect the quarterbacks thumb grip, whilst the white stripes helped to illuminate the footballs as most college stadiums are not well lit (Wilson 2005).

Canadian Football Specification

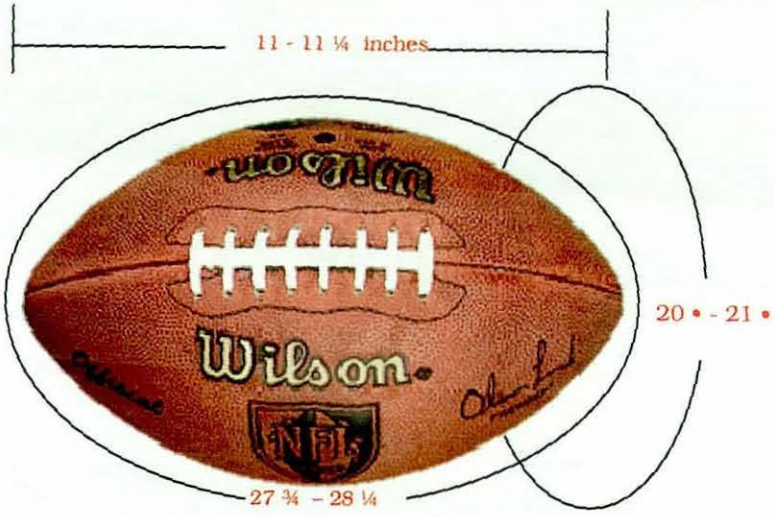

Figure A-3 Canadian football dimensions

Dimensions

Length - 11 to 11 1/4 inches

Equilateral axis circumference - 27 3/4 to 28 1/4 inches.

Polar axis circumference - 20 7/8 to 21 1/8 inches.

Materials

Four panels of Horween red leather.

Pressure

Inflated to the pressure of 12.5 to 13.5 pounds per square inch (psi).

Weight

Weight of 14 to 15 ounces.

Laces

Maximum length - 4 3/8 inches.

Maximum width - 1 1/8 inches.

Stripe

The ball shall be painted with 1-inch white stripes around the polar axis, 3 inches away from the point of greatest circumference of the polar axis.

General

A minimum of seven balls shall be used in a game and changed at the discretion of the referee. The balls shall be kept clean and in playable condition.

Australian Rules Football

Figure A-4 Australian rules dimensions

Dimensions

Length - 270 to 280 mm.

Equilateral axis circumference - 720 to 735 mm.

Polar axis circumference - 545 to 555 mm.

Materials

Made from leather, tan (day use) or yellow (night use) in colour.

Weight

450 - 500 grams (dry weight)

Comparison of Ovoid Ball Specification

Table A.1 details the main parameters specified by the ovoid ball governing bodies. Units have been converted to allow comparison, dimensions (mm), weight (g) and pressure (psi).

Table A.1 Comparison of ovoid ball specification

	Rugby	American Football	Canadian Football	Australian Rules
Length	280 - 300	276.2 - 301.2	279.4 - 280	270 - 280
Equilateral Circumference	740 - 770	704.9 - 723.9	707.9 - 717.6	720 - 730
Polar Circumference	580 - 620	524.9 - 539.8	530.2 - 536.6	545 - 555
Weight	410 - 460	393.9 - 425.2	393.9 - 425.2	450 - 500
Pressure	9.5 – 10	12.5 - 13.5	12.5 - 13.5	

Appendix B

The Tennis Racket Theorem

Barger and Olsson (1938) used Euler's rigid body equations to explain unstable rotation of a tennis racket. The method for deriving the stability of the rotation about the three principal axes is detailed below.

Euler's equations can be simplified to;

$$I_1\dot{\omega}_1 + (I_3 - I_2)\omega_3\omega_2 = 0 \qquad \text{(B1)}$$

$$I_2\dot{\omega}_2 + (I_1 - I_3)\omega_1\omega_3 = 0 \qquad \text{(B2)}$$

$$I_3\dot{\omega}_3 + (I_2 - I_1)\omega_2\omega_1 = 0 \qquad \text{(B3)}$$

The authors used a simplified model for the tennis racket depicted in Figure B1, with a circular hoop of radius a and mass m_a connected to a thin rod of length l and mass m.

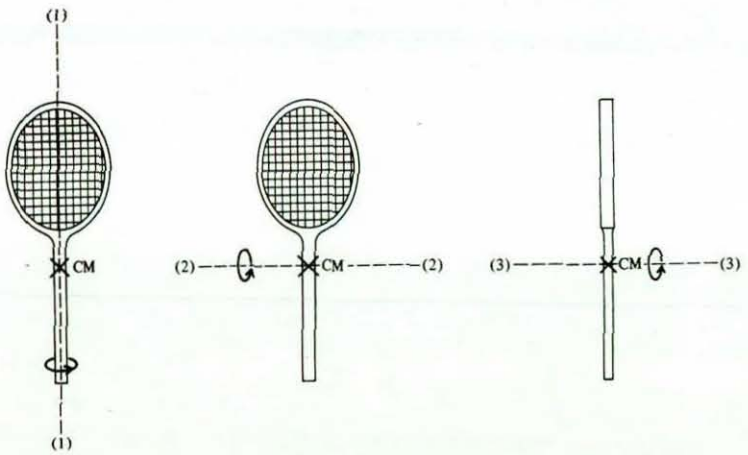

Figure B1 Principle axes of the tennis racket

The total mass of the racket, $M = m_a + m_b$ with the centre of mass (CM) located on the principal axis (1) at a distance R from the centre of the hoop.

$$R = \frac{m_l}{M}\left(a + \frac{l}{2}\right) \qquad \text{(B4)}$$

The moment of inertia about the principal axes are defined below, Equations B5-B8. I_2 was calculated by analysing the contribution of the hoop and the handle separately.

$$I_1 = \frac{1}{2} m_a a^2 \tag{B5}$$

$$I_{2(hoop)} = \frac{1}{2} m_a a^2 + m_a R^2 \tag{B6}$$

$$I_{2(handle)} = \frac{1}{12} m_l^{\ 2} + m_l \left(a + \frac{l}{2} - R \right)^2 \tag{B7}$$

$$I_3 = I_1 + I_2 \tag{B8}$$

Combining $I_{2(hoop)}$ and $I_{2(handle)}$ the authors calculated I_2, Equation B9.

$$I_2 = \frac{1}{2} m_a a^2 + \frac{1}{12} m_l l^2 + \frac{m_a m_l}{M} \left(a + \frac{1}{2})^2 \right) \tag{B9}$$

The parameters for a classic wooden tennis racket are;

a	=0.13m	l	=0.38
R	=0.18m	M	=0.34kg
m_l	=0.18kg	m_a	=0.15kg

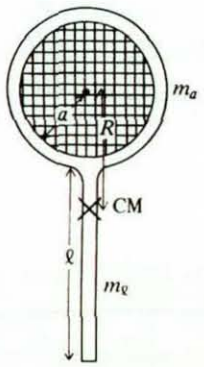

Figure B2 Dimensions of the tennis racket model

The moments of inertia about the principal axes were;

I_1=0.1 x 10^{-2} k·gm^2

I_2=1.2 x 10^{-2} k·gm^2

I_3=0.18 x 10^{-2} k·gm^2

I_3 defined in Equation B8, was then substituted into the Euler equations, and derived Equations B10-B13.

$$\dot{\omega}_1 + \omega_3 \omega_2 = 0 \tag{B10}$$

$$\dot{\omega}_2 - \omega_1 \omega_3 = 0 \tag{B11}$$

$$\dot{\omega}_3 + r\omega_2\omega_1 = 0 \qquad \text{(B12)}$$

where;

$$r = \frac{(I_2 - I_1)}{(I_2 + I_1)}$$

The authors stated that $r \approx 1$, and this value was used throughout the remaining calculations. If initially rotated about axis (1), the product $\omega_3\omega_2$ from Equation B10 can be neglected and it was found that ω_1 remained constant. Solving Equations B11 – B12, introduced a complex variable, Equation B13.

$$\tilde{\omega} = \omega_3 + i\omega_2 \qquad \text{(B13)}$$

Since $\omega_2 = \text{Im}\,\tilde{\omega}$ and $\omega_3 = \text{Re}\,\tilde{\omega}$, Equations B11-B12 became;

$$\text{Im}\,\dot{\tilde{\omega}} - \omega_1\,\text{Re}\,\tilde{\omega} = 0 \qquad \text{(B14)}$$

$$\text{Re}\,\dot{\tilde{\omega}} + \omega_1\,\text{Im}\,\tilde{\omega} = 0 \qquad \text{(B15)}$$

which were combined as a single equation;

$$\dot{\tilde{\omega}} - i\omega_1\tilde{\omega} = 0 \qquad \text{(B16)}$$

The exponential solution of this differential was defined by Equation B17.

$$\tilde{\omega}(t) - ae^{i(\omega_1 t + \alpha)} \qquad \text{(B17)}$$

The corresponding results for ω_2 and ω_3 were defined in Equations B18-B19.

$$\omega_2(t) = a\sin(\omega_1 t + \alpha) \qquad \text{(B18)}$$

$$\omega_3(t) = a\cos(\omega_1 t + \alpha) \qquad \text{(B19)}$$

The authors stated that by the initial conditions the amplitude a was small, and these components of the angular velocity remained small, with an approximate solution defined by Equation B20.

$$\omega = \sqrt{\omega\,(t)^2 + \omega_2}(t)^2 + \omega_3(t)^2 = \sqrt{\omega_1^{\,2} + a^2} \qquad \text{(B20)}$$

The authors stated that the angular velocity vector ω, precesses in a small cone about the principal axis (1), depicted in Figure B3, which explains the stability of the racket when rotated about this axis.

Figure B3 Stable Precession about principle axis (1)

The authors stated that if initially rotated about axis (3), the solution to Euler's equations was similar to rotation about axis (1). Equations B21-B22 were derived by interchanging ω_3 and ω_1 in Equations B18 and B19.

$$\omega_1(t) = a\cos(\omega_3 t + \alpha) \qquad \text{(B21)}$$

$$\omega_2(t) = a\sin(\omega_3 t + \alpha) \qquad \text{(B22)}$$

The motion about this axis was also defined as stable.

If the racket was initially rotated about the axis (2) the product $\omega_1\,\omega_3$ was neglected, which derived Equation B23.

$$\omega_2(t) = \omega_2(0) \qquad \text{(B23)}$$

Addition and subtracting of Equations B10 and B12 derived Equations B24 - B25

$$(\dot{\omega}_1 + \dot{\omega}_3) + \omega_2(\omega_1 + \omega_3) = 0 \qquad \text{(B24)}$$

$$(\dot{\omega}_1 - \dot{\omega}_3) - \omega_2(\omega_1 - \omega_3) = 0 \qquad \text{(B25)}$$

The authors stated that the solutions for the linear combinations in Equations B24 and B25 are;

$$(\omega_1 + \omega_3) = ae^{-\omega 2t} \qquad \text{(B26)}$$

$$(\omega_1 - \omega_3) = be^{+\omega 2t} \qquad \text{(B27)}$$

therefore;

$$\omega_1(t) = \frac{1}{2}(ae^{-\omega 2t} + be^{+\omega 2t}) \qquad \text{(B28)}$$

$$\omega_3(t) = \frac{1}{2}(ae^{-\omega 2t} - be^{+\omega 2t}) \qquad \text{(B29)}$$

The authors noted that during rotation about axis (2), the angular velocities about axes (1) and (3) grow rapidly with time, causing the racket to tumble, hence unstable rotation. This condition would apply as long as the product $\omega_1 \omega_3$ in Equation B11 was negligible.